

General Disclaimer

One or more of the Following Statements may affect this Document

- This document has been reproduced from the best copy furnished by the organizational source. It is being released in the interest of making available as much information as possible.
- This document may contain data, which exceeds the sheet parameters. It was furnished in this condition by the organizational source and is the best copy available.
- This document may contain tone-on-tone or color graphs, charts and/or pictures, which have been reproduced in black and white.
- This document is paginated as submitted by the original source.
- Portions of this document are not fully legible due to the historical nature of some of the material. However, it is the best reproduction available from the original submission.

MICROFILMED

FROM BEST

AVAILABLE

COPY

NASA TECHNICAL
MEMORANDUM

NASA TM X-53151

OCTOBER 21, 1964

N65 14933

NASA TM X-53151

FACILITY FORM ONE

(ACCESSION NUMBER)	205	(THRU)	1
(PAGES)	TMX 53151	(CODE)	30
(NASA CR OR TMX OR AD NUMBER)		(CATEGORY)	

A COMPREHENSIVE ASTRODYNAMIC EXPOSITION AND CLASSIFICATION OF EARTH-MOON TRANSITS

by GARY P. HERRING
Aero-Astrodynamics Laboratory

NASA

*George C. Marshall
Space Flight Center,
Huntsville, Alabama*

GPO PRICE \$ _____

OTS PRICE(S) \$ _____

Hard copy (HC) 6.00

Microfiche (MF) 1.25

TECHNICAL MEMORANDUM X-53151

A COMPREHENSIVE ASTRODYNAMIC EXPOSITION AND
CLASSIFICATION OF EARTH-MOON TRANSITS

By

Gary P. Herring

George C. Marshall Space Flight Center

Huntsville, Alabama

ABSTRACT

14939

The restricted three-body model is used to develop a geometrical and topological taxonomy of the field of earth-moon transits (both directions) which is based on conditions at the terminals (perigee and periselenium). It is presented in such a way as to promote mental control of the subject.

The classifying techniques are then employed in the analysis of free-return transits as well as such problems as the lighting conditions upon landing.

The report provides convenient reference material for the engineer involved in the layout of Apollo type missions.

Author

NASA - GEORGE C. MARSHALL SPACE FLIGHT CENTER

NASA - GEORGE C. MARSHALL SPACE FLIGHT CENTER

Technical Memorandum X-53151

October 21, 1964

A COMPREHENSIVE ASTRODYNAMIC EXPOSITION AND
CLASSIFICATION OF EARTH-MOON TRANSITS

By

Gary P. Herring

ASTRODYNAMICS BRANCH
ASTRODYNAMIC AND GUIDANCE THEORY DIVISION
AERO-ASTRODYNAMICS LABORATORY

TABLE OF CONTENTS

	<u>Page</u>
INTRODUCTION	
CHAPTER I. GEOMETRICAL CONSIDERATIONS	
Section 1. Reduction of the n-Body Problem.....	2
Section 2. The Restricted Three-Body Problem and Related Coordinate Systems.....	4
Section 3. Reduction of the Problem to the Basic Class, $C(\tau, \rho_e, \rho_m)$	9
CHAPTER II. THE STRUCTURE OF THE BASIC CLASSES $C(\tau, \rho_e, \rho_m)$	
Section 1. The Numerical Development of a Particular Class.....	11
Section 2. Body Symmetry of the Basic Class.....	15
Section 3. Quantitative Analysis of the Classes $C(T_i, 6555 \text{ km}, 1923 \text{ km}), 60 \leq T_i \leq 96 \text{ Hours}$	16
CHAPTER III. SYSTEMS OF CLASSES $C(T_i, R_{e_s}, R_{m_s})$ CONTAINING ALL TRANSITS IN THE FIELD OF INTEREST	
Section 1. The System $C(T_i, R_e, R_{m_s})$	19
A. Variation of the Lunar Terminal Radius.....	19
B. Development of Injection Loci for Variations in the Lunar Terminal Radius.....	24
Section 2. Lunar Impacts.....	27
Section 3. The System $C(T_i, R_{e_s}, R_m)$	29
A. Variation of the Earth Terminal Radius.....	29
B. Transits Having Perigee Inside the Earth.....	30

TABLE OF CONTENTS (Continued)

	<u>Page</u>
CHAPTER IV. APPLICATIONS	
Section 1. Free-Return Transits.....	31
A. Requirements for Free Return.....	31
B. Symmetric Free-Return Transits.....	32
C. Nonsymmetric Free-Return Transits.....	33
Section 2. Phases of the Moon at Approach and Lighting Conditions for Rendezvous and Impact.....	36
CHAPTER V. TRANSFORMATION FROM THE MEP SYSTEM TO GEOCENTRIC AND SELENOCENTRIC SYSTEMS	
Section 1. Launch Restrictions.....	39
Section 2. Selenographic Arrival Conditions.....	43
References.....	182

DEFINITION OF SYMBOLS

<u>Symbol</u>	<u>Definition</u>
$Az_e, (Az_m)$	azimuth with respect to earth (moon)
C	see page 13, Chapter II, Section 1
$C(\tau, \rho_e, \rho_m)$	the basic class of transits (see Chapter I, Section 3)
$C'(\tau, \rho_e, \rho_m)$	the reflection across the earth-moon polar plane of the class $C(\tau, \rho_e, \rho_m)$ by Miele's theorem
d_{em}	distance between earth and moon
G	universal gravitational constant
i	the inclination of the lunar orbit plane (MEP) to the ecliptic
$I_e, (I_m)$	inclination of a transit defined at the point of closest approach to the earth (moon) (see page 17, Chapter II, Section 3)
L	the geometric mean longitude from the mean equinox of date
MEP	moon-earth plane (the plane containing the motion of the earth and moon)
M_m	mass of the moon
M_e	mass of the earth
R_e	distance from the center of the earth to the space vehicle
R_m	distance from the center of the moon to the space vehicle
T, t	transit time
V	velocity of space vehicle
X_e	position vector of the earth

DEFINITION OF SYMBOLS (Continued)

<u>Symbol</u>	<u>Definition</u>
X_m	position vector of the moon
X	position vector of the space vehicle
$\beta = M_e + M_m$	total mass of the system
$\gamma = [d_{em}^3/G\beta]^{1/2}$	the reciprocal of the mean motion of the earth and moon about the center of mass
Δ	see page 13, Chapter II, Section 1
ϵ	the inclination of the earth equatorial plane to the ecliptic
λ	longitude
$\mu = M_m/\beta$	moon's fraction of the total mass
$1 - \mu = M_e/\beta$	earth's fraction of the total mass
$\xi = X/d_{em}$	the normalized position vector
$\xi' = \dot{X}\gamma/d_{em}$	normalized velocity vector
$\xi'' = \ddot{X}\gamma^2/d_{em}$	normalized acceleration vector
ρ_e	normalized distance from the center of the earth to the perigee of a transit
ρ_m	normalized distance from the center of the moon to the perisel of transit
σ	the vertex phase angle (see page 15, Chapter II, Section 2)
$\tau = t/\gamma$	normalized transit time
φ	latitude
Φ	see page 13, Chapter II, Section 1

DEFINITION OF SYMBOLS (Continued)

<u>Symbol</u>	<u>Definition</u>
Ω	the longitude of the mean ascending node of the lunar orbit on the ecliptic, measured from the mean equinox of date
λ	the mean longitude of the moon, measured in the ecliptic from the mean equinox of date to the mean ascending node of the lunar orbit, and then along the orbit

SUBSCRIPTS

$()_e$	referenced to the earth
$()_m$	referenced to the moon
$()_S$	referenced to a space-fixed coordinate system
$()_s$	denoting an entire system of continuous variations of the indicated parameter
$()_R$	referenced to a rotating coordinate system

DIFFERENTIATION

$$\dot{} = d/dt$$

$$\dot{}' = d/d\tau$$

LIST OF DEFINITIONS

- Azimuth (λ_z) - the angle between the velocity vector and local north
- Corotational - in the direction of the rotation of the system
- Counterrotational - opposite the direction of the rotation of the system
- Earth-Moon Polar Plane - the plane containing the polar axes of the earth and moon (and the line between the earth and moon)
- Free-Return Transit - a ballistic trajectory from the vicinity of the earth which reaches the vicinity of the moon and returns to the vicinity of the earth
- Inclination (I) - the angle between the instantaneous flight plane and the MEP (see page 17, Chapter II, Section 3)
- Latitude (ϕ) - the polar angle of a spherical coordinate system measured from the MEP, positive north and negative south, $-90^\circ \leq \phi \leq +90^\circ$
- Longitude (λ) - the angle in the MEP measured from a reference meridian (for the earth - the point farthest from the moon; for the moon - the point nearest the earth) to the meridian of interest in the direction of rotation of the system, $0 \leq \lambda \leq 360^\circ$
- Perigee - the point of closest approach of a transit to the earth
- Perigee Belt - the annular region containing all possible perigees of any one of the basic classes of transits having fixed transit time, perigee radius and perisel radius
- Perigee Horn - the horn-shaped region containing all possible perigees of the system of classes having fixed transit time and perisel radius
- Perigee Station - a segment of a great circle on which all possible perigees of a given basic class and phase angle ϕ occur

LIST OF DEFINITIONS (Continued)

- Perisel - the point of closest approach of a transit to the moon
- Perisel Belt - the annular region containing all possible perisels of any one of the basic classes of transits having fixed transit time, perigee radius and perisel radius
- Perisel Horn - the horn-shaped region containing all possible perisels of the system of classes having fixed transit time and perigee radius
- Transit - the path of the space vehicle
- Transit time - the time lapsed from some initial point on a transit to some other point on the transit (generally between perigee and perisel)
- Transit, Inbound - a transit from the moon to the earth
- Transit, Outbound - a transit from the earth to the moon
- Vertex Point - the point on the moon (or earth) which is overflown by all transits of a given class having the same Φ_e (or Φ_m)

LIST OF ILLUSTRATIONS

Figure	Title	Page
1.	Sun-Earth-Moon Geometry in 1966-1967.....	46
2.	Solar System in 1960 and 1969.....	47
3.	Earth-Moon Geometry in Oct. 1966.....	48
4.	The Moon-Earth Plane and Barycentric Rotating and Space Fixed Coordinate Systems.....	49
5.	Rotating Body-Centered Coordinate Systems.....	50
6.	MEP-Related Spherical Coordinate Systems.....	51
7.	An Individual Transit is Described by Reference to Its Coordinates at the Point of Nearest Approach to Earth or to Moon.....	52
8.	Sample Transit.....	53
9.	Principle of Reflection on the Moon-Earth Plane.....	54
10.	Principle of Reflection on the Polar Plane.....	55
11.	Principle of Reflection on the Earth-Moon Line.....	56
12.	Quadrants in Rotating Earth-Moon Space.....	57
13.	The Four Transits of a Class that are Embedded in the Earth-Moon Plane.....	58
14.	The Family of Transits that Depart from MEP- Equatorial Perigees in Co-Rotational Direction.....	59
15.	The Family of Transits that Depart from MEP- Equatorial Perigees in Counter-Rotational Direction.....	60
16.	Transits of a Family Pass Through a Region Small Enough as to be Represented by a Point (the term "Vertex" is adopted for this point).....	61
17.	The Pencil of Half Great-Circles Along Which the Search for Transits of the Class is Conducted.....	62

LIST OF ILLUSTRATIONS (Cont'd)

Figure	Title	Page
18.	Structural Behavior of Three Transit-Families Near Earth and Moon.....	63
19.	Locations of Perigees and Perisels of the Class $C(\tau^*, \rho_e^*, \rho_m^*)$ are Restricted to the Annular Regions ('Belts') Shown Here.....	21
20.	Loci of All Possible Perigees for the Classes $C(T_i, 6555 \text{ km}, 1923 \text{ km})$, $T_i = 60, 72, 84$ and 96 hr.....	64
21.	Survey of Arrival Areas at Moon for Transit Classes $C(60 \text{ hr}, 6555 \text{ km}, 1923 \text{ km})$ and $C(72 \text{ hr}, 6555 \text{ km},$ $1923 \text{ km})$	65
22.	Survey of Arrival Areas at Moon for Transit Classes $C(84 \text{ hr}, 6555 \text{ km}, 1923 \text{ km})$ and $C(96 \text{ hr}, 6555 \text{ km},$ $1923 \text{ km})$	66
23.	Transits Reaching Moon on Common Lunar Phase Angle.....	67
24.	The Property of 'Vertexing' is Exhibited at the Earth by Those Transits Whose Perisels are Positioned on a Common Lunar Phase Angle.....	68
25.	Schematic Showing of the Fundamental Relationships Between Vertices at One Body and Belt-Segments at the Other Body.....	69
26.	The (Φ, σ) -Coordinate System with Its Two Fundamental Phase Angles Φ and σ , Determining a Particular Transit System is Shown Here for Earth. A Corresponding Reference System is Defined for the Moon.....	70
27.	Schematics Illustrating the Symmetry Between the Field of Outbound Transits and Return Field.....	71
28.	The Variation of Departure Azimuth Along Various Phase Angles as a Function of the Distance Angle for $C(60 \text{ hr}, 6555 \text{ km}, 1923 \text{ km})$	72
29.	The Variation of Departure Azimuth Along Various Phase Angles as a Function of the Distance Angle for $C(72 \text{ hr}, 6555 \text{ km}, 1923 \text{ km})$	73

LIST OF ILLUSTRATIONS (Cont'd)

Figure	Title	Page
30.	The Variation of Departure Azimuth Along Various Phase Angles as a Function of the Distance Angle for C(84 hr, 6555 km, 1923 km).....	74
31.	The Variation of Departure Azimuth Along Various Phase Angles as a Function of the Distance Angle for C(96 hr, 6555 km, 1923 km).....	75
32.	Velocity Requirements for the Indicated Departure Phase Angles vs the Distance Angle for C(60 hr, 6555 km, 1923 km).....	76
33.	Velocity Requirements for the Indicated Departure Phase Angles vs the Distance Angle for C(72 hr, 6555 km, 1923 km).....	77
34.	Velocity Requirements for the Indicated Departure Phase Angles vs the Distance Angle for C(84 hr, 6555 km, 1923 km).....	78
35.	Velocity Requirements for the Indicated Departure Phase Angles vs the Distance Angle for C(96 hr, 6555 km, 1923 km).....	79
36.	Perigee Velocity vs Earth Phase Angle, Φ_e , for Various Inclinations of the Perisel Conic for the Class C(60 hr, 6555 km, 1923 km).....	80
37.	Perigee Velocity vs Earth Phase Angle, Φ_e , for Various Inclinations of the Perisel Conic for the Class C(72 hr, 6555 km, 1923 km).....	81
38.	Perigee Velocity vs Earth Phase Angle, Φ_e , for Various Inclinations of the Perisel Conic for the Class C(84 hr, 6555 km, 1923 km).....	82
39.	Perigee Velocity vs Earth Phase Angle, Φ_e , for Various Inclinations of the Perisel Conic for the Class C(96 hr, 6555 km, 1923 km).....	83
40.	Typical Loci of Constant Velocity, and of Lunar Arrival Inclination for the Class C(72 hr, 6555 km, 1923 km).....	84

LIST OF ILLUSTRATIONS (Cont'd)

Figure	Title	Page
41.	Azimuth at Perigee vs Phase Angle for C(60 hr, 6555 km, 1923 km).....	85
42.	Azimuth at Perigee vs Phase Angle for C(72 hr, 6555 km, 1923 km).....	86
43.	Azimuth at Perigee vs Phase Angle for C(84 hr, 6555 km, 1923 km).....	87
44.	Azimuth at Perigee vs Phase Angle for C(96 hr, 6555 km, 1923 km).....	88
45.	Lunar Arrival Velocity Corresponding to the Injection Velocities Shown by Fig. 36, C(60 hr, 6555 km, 1923 km).....	89
46.	Lunar Arrival Velocity Corresponding to the Injection Velocities Shown by Fig. 37, C(72 hr, 6555 km, 1923 km).....	90
47.	Lunar Arrival Velocity Corresponding to the Injection Velocities Shown by Fig. 38, C(84 hr, 6555 km, 1923 km).....	91
48.	Lunar Arrival Velocity Corresponding to the Injection Velocities Shown by Fig. 39, C(96 hr, 6555 km, 1923 km).....	92
49.	Perisel Azimuth vs Distance Angle for Various Φ_m for C(72 hr, 6555 km, 1923 km).....	93
50.	Perisel Azimuth vs Δ_m for Various Φ_m for C(96 hr, 6555 km, 1923 km).....	94
51.	Perisel Velocity vs Δ_m with Φ_m and I_e as Parameters, for the Class C(72 hr, 6555 km, 1923 km).....	95
52.	Perisel Velocity vs Δ_m with Φ_m and I_e as Parameters, for the Class C(96 hr, 6555 km, 1923 km).....	96
53.	Perigee Conic Inclination Related to Perisel Velocity and Lunar Phase Angle for the Class C(72 hr, 6555 km, 1923 km).....	97

LIST OF ILLUSTRATIONS (Cont'd)

Figure	Title	Page
54.	Perigee Conic Inclination Related to Perisel Velocity and Lunar Phase Angle for the Class C(96 hr, 6555 km, 1923 km).....	98
55.	Perisel Azimuth vs Lunar Phase Angle for the Class C(72 hr, 6555 km, 1923 km).....	99
56.	Perisel Azimuth vs Lunar Phase Angle for the Class C(96 hr, 6555 km, 1923 km).....	100
57.	Perigee Velocity vs Lunar Phase Angle for Various I_e for C(72 hr, 6555 km, 1923 km).....	101
58.	Perigee Velocity vs Lunar Phase Angle for Various I_e for C(96 hr, 6555 km, 1923 km).....	102
59.	Lunar Departure Belt for C(72 hr, 6555 km, 1923 km) with Loci of Constant Perigee Conic Inclinations.....	103
60.	Lunar Departure Belt for C(96 hr, 6555 km, 1923 km) with Loci of Constant Perigee Conic Inclinations.....	104
61.	Perisel Circles at Various Radii Corresponding to $\phi_e = 0^\circ$	105
62.	The Surface Containing All Possible Perisels Corresponding to $\phi_e = 0^\circ$ from the Class C(T, R_e, R_m).....	106
63.	The Perisel Surface for $\phi_e = 0^\circ$ with Its Line of Vertices.....	107
64.	The Intersection of the Perisel Surface with (a) the MEP and (b) A Polar Plane Containing the Vertex Line.....	108
65.	The Continuation of the Embedded and Polar Transits Past Perisel to the Vertex Line for $\phi_e = 0^\circ$	109
66.	The Continuation of Transits, Having Polar Arrival, Past Perisel to the Vertex for $\phi_e = 90^\circ$	110

LIST OF ILLUSTRATIONS (Cont'd)

Figure	Title	Page
67.	The Continuation of the Embedded and Polar Transits Past Perisel to the Vertex Line for $\Phi_e = 180^\circ$	111
68.	The Perisel Horn Containing All Perisels for the System C(72 hr, 6555 km, R_{mS}), $R_{mS} < 250$ km.....	112
69.	The Perisel Horn for the System C(72 hr, 6555 km, R_{mS}), $R_{mS} < 2500$ km with Its Vertex Cone.....	113
70.	The Intersection of the Perisel and Vertex Locus with the MEP and a Polar Plane Containing C_m for C(72 hr, 6555 km, R_{mS}).....	114
71.	Location of Perigees for Transits from $\Phi_e = 0^\circ$ Belonging to the System C(72 hr, 6555 km, R_{mS}).....	115
72.	Three Families of Transits from $\Phi_e = 0^\circ$ Belonging to the System C(72 hr, 6555 km, R_{mS}).....	23
73.	Location of Perigees for Transits from $\Phi_e = 180^\circ$ Belonging to the System C(72 hr, 6555 km, R_{mS}).....	116
74.	Three Families of Transits from $\Phi_e = 180^\circ$ Belonging to the System C(72 hr, 6555 km, R_{mI}).....	25
75.	Perigee Belts from the System C(72 hr, 6555 km, R_{mS}), $R_m = 1000$ km, 1923 km, and 3000 km.....	117
76.	Projections of Perisel Belts at $R_m = 1000$ km, 1923 km and 3000 km from the System C(72 hr, 6555 km, R_{mS}) Onto a Common Sphere.....	118
77.	Azimuth at Perigee Required Along Various Phase Stations for C(72 hr, 6555 km, R_{mS}) for $R_m = 1000$ km, 1923 km, and 3000 km).....	119
78.	Azimuths Required to Envelop the Moon from Various Phase Stations vs Perisel Radius for the System C(72 hr, 6555 km, R_{mS}).....	120
79.	Perigee Velocity Requirements for Points Along the Given Phase Stations for Perisel Radii of 1000 km, 1923 km, and 3000 km from the Classes C(72 hr, 6555 km, R_{mS}).....	121

LIST OF ILLUSTRATIONS (Cont'd)

Figure	Title	Page
80.	Perigee Azimuth vs Φ_e for Typical Perisel Conic Inclinations for the Class C(72 hr, 6555 km, 1000 km).....	122
81.	Perigee Azimuth vs Φ_e for Typical Perisel Conic Inclinations for the Class C(72 hr, 6555 km, 1923 km).....	123
82.	Perigee Azimuth vs Φ_e for Typical Perisel Conic Inclinations for the Class C(72 hr, 6555 km, 3000 km).....	124
83.	Perigee Velocity Required for Lunar Arrival Inclinations of 30° , 60° , 90° , 120° , and 150° for Perisel Radius of 1000 km, C(72 hr, 6555 km, 1000 km).....	125
84.	Perigee Velocity Required for Lunar Arrival Inclinations of 30° , 60° , 90° , 120° , and 150° for Perisel Radius of C(72 hr, 6555 km, 1923 km).....	126
85.	Perigee Velocity Required for Lunar Arrival Inclinations of 30° , 60° , 90° , 120° , and 150° for Perisel Radius of 3000 km, C(72 hr, 6555 km, 3000 km).....	127
86.	Lunar Arrival Velocity for Various Arrival Inclinations at Perisel Radius of 1000 km, C(72 hr, 6555 km, 1000 km).....	128
87.	Lunar Arrival Velocity for Various Arrival Inclinations at Perisel Radius of 1923 km, C(72 hr, 6555 km, 1923 km).....	129
88.	Lunar Arrival Velocity for Various Arrival Inclinations at Perisel Radius of 3000 km, C(72 hr, 6555 km, 3000 km).....	130
89.	Impact Parameters for Transits from the System C(72 hr, 6555 km, R_{ms}) for $\Phi_e = 0^\circ$ and $I_m =$ (a) 0° , 180° , and (b) 90° , -90°	131
90.	The Continuation of Impact Transits to Their Associated Perisel Circles.....	132

LIST OF ILLUSTRATIONS (Cont'd)

Figure	Title	Page
91.	Circles of Constant Impact Time and Path Angle Associated with Perisel Circles.....	133
92.	Impact Area Defined by a Perisel Radius of 627 km in which Essentially Constant Time and Path Angle May be Obtained.....	134
93.	Areas of Essentially Constant Path Angle and Transit Time at Impact for Perisel Radii 258 km, 627 km, and 1183 km.....	135
94.	Path Angle at Impact Associated with Perisel Radius for the System C(72 hr, 6555 km, R_{mS}).....	136
95.	Transit Time to Impact Associated with Perisel Radius for the System C(72 hr, 6555 km, R_{mS}).....	137
96.	Velocity at Impact for Counter and Co-Rotational Earth Departure, C(72 hr, 6555 km, R_{mS}).....	138
97.	Comparison of Impact and Perisel Velocities for Transits from $\phi_e = 0^\circ$, and 180° for the System C(72 hr, 6555 km, R_{mS}).....	139
98.	Longitude of Impact and Perisel for Transits from $\phi_e = 0^\circ$, and 180° for the System C(72 hr, 6555 km, R_{mS}).....	140
99.	Perigee Velocity Required for the Embedded Transits vs Perisel Radius, C(72 hr, 6555 km, R_{mS}).....	141
100.	Perpendicular Impact Loci at the Lunar Surface for C(T_i , 6555 km, 0).....	142
101.	The Center and the Major and Minor Axis of the Perpendicular Impact Loci Versus Transit Time.....	143
102.	Perigee Loci for Perpendicular Impacts for C(T_i , 6555 km, 0) $T_i = 60, 72, 84,$ and 96 hr.....	144
103.	The Center and the Radius of the Perigee Loci for Perpendicular Impact Versus Transit Time.....	145

LIST OF ILLUSTRATIONS (Cont'd)

Figure	Title	Page
104.	Comparison of the Perturbations in the Shape of the Embedded Transits for Variations in R_e for the System C(72 hr, R_{eS} , 1923 km).....	146
105a.	Relative Positions of Perigee Belts for C(72 hr, R_e , 1923 km).....	147
105b.	Perisel Belts for C(72 hr, R_e , 1923 km).....	148
106.	The Intersection of the Perigee Horn with the MEP for the System C(72 hr, R_{eS} , 1923 km).....	149
107.	The Intersection of the Perigee Horn with a Polar Plane Containing C_e , for the System C(72 hr, R_{eS} , 1923 km).....	150
108.	Longitudes of Intersection of Perisel Belts with the MEP for the System C(72 hr, R_{eS} , 1923 km).....	151
109.	Co-Rotational Transits Having Perigee Inside the Earth for the System C(72 hr, R_{eS} , 1923 km)(Velocity and Path Angle Given at Surface and 185 km Altitude)....	152
110.	Counter-Rotational Transits Having Perigee Inside the Earth, for the System C(72 hr, R_{eS} , 1923 km)(Velocity and Path Angle Given at Surface and 185 km Altitude).....	153
111.	Polar Transits Having Perigee Inside the Earth for the System C(72 hr, R_{eS} , 1923 km)(Velocity and Path Angle Given at Surface and 185 km Altitude)....	154
112.	Schematic of Segments of the Perisel Belts for the Classes C(T^* , 6555 km, R_1^*) and C'(T^* , 6555 km, R_1^*)....	155
113.	The Symmetric Free Return for $\Phi_e = \Phi_e' = 0^\circ$ and $I_m = 180^\circ$ for the Classes C(T^* , 6555 km, R_2^*) and C'(T^* , 6555 km, R_2^*).....	156
114.	The Plane Symmetric Free Return for $\Phi_e = \Phi_e' = 90^\circ$, 270° and Maximum and Minimum I_m for the Classes C(T^* , 6555 km, R_3^*) and C'(T^* , 6555 km, R_3^*).....	157

LIST OF ILLUSTRATIONS (Cont'd)

Figure	Title	Page
115.	The Line Symmetric Free Returns for $\phi_e = 270^\circ$, $\phi_e' = 90^\circ$ and $\phi_e = 90^\circ$, $\phi_e' = 270^\circ$ for the Classes $C(T^*, 6555 \text{ km}, R_4^*)$ and $C'(T^*, 6555 \text{ km}, R_4^*)$	158
116.	The Symmetric Free Return for $\phi_e = \phi_e' = 180^\circ$ and $L_m = 180^\circ$ for the Classes $C(T^*, 6555 \text{ km}, R^*)$	159
117.	The Locus of Free Returns and Their Corresponding Vertex Points (About the MEP) for the Classes $C(T^*, 6555 \text{ km}, R_{ms}^*)$ and $C'(T^*, 6555 \text{ km}, R_{ms}^*)$	160
118.	Perisel Loci for Symmetric Free Returns for the System $C(T_s, 6555 \text{ km}, R_{ms})$, $T_s = 60, 72, 84,$ and 96 hr	161
119.	Near Moon Boundary for Symmetric Free Returns Representing Maximum and Minimum Inclination of Perisel Conic at Any R_m	162
120.	Transit Time and ϕ_e for Maximum Inclination of Perisel Conic for Free Returns in Neighborhood of Moon.....	163
121.	Velocity and Longitude of Perisels in the MEP vs Transit Time for $C(T_s, 6555 \text{ km}, 1923 \text{ km})$ and $C'(T_s, 6555 \text{ km}, 1923 \text{ km})$ for Determination of Free Return Boundaries in the Three Parameters.....	164
122.	Non-Symmetric Free Return Perisel Loci for the Indicated Transit Times (--) and Corresponding Velocity Direction at Perisel (—).....	165
123.	Velocity and Longitude of Perisels in the MEP vs Transit Time for $C(T_s, 6555 \text{ km}, 1000 \text{ km})$ and $C'(T_s, 6555 \text{ km}, 1000 \text{ km})$ for Determination of Free Return Boundaries in the Three Parameters.....	166
124.	Velocity and Longitude of Perisels in the MEP vs Transit Time for $C(T_s, 6555 \text{ km}, 3000 \text{ km})$ and $C'(T_s, 6555 \text{ km}, 3000 \text{ km})$ for Determination of Free Return Boundaries in the Three Parameters.....	167
125.	Earth-Moon-Sun Geometry Referenced to a Coordinate System in the Plane of the Ecliptic.....	168

LIST OF ILLUSTRATIONS (Cont'd)

Figure	Title	Page
126.	Lighting Conditions at Arrival for the Embedded and Polar Transits from $\Phi_e = 0$, and Perisel Belt for $T = 72$ hr for a Particular Earth-Moon-Sun Geometry.....	169
127.	Earth-Moon Geometry Referenced to the Vernal Equinox for Two Times a Month.....	170
128.	An Arbitrary but Typical Position of the True Earth Axis and Equator to the MEP-Reference System Launch Site Locations are Indicated According to Three Different Times of a Day.....	171
129.	Illustrations of the Initial and Last Timepoints of the Period at Which a Full Coverage of the Vertex Locus by Two-Dimensional Trajectories can be Accomplished.....	172
130.	Illustration of the Second Period for Which Two-Dimensional Flights from the Launch Site Allow Full Coverage of the Vertex Locus. These Flights Take a Longer Central Angle Before Reaching the Vertex Than Those of Fig. 129.....	173
131.	The Two Sections Encompassing the Departure Directions for Which Two-Dimensional Flights from Launch to Transit are Feasible at the Particular Day Chosen.....	174
132.	Examples of a Trajectory with Two Launch Opportunities (T_A and T_C) and of One Launched Due East Allowing Only One Launch Opportunity (T_B).....	175
133.	Precession of Certain Orbit Planes and the Earth-Moon Line, Exhibited for Approximately Four Days Between Launch and Injection Into Lunar Orbit.....	176
134.	The Relationship of the LNL (Lunar-Nodal-Line) Coordinate System to the Earth at Two Times of a Month.....	177
135.	Co- and Counter-Rotational Arrival Geometry for Transits from C(T, R_e, R_m) Which Pass Over a Common Point on the Lunar Surface.....	178

LIST OF ILLUSTRATIONS (Concluded)

Figure	Title	Page
136.	The Earth Launch Sectors Reduced by Requirement that the Transits Pass Over a Given Point on the Lunar Surface.....	179
137.	The Lunar Arrival Sectors as Reduced by Launch Restrictions on Azimuth, the Time of Launch, and the Launch Side.....	180
138.	An Indication of the Movement of the Sectors for Lunar Approach as Time Increases ($\tau_1 < \tau_2$).....	181

TECHNICAL MEMORANDUM X-53151

A COMPREHENSIVE ASTRODYNAMIC EXPOSITION AND CLASSIFICATION OF EARTH-MOON TRANSITS

SUMMARY

The classical restricted three-body model is used in obtaining an astrodynamical survey and classification of the field of trajectories (traveling in both directions) between the earth and the moon.

The space-fixed equations of motion are normalized and transformed to a rotating system. The classification accomplished in this rotating system is geometrical and is based on the time of travel from perigee to perisel (or perisel to perigee) and the distances of nearest approach to the centers of the earth and the moon. Classes so defined exhibit identical structural characteristics as to shape of feasible regions of perigee and perisel locations and as to the directional behavior of transits near the celestial bodies.

A class-eigen coordinate system is introduced which is intrinsically suited for the approximative solution of the fundamental two-point boundary problem of earth-moon transits.

The resulting classes are applied to the determination of regions of existence of free-return transits (both symmetrical and asymmetrical) and to the determination of lighting conditions at lunar arrival for both impact and "fly-by" transits.

The modes of transition from this system to the geographic and selenographic systems are exemplified in discussing the problems of launch from the Atlantic Missile Range into a lunar transit under general mission constraints at launch and lunar arrival.

INTRODUCTION

The concentration on the Apollo project in this country has placed demands on certain segments of the scientific community for more complete and comprehensive understanding of many astrodynamic problems. Prominent among them is an understanding of the field of transits in earth-moon space. Because of the nature of the Apollo mission, it is mandatory that this problem be under firm mental control.

The gathering of the body of knowledge necessary for mental control of the field of earth-moon transits should be conducted to meet a dual purpose. Firstly, it should aim for simplicity of presentation to promote understanding and retention of concepts. Secondly, it should be of a form which can be used by any member of the scientific community who should have need for such information in his work. The mode of development and presentation of the survey of earth-moon transits presented herein is an attempt at satisfying this two-fold objective.

In the approach pursued to meet our study objectives, the Classical Restricted Three-Body Problem is used, which yields a good approximation of the physical system. In presenting the material generated from this mathematical model, geometrical and topological concepts are used rather than the conventional graphs and tabulated data.

It is felt that this approach meets the study objectives; i.e., it results in easily retainable mental concepts which can be applied directly by the scientist involved in the analysis of earth-moon transits.

CHAPTER I. GEOMETRICAL CONSIDERATIONS

Section 1. Reduction of the n-Body Problem

The environment in which an Apollo spacecraft must operate is a dynamical system, classically referred to as the n-body system. In this system each body operates in an inverse gravity field, attracting and being attracted by every body within the system. The forces of attraction are dependent upon the relative sizes and distances between bodies. To compute transits with complete accuracy in earth-moon space, which is only a small portion of the n-body system, the forces exerted by all bodies need to be considered. This, however, is not necessary because some of the bodies exert forces too small to be within the scope of present computer techniques. Thus, the earth, moon and sun would be the bodies of major concern. The relative geometry of the physical system, having primary influence on transits in earth-moon space, is described in the following.

The motion of the center of mass of the earth-moon system about the sun takes place in a plane referred to as the ecliptic. This plane provides a convenient reference from which a brief description of earth-moon-sun geometry can be constructed. As the earth orbits the sun, it rotates about an axis inclined by some 23.4° to the pole of the ecliptic. The earth equator, being orthogonal to its pole, has the same 23.4° inclination with respect to the ecliptic. There is also a very slow motion or precession of the equatorial plane of the earth, with a cycle of some 26,000 years.

Next, the plane of the moon's motion about the earth describes a varying angle of about 5.15° with respect to the ecliptic. This geometry is depicted in Figure 1 where a yearly cycle (1966-67) is illustrated. It may be pointed out that the lunar orbit plane precesses in space at a rate of one cycle per 18.6 years (or 19.3° per year). When comparing this plane with the plane of the earth's equator, and considering the precessional motion, there results a variation in their relative inclinations between 18.5 and 28.5 degrees. The two limiting cases of this geometry are schematically shown in their 1960 and 1969 orientation on Figure 2.

With reference to the 1969 geometry in Figure 2, another plane of interest is that of the lunar equator, which has a constant inclination of about 1.5° with respect to the ecliptic. According to one of the laws of Cassini, the pole of the ecliptic, the pole of the lunar plane of motion, and the pole of the lunar rotation lie in one great circle. Thus, there is a resultant constant inclination of about 6.7 degrees between the lunar equator plane and the lunar plane of motion. The geometry for the lunar equator during October 1966 is shown in Figure 3 as well as the varying distance of the moon in its elliptic orbit.

The motions described above are the ones of major influence upon earth-moon transits; however, included among them are certain conditions which render a clear analysis somewhat difficult to achieve. A general survey of the field of earth-moon transits requires the development of a model which is applicable for any instant of time. Therefore, the following additional reductions are made to achieve this end.

First, for the duration of a given transit, the moon may be restricted to travel on a circular path around the earth rather than its conventional elliptic path. Secondly, the effect of the sun may be neglected without much sacrifice of realism because the major influence on earth-moon transits is due to these (earth-moon) two bodies. Thirdly, a coordinate system, referenced to the plane of the lunar orbit about the earth and the earth-moon line, may be used so that the transits are independent of the varying inclination between the earth and lunar equatorial planes. In addition, the proper selection of a coordinate system for computation makes it unnecessary to generate information for varying distance between earth and moon.

A trajectory computed in such a system, where the equations of motion are independent of earth-moon distance, is unique and valid under the proper transformation for any assumed earth-moon distance.

The reduction and coordinate systems are made clearer by the developments which follow in the next section.

Section 2. The Restricted Three-Body Problem and Related Coordinate Systems

As suggested in the previous section, for short periods of time within any month of reference in the ephemeris, the earth and moon may be considered to move, separated by a constant distance, in a common plane, describing circles about their center of mass (the barycenter). The motion of a massless space vehicle in such a system is described by the equations of motion of the classical restricted three-body problem.

Two Cartesian coordinate systems are chosen for representation of the vehicle's motion in this model: space fixed and rotating. Both systems have their origins at the center of mass. At some initial time, the space-fixed system has its positive x-axis passing from the center of the earth, through the barycenter, to the center of the moon; the z-axis is the axis of rotation of the system; and the y-axis is such that the system is right-handed. The rotating system has the same definition as the space-fixed system at the initial time, but rotates about the z-axis with an angular velocity equal to that of the earth-moon system. (In this system, the earth and moon remain on the x-axis at all times.) These systems are shown by Figure 4 for the initial time, $t = 0$, and at a later time, $t = \Delta t$, with the subscripts "S" and "R" denoting "space fixed" and "rotating."

In the space-fixed coordinate system, the equations of motion may be written

$$\ddot{\mathbf{X}} = G \left(\frac{M_e}{R_e^3} (\mathbf{X}_e - \mathbf{X}) + \frac{M_m}{R_m^3} (\mathbf{X}_m - \mathbf{X}) \right) \quad (1)$$

where

$$\mathbf{X} = \begin{bmatrix} x_S \\ y_S \\ z_S \end{bmatrix},$$

\mathbf{X}_e is the position vector of the earth,

\mathbf{X}_m is the position vector of the moon,

X is the position vector of the space vehicle,

$$R_e = |X_e - X|,$$

and

$$R_m = |X_m - X|.$$

As previously indicated, by proper selection of the coordinate system for computation, the equations of motion become independent of d_{em} . The obvious advantage of this is that a trajectory computed in such a system may be transformed into a corresponding trajectory for every value of d_{em} . This is accomplished by normalization of (1) as follows [7]: Let

$$X = d_{em}\xi, \quad (2)$$

where ξ is the normalized position vector. Let

$$M_e + M_m = \beta, \quad (3a)$$

so that

$$1 - \mu = \frac{M_e}{\beta}, \quad \mu = \frac{M_m}{\beta} \quad (3b)$$

are the earth's and moon's fraction of the total mass. Then

$$M_e = \beta(1 - \mu), \quad M_m = \beta\mu. \quad (3c)$$

Let

$$t = \gamma\tau, \quad (4)$$

τ is the normalized time variable and γ is a constant. From equations (2), (3), and (4), we see that

$$X(t) = X(\gamma\tau) = X^*(t)$$

so that

$$\dot{X} = \frac{dX}{d\tau} \frac{d\tau}{dt} = X^{*'} \frac{1}{\gamma}, \quad (5)$$

and likewise,

$$\ddot{X} = X^{*''} \frac{1}{\gamma^2}. \quad (6)$$

Now dropping the * notation and substituting (2) into (5) and (6), we may write

$$\dot{X} = X' \frac{1}{\gamma} = \frac{d_{em}}{\gamma} \xi', \text{ velocity} \quad (7)$$

and

$$\ddot{X} = X'' \frac{1}{\gamma^2} = \frac{d_{em}}{\gamma^2} \xi'', \text{ acceleration.} \quad (8)$$

Substituting (2) and (8) into (1) and factoring β out of the right-hand side, we obtain

$$\begin{aligned} \frac{d_{em}}{\gamma^2} \xi'' &= G\beta \left(\frac{1 - \mu}{d_{em}^3 |\xi_e - \xi|^3} d_{em} (\xi_e - \xi) + \frac{\mu}{d_{em}^3 |\xi_m - \xi|^3} d_{em} (\xi_m - \xi) \right) \\ &= \frac{G\beta}{d_{em}^2} \left((1 - \mu) \frac{\xi_e - \xi}{|\xi_e - \xi|^3} + \mu \frac{\xi_m - \xi}{|\xi_m - \xi|^3} \right). \end{aligned} \quad (9)$$

The normalization is now accomplished by setting

$$\frac{d_{em}^3}{G\beta\gamma^2} = 1,$$

so that

$$\gamma = \left(\frac{d_{em}^3}{G\beta} \right)^{1/2}. \quad (10)$$

Therefore, the equations of motion are expressed in the normalized system as

$$\xi'' = (1 - \mu) \frac{\xi_e - \xi}{|\xi_e - \xi|^3} + \mu \frac{\xi_m - \xi}{|\xi_m - \xi|^3}. \quad (11)$$

For engineering application, the trajectories calculated in this normalized system may be transformed point for point to the corresponding trajectory for any specific d_{em} by

$$t = \gamma\tau, \quad (4)$$

$$X = d_{em} \xi, \quad (2)$$

$$\dot{X} = \frac{d_{em}}{\gamma} \xi', \quad (7)$$

and

$$\ddot{X} = \frac{d_{em}}{\gamma^2} \xi''. \quad (8)$$

The equations of motion for the rotating normalized coordinate system are written

$$\xi'' = \begin{bmatrix} \xi_1 - 2\dot{\xi}_2 \\ \xi_2 - 2\dot{\xi}_1 \\ 0 \end{bmatrix} + (1 - \mu) \frac{\xi_e - \xi}{|\xi_e - \xi|^3} + \mu \frac{\xi_m - \xi}{|\xi_m - \xi|^3},$$

where ξ in this case refers to the vectors expressed in the rotating coordinate system, and ξ_i is the i th component of ξ . The same transformations, (4), (2), (7), and (8), may be applied to the position, velocity, and acceleration expressed in this system. (In general, the information presented in the following chapters will be in the rotating system.)

To avoid confusion, ξ_1 , ξ_2 , and ξ_3 will now be replaced by x , y , and z , respectively, and the subscript "R" will denote the rotating system and "S" the space-fixed system. The subscript "e" and "m" will denote earth and moon. In the space-fixed system, $z_{S_e} = z_{S_m} = 0$, and in the rotating system, $y_{R_e} = z_{R_e} = y_{R_m} = z_{R_m} = 0$, for all time, (t) .

For the purpose of presentation of the results, four additional coordinate systems are needed. Two of these systems are Cartesian and parallel to the rotating system, the only difference being the location of the origin. For one, the origin is fixed at the center of the earth, and for the other, at the center of the moon (Figure 5).

The other two are spherical coordinate systems, fixed in either the earth-centered or the moon-centered rotating system. These systems are defined as follows: On the earth and the moon, equatorial planes are defined as the intersections of the moon-earth travel plane (designated as the MEP) with the bodies. MEP-poles are perpendicular to the MEP through the centers of the bodies with the north direction along the positive direction of the axis of rotation of the system. On both bodies, the MEP-latitude (φ) is defined in consistency with the definition of MEP-equators and MEP-poles, positive latitudes measured north through 90 degrees and negative, south through -90 degrees. MEP-longitudes (λ) are measured by great half-circles from pole to pole, the zero reference at the moon being that half-circle nearest the earth, and the zero reference at the earth being that half-circle farthest from the moon. The longitude is defined eastward (the direction of rotation of the system) through 360 degrees. These systems are shown by Figure 6. Within any of these coordinate systems, transits are identified, for the purpose of this study, by reference to their six state variables, in position and velocity, at the points of nearest approach to the center of the earth and the moon. These points are called perigee and periselenium (for brevity, "perisel"). Alternately, the terms "departure" and "arrival" or collectively "terminals" are used (Figure 7).

Section 3. Reduction of the Problem to the Basic Class $C(\tau, \rho_e, \rho_m)$

The continuing effort to reduce the problem to its fundamentals is realized by using what is referred to as a basic class. This basic class possesses geometrical features which are well suited for mental control of the problem. Before defining the basic class, it is convenient to discuss a theorem which proves helpful in the problem.

Quoting from Reference 1: "The Theorem of Image Trajectories states that if a trajectory is physically possible in the earth-moon space,¹ three image trajectories are also physically possible:

- (a) The image with respect to the plane which contains the earth-moon axis and is perpendicular to the axis of rotation of the earth-moon system.²
- (b) The image with respect to the plane which contains the earth-moon axis and the axis of rotation of the earth-moon system.³
- (c) The image with respect to the earth-moon axis.⁴

The first of these image trajectories must be flown in the same sense as that of the basic trajectory, while the other two must be flown in the opposite sense." It should be emphasized that these trajectories are exact images of each other in all components of position for arbitrarily large periods of time; i.e., every point of a given trajectory, and therefore any trajectory point, has exactly three unique images.

Author's Notes:

¹Such a trajectory is depicted in Figure 8.

²The image of the sample trajectory as reflected across the MEP, Figure 9.

³The image of the sample trajectory as reflected across the polar plane, Figure 10.

⁴The image of the sample trajectory as reflected across the earth-moon line (or a composite of the reflections (a) and (b)), Figure 11.

By taking advantage of this theorem, the magnitude of the problem is reduced as follows.

Consider the earth-moon space to be divided into four quadrants by the MEP and the polar plane containing the earth-moon-line and the polar axis. Let the position vector X_R be denoted by the ordered 3-tuple $X_R = (x, y, z)$. Then, for positive or negative x , y , and z , Quadrant I contains all those points $X = (\pm, -, +)$, Quadrant II contains the points $X = (\pm, +, +)$, Quadrant III contains the points $X = (\pm, +, -)$, and Quadrant IV contains the points $X = (\pm, -, -)$. This quadrant definition is illustrated in Figure 11.

Now, referring to the theorem and Figure 12, by (a), every transit having a perigee in Quadrant IV has an image transit (flown in the same sense) with perigee in Quadrant I. Likewise, by (b), every transit having a perigee in Quadrant II has an image transit (flown in the opposite sense) with a perigee in Quadrant I; and by (c), every transit having a perigee in Quadrant III has an image transit (flown in the opposite sense) with a perigee in Quadrant I. Thus, it is necessary to investigate only those transits having a perigee in Quadrant I, since all other transits may be obtained from these by simple reflections as defined by the Theorem of Images. The images of transits with perigee occurring in one of the two planes follow trivially from the points along the transit in the neighborhood of perigee. To include these transits, Quadrant I is defined to include that half of the polar plane in which $z_R \geq 0$ and that half of the MEP in which $y_R \leq 0$.

In the investigation of these transits, consideration of absolute time for departure or arrival has been made unnecessary by the use of the restricted three-body model, in that the terminals are referenced position-wise to the MEP system. However, the time, τ , spent between terminals (referred to as "transit time") remains as an important parameter.

By using the spherical coordinate systems described in the previous section, one of the six state variables, flight path angle (ϑ) is fixed by definition of the terminals, and is equal to 90 degrees (or horizontal) at both end-points.

Now, arbitrarily fixing the terminal radii and the transit time, a basic class $C(\tau, \rho_e, \rho_m)$ of transits is defined, where τ = transit time, ρ_e = perigee radius, and ρ_m = perisel radius. That is, all transits which have perigee on a sphere about the earth of radius ρ_e , perisel on a sphere of radius ρ_m about the moon, and transit time, τ , are grouped into one class designated by $C(\tau, \rho_e, \rho_m)$.

The variables on this class are longitude at perigee (λ_e) and perisel (λ_m), latitude at perigee (ϕ_e) and perisel (ϕ_m), azimuth at perigee (Az_e) and perisel (Az_m), and velocity magnitude at perigee (V_e) and perisel (V_m).

The numerical development and application of these classes are the subjects of the following chapters.

CHAPTER II. THE STRUCTURE OF THE BASIC CLASSES $C(\tau, \rho_e, \rho_m)$

Section 1. The Numerical Development of a Particular Class

The attempt to collect individual transits into a hierarchy of families of subclasses defining a class of particular order, which satisfies the definition of $C(\tau, \rho_e, \rho_m)$, demands a search for characteristics common to several transits. Since all classes, $C(\tau, \rho_e, \rho_m)$, will be shown to have topologically identical structure, it will suffice to analyze only one particular class in detail. The class

$$C(.68902785, .17022437 \times 10^{-2}, .49937675 \times 10^{-3})$$

is chosen for illustration. (It should be remembered that $\tau = .68902785$, $\rho_e = .17022437 \times 10^{-2}$, and $\rho_m = .49937675 \times 10^{-3}$ are dimensionless quantities as expressed in the normalized coordinate systems of Chapter I, Section 2. For convenience in notation, let $\tau = .68902785 = \tau^*$, $\rho_e = .17022437 \times 10^{-2} = \rho_e^*$, and $\rho_m = .49937675 \times 10^{-3} = \rho_m^*$.)

As an arbitrary starting point in the determination of characteristics common to several transits, a numerical search is made for all transits satisfying the class restrictions and fully embedded in the earth-moon plane. Four such transits evolve as shown in Figure 13. They can be paired according to common departure directions, two leaving the earth corotationally, in congruence to the system rotation, and two counterrotationally. Each pair entwines the moon.

To enlarge this small family, the numerical search is extended to include all such transits of the chosen class having their departure from the MEP. The results of this search are indicative of the characteristics sought. Two well defined families emerge. The two families, consisting of an infinite number of transits, leave the earth in opposite directions as depicted on Figures 14 and 15. The points from which the transits of these two families depart define two small arcs (referred to as perigee stations) in the MEP of less than 1.2 degrees, measured by earth central angle. The velocity vectors have a largest relative

azimuth from the MEP of ± 5.4 degrees. The two families define tubular surfaces of transits which envelop the moon densely. The perisel locations form an almost circular pattern (with geometric center in the MEP) for each family. These transits, if continued past their perisel points, cross through a small volume above the center of their perisel circle (as observed from the center of the moon). This is illustrated by Figure 16. The small volume within which the transits have common crossings is defined to be the vertex of the family. It should be emphasized here that these two families contain all possible transits which belong to the class $C(\tau^*, \rho_e^*, \rho_m^*)$ and have perigees in the MEP.

Consideration of these two families suggests an investigation of the existence of transits which pass over one of the earth's poles and one of the moon's poles. A numerical search yields only four such transits, all of which depart from the same longitude. Two depart from northern latitudes, passing over the north pole of the earth, one of which passes over the lunar south pole, and the other passing over the lunar north pole. The other two transits are exact reflections of the first two about the MEP. As in the previous case, it is found that the totality of transits, belonging to $C(\tau^*, \rho_e^*, \rho_m^*)$, which depart from this longitude, form two well defined families, one being the image of the other about the MEP. These two families have every structural feature ascribed to the first families discussed; that is,

- (a) transits depart from small continuous arcs of great circles, with small relative azimuths for a given arc,
- (b) transits from a given arc form a dense family, defining a tubular surface which envelopes the moon,
- (c) the perisel locations for a given family form a circular pattern,
- (d) the transits of a given family have common crossings in a "vertex point," which projects to the center of the circular perisel pattern.

These characteristics indicate the existence of a somewhat annular region of arcs of great circles (perigee stations) from which similar unique families or subclasses depart. Therefore, a new coordinate system is introduced to expedite the search process for the generation of other subclasses.

A pencil of great circles of radius ρ_e^* is oriented such that one of the intersection points (C_e) is in the MEP, and at the longitude of the "polar family" just discussed. The line containing C_e and the center of the earth is referred to as the centerline. This pencil is shown on Figure 17. It is considered as consisting of great half-circles, each half-circle being defined by the dihedral angle ϕ_e (referred to as "earth phase angle") measured counterclockwise from the MEP to the plane of the half-circle, through 360° (or equivalently, through $\pm 180^\circ$).

Any point on the spherical surface can now be defined by two coordinates: (a) the particular half-circle on which the point lies, and (b) the "distance angle," Δ_e , measured at the center of the earth, from C_e along the half-circle to the point.

Using this coordinate system, it is found that on each half-circle there is only a small arc from which departures are possible for transits belonging to the class $C(\tau^*, \rho_e^*, \rho_m^*)$. Every subclass found in this manner exhibits the characteristics ascribed to the first subclasses mentioned. The departure and arrival structure of three of those subclasses, identified by their respective phase angles, ϕ_e , of 0° , 90° , and 180° , is illustrated by Figure 18. The corresponding vertices are also identified by reference to ϕ_e .

The somewhat annular region (or belt) containing all possible departure positions for transits of this class is given at the left of Figure 19. The diameter of this region is about 15° earth's central angle, and its width varies from less than 1° in the west to about 1.2° on the east. At the moon, the area containing all possible perisel circles for the class $C(\tau^*, \rho_e^*, \rho_m^*)$ is also an annular belt (Figure 19 on right). Its diameter is near 120° moon's central angle, with the belt width varying from about 20° in the west to only a few degrees in the east. Representative perisel circles and vertices are exhibited within the belt, referred to by their earth phase angles ϕ_e . All vertices for this class lie on the indicated locus of vertices.

Departures from $0^\circ < \phi_e < 180^\circ$ produce families with vertex points below the MEP, and symmetrically, those from $180^\circ < \phi_e < 360^\circ$ produce vertex points above the MEP. This symmetry follows from application of the theorem of images, for example, the families from $0^\circ < \phi_e < 180^\circ$; i.e., the families departing from below the MEP are exact reflections of those departing above the MEP.

Within the field of interest for the Apollo project, all classes $C(\tau, \rho_e, \rho_m)$ may be generated numerically in the same manner as $C(\tau^*, \rho_e^*, \rho_m^*)$, and the same basic features will be found for each class.

There are structural relationships between these basic classes which may be used in the determination of classes of higher order. It is through the use of these higher order classes that a conceptual control of the entire field of transits is gained. So that the engineer may gain a better "feel" for the classifications, the expansion to higher order classes is deferred to later chapters in which the material will be presented as transformed for a specific d_{em} . This will not restrict the use of the data presented as might be expected, for the inverse transformation is easily obtained from the material presented in Chapter I, Section 2. That is, the inverse transformation, applied to data given for a specific d_{em} will yield data in the normalized coordinate system, which in turn may be transformed to any d_{em} .

The classes of higher order will be developed from systems of basic classes having common transit times. For this reason a brief comparison of specific classes having $.57418988 \leq \tau_i \leq .91870380$ will be given in Section 3 of this chapter to emphasize the shapes and relationship between the departure and arrival areas (trajectories from these classes, $C(\tau_i, \rho_e^*, \rho_m^*)$, which when transformed, according to Chapter I, Section 2, to $d_{em} = \text{mean distance } (385,080 \text{ km})^1$ belong to $C(T_i, 6555 \text{ km}, 1923 \text{ km})$ where $60 \leq T_i \leq 96$ hours). This transit time region is of interest for Apollo type missions. Classes from this region will be compared at four points, $\tau = .57418988, .68902785, .80386583, \text{ and } .91870380$ (corresponding to $T = 60$ hours, 72 hours, 84 hours, and 96 hours). The method of development described for $\tau = \tau^*$ is identical for the other three transit times.

Figure 20 shows the areas of all possible perigees corresponding to these four transit times. As transit time increases, the perigee area shifts continuously to larger MEP-longitudes, and the over-all diameter of the annular areas continuously decreases with increasing transit time.

The corresponding perisel belts shift to smaller lunar longitudes as shown by Figures 21 and 22. A detailed quantitative analysis of these four classes is given in Section of this chapter.

¹All results presented for a specific d_{em} will be for $d_{em} = 385,080 \text{ km}$, approximately the mean earth-moon distance, and $\gamma = 104.49505$ hours.

Section 2. Body-Symmetry of the Basic Class

The similarity in the shape of perigee and perisel belts suggests a symmetry in their structural features. Investigations for this symmetry yield a functional relationship between the terminal conditions of arbitrary transits. This functional relationship is necessary for the solution of the question typical for Apollo flights: What are the departure conditions for a transit that is to approach a preselected landing point on the moon in a preselected direction? Or a more fundamental question: In a given class, does a transit exist that accomplishes certain approach conditions?

To this end, the coordinate system used for generation of the basic class is applied to the transits arriving at the moon. A pencil of great half-circles of radius R_m is positioned at the moon such that one of its intersections is located in the MEP at the longitude of the perisels for the polar-earth-polar-moon transits. The lunar phase angle, Φ_m , and distance angle, Δ_{ms} , are defined as in the previous case.

Transits that reach their perisels on a common lunar phase angle (Figure 23) show the following characteristics when traced back to earth: (a) They envelop the earth densely. (b) They have an almost circular perigee locus. (c) When followed further back, beyond their perigees, they pass through a small volume representable by a vertex (Figure 24). How this "body-symmetrical" behavior of the class structural features furnishes a key to the terminal correspondence problem is shown in the following.

Figure 25 states (a) that transits emanating from a common vertex at the earth have a common lunar phase angle, Φ_m ; and (b) that transits with a common earth phase angle Φ_e have a common vertex at the moon. This relationship may be restated: There exists a one-to-one mapping of vertex points at one body into station segments of the other body. Since now the identification of its vertex and its station segment defines a transit at one body, the knowledge of this transit's geometry at the other body may be determined by a mapping function. A very simple function may be obtained by introducing a vertex-phase angle, σ , defined in the same way as ϕ , with C_e (or C_m) as the pencil of the great half-circles through the points on the vertex locus.

If reference is taken to the pencils of great half-circles introduced previously at earth and moon, and if the locations of vertices and belt-stations are measured by their respective phase angles (Figure 26), a rule of quadrants holds which says that quadrants map negatively. To elaborate on this, consider one example of a given transit for which the phase angle of the vertex on earth, σ_e , is between 0 and 90 degrees, and

the perigee phase angle, ϕ_e , lies between 90 and 180 degrees. This transit will arrive at the moon such that its perisel phase angle, ϕ_m , is between 0 and -90 degrees, and its vertex phase angle at the moon, σ_m , is between -90 and -180 degrees. Thus, the functional relationship between terminals may be restated as

$$Q(\sigma_e) = -Q(\phi_m) \quad \text{and} \quad Q(\sigma_m) = -Q(\phi_e),$$

where the symbol $Q()$ reads "quadrant of."

Although a quantitative discussion will be omitted in favor of the more relevant conceptual control of the problem and the general classification of transits, the uniqueness of transits defined by these phase angles deserves special emphasis. It will suffice to strongly emphasize the following:

In the planning of specific missions it should be remembered that once a class $C(T, R_e, R_m)$ has been chosen, (a) selecting both σ and ϕ at one body defines a unique transit, and (b) selecting either σ at each body or ϕ at each body defines a unique transit.

Section 3. Quantitative Analysis of the Classes $C(T_i, 6555 \text{ km}, 1923 \text{ km}), 60 \leq T_i \leq 96 \text{ Hours}$

The basis for the development of the astrodynamical concepts needed for classification of transits in the earth-moon space has been presented thus far within a geometrical framework and a normalized coordinate system. Although this is sufficient for the purposes of this study, the remainder of the development will be presented as transformed for $d_{em} = 385,080 \text{ km}$ along with substantiating graphical representations of the more interesting parameters.

The perigee and perisel areas defined by the classes $C(\tau_i, \rho_e^*, \rho_m^*)$ in the first section of this chapter are not altered by the transformation to $C(T_i, 6555 \text{ km}, 1923 \text{ km})$, since these areas were given in a spherical coordinate system. A quantitative analysis of these classes is furnished by the following series of figures.

By application of Miele's Theorem of Images, terminal belts (and points) and vertex curves can be quantitatively reflected across the polar plane (containing the earth-moon line and the north pole of the system). Also, the phase angle relationships given in Section 2 of this chapter hold quantitatively for both lunar arrival and departure transits. Figure 27 schematically illustrates this reflection principle. Thus, the following information may be interpreted as either earth-moon transits or moon-earth transits. (It should be remembered, that in performing this analysis, the rotating coordinate system is utilized.)

Figures 28, 29, 30, and 31: The variation of earth perigee azimuth along various phase angles is given as a function of the distance angle Δ_e for the transit time classes C(T_i , 6555 km, 1923 km), $T_i = 60, 72, 84, \text{ and } 96$ hours. These graphs show that to every point Δ_e of a perigee station on a given phase angle, there are associated exactly two azimuths, with the exception of the boundary points where the azimuth is unique for the given phase angle. Various inclinations of these transits (at perisel) are indicated on the phase angle loci. Inclination as used in this study is defined as follows:

$$\cos I' = \sin A_z \cos \varphi, \quad 0^\circ \leq I' \leq 180^\circ.$$

If $\dot{z} \gtrless 0$,

$$I = \begin{cases} I' & \text{if } \dot{z} > 0 \\ -I' & \text{if } \dot{z} < 0. \end{cases}$$

If $\dot{z} = 0$,

$$I = \begin{cases} 0 & \text{if } \varphi = 0 \\ -I' & \text{if } \varphi > 0 \\ I' & \text{if } \varphi < 0 \end{cases}$$

where I is the inclination and $0^\circ \leq I \leq 180^\circ$ or $-180^\circ \leq I \leq 0^\circ$. Thus, inclination is defined through 360° instead of the usual definition through 180° and without the usual reference to the ascending node.

This definition is equivalent to the customary one, but allows the numerical isolation of transits having inclinations near the relative minimum and maximum inclinations possible within given classes as pointed out in the following. The perisel (or perigee) conic defines a plane containing the center of the moon (or earth), the perisel (perigee), and the vertex. For any phase angle, there exists a conic which has a relative minimum inclination equal to the latitude of the vertex point, and a conic with maximum inclination equal to 180° minus the latitude of the vertex point. These maximum and minimum inclinations could become important in mission definition, and should be considered in conjunction with the last paragraph of Section 2 of this chapter.

Figures 32, 33, 34, and 35: The injection velocity requirements for the transits indicated by Figures 28 through 31 are given as a function of the distance angle, Δ_e , to points along the given phase angles. The two velocities corresponding to the two azimuths for a given point may be related through the inclination of the perisel conic.

Figures 36, 37, 38 and 39: A representation of the relationships of perigee velocity on the perisel inclination may be obtained by cross plots from Figures 32 through 35, i.e., perigee velocity versus phase angle, with inclination of the lunar arrival plane as a parameter.

Figures 32 through 35 and 36 through 39 may be combined to obtain loci of constant velocity and lunar arrival inclination within the perigee areas for each class C(T_i , 6555 km, 1923 km) such as those given by Figure 40 for $T = 72$ hours. It should be remembered that by Miele's Theorem of Images these loci may be reflected about the x-y plane. The negative arrival inclinations shown here were obtained by this method.

Figures 41, 42, 43, and 44: The azimuth at perigee plotted over Φ_e yields a narrow band very nearly the same width over all Φ_e . The width of this band increases, as indicated, as transit time increases.

Figures 45, 46, 47, and 48: The velocity at perisel for transits which leave the earth with the velocities shown by Figures 36 through 39 are shown as a function of Φ_e . The correspondence between individual transits is made through the parameter inclination of the arrival plane.

For the remaining part of this section, only the classes for $T = 72$ and 96 hours will be discussed. These two classes are sufficient to indicate the variations in the parameters with respect to the lunar phase angle Φ_m , since most of these patterns are similar to the ones just presented.

Figures 49 and 50: The variation of perisel azimuth along various lunar phase angles is given as a function of the distance angle Δ_m for C(72 hr, 6555 km, 1923 km) and C(96 hr, 6555 km, 1923 km).

Figures 51 and 52: The perisel velocities for the transits indicated by Figures 49 and 50 are given as a function of Δ_m . The velocities and azimuths of the two transits having a given perisel in common may be related through Δ_m and the inclination of the perisel conic (constant $|I_m|$ loci are drawn in to aid further cross plotting). For $0 \leq \Phi_m \leq 180^\circ$, the positive I_m are the intersections of the $|I_m|$ loci with the upper part of the Φ_m curves, and the negative I_m are the intersections of the $|I_m|$ loci with the lower part of the Φ_m curves. The dotted lines at each end of the figure are the loci for minimum inclination of the perigee conics. Application of Miele's Theorem of Images to these figures yields the phase angles $180^\circ < \Phi_m < 360^\circ$. For these phase angles, the sign of the inclination of the perigee conic reverses.

Figures 53 and 54: Perigee conic inclination is related to the velocity at perisel and ϕ_m . The positive inclinations shown here may be reflected by the image theorem to obtain their negatives.

Figures 55 and 56: The behavior of the perisel azimuth over ϕ_m is very similar to that at the earth; however, the variation in the width of the azimuth belts is smaller between transit time classes as indicated by these two figures.

Figures 57 and 58: These two figures show the variation of perigee velocity over ϕ_m for various inclinations of the perigee conic. These curves may also be reflected to obtain the negative inclinations.

Figures 59 and 60 illustrate the loci of perisels, corresponding to the perigee conic inclinations of 30° , 60° , 90° , 120° , and 150° , which make up the perisel belts. The belts as shown here represent the lunar injection loci for moon-earth transits. The same figures may be obtained for lunar arrivals by reflection. The shaded area represents the total area of the belts.

CHAPTER III. SYSTEMS OF CLASSES $C(T_i, R_{e_s}, R_{m_s})^1$ CONTAINING ALL TRANSITS IN THE FIELD OF INTEREST

Section 1. The Systems $C(T_i, R_e, R_{m_s})$

A. Variation of the Lunar Terminal Radius

The systems of classes $C(T_i, R_e, R_{m_s})$ are developed by stepwise variations in the element R_m of a basic class $C(T, R_e, R_m)$, for fixed values of T_i within the range of interest. For this system of classes, R_e is held constant and equals 6555 km. To facilitate understanding, the development will be made by expansion of a particular class $C(72 \text{ hr}, 6555 \text{ km}, 1923 \text{ km})$.

¹ The subscript (s) will be used to denote systems of basic classes for which the subscripted parameter, although unique for a specific basic class, varies continuously over the system.

For fixed values of R_m , $0 < R_{m_1} < R_{m_2} < \dots < 1923 \text{ km} < \dots < R_{m_k}$, basic classes are developed by the methods outlined in Chapter II. Since, mathematically, the equations of motion treat the moon as a mass point, the perisel radius R_m may approach zero.² Each of these classes exhibits the structural features attributed to the particular class $C(72 \text{ hr}, 6555 \text{ km}, 1923 \text{ km})$ and have the same centerline, C_m .

The geometrical relationship between these classes is best seen by considering first the relationship between individual perisel circles from each class, for example, those generated from $\phi_e = 0^\circ$ for various values of R_m . Examples of these perisel circles are shown by Figure 61. Such perisel circles exist for every perisel radius in the vicinity of the moon. They form a dense horn-shaped surface associated with the given phase angle (Figure 62). The transits defining these families, if continued beyond the perisel surface, cross through a continuum (or line) of vertices at the center of the surface. Each point of the line is associated with a particular perisel radius (Figure 63).

A graphical representation of the intersections of the surface by two perpendicular planes containing the vertex line (for instance, the MEP and a polar plane) gives a more exact definition of the shape of this surface. Figure 64 (in the MEP) shows the locus of perisel points associated with the embedded transits. The polar plane is the plane of flight at arrival defined by the transits leaving the earth with the largest relative azimuths from the MEP (for each perisel radius) and arriving over the north or south pole of the moon (Figure 64b). Figure 65 shows the continuation of several typical transits through the perisel loci to the vertex points associated with the given perisel radii. The general features of these transits are conserved for all transits in the vicinity of the moon.

Now, investigating all other phase angles, the same general behavior as that discussed above is found for each phase angle. The location of the surfaces generated, their vertex lines, and their cross-sectional diameter at any perisel radius are functions of the departure phase angle. An indication of the relative size and location of these surfaces is found in the information presented in Chapter II (Figure 19)

² The equations of motion have singularities at the centers of the earth and moon. However, there now exists a computation procedure by which limiting radii, including zero, may be studied. Richard F. Arenstorf accomplishes the removal of these singularities simultaneously in his paper, "On the Best Regularization of the Restricted Three-Body Problem," MTP-COMP-63-1.

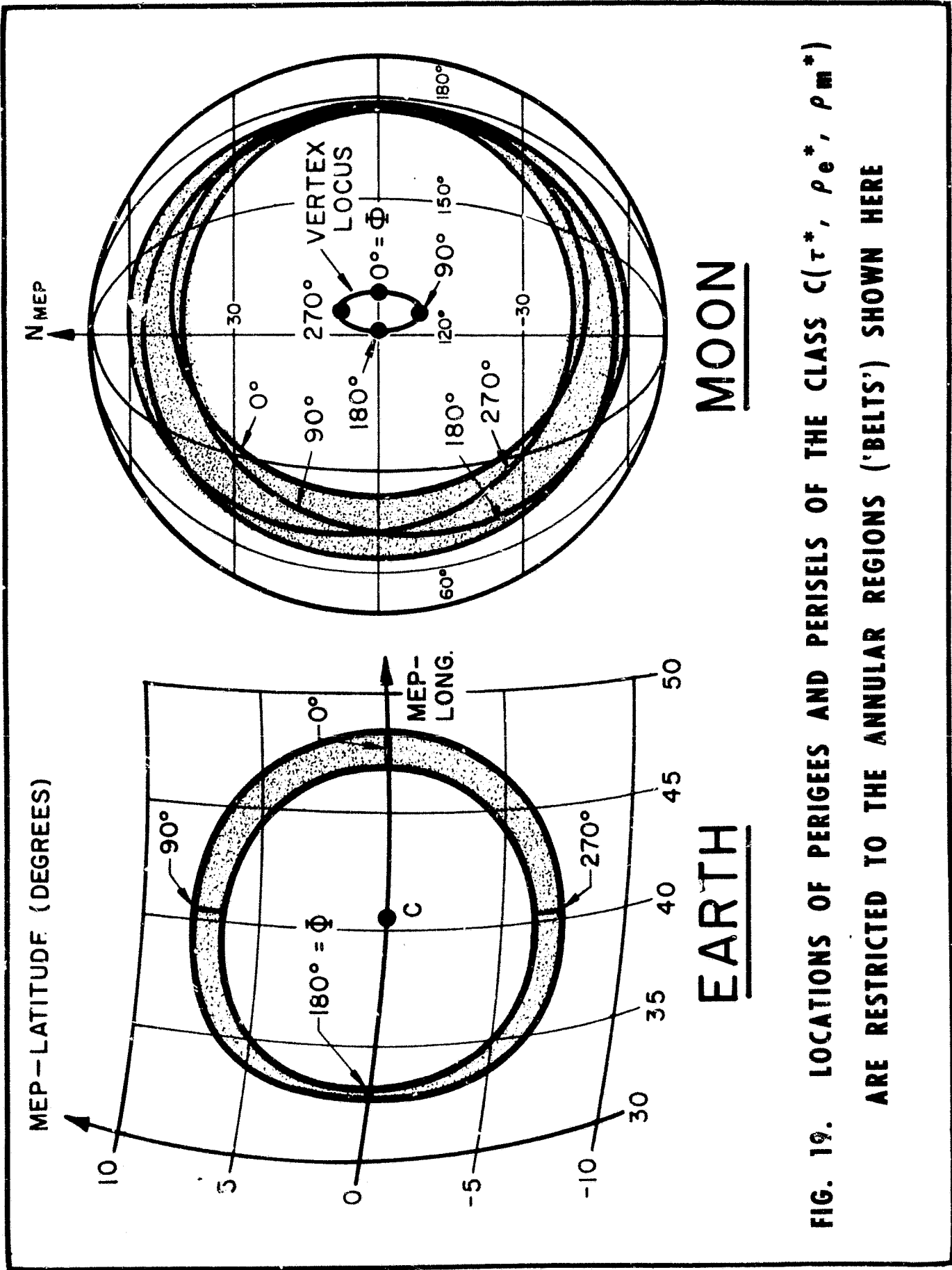


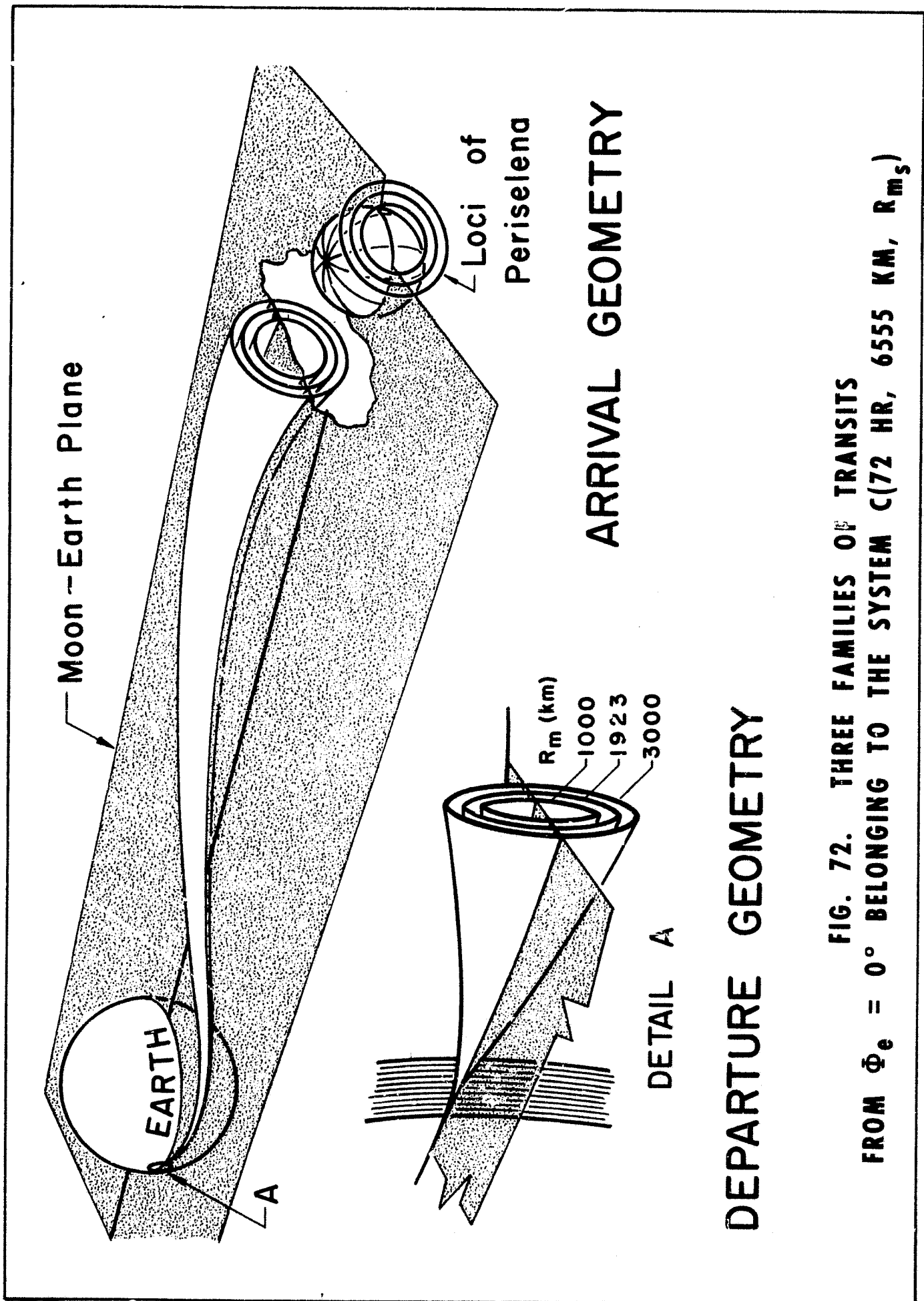
FIG. 19. LOCATIONS OF PERIGEES AND PERISELS OF THE CLASS $C(\tau^*, \rho_e^*, \rho_m^*)$ ARE RESTRICTED TO THE ANNULAR REGIONS ('BELTS') SHOWN HERE

for the class $C(\tau^*, \rho_e^*, \rho_m^*)$ transformed to $C(72 \text{ hr}, 6555 \text{ km}, 1923 \text{ km})$. The perisel circles (perisel radius 1923 km) shown here are elements of the perisel surfaces generated for phase angles of 0° , 90° , 180° , and 270° . The shaded area represents the continuum of perisel circles found at the intersection of a sphere of radius 1923 km with the continuum of perisel surfaces generated from consideration of all possible phase angles, i.e., the perisel locations for $C(72 \text{ hr}, 6555 \text{ km}, 1923 \text{ km})$.

It was noted in Chapter II that, as departure phase angle increases from 0° to 90° , the vertex point associated with the perisel circle at 1923 km moves away from the MEP to a maximum latitude for $\phi_e = 90^\circ$. Likewise, the vertex lines associated with these surfaces move to a maximum latitude (about -9°). The polar plane in which this maximum occurs is shown in Figure 66. A plane containing this vertex line and perpendicular to the polar plane shown would be that plane defined by the transits arriving with the smallest possible relative inclination to the MEP for this phase angle. This inclination is determined by the latitude of the vertex line for a given phase angle (as discussed in Chapter II). The arrival situation for transits leaving from $\phi_e = 270^\circ$ is the image (about the MEP) of that for $\phi_e = 90^\circ$. This image may be obtained by application of Miele's Theorem of Images to the transits leaving from $\phi_e = 90^\circ$.

The moon arrival situation for those transits which depart from the earth with a counterrotational velocity component is topologically the same as for those departing corotationally. Figure 67, analogous to Figure 65, shows the intersections of the perisel surface defined by $\phi_e = 180^\circ$ with (a) the MEP, and (b) with a plane containing the polar arrivals. By comparison of the perisel loci given for phase angles of 0° , 90° , and 180° (Figures 64, 65, and 67), the perisel surfaces, defined as ϕ_e increases from 0° to 180° , are shown to increase in cross-sectional diameter at a given perisel radius, and the vertex lines move to smaller longitudes (as indicated by the perisel circles in Figure 19).

The locus of all such surfaces forms a perisel horn of varying thickness, and generally the same shape as the surfaces of which it is composed (Figure 68). The perisel horn contains all perisels for the system $C(72 \text{ hr}, 6555 \text{ km}, R_{m_s})$. The vertex lines of these surfaces form a smaller cone shaped surface about a line through the center of the horn (Figure 69). This centerline is defined by the line from the center of the moon through ρ_m (discussed in Chapter II). Figure 70 gives a more exact representation of this volume of perisel points. The intersection of the perisel horn and the cone of vertices with the MEP is given in Figure 70 part (a). The boundaries of the area of intersection are practically the loci of perisel points corresponding to the embedded transits from phase angles $\phi_e = 0$ and $\phi_e = 180^\circ$ (shown earlier in Figures 65 and 67). The intersection of the perisel horn with a plane perpendicular to the MEP and containing C_m is shown in Figure 70 part (b).



ARRIVAL GEOMETRY

DEPARTURE GEOMETRY

FIG. 72. THREE FAMILIES OF TRANSITS FROM $\Phi_e = 0^\circ$ BELONGING TO THE SYSTEM C(72 HR, 6555 KM, R_{ms})

In summary, for fixed transit time (72 hours) and perigee altitude (185 km), and a given phase angle, the variation of perisel radius generates a continuum of perisel circles which form a horn-shaped surface (the cross-sectional diameter increasing with perisel radius). The continuation of these transits past the perisel surface defines a line of vertices through the center of the surface. A similar unique perisel surface and line of vertices are found for each earth phase angle ($0^\circ \leq \phi_e \leq 360^\circ$). As all other earth phase angles are considered, a continuum of associated perisel surfaces is constructed which forms a horn-shaped volume containing all possible perisel points belonging to the system C(72 hr, 6555 km, R_{ms}). The locus of the associated vertex lines is a smaller cone-shaped surface about the centerline C_m .

Similar perisel horns are generated by the system of classes for every transit time in the range from 60 to 96 hours. An indication of the shape and location of these systems for other such transit times is given by the basic classes presented in Chapter II for $T_i = 60, 84,$ and 96 hours.

P. Development of Injection Loci for Variations in Lunar Terminal Radius

So that the development of the geometrical properties of earth-moon transits may proceed smoothly, the variations in earth terminal conditions were neglected in the previous section. Now, having developed the general properties of the perisel horn in the vicinity of the moon, the variation in earth parameters required to form the horn will be investigated.

Consider first the continuum of families (corresponding to various perisel radii) resulting from the injection phase angle $\phi_e = 0^\circ$. As discussed previously, these transits all have their injection points in the MEP and result in perisels which form a horn-shaped surface. The perigee stations associated with these families are colinear, but increase in length with perisel radius (Figure 71); and also, for increasing radii, each station and the resulting family contain all those stations and families for smaller perisel radii (Figure 72). A similar situation exists for those families of transits leaving the earth from $\phi_e = 180^\circ$. Again the perigee stations are in the MEP, and these stations increase in length with perisel radius. However, along with an increase in length, the stations for $\phi_e = 180^\circ$ shift toward zero earth longitude as perisel radius increases. In this case, the resulting families do not initially contain those for smaller perisel radii. This is shown graphically in Figure 73 and pictorially in Figure 74.

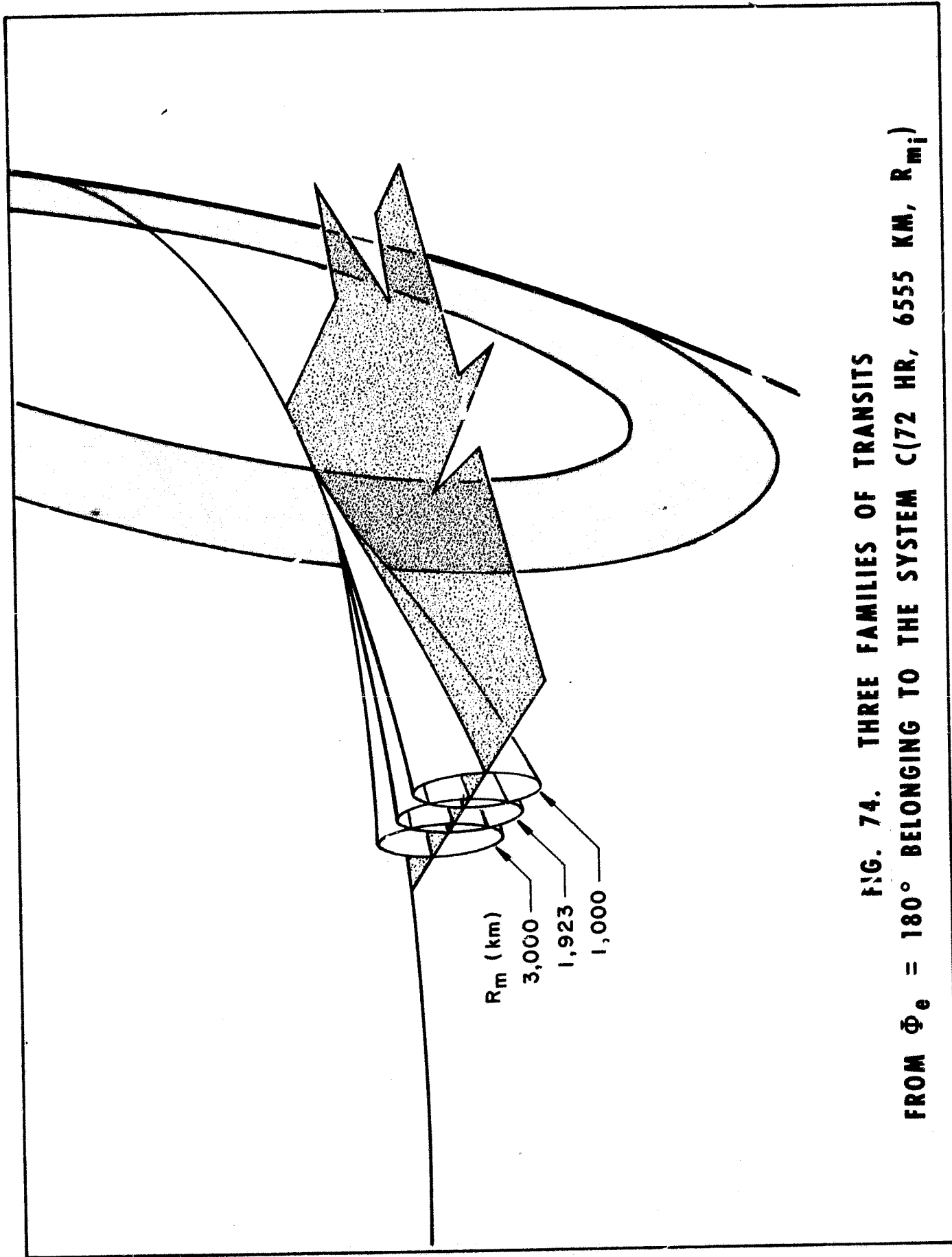


**FIG. 74. THREE FAMILIES OF TRANSITS
FROM $\Phi_e = 180^\circ$ BELONGING TO THE SYSTEM C(72 HR, 6555 KM, R_{m_i})**

In general, the features exhibited for perigee stations at phase angles of 0° and 180° are conserved for all phase angles from 0° to 360° , with those features at $\phi_e = 0^\circ$ being gradually deformed into those for $\phi_e = 180^\circ$, and symmetrically from $\phi_e = 180^\circ$ to $\phi_e = 360^\circ$. In the previous section the intersection of a sphere of radius 1923 km with the perisel horn was shown to be the perisel belt which corresponded to the perigee belt for 72-hour transits discussed in Chapter II. A similar unique perigee belt is formed for every perisel radius by construction of the associated perigee stations for all phase angles. Perigee belts corresponding to perisel radii of 1000 km, 1923 km, and 3000 km are shown by Figure 75. The features discussed above for perigee stations at phase angles of 0° and 180° are perhaps more easily generalized to other phase angles by consideration of this figure. The projections of the resulting perisel belts formed at the intersections of the horn with spheres of radii 1000 km, 1923 km and 3000 km onto a common sphere are given by Figure 76.

For such perigee stations associated with any given phase angle, the range of variation in velocity direction (or azimuth) required for enveloping the moon increases as the length of the station increases (corresponding to increasing perisel radii). An indication of this is given in Figure 77, which shows the azimuth required at each point along the perigee stations associated with the above perisel radii for several phase angles. The coordinates are perigee azimuth and Δ_e , the distance angle from the center, C_e , to the perigee point. By application of Miele's Theorem of Images, $\phi_e = +45^\circ, +90^\circ, \text{ and } +135^\circ$ may be obtained from $\phi_e = -45^\circ, -90^\circ, \text{ and } -135^\circ$. The double-valued nature of Δ_e in Az_i , for each of these curves, corresponds to transits having the same position at perigee, but having different velocity directions.

This increasing range of variation in Az_i required for increasing perisel radii is given explicitly as a function of perisel radius in Figure 78 for phase angles of $0^\circ, 45^\circ, 90^\circ, 135^\circ, \text{ and } 180^\circ$ (and by the proper reflections according to Miele's Theorem of Images, phase angles of $225^\circ, 270^\circ, \text{ and } 315^\circ$).

Similarly, the range of variation in velocity magnitude required for enveloping the moon from a given phase angle increases with the perisel radius. Velocity magnitude requirements for each point along the perigee stations associated with the perisel radii 1000 km, 1923 km, and 3000 km are given for several phase angles in Figure 79. As shown here Δ_e is also double-valued in velocity magnitude for each phase angle and perisel radius. From consideration of this double-valued nature of Δ_e in velocity direction and magnitude, two unique transits for each perisel radius are seen to be possible from each point of the corresponding perigee belt (with the exception of the boundary points) which have different velocity directions and magnitudes at perigee. (In the case $\phi_e = 0^\circ$ or $\phi_e = 180^\circ$, the velocity magnitude is the same for the two transits.) The ensuing

transits yield different perisel points and directions of arrival. Inclinations of the perisel conics are indicated in both of these figures (77 and 79) to give more insight into the moon arrival (or departure) situation, as well as being a convenient parameter for matching the proper azimuths and velocity magnitudes on these graphs for given positions in the perigee belts.

Another means of representation of the information contained in Figures 77 and 79, which gives stronger emphasis to the inclination of the moon arrival conic, merits at least graphical presentation. Figures 80, 81, and 82 are plots of velocity direction at perigee vs phase angle, with the inclination of the perisel conic as a parameter. Figures 83, 84, and 85 are plots of perigee velocity magnitude vs phase angle with the lunar arrival inclination as a parameter. In these figures, only inclinations of 30° , 60° , 90° , 120° , and 150° are given. Inclinations of 225° , 270° , and 315° may be found by proper application of Miele's Theorem of Images. It is interesting to note the shape similarity of the corresponding plots (Figures 86, 87, and 88) for velocity magnitude at perisel with those above for perigee.

Section 2. Lunar Impacts

The preceding discussion of variations in perisel radius was without regard to the volume of the moon. This approach was taken so that the families of constant transit time would be consistent families, i.e., the time of transit was to be measured from earth perigee to the (mathematical) point of lunar close approach. In the physical situation, assuming the moon to have a radius of 1738 km, all those transits with perisel radius less than 1738 km will impact on the surface of the moon at some time before periselenium. Therefore, those points of the perisel horn which lie within the surface of the moon are to be associated with impact transits.

Recall Figure 63 which was generated from the phase angle $\phi_e = 0^\circ$. The surface represented here is that which was defined by investigation of all possible perisel points in the vicinity of the moon, corresponding to 72-hour transits which have their earth perigee at 6555 km (100 n.m. altitude) and station phase angle $\phi_e = 0^\circ$. The perisel circles shown on the surface are those for perisel radii of 828 km, 1368 km, 1923 km, and 2500 km.

To facilitate the association of perisel points with points of impact, the intersections of this surface with the MEP and a polar plane containing the vertex line are given by Figures 89a and 89b. (The dotted circle represents the surface of the moon and the dotted lines represent the extension of the vertex lines through the center of the moon.) Now retracing the paths of the transits for these radii (dashed)

back to the surface of the moon, points of constant transit times and constant path angles are found in the MEP and in the polar plane corresponding to each perisel radius. These points are symmetric about the vertex line. Figure 90 shows these transits impacting on the surface of the moon and their continuation to the horn-shaped surface of perisels associated with $\phi_e = 0$. If all such transits defining the given perisel circles are traced back to the surface of the moon, circular loci of almost constant transit time to impact and impact path angle are formed for every perisel radius (Figure 91). (The variation in τ and β is in the second decimal place.)

The development of loci of constant transit time to impact, and impact path angle for other earth phase angles proceeds in the same manner. Similar concentric circular loci are described for each phase angle. The impact loci for all earth phase angles, corresponding to a given perisel radius, for example, $R_m = 627$ km, form an annular region on the surface of the moon similar in shape to the perisel belt for the given radius. In this annular region, impacts may be obtained with fixed values of impact time and path angle from each earth phase angle (Figure 92). Similar annular regions are formed for every perisel radius. Figure 93 shows the regions associated with the perisel radii, i.e., 258 km, 627 km, and 1183 km. The maximum variation of time and path angle for any perisel radius over all ϕ_e is about .06 hour and 1.5° as shown below. The impact time and path angle are not unique for a given position on the moon. Neighboring perisel radii within the moon determine overlapping annular regions of impact with different impact times and path angles.

The variation of the impact path angle with perisel radius is somewhat sinusoidal with the impact path angle single-valued and changing from 90° to 180° , as perisel radius varies from 1738 km approaching zero. This is shown for the phase angles $\phi_e = 0^\circ$, and 180° in Figure 94. The transits having a zero perisel radius and an impact path angle of 180° (i.e., the transit impacting perpendicular to the surface of the moon) are found to be colinear with the extension of the corresponding vertex lines mentioned before. As perisel radius decreases from 1738 km to zero, the arc length between impact and perisel first increases to a maximum, and then decreases to the radius of the moon for the limiting case of zero perisel radius. At the same time, perisel velocity is increasing. The combined effects of the first increasing and then decreasing arc length between impact and perisel and the increasing velocity result in transit time to impact being double-valued (Figure 95). The variations of impact and perisel velocity with decreasing radius of perisel are given for $\phi_e = 0^\circ$, and 180° by Figures 96 and 97. The corresponding longitudes of impact and periselenium are given in Figure 98, and the velocity magnitude at perigee for the embedded transits is given in Figure 99.

Perpendicular impact loci (corresponding to the limiting cases of $R_m = 0$) are given by Figure 100 for the transit times of 60, 72, 84, and 96 hours. These are the only possible perpendicular impacts from the systems $C(T_i, 6555 \text{ km}, R_{ms})$ $T_i = 60, 72, 84, \text{ and } 96$ hours. An indication of the similar loci for any transit time in $60 \leq T_i \leq 96$ is given by Figure 101. This figure shows the center (which lies on C_m), the major axis, and the minor axis of the loci versus transit time. Since these loci lie on the vertex lines, their reflection through the center of the moon results in the corresponding vertex loci.

Corresponding perigee positions are given by Figure 102. These loci are very nearly circular for the lower transit times, and even for the higher transit times the locus may be at least approximated by circles; therefore, Figure 103 indicates the positions of the centers and radii of the loci for transit times $60 \leq T_i \leq 96$.

Section 3. The System $C(T_i, R_{es}, R_m)$

A. Variation of Earth Terminal Radius

The somewhat arbitrary restriction of the earth terminal radius to 6555 km (185 km altitude) has allowed an extensive study of the behavior of transits in the earth-moon systems. However, only after allowing variations in the earth terminal radius will the purpose of this study have been accomplished, i.e., the classification of all transits with successive close approaches in the vicinity of the earth and the moon.

The systems of classes $C(T_i, R_{es}, R_m)$ are developed in the same way as were the systems $C(T_i, R_e, R_{ms})$, i.e., by stepwise variations in the element R_e of a basic class $C(72 \text{ hr}, 6555 \text{ km}, 1923 \text{ km})$. Thus, basic classes are generated for $0 < R_{e_1} < R_{e_2} < \dots < 6555 \text{ km} < \dots < R_{e_k}$. Once more, each of these classes exhibits the structural features attributed to the particular class $C(72 \text{ hr}, 6555 \text{ km}, 1923 \text{ km})$ and have the same centerline, C_e .

Figure 104 gives a comparison of the perturbations in the actual trajectory shape for $R_e = 6555 \text{ km}$ (100 n.m., altitude), 7665 km (700 n.m., altitude), 8775 km (1300 n.m., altitude), and 9885 km (1900 n.m., altitude). The perturbations in the shape of trajectories from phase angles other than 0° and 180° are very similar to the trends shown here.

Figure 105a shows the relative positions of the perigee belts for these classes, and Figure 105b shows the corresponding perisel belts for $R_{e_i} = 6555$ km, 9885 km. From this figure, we see very little variation in the perisel belt for variations in R_e . As indicated by the dotted lines on Figure 105a, a horn-shaped continuum of such perigee belts is found when R_e is allowed to vary continuously between $0 < R_e \leq R_{e_k}$. The intersection of this perigee horn with a sphere of any fixed radius R_{e_j} is, therefore, the locus of all possible perigee locations for transits from the classes $C(T, R_{e_j}, 1923$ km), and the horn contains all transits of the system $C(T, R_{e_s}, 1923$ km).

The intersections of this perigee horn with the MEP and with a polar plane containing C_e are shown by Figure 106 and Figure 107. The intersections of the corresponding perisel belts (at $R_m = 1923$ km) with the MEP are given as a function of perigee radius by Figure 108.

B. Transits Having Perigee Stations Inside the Earth

The consideration of transits having perigee inside the earth (analogous to the previous discussion of perisels within the moon) has its value in the possibility of future direct ascent missions, or the desire for injection with a path angle other than 90° .³

Since the general characteristics of such transits are very similar to those discussed previously, only the perigee geometry is presented. Injection altitude has been chosen arbitrarily as 185 km (100 n.m.). The patterns existing here are typical of the situations to be encountered at any other altitude near the earth. Further, numerical data are presented only for the embedded transits and the polar (earth and moon) transits. The trends indicated by these transits are in general applicable to other departure phase angles and directions of lunar approach.

Figures 109, 110, and 111 illustrate the (mathematical) behavior of the embedded and polar transits between perigee and the 185 km injection altitude. Almost any geometrical restraint imposed at the moon, which can be satisfied by injection at 185 km perigee altitude, can also be satisfied by this type of transit when referenced to the corresponding perigee class. Such transits may be easily referenced to the corresponding perigee class by the simple two-body relationships, and by the same means, injection requirements may be obtained for injection into these transits at higher altitudes (This two-body approximation is very good for short periods of time near the earth).

³ The discussion here is not intended to show practicality, but possibility.

CHAPTER IV. APPLICATIONS

Section 1. Free-Return Transits

A. Requirements for Free Returns

An important application of the geometrical concepts developed in the previous chapters is found in the implication of the existence or, just as important, the nonexistence of certain types of transits satisfying given mission requirements.

One such mission of immediate importance is that of free flight transits which, after passing arbitrarily near the moon, return to the vicinity of the earth with position and velocity coordinates conducive to reentry and recovery. The utility of such a mission definition lies in its applicability to Apollo type missions, for which mission abort in the vicinity of the moon, without thrusting maneuvers, and return to earth may be desirable or necessary, or simply to missions for which lunar fly-by and earth-return is required.

These free-return transits can be defined within the context of the classification methods of this study by the following restrictions on position, velocity direction and velocity magnitude at the perisel point:

1. Position - Two perisel circles must have this point in common; one a lunar arrival circle defined by earth-moon transits (outbound legs), and the other, a lunar departure circle, defined by moon-earth transits (inbound leg) corresponding to the reflection across the M-E polar plane of the same or any other arrival circle.
2. Velocity Direction - The two perisel circles must be tangent at this point. Since the transits are normal to their perisel circles, tangency of the two circles is required for the velocity directions to be colinear.
3. Velocity Magnitude - The velocity magnitude for the two transits must be the same at this point.

Neither flight time, perisel radius, nor the perigee radii appear explicitly in these restrictions. However, they do appear implicitly, defining boundaries of regions for which all three restrictions may be satisfied. The properties of these boundaries and certain elements of the region of existence are the topics pursued in the following.

Without loss of generality, the discussion may be simplified by assuming the perigee radius of the outbound leg and that of the inbound leg to be the same; i.e., the classes of transits discussed belong to $C(T_S, 6555 \text{ km}, R_{m_S})$, where T_S and R_{m_S} are dependent. The analysis and the patterns which would be developed for different combinations of the two perigee radii are similar to that to be presented.

B. Symmetric Free Returns

The most easily conceived free returns are those for which perisel occurs in the M-E polar plane. The principles for the development of such free return transits are outlined in the following idealized example.

Consider the classes $C(T^*, 6555 \text{ km}, R_1^*)$, defined by the intersection of a sphere of radius R_1^* , about the center of the moon, with the perisel horn corresponding to the transit time T^* (* denotes the idealized example) and $C'(T^*, 6555 \text{ km}, R_1^*)$, the reflection of $C(T^*, 6555 \text{ km}, R_1^*)$ across the M-E polar plane. Segments of the two perisel belts defined at the intersections are shown on Figure 112, with the perisel circles for the phase angles 0° , 90° , 180° , and 270° superimposed. The loci of vertices are also projected onto the sphere.¹

Figures 113, 114, 115, and 116 show the classes from the system $C(T^*, 6555 \text{ km}, R_{m_S}^*)$ defined at the intersections of spheres of radii $R_2^* < R_3^* < R_4^* < R_5^*$, respectively, with the same perisel horn. These five figures show that, as the perisel increases, at some radius R_2^* the perisel horns intersect the moon-earth polar plane. The first possible symmetric free return for $C(T^*, 6555 \text{ km}, R_{m_S}^*)$ occurs at this point. Here the perisel circles for $\phi_e = 0$ from $C(T^*, 6555 \text{ km}, R_2^*)$ and $C'(T^*, 6555 \text{ km}, R_2^*)$ are tangent forming the inbound and outbound legs of the free return. In the same manner, with further increases of the perisel radius, a free return occurs for every phase angle as the corresponding perisel circles become tangent (in the M-E polar plane). The latitude of the perisel point for these free returns increases from $\phi_m = 0^\circ$, for $\phi_e = 0^\circ$, to a maximum for $\phi_e = 90^\circ$ (Figure 114), and back to $\phi_m = 0^\circ$ for $\phi_e = 180^\circ$. Simultaneously ϕ decreases to a minimum for the corresponding phase angles symmetric about the MEP ($360^\circ > \phi_e > 180^\circ$).

Free returns of the type depicted by Figure 114, having perisel latitude $\phi_m \neq 0$, have been called free returns of the second kind by Schwaniger [6] and others, but will be referred to here as "plane symmetric free returns." "Line symmetric free returns" also described in Reference 6, as those of type 1 or the first kind, have their perisel

¹The two perigee belts are reflections across the x-z plane.

on the earth-moon line, and also occur in pairs, with azimuth symmetric about 270° , (for earth phase angles symmetric about the MEP) as the corresponding perisel circles become tangent to the earth-moon line, as shown for $\phi_e = 90^\circ$ and 270° on Figure 115. Here, the perisel circles become tangent to their reflection across the earth-moon line; i.e., the perisel circles for $\phi_e = 90^\circ$ and $\phi_e' = 270^\circ$ define a free return which has an azimuth less than 270° , and symmetrically, $\phi_e = 270^\circ$ and $\phi_e' = 90^\circ$ define a free return which has an azimuth greater than 270° . The azimuth increases from 270° to a maximum as ϕ_e increases from 0° to 90° , then decreases to 270° as ϕ_e continues to increase to 180° , and symmetrically for $180^\circ < \phi_e < 360^\circ$.

A three-dimensional representation of the development of the free return patterns as described with reference to Figures 113, 114, 115, and 116 is given by Figure 117. The plane symmetric free returns, defined at the points of tangency of Figures 113, 114, and 116, correspond to the perisel points A, D, and G in the x-z plane of Figure 117. Likewise, the perisel points at d, for $\phi_e = 90^\circ, 270^\circ$, belong to the line symmetric free returns defined at the point of tangencies of Figure 115.

Thus, there is a line symmetric and a plane symmetric free return for every earth phase angle except 0° and 180° , where the single free returns satisfy the definitions for both types. The locus for the plane symmetric returns is somewhat elliptical, and the locus for the line symmetric is then the axis of the ellipse colinear with the earth-moon line. The locus of the vertex points for free returns belonging to $C(T_O^*, 6555 \text{ km}, R_{m_s}^*)$ is indicated on the vertex cone, also shown on Figure 117.

At this point, it should be reiterated that the example used is an idealized case. The true geometrical patterns for the loci of perisels corresponding to free return transits become distorted over variations in transit time. Figure 118 indicates the variation in the shape of the perisel loci for symmetric free returns of the systems $C(T_s, 6555 \text{ km}, R_{m_s})$, $T_i = 60, 72, 84, \text{ and } 96$ hours. The near-moon boundary for symmetric free returns is given by Figure 119. Figure 120 gives the transit time and earth phase angle for the maximum inclination achievable in a neighborhood of the moon.

The discussion may be summarized here by the following:

1. The perisel points of all possible symmetric free returns lie in the x-z plane.²

²This is also implied by Miele's Theorem of Images.

2. For a given transit time and perigee radius, there exist two symmetric free returns (one line symmetric and one plane symmetric for every earth phase angle $0^\circ < \phi_e < 360^\circ$, with the pairs for 0° and for 180° being identical. Each free return has its perisel and vertex point at unique distances from the center of the moon.
3. The perisel loci for the free returns of neighboring transit times intersect densely, forming a region, within which the perisels of an infinity of line symmetric free returns exist at every point along the x-axis.
4. At any other point of the region, there exist exactly two plane symmetric free returns, except at the near-moon boundary of the region, where there is only one.

C. Nonsymmetric Free Returns

The use of a symmetric free return transit for a given mission may place undue restrictions on the position of perisel or the return perigee. It is very likely that due to tracking (and other) restrictions on reentry, returns to a position symmetric to that of launch would be undesirable, yet return to a specified altitude may be necessary for successful recovery.

Such mission constraints may be satisfied by application of the restrictions given in Section 1 to the systems of classes $C(T_s, R_{es}, R_{ms})$ and $C'(T_s, R'_{es}, R'_{ms})$, where $T_i \neq T'_i$, $R_{mi} = R'_{mi}$, and $R_{ei} \neq R'_{ei}$. The development of such "nonsymmetric" free returns is a straightforward continuation of that for the symmetric cases discussed in the previous section.

Consider, for example, the class $C(T^*, R_e, R_2^*)$ shown by Figure 113 and, $C'(T_1^*, R_e, R_2^*)$ instead of $C(T^*, R_e, R_2^*)$, where T_1^* is arbitrarily near T^* . There exist two perisel circles, one from each class, corresponding to different earth phase angles, which are tangent at a point where the velocities are the same, thus producing a nonsymmetric free return with $\lambda_m \neq 180^\circ$ and $Az_m \neq 270^\circ$. The coordinates of the earth perigees for the two legs, as well as the transit times, differ.

As increasing and decreasing transit time classes are considered, i.e., $C'(T_1^*, R_e, R_2^*)$, $T_1^* \geq T^*$, two nonsymmetric free returns occur for every earth phase angle in $C(T^*, R_e, R_2^*)$, one above the MEP and one below the MEP.

The outbound legs of these nonsymmetric free returns all have the same transit time T^* , and each of the inbound legs has different transit times.

The approximate bounds on T_i^* for any R_m may be found by comparing velocities and positions for perisels in the MEP, over transit time, for the systems $C(T_s, R_e, R_{ms})$ and $C'(T_s', R_e', R_{ms})$. This is illustrated by Figure 121 for $R_e = R_e' = 6555$ km and $R_m = 1923$ km. For these systems of classes, there exists a continuum between the transit times of about 60 hours and 82 hours within which transits may have the same perisel velocities and longitudes. The free returns are also dependent on perisel azimuth and latitude, but for the determination of boundaries these parameters are not needed.

As an example for reading this graph, choose an outbound transit time $T = 65$ hours. The transit times of possible inbound transits having comparable perisel longitudes are between about 73 hours and 76.5 hours shown by the shaded area. The limits on perisel velocity for these free returns are shown by the dotted lines within the velocity region. Further identity of these transits with respect to perigee conditions may be obtained from cross plots of the graphs of perigee parameters presented in Chapter III.

Nonsymmetric free returns traveling in the opposite direction to those discussed above may be obtained in the same manner from the same figure. These transits are reflections of the above transits across the earth-moon polar plane. The perisel velocities are the same, and the longitudes are reflections about 180° , i.e., the positive portion of the longitude curves in Figure 121.

Note that, for $\lambda_m = 180^\circ$, there exist perisels in the x-z plane for transit times between about 69 hours and 70 hours. These points represent symmetric free returns.

Figure 122 is given only as an indication of the shape of the perisel loci for nonsymmetric free returns from the systems (T_i , 6555 km, 1938 km). The solid curves are the free return loci for transit times of 65, 70, 75 and 80 hours, and the dotted lines of constant azimuth at perisel indicate the velocity direction of the free returns. Note that the intersections of the 70 hour locus with the moon-earth polar plane ($\lambda_m = 180^\circ$) are symmetric free returns. This figure may be reflected by Miele's Theorem of Images to obtain transits with the same transit time in the opposite direction.

Figures 123 and 124 for $R_m = 1000$ km and 3000 km, respectively, give the same information as Figure 121 for $R_m = 1923$ km, i.e., boundaries in transit time perisel longitude and velocity for both symmetric and nonsymmetric free returns. Although $R_m = 1000$ km is physically meaningless, Figure 123 is very useful along with Figures 121 and 124 for cross plots over perisel radii of greatest interest, i.e., $1738 \text{ km} < R_m < 3000 \text{ km}$.

A more detailed study of free return transits is to be published in the near future by A. J. Schwaniger of this office (also see references 6 and 9).

Section 2. Phases of the Moon at Approach and Lighting Conditions for Rendezvous and Impact

Almost any lunar mission places restrictions on the lighting conditions at lunar approach. A complete treatment of this subject, however, would very well comprise a complete study in itself. For this reason, the following is intended only as an indication of another of many possible applications of the concepts developed in Chapters I-III. No numerical data are presented - only the method of application.

Figure 125 is an arbitrary representation of the earth, moon and sun with respect to the plane of the ecliptic and the vernal equinox. The parameters indicated may be determined at any time from "The Astronomical Ephemeris and the American Ephemeris and Nautical Almanac"³ as defined below:

λ = the mean longitude of the moon, measured in the ecliptic from the mean equinox of date to the mean ascending node of the lunar orbit, and then along the orbit,

Ω = the longitude of the mean ascending node of the lunar orbit on the ecliptic, measured from the mean equinox of date,

$\lambda = \Omega + \omega,$

i = the inclination of the lunar orbit plane to the ecliptic,

L = the geometric mean longitude from the mean equinox of date,

³Hereafter referred to as AEAENA.

\bar{R}_{es} = the vector from the earth to the sun,

\bar{R}_{em} = the vector from the earth to the moon,

\bar{R}_{sm} = the vector from the sun to the moon.

A vector expressed in the earth centered ecliptic coordinate system may be expressed in the MEP earth-centered system by the following rotations:

$$\bar{X}_{MEP_e} = (\omega)_3 (i)_1 (\Omega)_3 \bar{X}_{Eec} = T \bar{X}_{Eec},$$

where

$$(\theta)_1 = \begin{bmatrix} 1 & 0 & 0 \\ 0 & \cos \theta & \sin \theta \\ 0 & -\sin \theta & \cos \theta \end{bmatrix}$$

$$(\theta)_3 = \begin{bmatrix} \cos \theta & \sin \theta & 0 \\ -\sin \theta & \cos \theta & 0 \\ 0 & 0 & 1 \end{bmatrix}.$$

With respect to the MEP moon-centered system, this is given as

$$\bar{X}_{MEP_m} = \bar{X}_{MEP_e} - \begin{bmatrix} d_{em} \\ 0 \\ 0 \end{bmatrix}.$$

Therefore, the vector from the sun to the moon may be calculated in the MEP moon-centered system by the above transformation of the following expressed in terms of data given in the AEAENA:

$$\varphi = \sin^{-1} (\sin i \sin \omega), \quad \varphi \neq \pm \frac{\pi}{2}$$

$$\cos \Delta\lambda = \frac{\cos \omega}{|\cos \varphi|}, \quad \omega \neq n \cdot \frac{\pi}{2}, \quad n = 0, 1, 2, 3$$

$$\sin \Delta\lambda = \tan \varphi / \tan i$$

$$\Delta\lambda = \tan^{-1} [\sin \Delta\lambda / \cos \Delta\lambda]$$

(if $\omega = n \frac{\pi}{2}$, $\Delta\lambda = \omega$). Therefore,

$$\bar{R}_{sm} = \bar{R}_{em} - \bar{R}_{es} = \begin{bmatrix} R_{em} \cos (\Omega + \Delta\lambda) \\ R_{em} \sin (\Omega + \Delta\lambda) \\ R_{em} \sin i \sin \omega \end{bmatrix} - \begin{bmatrix} R_{es} \cos L \\ R_{es} \sin L \\ 0 \end{bmatrix}.$$

Transforming to MEP moon-centered coordinates, the latitude, φ_m , and longitude, λ_m , of the "midnight point" on the moon are found from the following:

$$\frac{\bar{X}_{MEP_m}}{|\bar{X}_{MEP_m}|} = \begin{bmatrix} \cos \varphi \cos (360 - \lambda_m) \\ \cos \varphi \sin (360 - \lambda_m) \\ \sin \varphi_m \end{bmatrix}.$$

This midnight point defines the hemispheres of "daylight and darkness" on the moon for the ephemeris time selected. For times in the neighborhood of the selected time, there will be no appreciable change in the areas of light and darkness.

If the time is selected to coincide with the arrival of some earth-moon transit, the lighting conditions available for rendezvous or lunar impact may be determined for any transit arriving at this time merely by reference to the centerline, C_m , for the corresponding transit time. Transits having a common transit time are essentially parallel in the neighborhood of the moon and lie within a tubular volume (having an almost circular cross section) which contains their perisels and decreases to a point at C_m .

For example, consider typical transits having a transit time of 72 hours arriving at the moon (at mean distance) at the ephemeris time represented by the geometry of Figure 125. C_m for 72 hours is approximately at 125° longitude. This arrival situation is depicted by Figure 126. Four transits (embedded and polar) for $\phi_e = 0$, and the associated perisel belt for 72 hours are given as typical. In this situation, transits may depart from the earth from any ϕ_e and arrive in a lighted region with arrival inclinations $90^\circ < I_m \leq 180^\circ$, and $-90^\circ > I_m \geq -180^\circ$. Similar conditions exist for impact transits.

(The location of C_m for other transit times in the region $60 \leq T \leq 96$ may be found in the information given in Chapter III, Section 2.)

CHAPTER V. GEOGRAPHIC AND SELENOGRAPHIC LAUNCH AND ARRIVAL CONDITIONS

Section 1. Launch Restrictions

For operational as well as flight reliability reasons, the Apollo project requires launch from the Atlantic Missile Range within specific limits on azimuth, and requires the lunar approach to be in a predetermined direction over a specified position on the lunar surface. Thus, implementation of the Apollo project requires the formulation of the necessary launch parameters in a geographical coordinate system, and similarly the arrival parameters must be formulated in a selenographic system.

In consistency with the aim of this paper - promoting the understanding of the problems and the ways of solving them, rather than bringing out quantitative data - a rigorous treatment of the transformations from the MEP to the geographic and selenographic systems is omitted,¹ and the development is, in general, by means of sequences of illustrations.

¹See "Explanatory Supplement to the Ephemeris," HMSO, 1961; and "Selenographic Coordinates," JPL TR 32-41, B. E. Kalensher, 24 Feb. 1961, for treatments including librations and nutations, etc.

The selection of a launch date and time, for the investigation of a mission's feasibility, fixes the MEP coordinate system with respect to the ephemeris and the Atlantic Missile Range. The situations available for launch are then determined by the perigee and perisel belts.

Four simple coordinate rotations, through ω , i , Ω , and ϵ , relates the perigee belt to the space-fixed (in direction) earth equatorial system as shown by Figure 119.

This transformation is given by $\bar{X}_{EEQ} = (\epsilon)_1(-\Omega)_3(i)_1(-\omega)_3\bar{X}_{MEPe}$ where ϵ , Ω , i , and ω are measured as shown in Figure 127.

One further rotation, through the angle of rotation of the earth about its pole, is necessary to reference the MEP system to a particular launch-site coordinate system.²

A typical case of relative axis alignment is illustrated on Figure 128, which intentionally does not represent the special geometric relationships encountered near 1968/9. Before and after these years, a geometry similar to that shown materializes once a month. Although it is not considered here, there is a small rotation of the MEP system as well as a precession of the flight plane between launch and perigee during the time periods shown on this and the next four diagrams, which must be considered in a numerical investigation. These factors are considered in a later discussion.

Rather than limiting the discussion to the possibility of effecting particular launch geometries from Atlantic Missile Range a more general question is posed: What departures, if any, are possible within a given class $C(T, R_e, R_m)$, if the flight from Atlantic Missile Range to the perigee of the lunar trajectory (including direct injections and injections into parking orbits, with subsequent injection into a lunar trajectory) is to be made without lateral maneuvers? The restrictions for such transits are that

- (1) the restrictions imposed on the flight parameters by the class $C(T, R_e, R_m)$ must be satisfied,
- (2) the flight plane must contain a point of the vertex locus for the class and (neglecting the precession of the nodes of the flight plane) the launch site, and
- (3) the flight plane must be within the limits of azimuths that are permissible for range safety as well as for tracking or other reasons.

²See "Methods for Trajectory Computation," MTP-AERO-63-9, William E. Miner, for typical coordinate systems and atmospheric trajectory computation methods.

Three geographical conditions (or times of a day) are referred to in Figure 128, arbitrarily as times A, B, and C. For each launch time, the launch azimuth limits are indicated, chosen here to be from 70° to 110° east from north. Now, since any plane of flight that will initiate a transit of the given class must contain a point of the vertex ellipse, it is clear that time A is too early, and time C is too late for launching into a transit of the class. A time of feasible launchings is represented here by the case of time B, but the times of possible launch extend to earlier and later time points forming a launch window during which transits of the class are possible.

The two time points allowing the first and last full coverage of the vertex ellipse are depicted on Figure 129. The total angular sector defined at the vertex curve, by the above first and last "full coverages," encompasses roughly all approach directions feasible within this time period. There is, however, a later, second period of feasible launches into transits of the class. Figure 130 shows the initial and final times of full vertex coverage by these flights which, in general, travel through larger central angles before reaching their vertices. The angular section cut out by these flights is, in the general case, separated from that of the earlier launch period.

Figure 131 gives an enlarged synopsis of the two sectors, where the belt of perigee stations is now superimposed. This diagram illustrates all possible transits remaining less than one revolution in a parking orbit which can be achieved by launch on this day without lateral maneuvers. These sectors are unique in that there are no two days for which the sectors are identical.

Reverting to the question of whether a particular set of departure conditions (i.e., a particular flight plane) can be met at a particular launch date, the answer is partially expressed by the above discussion. If the set of conditions is compatible with the sectorial description of the feasible launches, the feasibility is established for (a) at least two³ opportunities (azimuth $\neq 90^\circ$) of ascending into (b) at least one transit, from (c) at least one lunar phase angle family, $0^\circ \leq \Phi_n < 360^\circ$ (which will not be determined here). This cumbersome statement can be understood by consideration of the following:

- (a) Under the assumption that the permissible launch azimuths lie symmetrical about 90° , i.e. there exists a launch opportunity with the azimuth $90^\circ \pm \alpha$ ($\alpha \neq 0$), then there exists another opportunity at a different

³At least one opportunity for azimuth = 90° .

time of the day (earlier for "+ α " and later for "- α ") for launching into the same flight plane, the azimuth for which is $90^\circ \mp \alpha$. This is illustrated by Figure 132, which shows that feasible launch trajectories cross the launch latitude twice, except the trajectory launched due east.

- (b) This follows from the assumption of compatibility of the desired flight plane with the sectorial description of the feasible launches.
- (c) The vertex locus here is defined by the lunar phase angle families, each point corresponding to a distinct ϕ_m . Thus, if the launch flight plane crosses the vertex locus twice (rather than being tangent to it), two distinct transits are possible by varying the position of the perigee. (A corresponding variation is required in the perigee velocity.) The perisel conditions of these two transits may be estimated by the ϕ - σ relationships given in Chapter II, Section 2. Note that ϕ_m for these two perisels may be separated by as much as 180° for the case that the launch plane contains C_e .

Another fact with respect to the launch problem is probably now self-evident: all launch opportunities for such maneuverless flights last only an instant. Launchings at times different from these require "out-of-plane" maneuvers at one or more powered phases of the flight. Out of plane maneuvers also are the only means of dealing with those transits for which the departure geometry does not lie within the angular sectors of feasible in-plane launches of the day.

If the mission restrictions will allow the vehicle to remain in the parking orbit for a large number of revolutions, launch windows may be greatly extended. As pointed out above, there are two possibilities for launch into a permissible orbit on a given launch date without lateral maneuvers. Consider now the launch time, T_3 , on Figure 130, the first time possible, in the second sector, for full coverage of the vertex ellipse on this day. If the vehicle is allowed to remain in the parking orbit for about four days, an additional sector (with azimuths between (b) and (c)) is available for launch at the same instant, T_3 , as shown by Figure 133 ((a) is the minimum, and (b) the maximum, allowable azimuth). The plane of the parking orbit will precess westwardly at about 6° per day (for typical parking orbits of interest here), and the vertex locus advances eastwardly at about 13° per day (as the moon revolves about the earth). Therefore, at T_5 , $T_5 \approx T_3 + 4$ days, the orbit planes between (b) and (c) will contain points of the vertex ellipse as shown on Figure 133 by the dotted lines. Note that (c) will reach the vertex ellipse before (b). This is due to the slower rate of precession of the orbit planes as the inclination increases to 90° .

This example shows that, in general, a lunar orbit can be achieved with any launch azimuth and any launch time, if only the parking orbit is maintained a sufficient length of time (the greatest time necessary being less than 1/2 month), and the parking orbit is chosen such that the vehicle reaches the perigee belt at the proper time.

This effectively yields an unlimited launch window for every allowable launch azimuth; however, perturbations on the parking orbit and velocity requirements for injection into the parking orbit, as well as other mission restrictions, may very well reduce this unlimited launch window to near zero, or even zero itself.

Section 2. Selenographic Arrival Conditions

The situation at lunar arrival, with respect to a selenographic coordinate system, is very similar to that at earth departure discussed in the previous section.

Neglecting once more the smaller perturbations on the system (physical libration, etc.), a simplified transformation can be made from the MEP coordinate system to a selenographic coordinate system as follows. Since the ascending node of the lunar equatorial plane on the ecliptic occurs at the descending node of the MEP, the nodal line of the MEP and the MEQ (moon-equatorial) plane (henceforth called the LNL (lunar nodal line)) remains essentially parallel to the nodal line of the MEP on the ecliptic. Thus, an intermediate coordinate system, convenient for geometrical representation of the lunar arrival situation, is defined as having its positive x-axis containing the LNL and pointed toward the center of the earth, at the descending node of the MEP on the ecliptic;⁴ and its positive z-axis in the direction of the lunar axis of rotation; and its y-axis such that it is a right-handed system. The relationship of LNL system to the earth is shown by Figure 134 which corresponds to the two times of the month depicted by Figure 127.

The transformation from the MEP moon-centered system to the LNL system is given by two rotations of the MEP moon-centered systems; i.e.,

$$\bar{X}_{LNL} = (- (I_{mec} + i))_1 (-\omega)_3 \bar{X}_m,$$

⁴So that the angle between the negative x-axis of the MEP and the LNL systems is always ω .

where

I_{mec} = the inclination of the lunar equator to the ecliptic

and

i = the inclination of the MEP to the ecliptic.

One further rotation, through the angle of rotation of the moon about its axis, defines a selenographic system. The treatment of the lunar arrival problem, referenced to the selenography, is now almost identical to that of the previous section for earth departure, with the exception that both corotational and counterrotational flight are to be considered. (It should be remembered that the terms "departure" and "arrival" are referenced to perigee and perisel points which may be reflected by Miele's Theorem of Images in which case "departure" and "arrival" are to be interchanged for the reflected flight in the opposite direction.)

If a particular point on the lunar surface is chosen to be overflowed by transits from some class $C(T, R_e, R_m)$, simple geometric considerations allow the determination of admissible transits as in the following example,

For a point on the lunar equator⁵ and the class $C(72 \text{ hr}, 6555 \text{ km}, 1923 \text{ km})$, all admissible transits are shown by Figure 135 to have lunar phase angles in two sectors between $\sim 160^\circ$ and 178° , for corotational arrival, and between $\sim 5^\circ$ and -10° , for counterrotational arrival. Since all vertex points are overflowed by transits of either sector, earth launch from any ϕ_e will accomplish this mission. If earth launch is restricted to the azimuth limitations of the previous section, the following reductions occur in the launch and arrival sectors.

⁵The point is chosen here to be on the lunar equator, but this does not restrict the generality. Also, for the purpose of this discussion, it is assumed that perisel occurs at the same time, τ , for all transits under discussion, and the difference in the time from perisel to the common crossing point is negligible (so that the discussion will not be unnecessarily complicated).

Consider Figure 131 once more. Since, from Figure 135, $160^\circ \leq \phi_m \leq 178^\circ$ and $-10^\circ \leq \phi_e \leq 5^\circ$, only those elements of the earth departure sectors which pass over the vertex points corresponding to these ϕ_m are available for launch. Figure 136 shows the reduced sectors to be composed of four distinct sectors which are much smaller than the original. These four sectors allow ϕ_e such that, approximately, $-10^\circ \leq \phi_e \leq +10^\circ$ for A, $20^\circ \leq \phi_e \leq 45^\circ$ for B, $-65^\circ \leq \phi_e \leq -45^\circ$ for C, and $-75^\circ \leq \phi_e \leq -60^\circ$ for D.

These restrictions must now be imposed on the lunar sectors. This is given by Figure 137, where the possible arrival transits must pass over the vertex points corresponding to the restriction on ϕ_e .

If the time of perigee for the above transits had occurred at some later time of the same day, in general, a different set of admissible transits would be developed since the orientation of the MEP and LNL systems changes with time. This is indicated by Figure 138, which shows the set of transits of Figure 135 for time, τ_1 , and the dashed lines those (which fly over the same point on the lunar surface) at a later time, corresponding to τ_2 .

This procedure may be repeated to obtain conceptual control over the launch conditions and arrival conditions necessary (and possible) for accomplishment of general lunar missions. For every launch time, the proper orientation of the MEP with the geographic and selenographic systems must be made in agreement with the ephemeris.

If a further restriction is placed in the mission definition, requiring a transit to pass over a given point on the lunar surface in a given direction, there is exactly one such transit from each class $C(T, R_e, R_m)$. Furthermore, these unique transits vary at each instant of time.

SUN-EARTH-MOON GEOMETRY IN 1966-1967

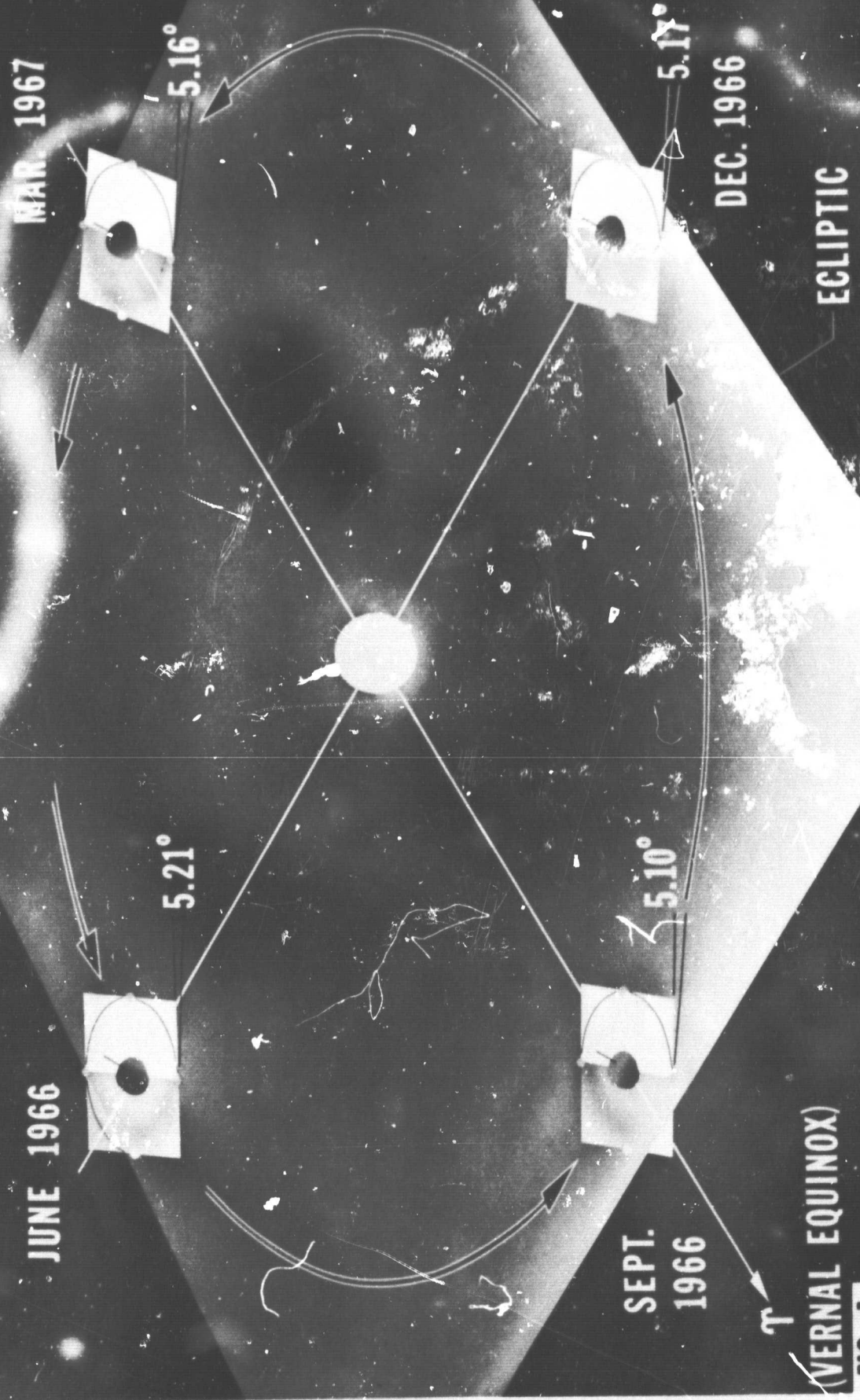


FIG. 1

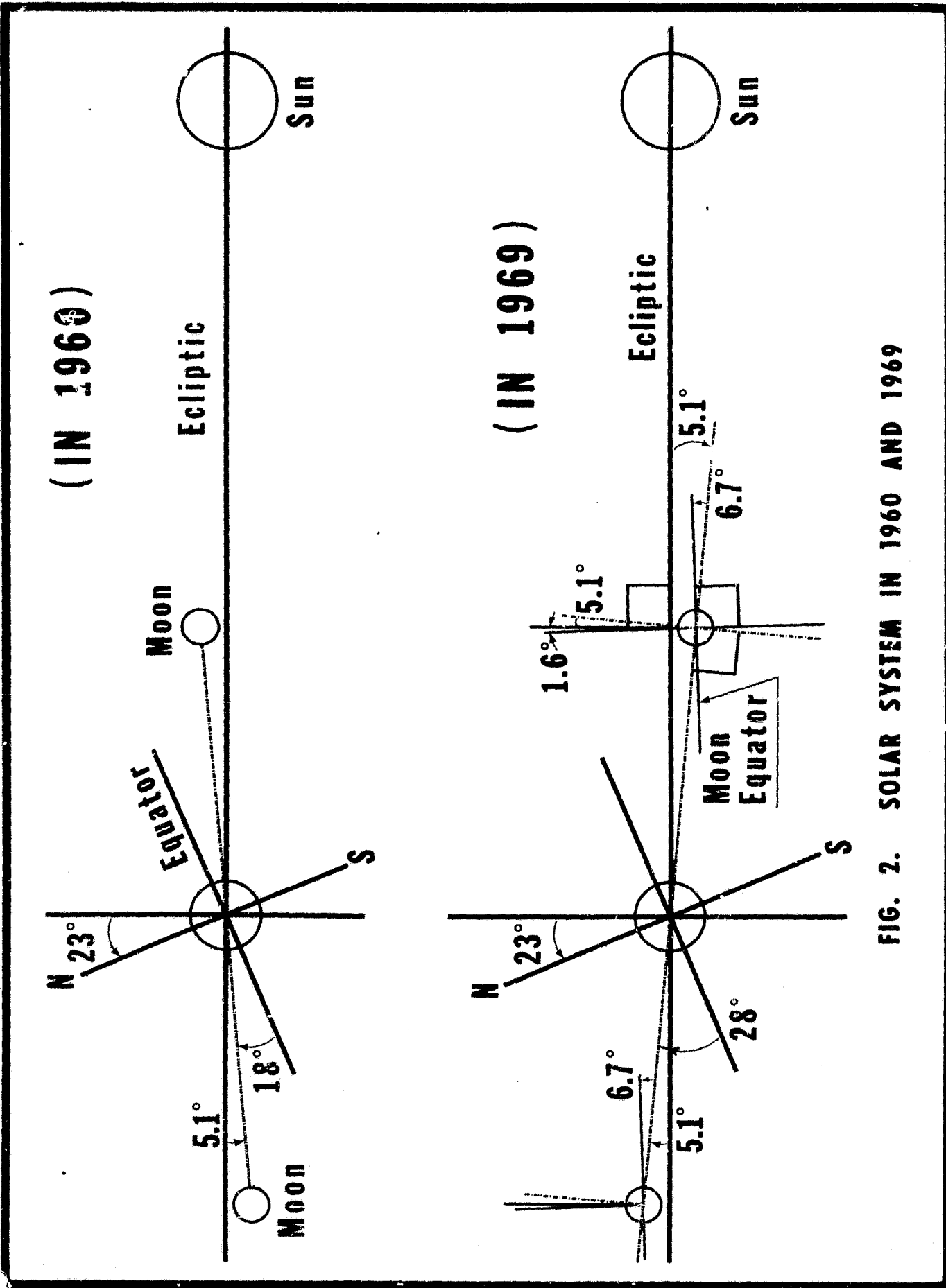


FIG. 2. SOLAR SYSTEM IN 1960 AND 1969

EARTH-MOON GEOMETRY IN OCT. 1966

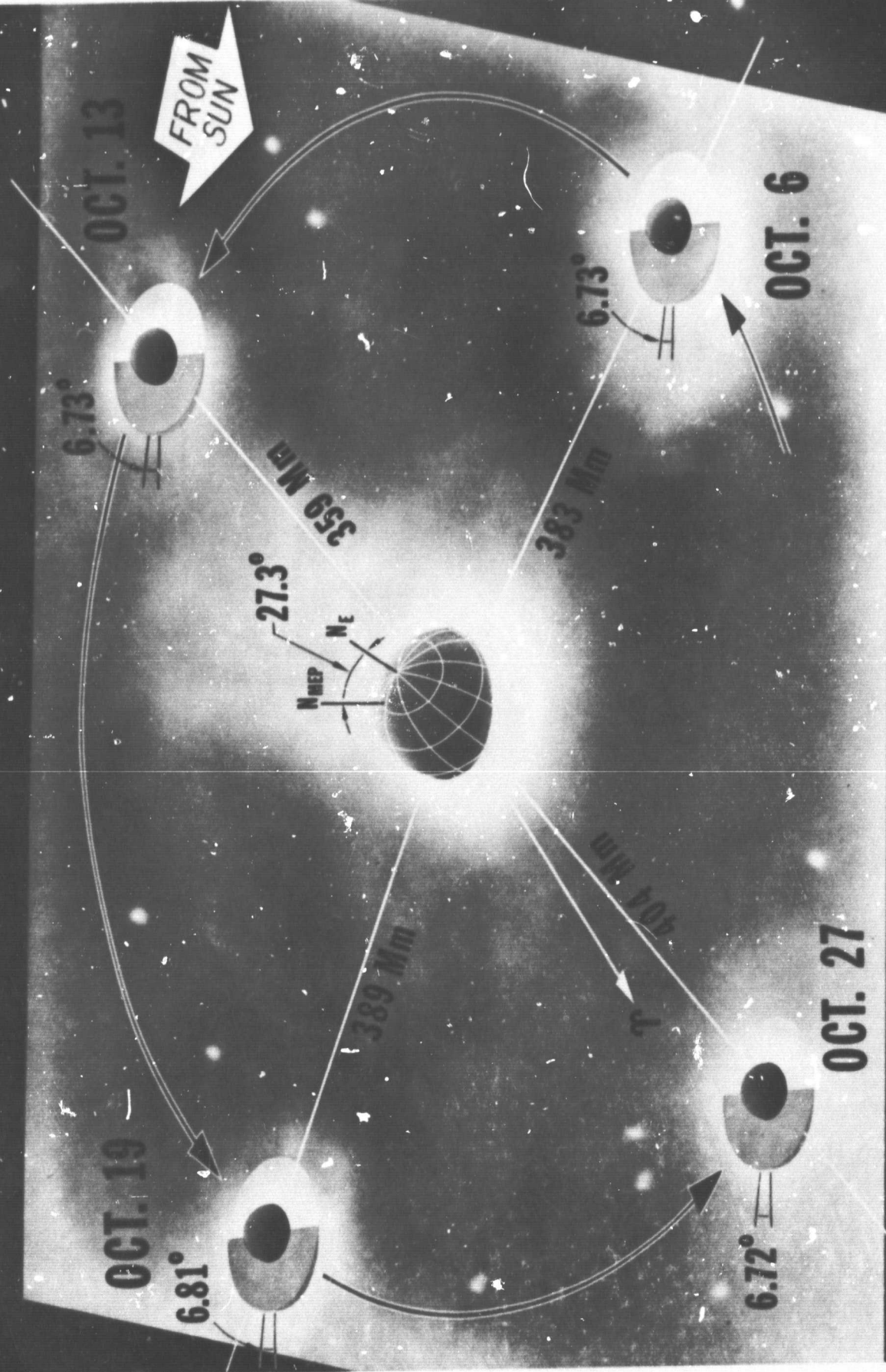


FIG. 3

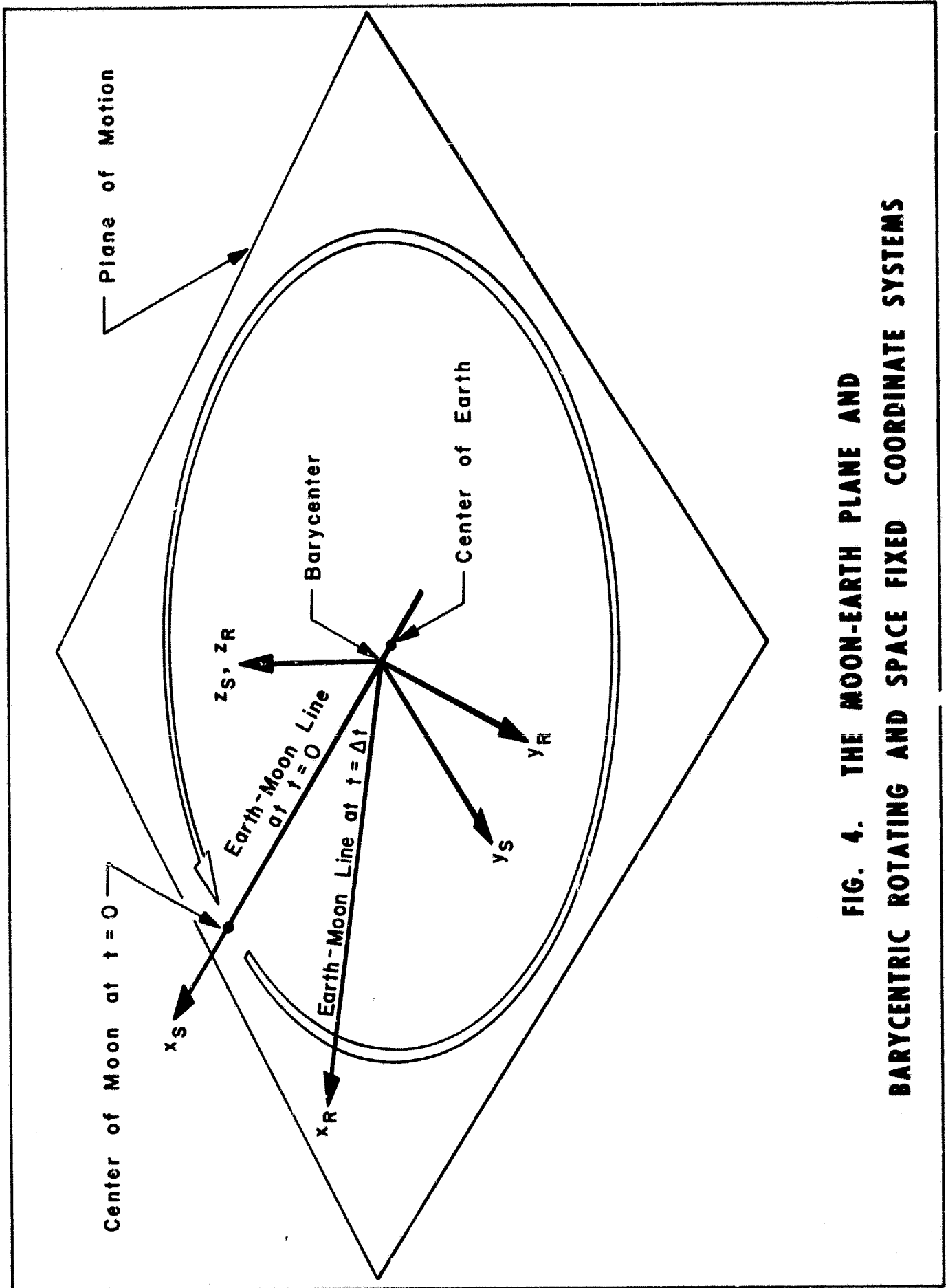


FIG. 4. THE MOON-EARTH PLANE AND BARYCENTRIC ROTATING AND SPACE FIXED COORDINATE SYSTEMS

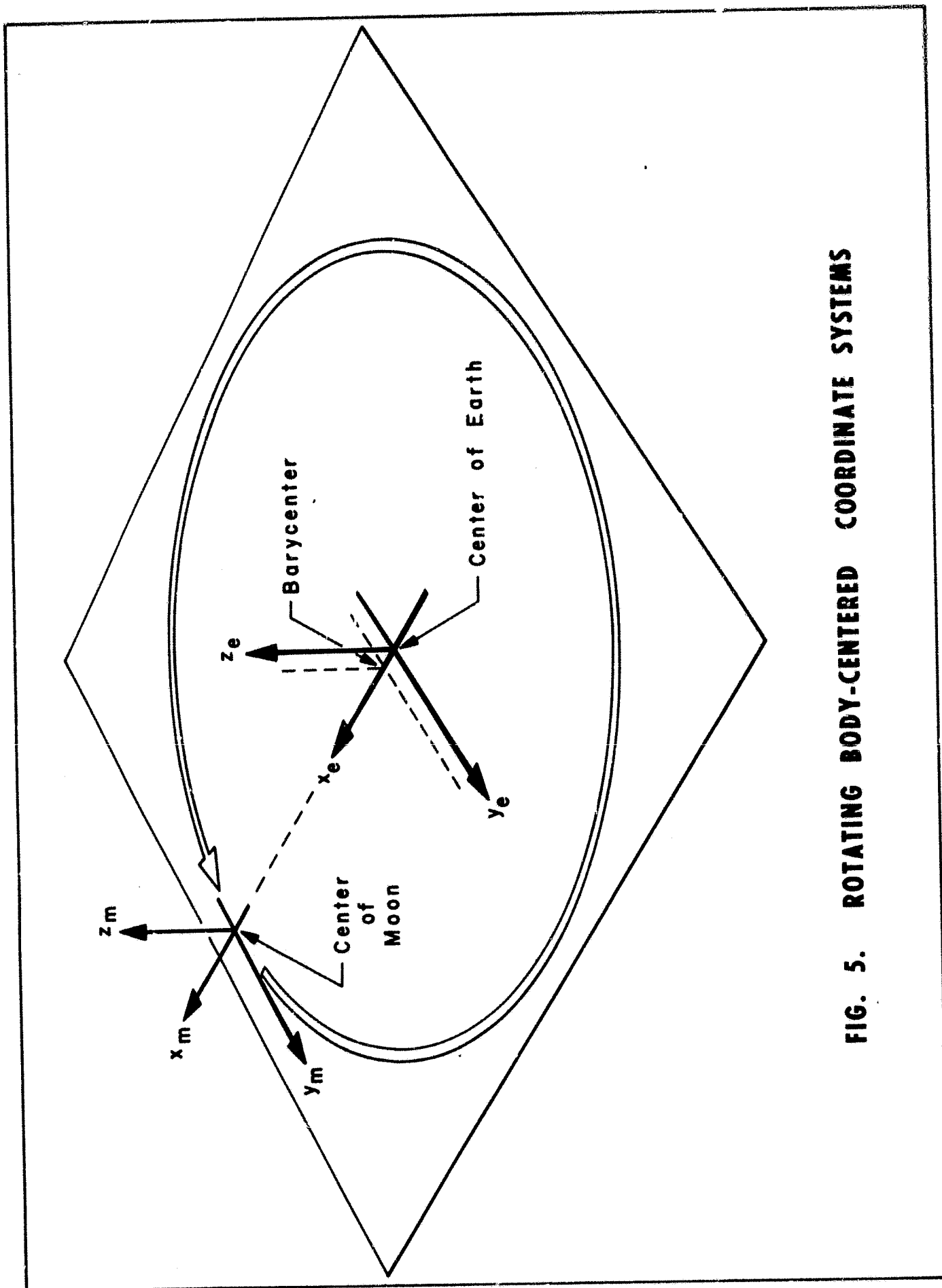


FIG. 5. ROTATING BODY-CENTERED COORDINATE SYSTEMS

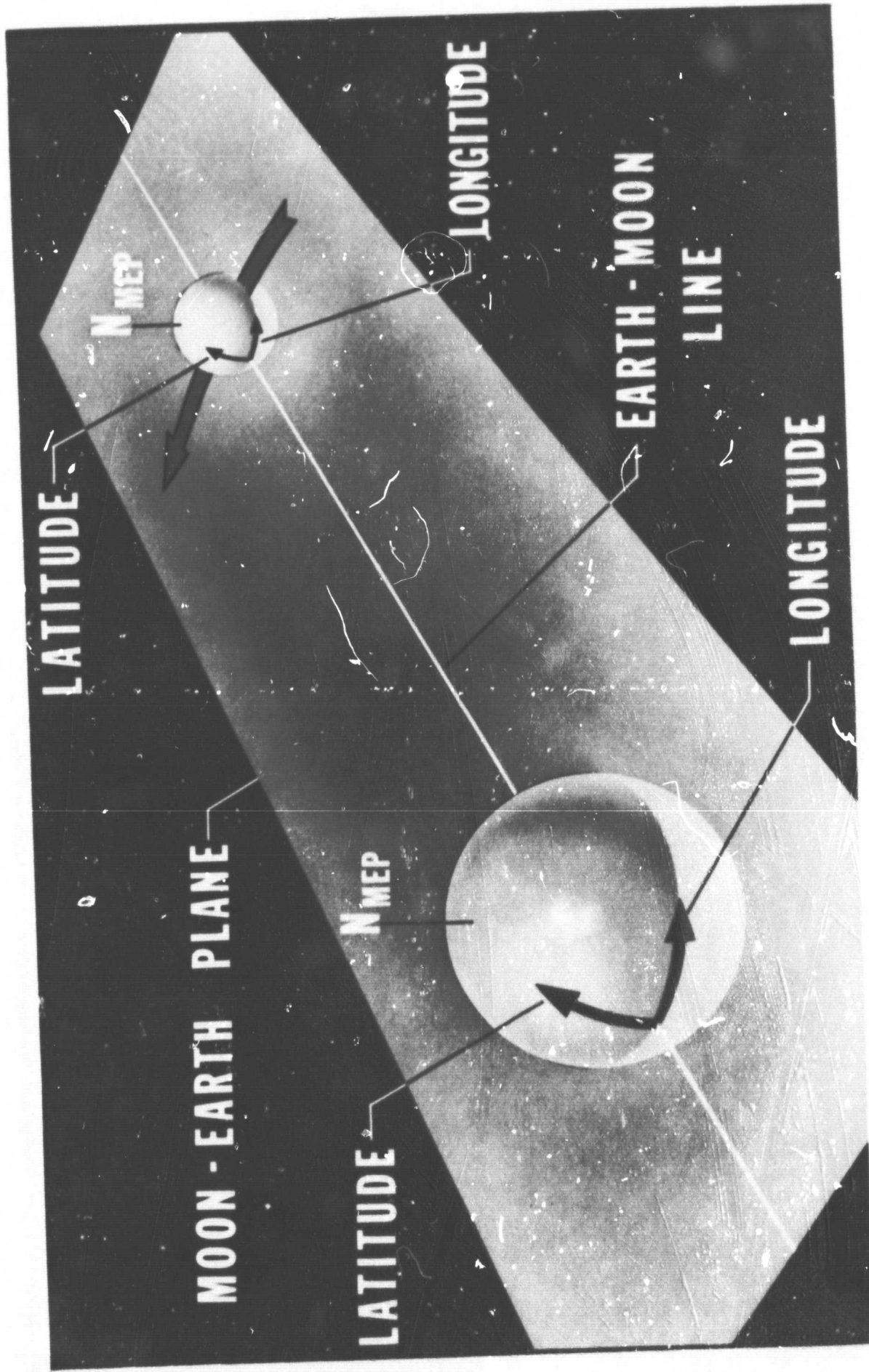


FIG. 6. N_{MEP} - RELATED SPHERICAL COORDINATE SYSTEMS

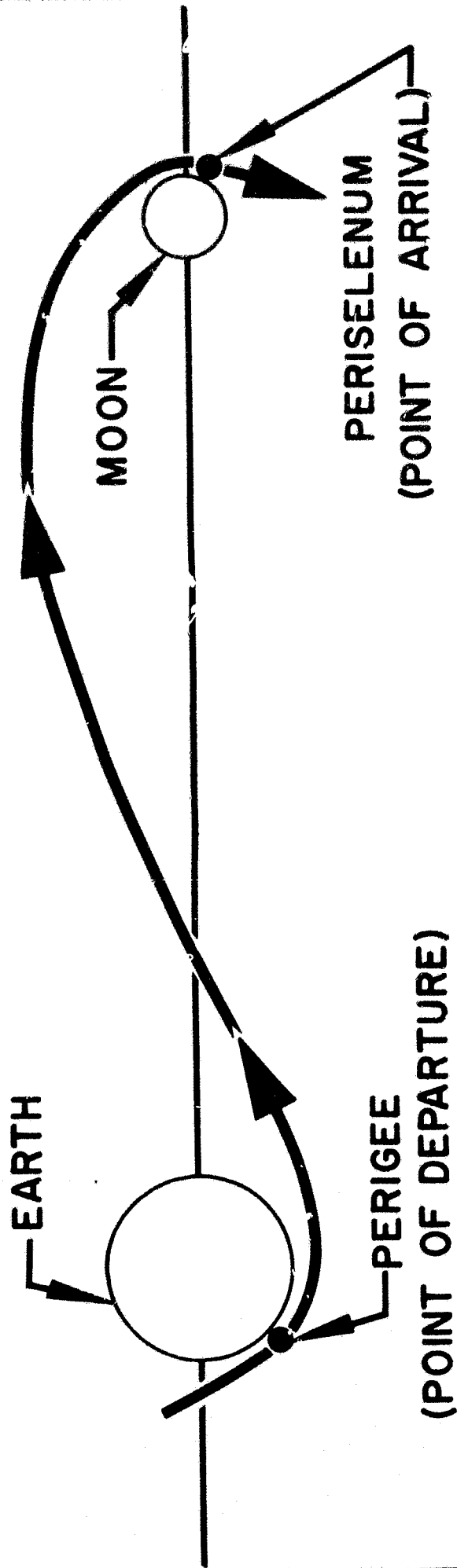
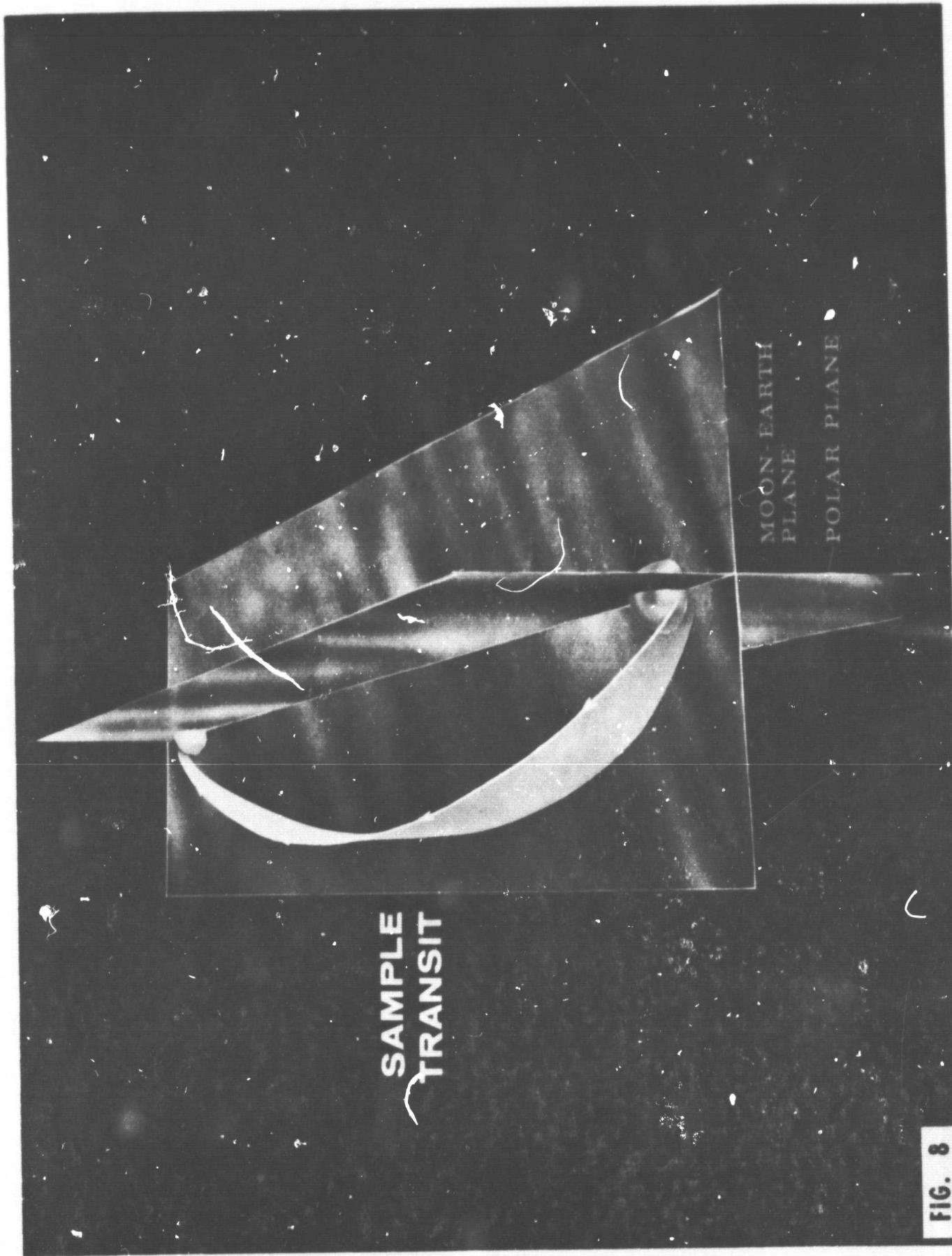


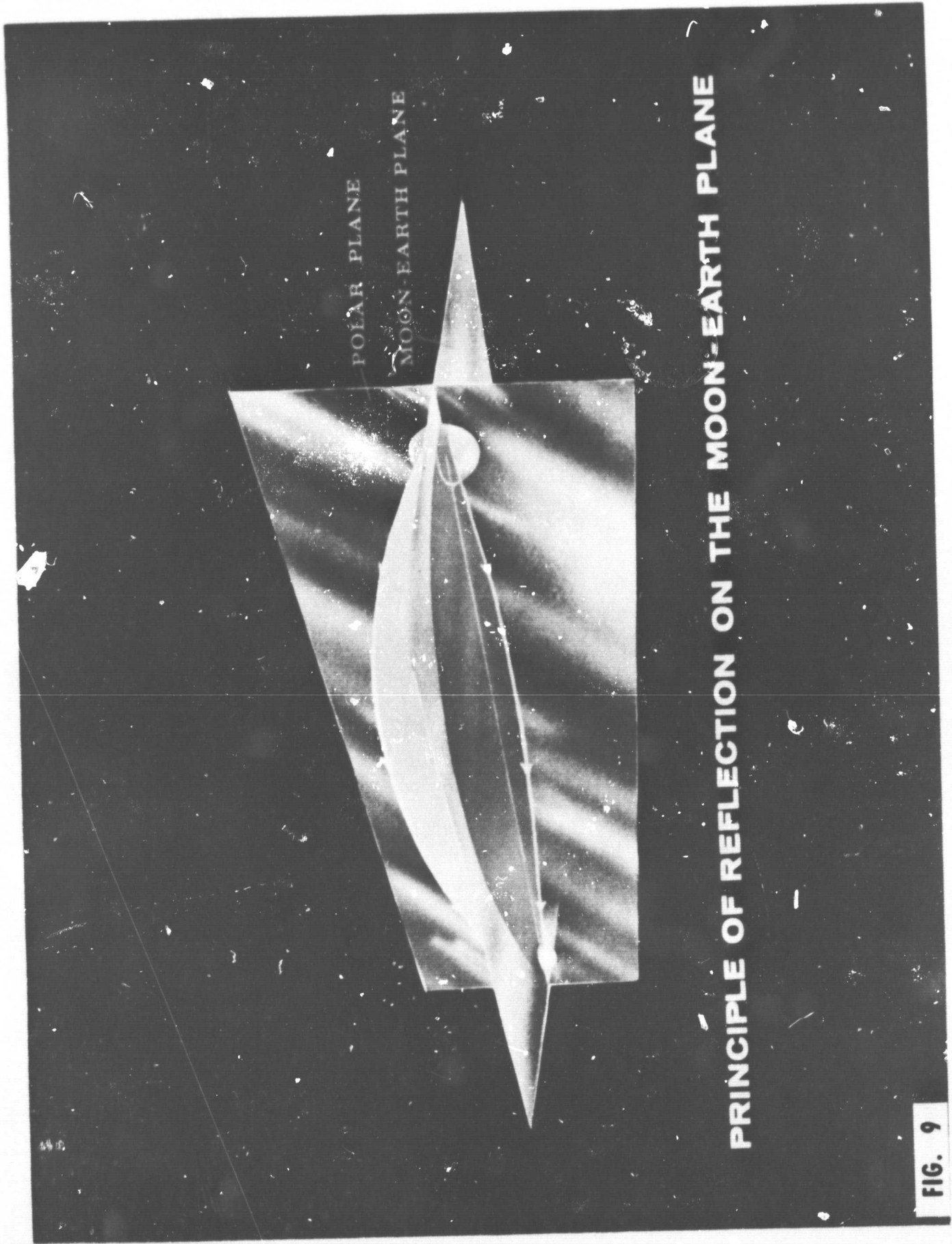
FIG. 7. AN INDIVIDUAL TRANSIT IS DESCRIBED BY REFERENCE TO ITS COORDINATES AT THE POINT OF NEAREST APPROACH TO EARTH OR TO MOON



SAMPLE
TRANSIT

MOON-EARTH
PLANE
POLAR PLANE

FIG. 8



PRINCIPLE OF REFLECTION ON THE MOON-EARTH PLANE

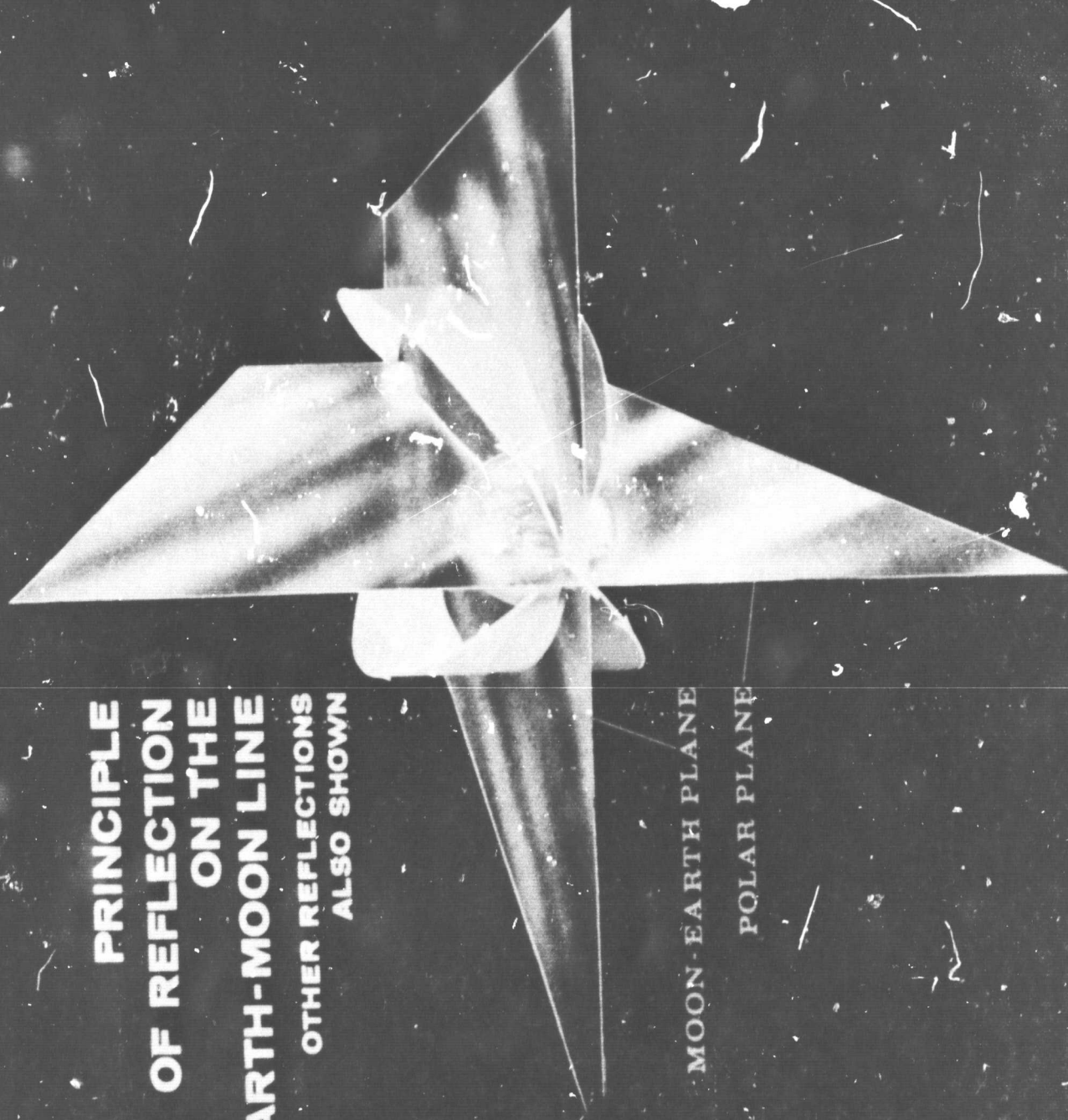
FIG. 9

**PRINCIPLE OF REFLECTION
ON THE POLAR PLANE**



FIG. 10

**PRINCIPLE
OF REFLECTION
ON THE
EARTH-MOON LINE
OTHER REFLECTIONS
ALSO SHOWN**



MOON-EARTH PLANE
POLAR PLANE

FIG. 11

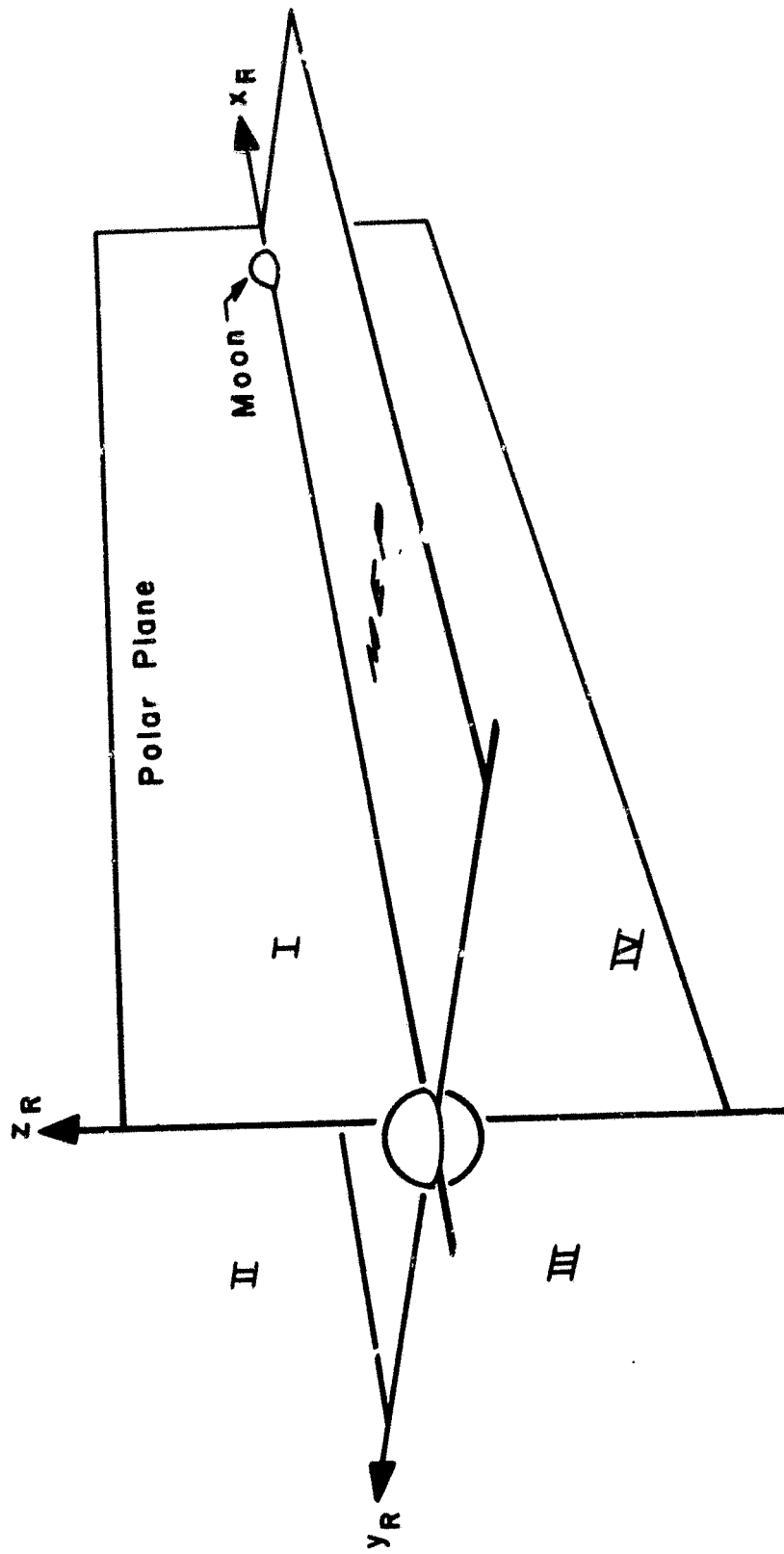


FIG. 12. QUADRANTS IN ROTATING EARTH-MOON SPACE

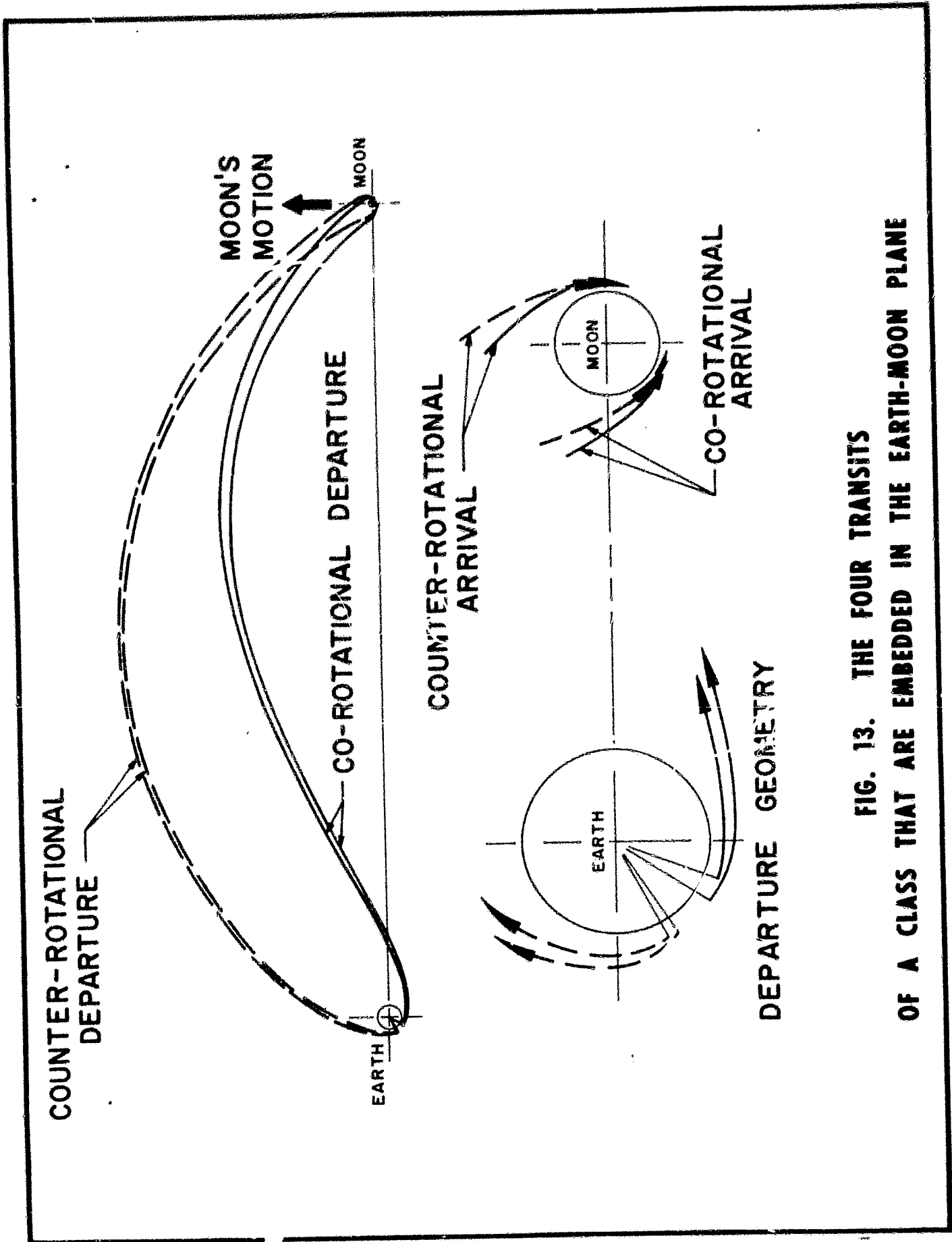
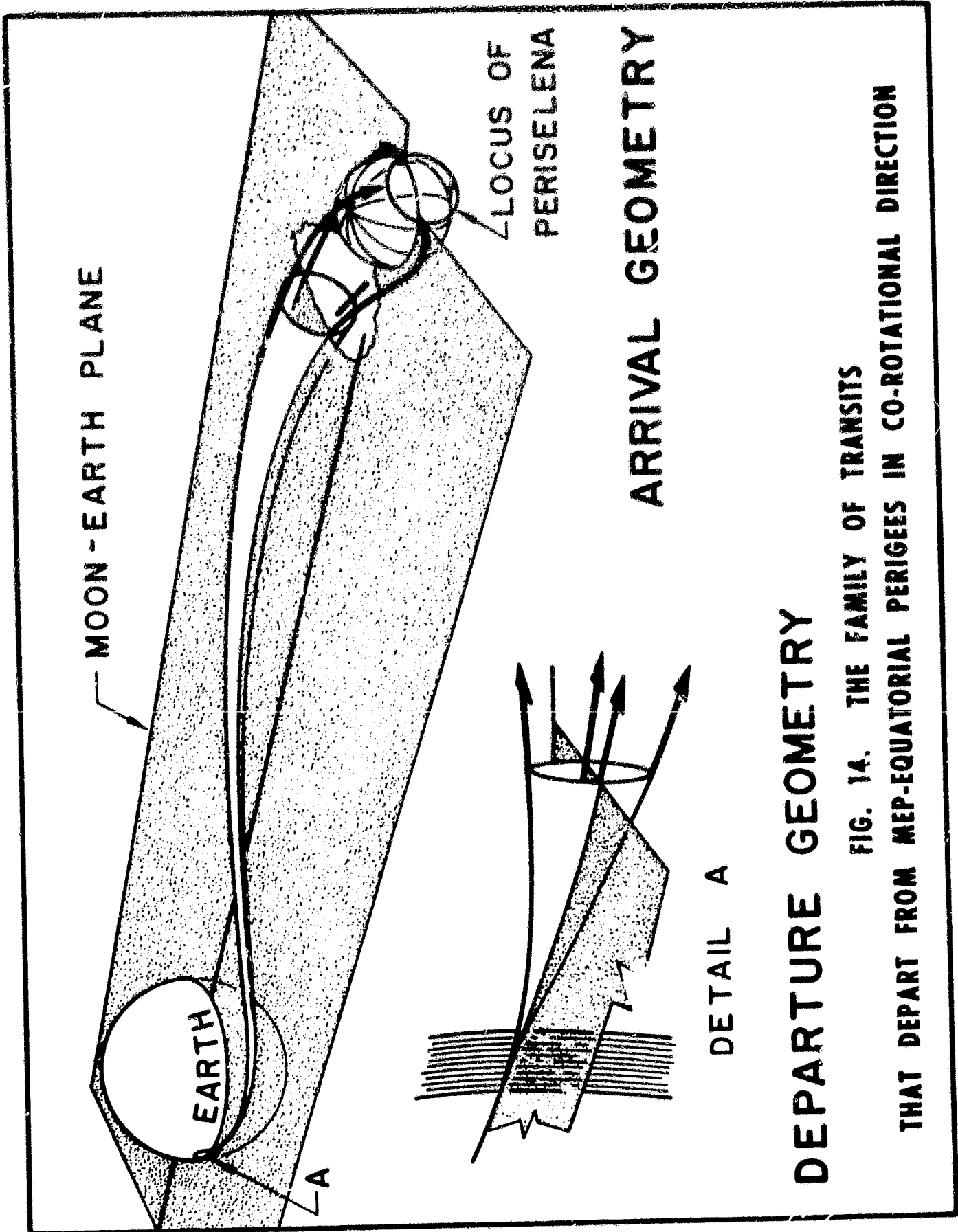


FIG. 13. THE FOUR TRANSITS OF A CLASS THAT ARE EMBEDDED IN THE EARTH-MOON PLANE



DEPARTURE GEOMETRY

FIG. 14. THE FAMILY OF TRANSITS THAT DEPART FROM MEP-EQUATORIAL PERIGEES IN CO-ROTATIONAL DIRECTION

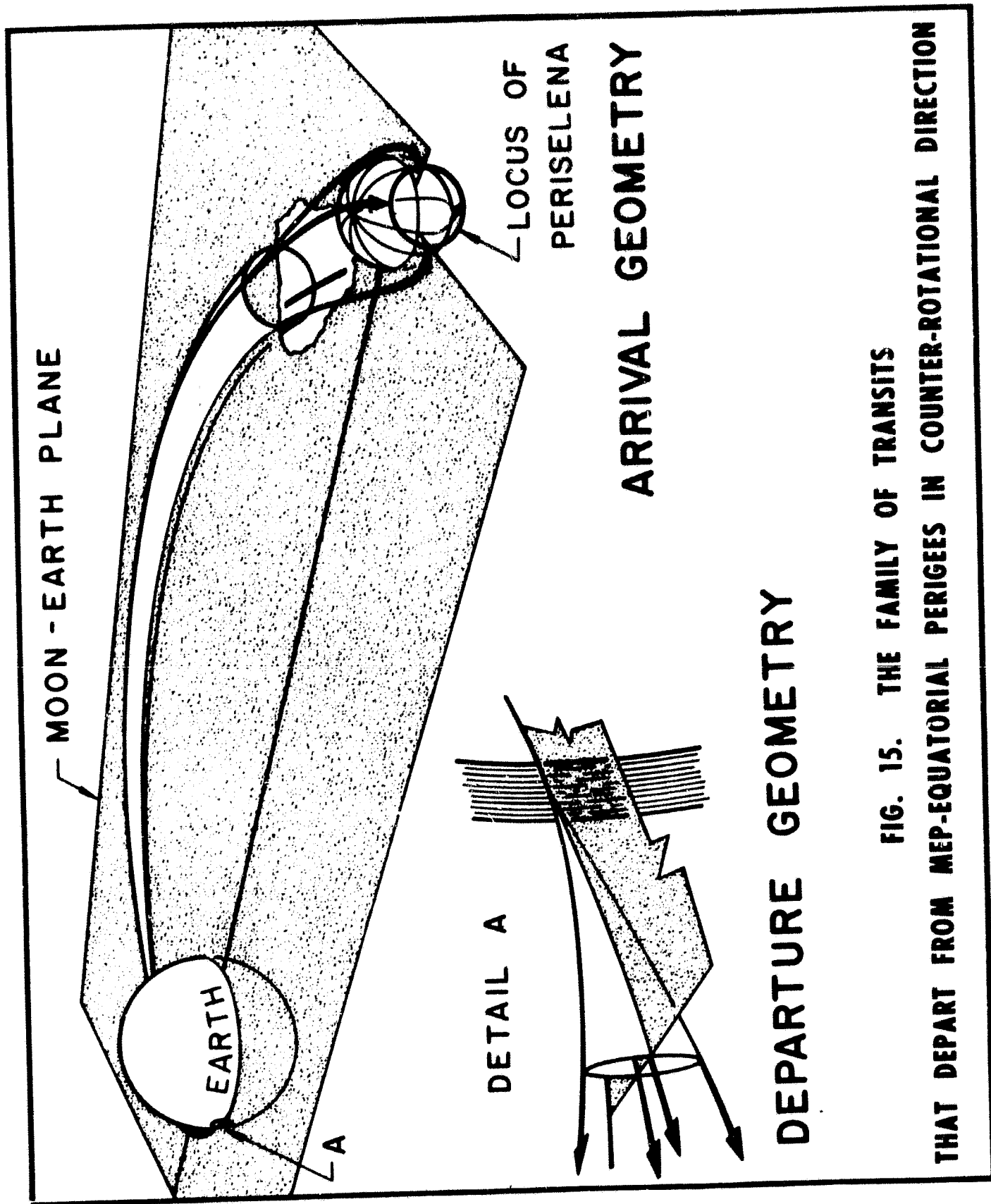
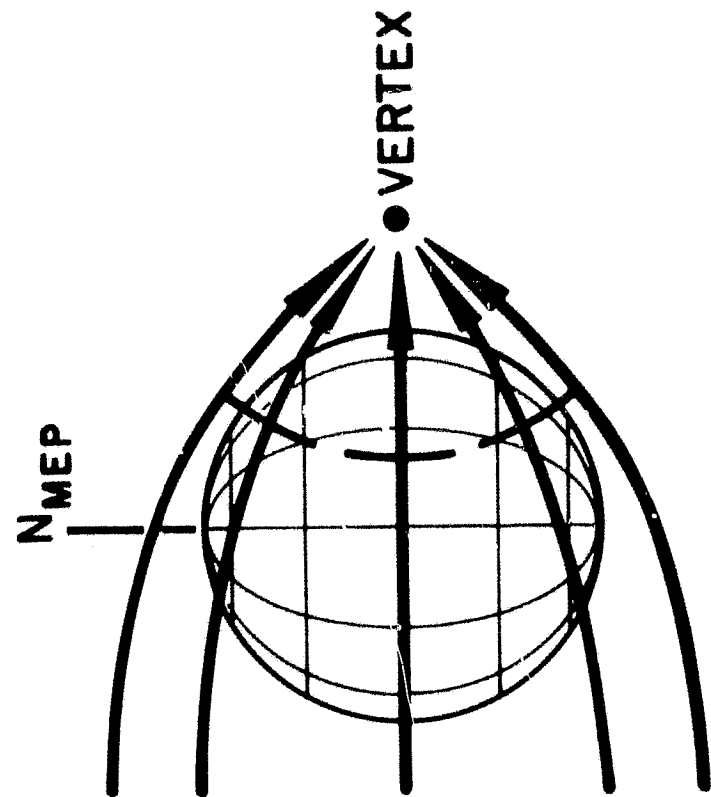
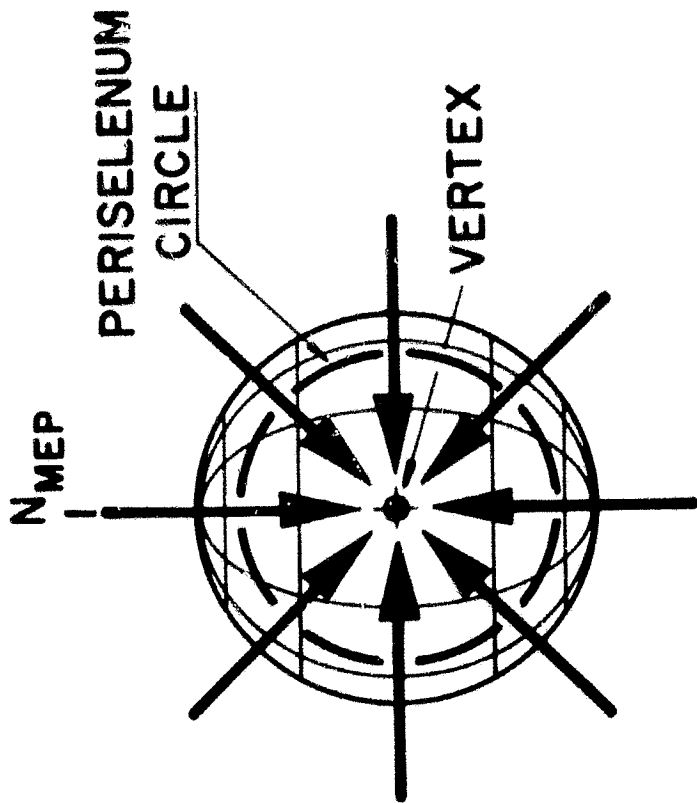


FIG. 15. THE FAMILY OF TRANSITS THAT DEPART FROM MEP-EQUATORIAL PERIGEES IN COUNTER-ROTATIONAL DIRECTION



**SIDE VIEW OF
TRANSITS NEAR MOON**



**VERTEX-CENTERED
VIEW OF TRANSITS**

**FIG. 16. TRANSITS OF A FAMILY PASS THROUGH A REGION
SMALL ENOUGH AS TO BE REPRESENTED BY A POINT
(THE TERM 'VERTEX' IS ADOPTED FOR THIS POINT)**

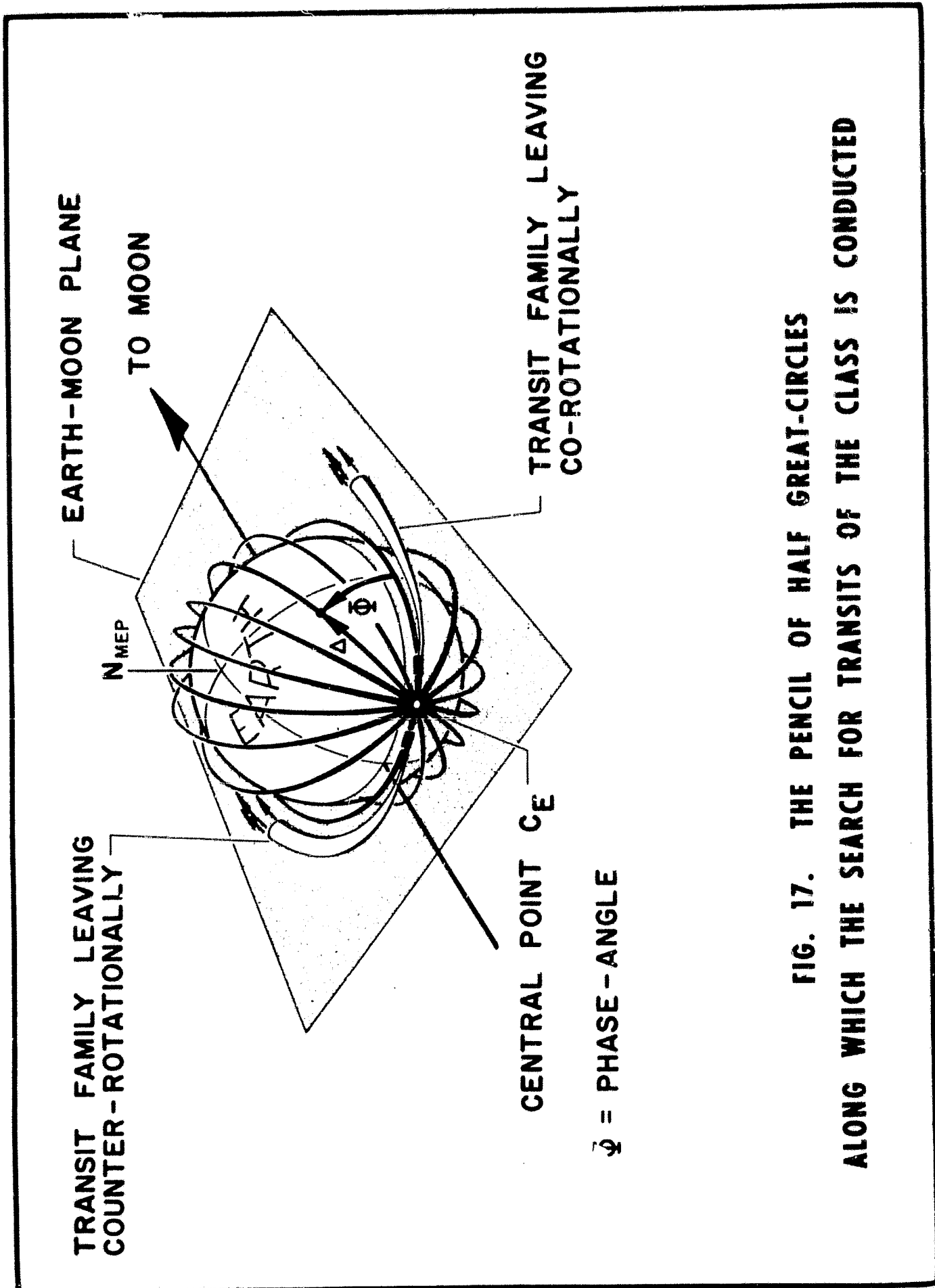


FIG. 17. THE PENCIL OF HALF GREAT-CIRCLES ALONG WHICH THE SEARCH FOR TRANSITS OF THE CLASS IS CONDUCTED

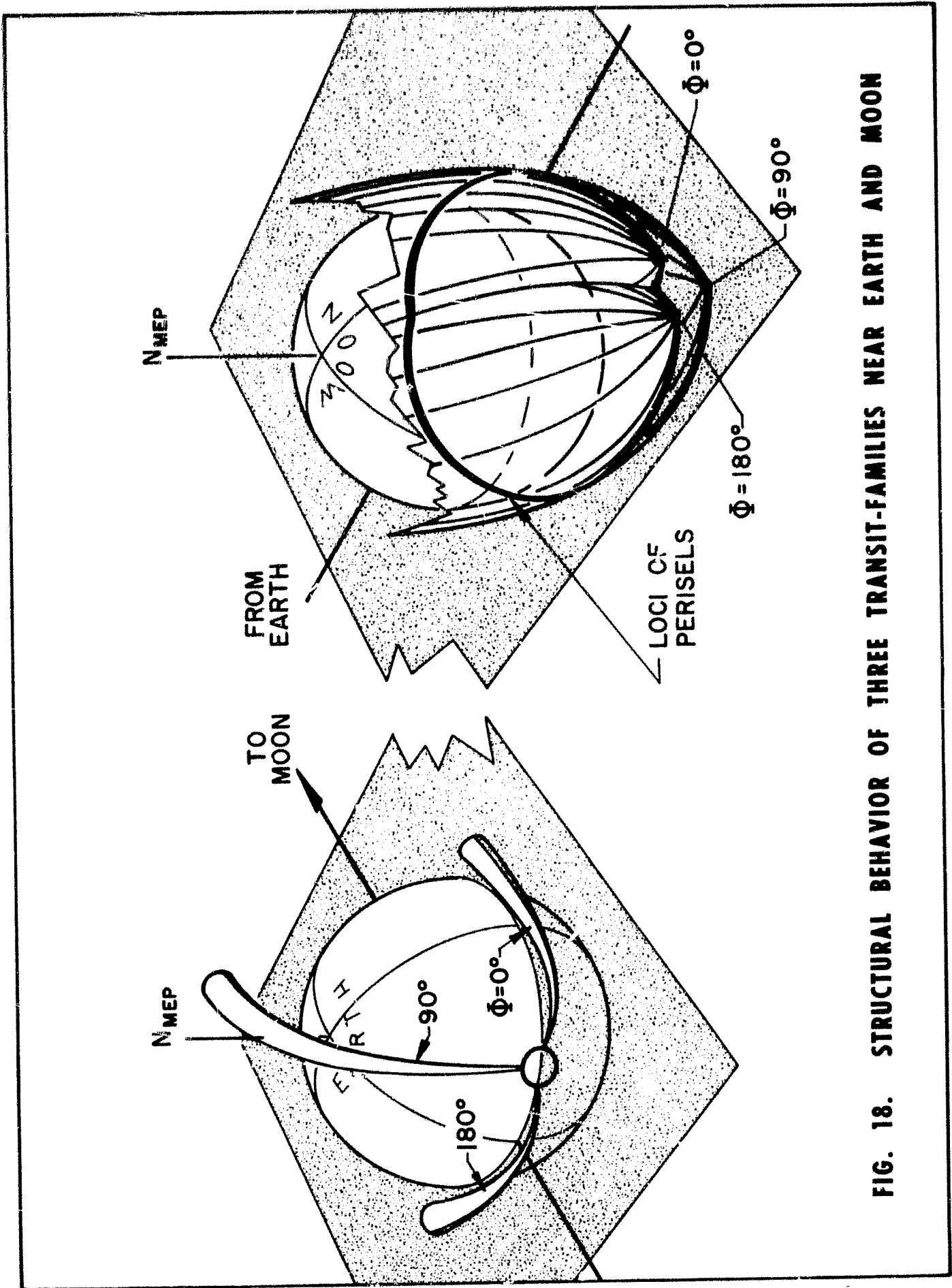


FIG. 18. STRUCTURAL BEHAVIOR OF THREE TRANSIT-FAMILIES NEAR EARTH AND MOON

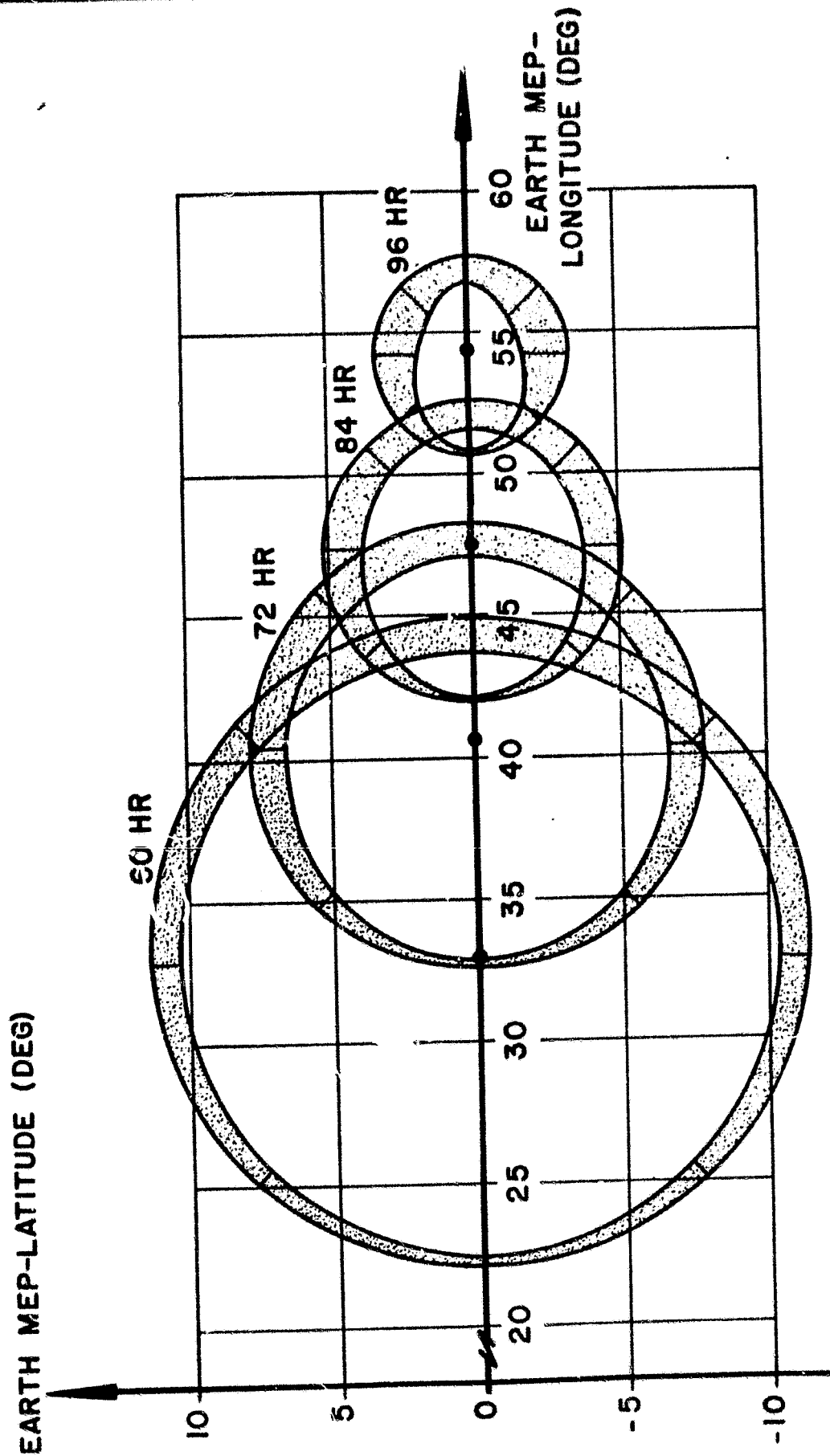
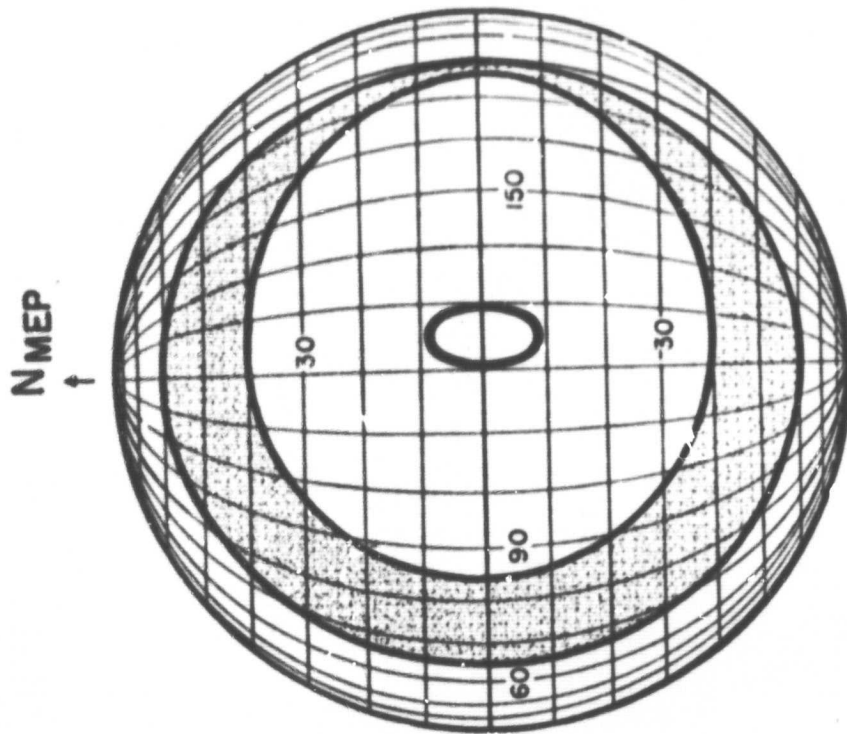
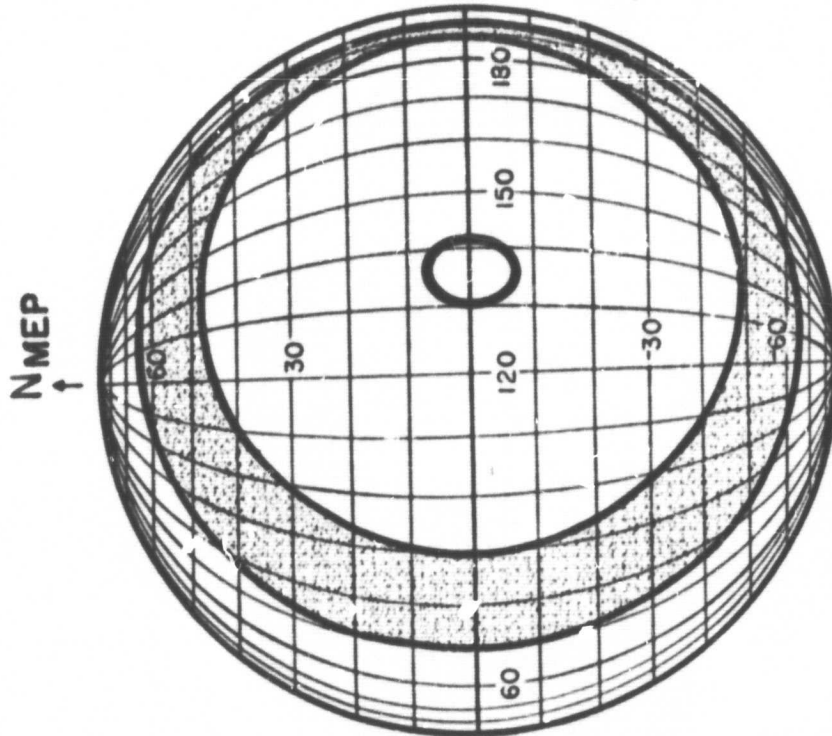


FIG. 20. LOCI OF ALL POSSIBLE PERIGEEES FOR THE CLASSES $C(T_i, 6,555 \text{ km}, 1,923 \text{ km})$, $T_i = 60, 72, 84 \text{ AND } 96 \text{ hr}$

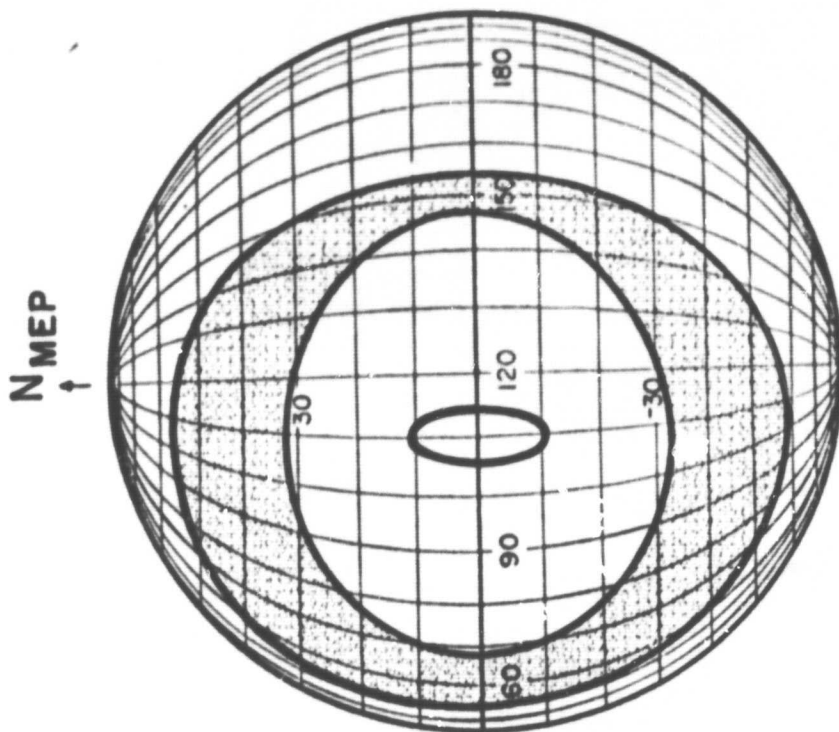


72 HR

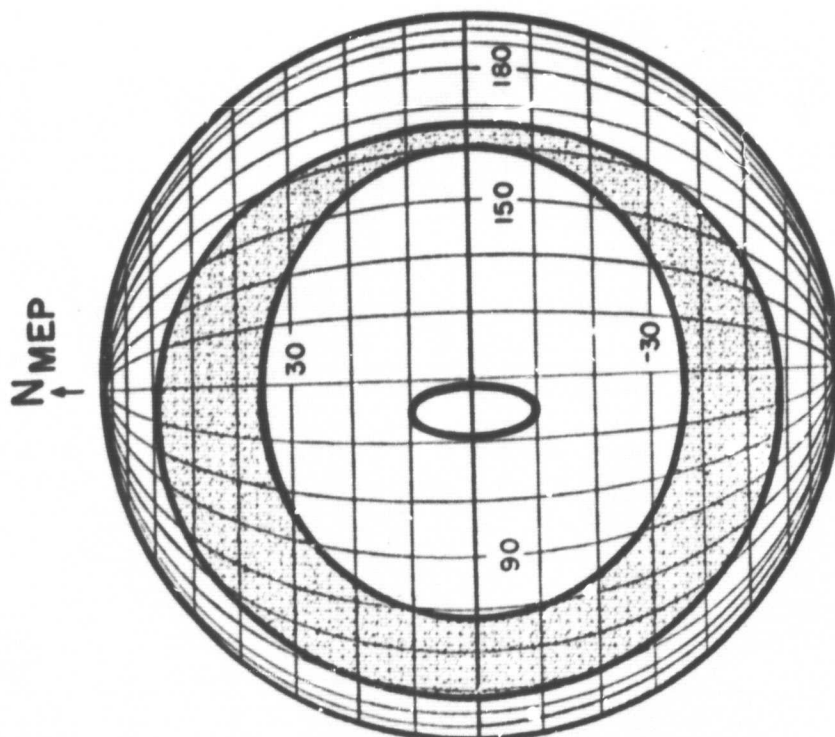


60 HR

FIG. 21. SURVEY OF ARRIVAL AREAS AT MOON FOR TRANSIT CLASSES C (60 HR, 6555 KM, 1923 KM) AND C (72 HR, 6555 KM, 1923 KM)



96 HR



84 HR

FIG. 22. SURVEY OF ARRIVAL AREAS AT MOON FOR TRANSIT CLASSES C (84 HR, 6555 KM, 1923 KM) AND C (96 HR, 6555 KM, 1923 KM)

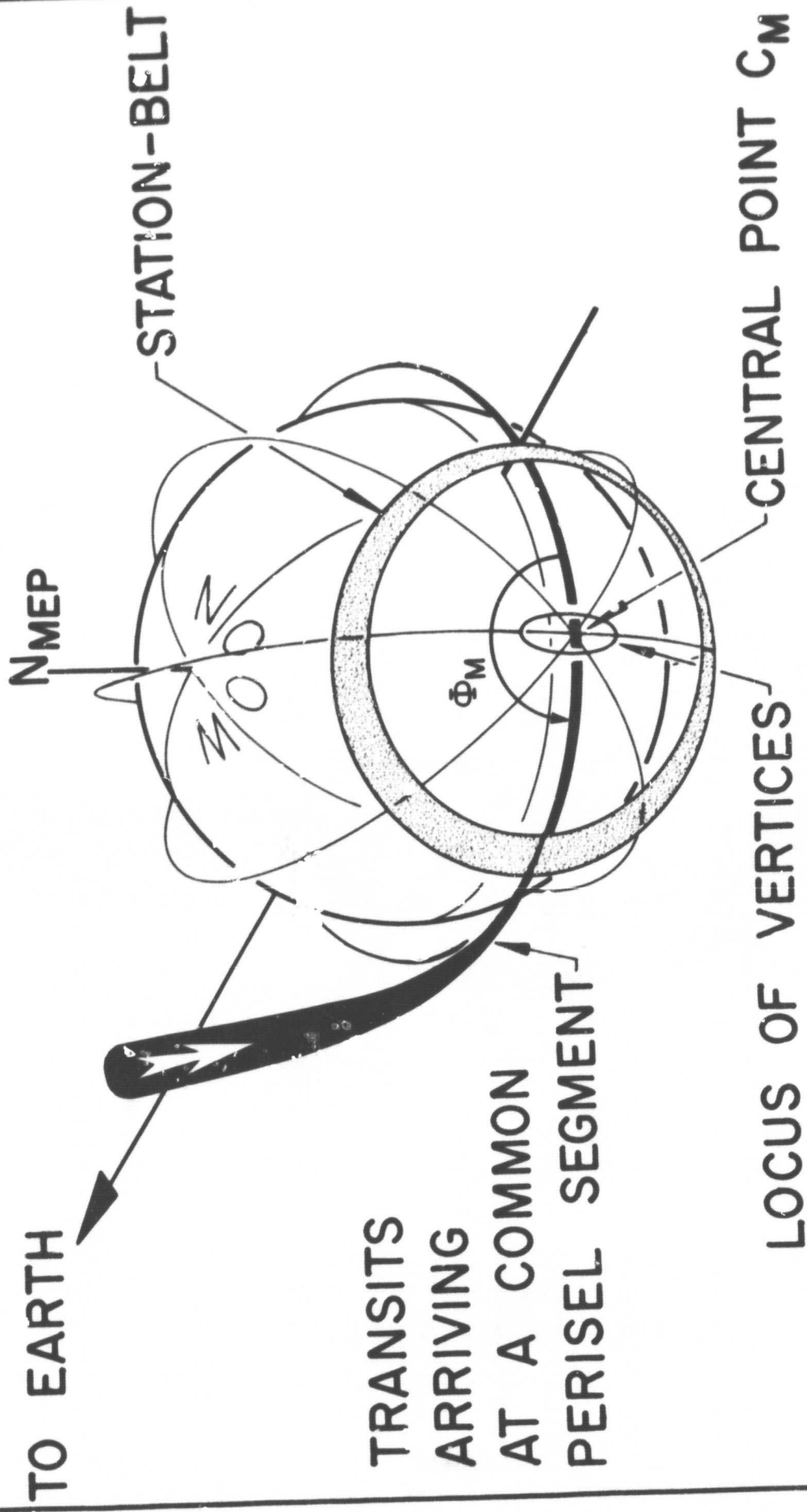


FIG. 23. TRANSITS REACHING MOON ON COMMON LUNAR PHASE ANGLE

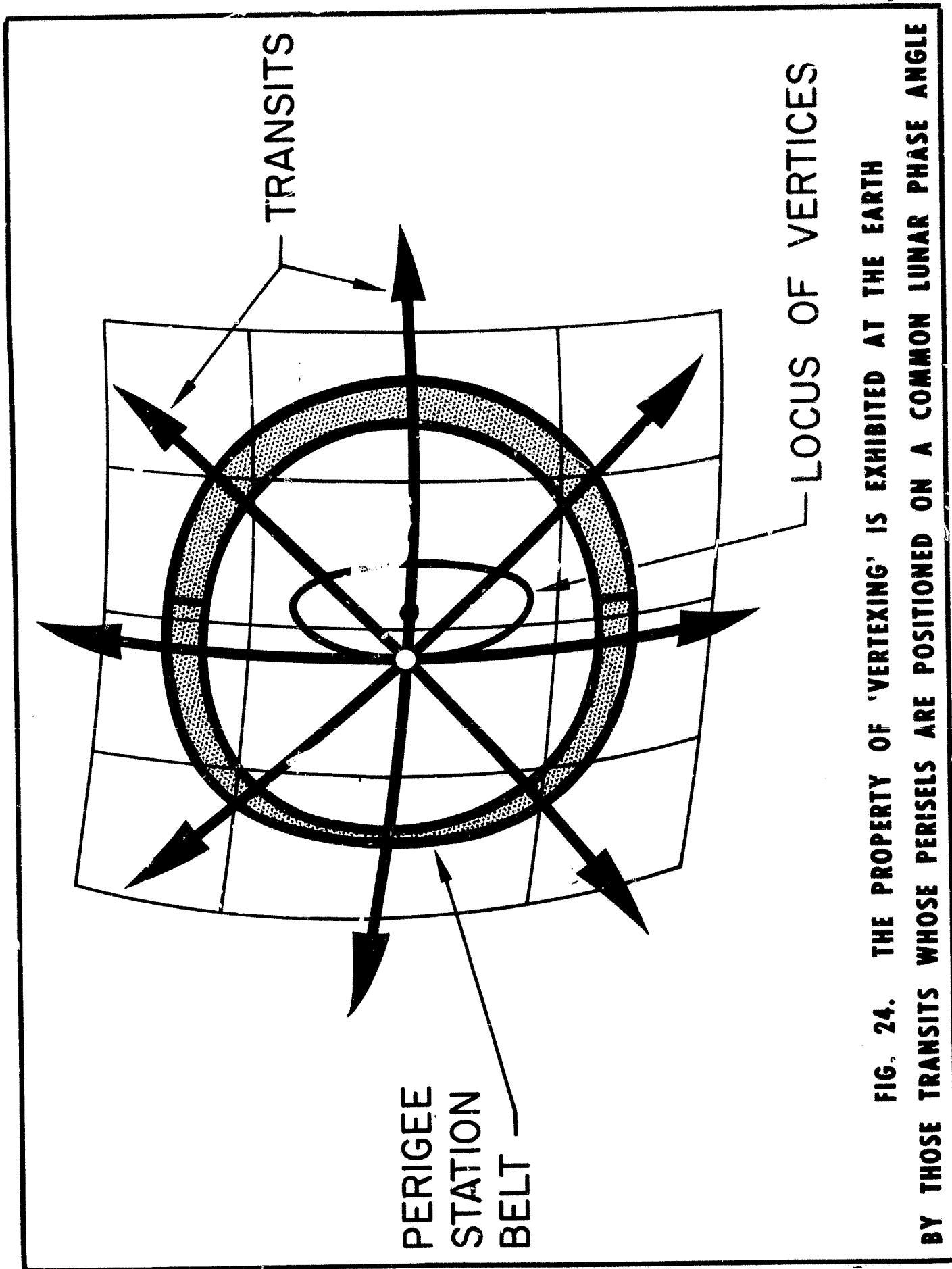
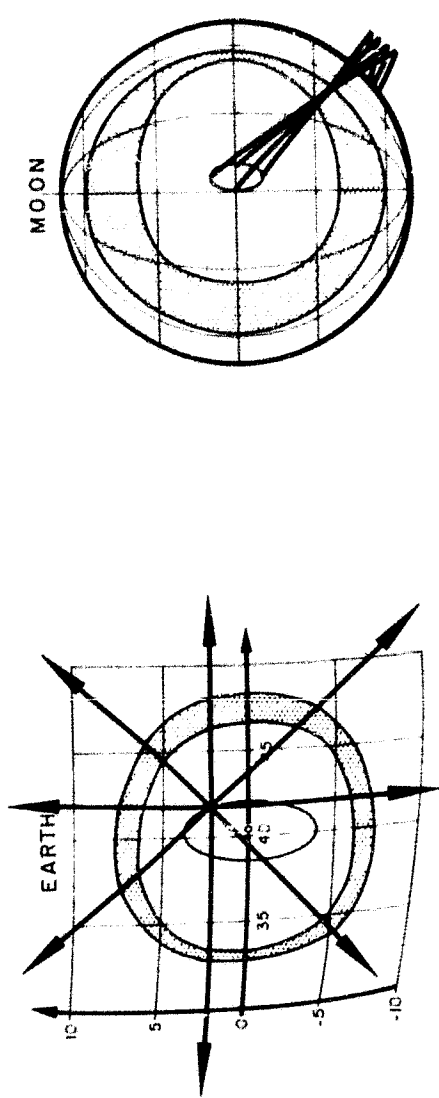
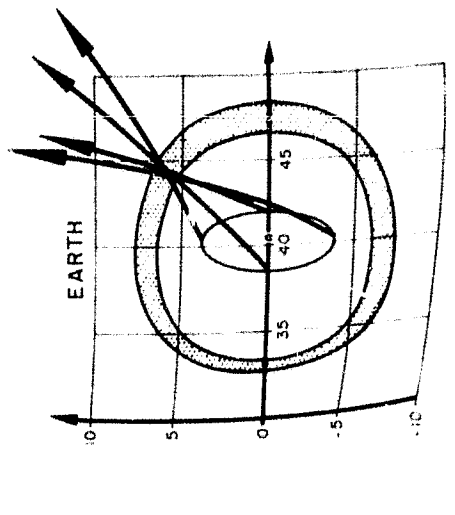


FIG. 24. THE PROPERTY OF 'VERTEXING' IS EXHIBITED AT THE EARTH BY THOSE TRANSITS WHOSE PERISELS ARE POSITIONED ON A COMMON LUNAR PHASE ANGLE



VERTEX ↔ STATION - SEGMENT



STATION - SEGMENT ↔ VERTEX

FIG. 25. SCHEMATIC SHOWING OF THE FUNDAMENTAL RELATIONSHIPS BETWEEN VERTICES AT ONE BODY AND BELT-SEGMENTS AT THE OTHER BODY

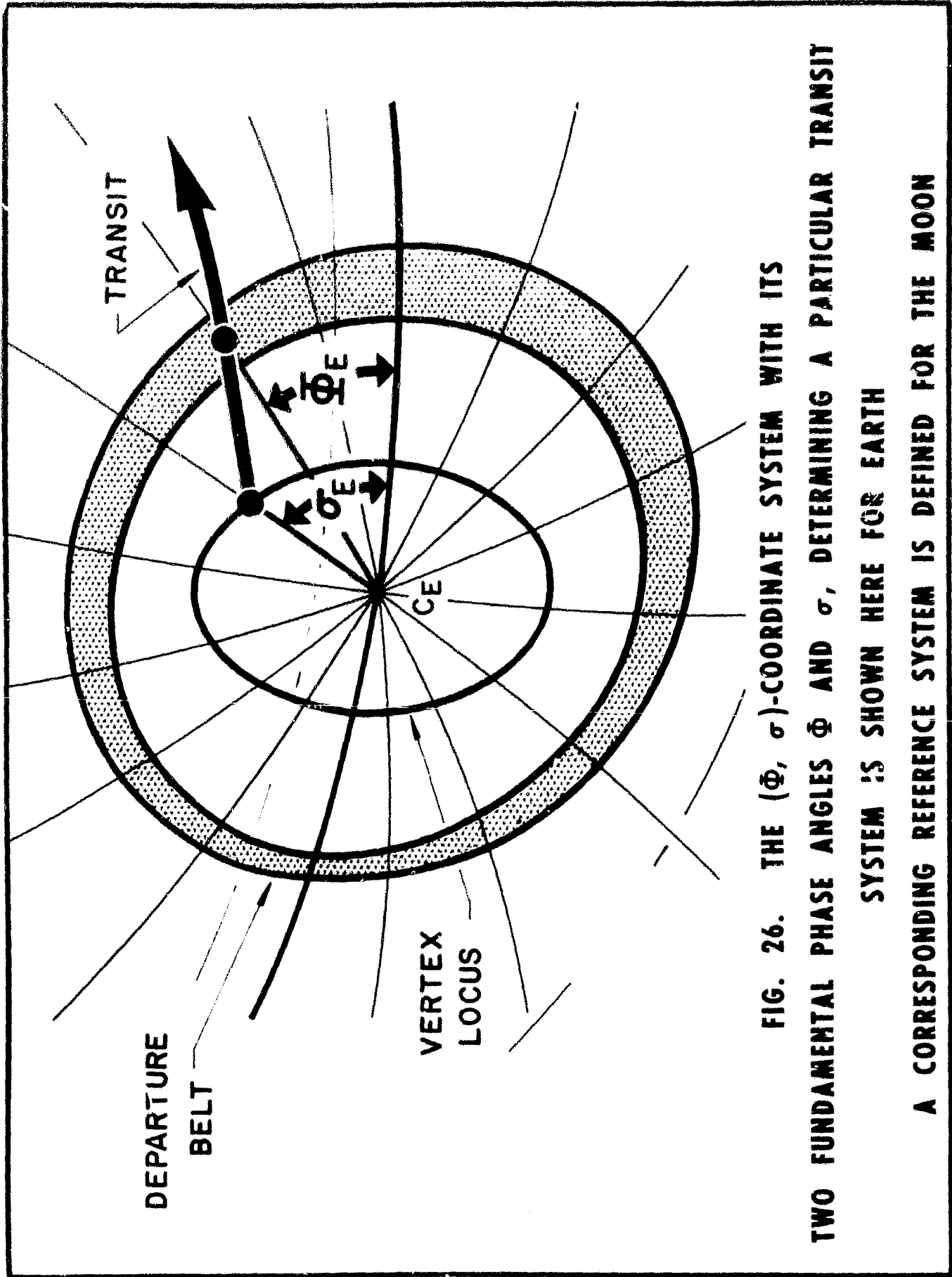


FIG. 26. THE (Φ, σ) -COORDINATE SYSTEM WITH ITS TWO FUNDAMENTAL PHASE ANGLES Φ AND σ , DETERMINING A PARTICULAR TRANSIT SYSTEM IS SHOWN HERE FOR EARTH A CORRESPONDING REFERENCE SYSTEM IS DEFINED FOR THE MOON

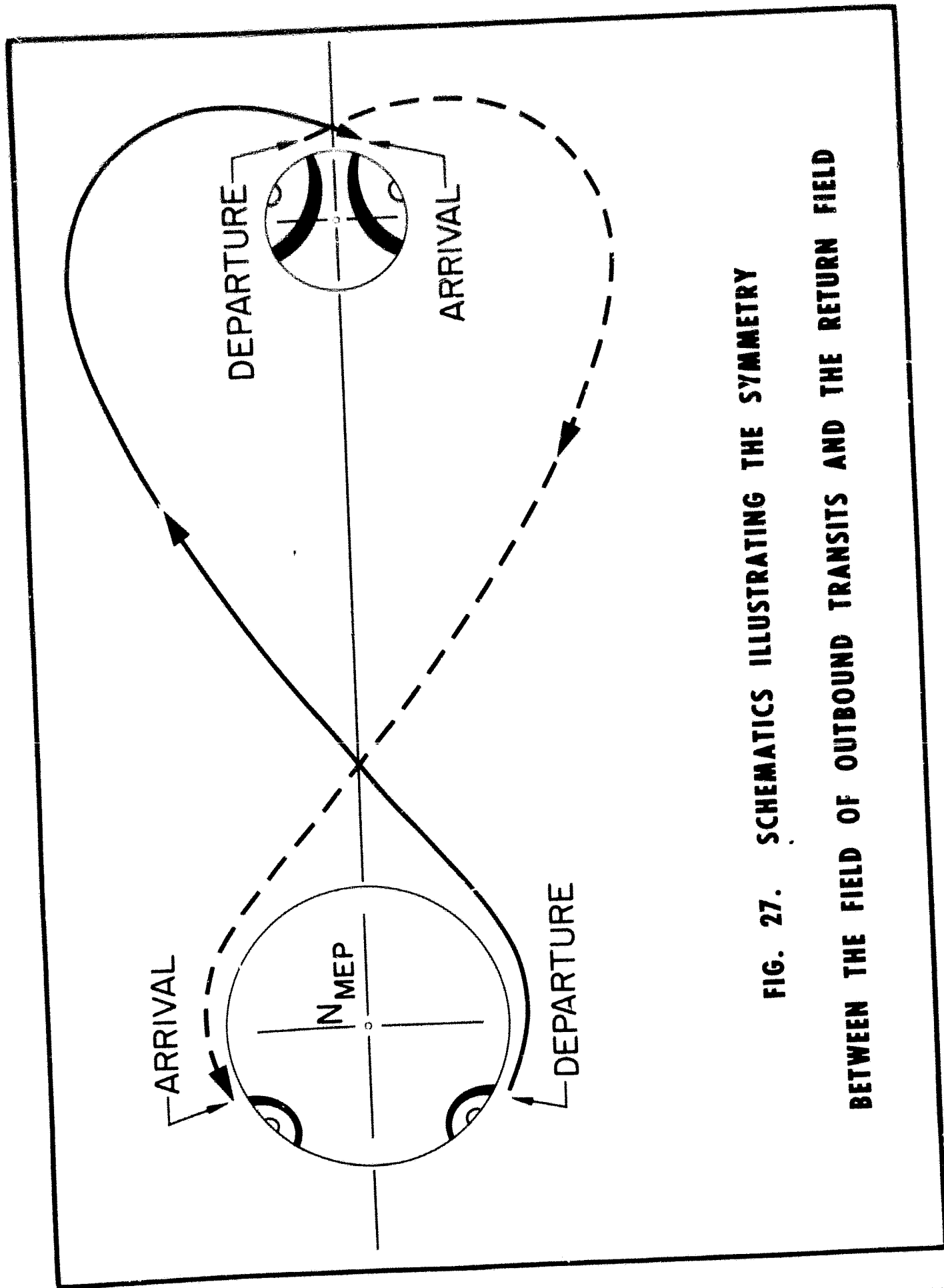


FIG. 27. SCHEMATICS ILLUSTRATING THE SYMMETRY BETWEEN THE FIELD OF OUTBOUND TRANSITS AND THE RETURN FIELD

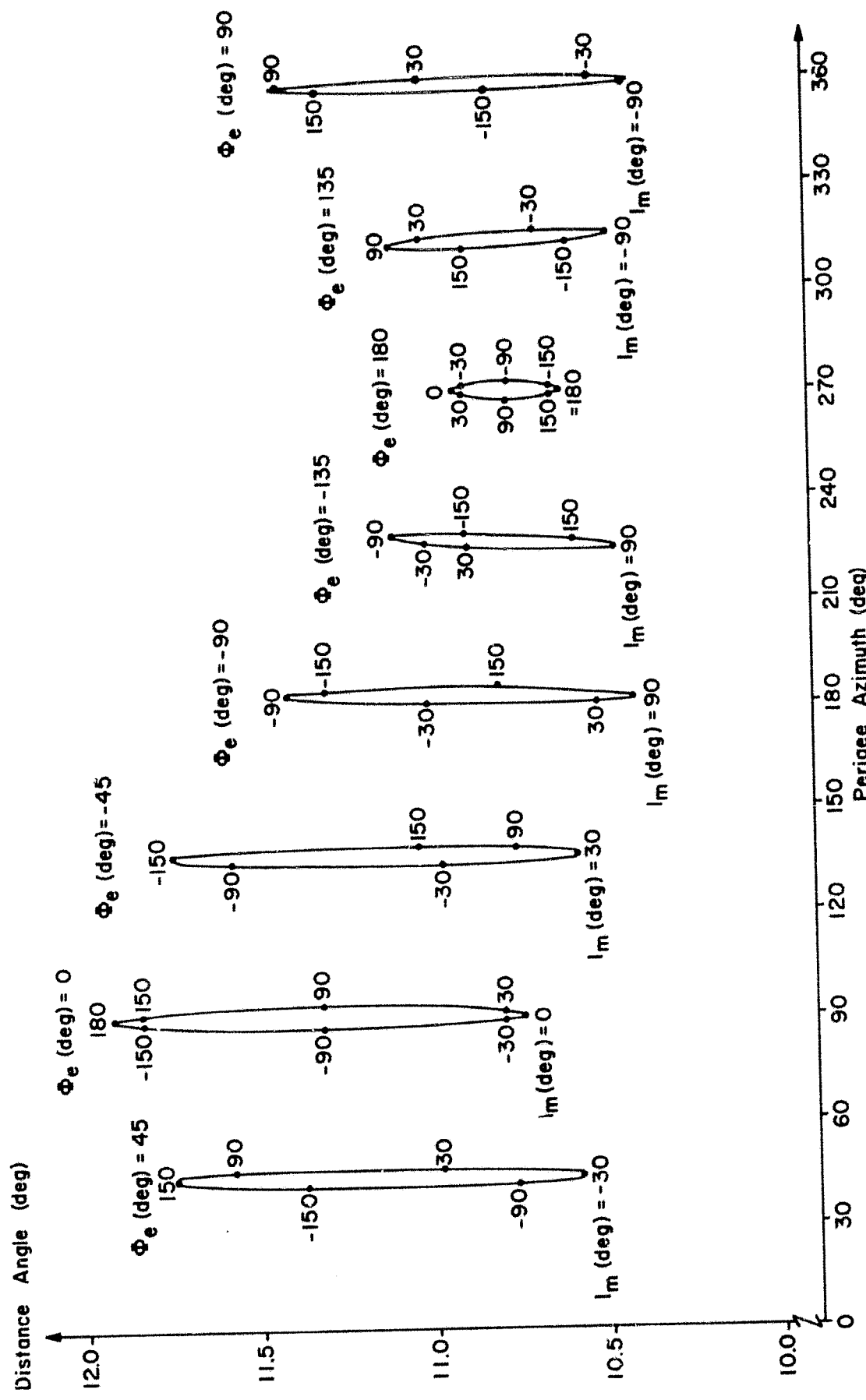


FIG. 28. THE VARIATION OF DEPARTURE AZIMUTH ANGLES AS A FUNCTION OF THE DISTANCE ANGLE FOR C (60 HR, 6555 KM, 1923 KM)

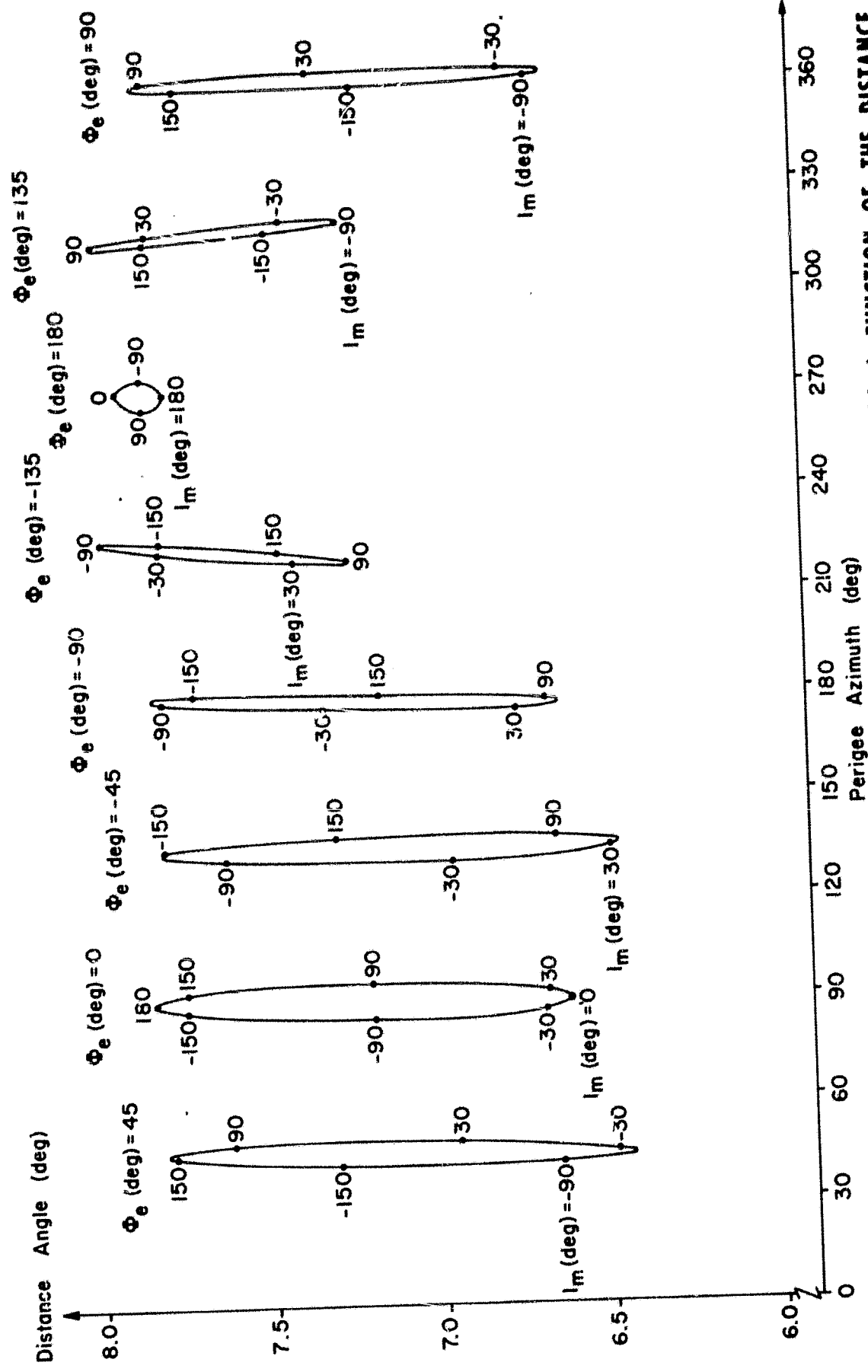


FIG. 29. THE VARIATION OF DEPARTURE AZIMUTH ANGLES AS A FUNCTION OF THE DISTANCE ANGLE FOR C (72 HR, 6555 KM, 1923 KM)

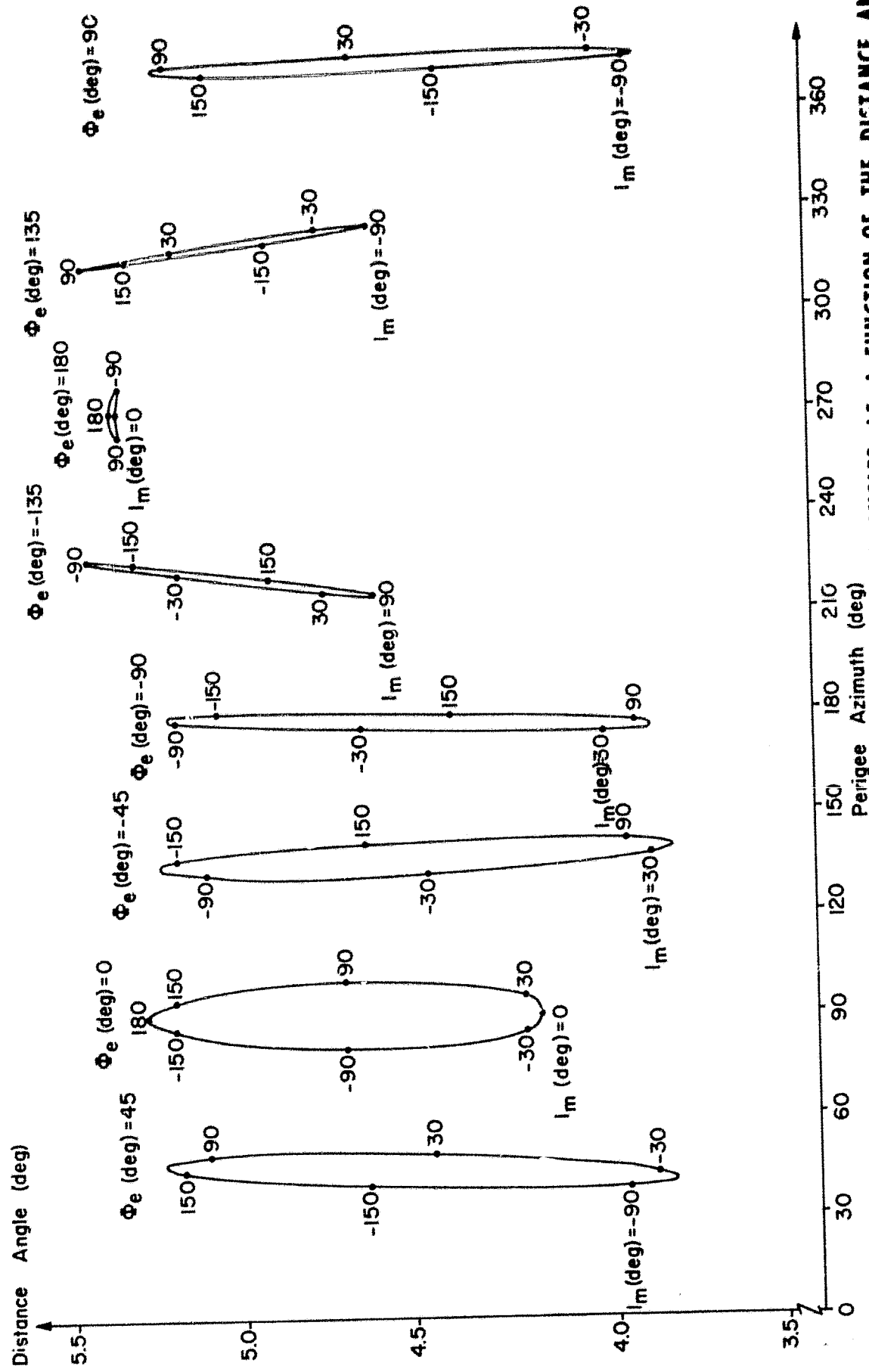


FIG. 30. THE VARIATION OF DEPARTURE AZIMUTH ANGLES AS A FUNCTION OF THE DISTANCE ANGLE FOR C (84 HR, 6555 KM, 1923 KM)

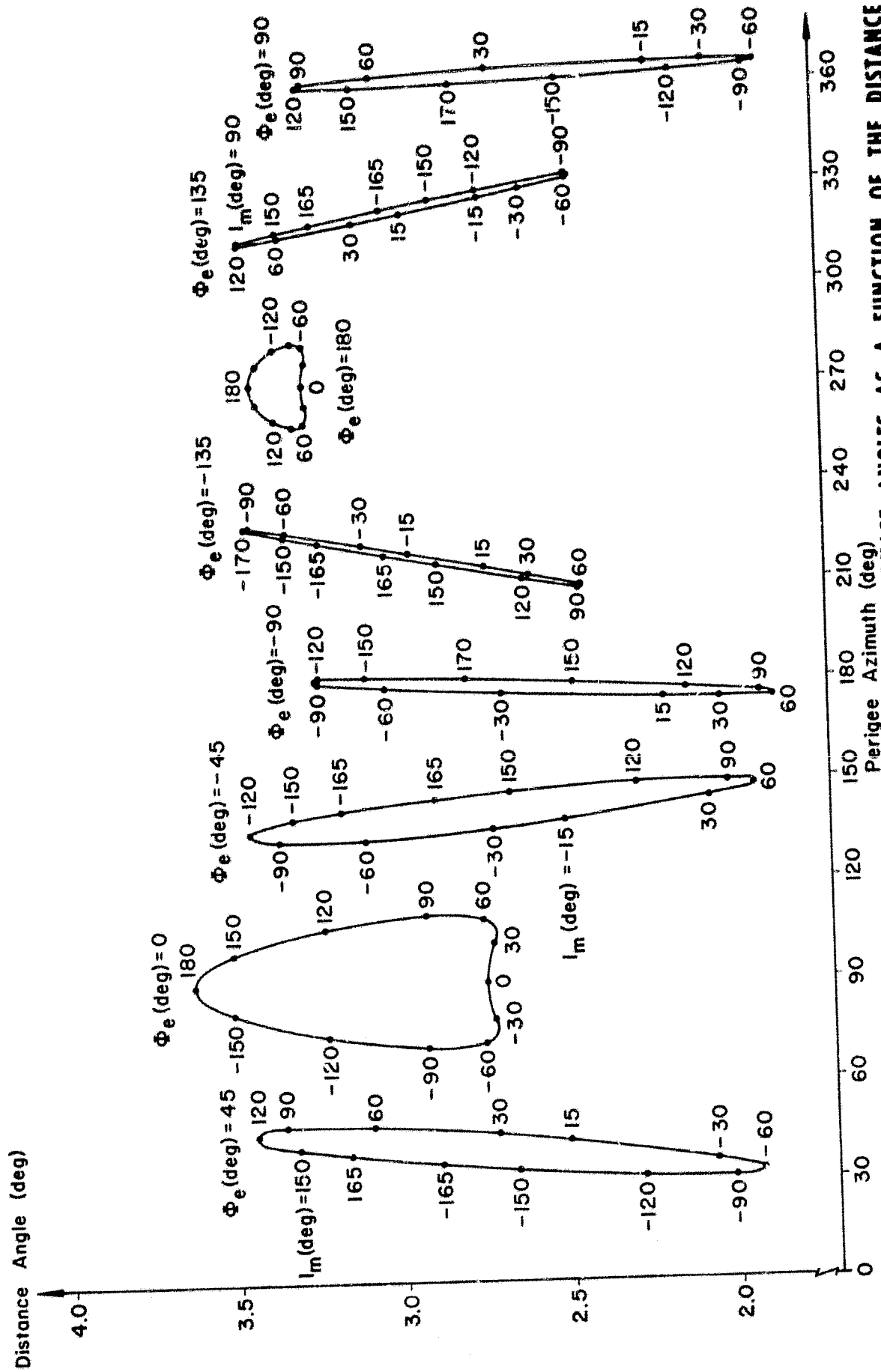


FIG. 31. THE VARIATION OF DEPARTURE AZIMUTH ANGLES AS A FUNCTION OF THE DISTANCE ANGLE ALONG VARIOUS PHASE ANGLES FOR C (96 HR, 6555 KM, 1923 KM)

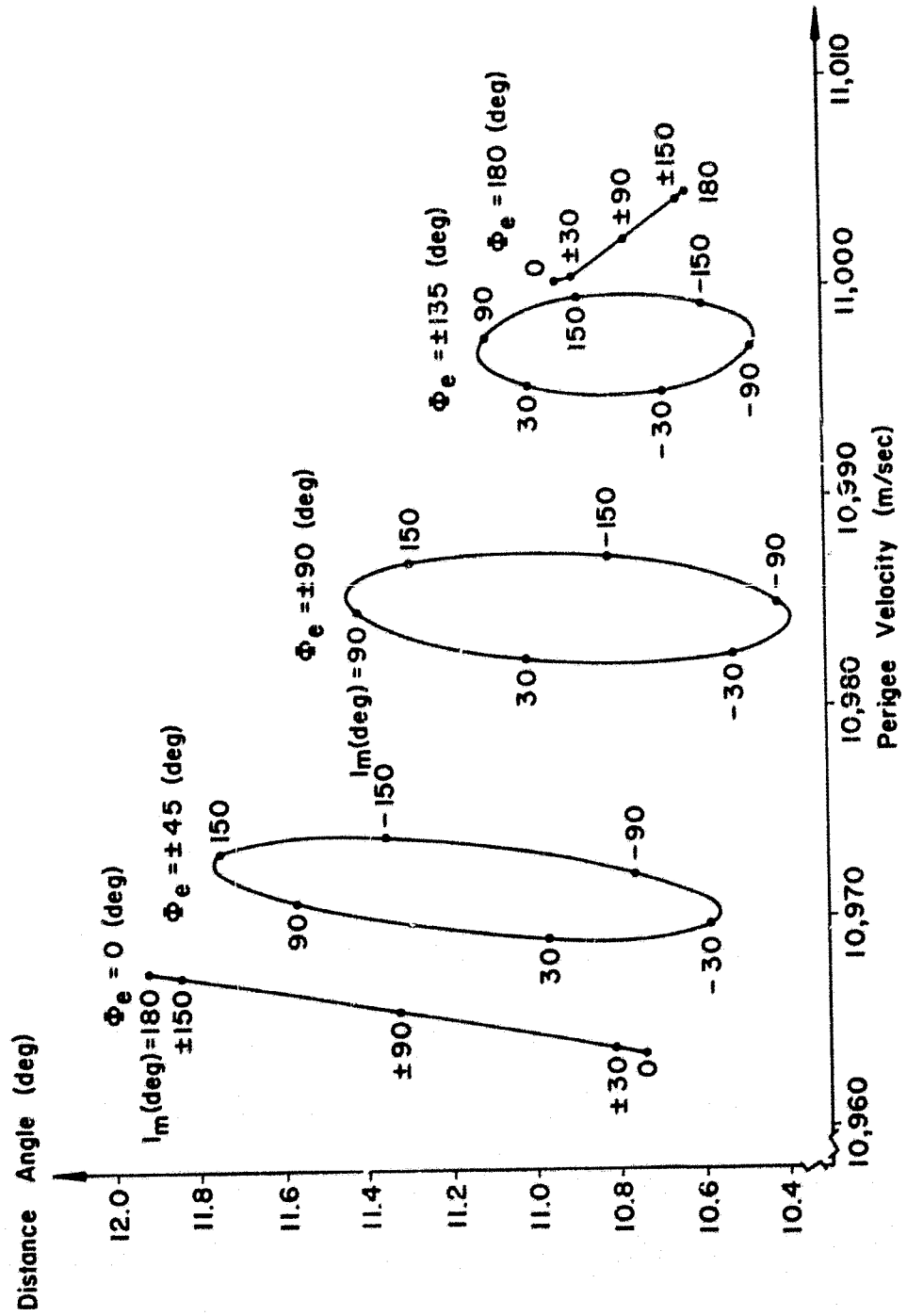


FIG. 32. VELOCITY REQUIREMENTS FOR THE INDICATED DEPARTURE PHASE ANGLES VS THE DISTANCE ANGLE FOR C (60 HR, 6555 KM, 1923 KM)

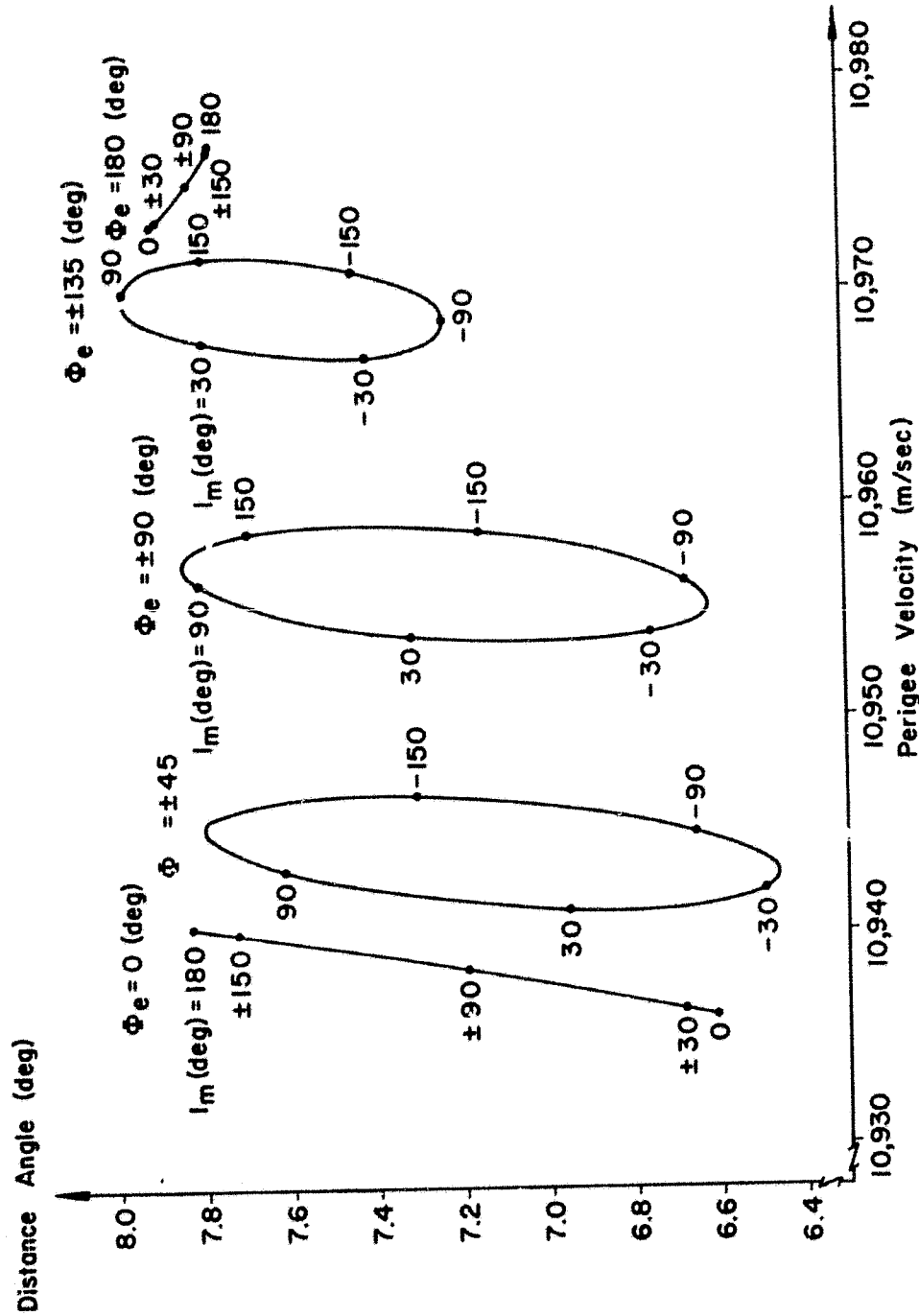


FIG. 33. VELOCITY REQUIREMENTS FOR THE INDICATED DEPARTURE PHASE ANGLES VS THE DISTANCE ANGLE FOR C (72 HR, 6555 KM, 1923 KM)

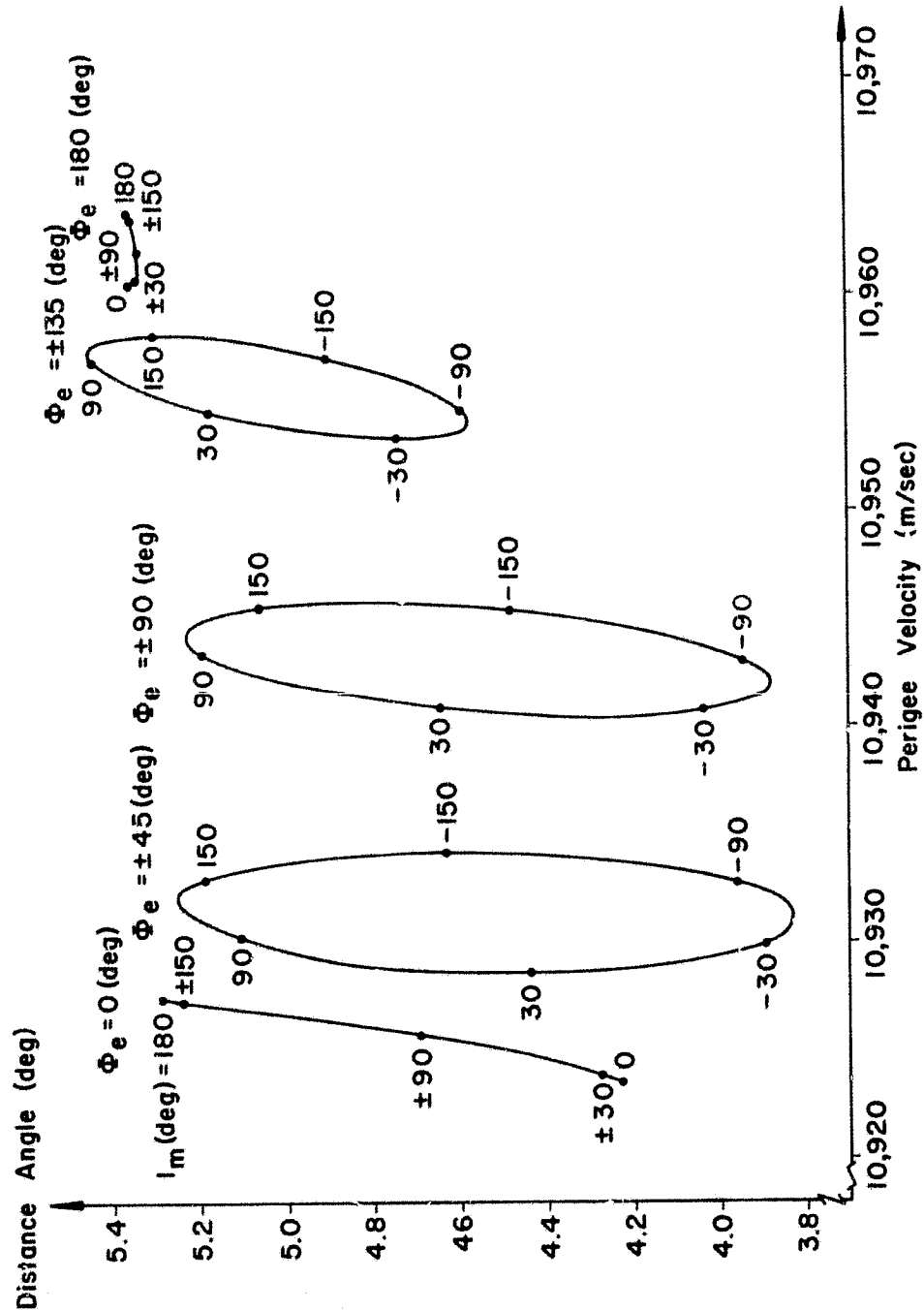


FIG. 34. VELOCITY REQUIREMENTS FOR THE INDICATED DEPARTURE PHASE ANGLES VS THE DISTANCE ANGLE FOR C (84 HR, 6555 KM, 1923 KM)

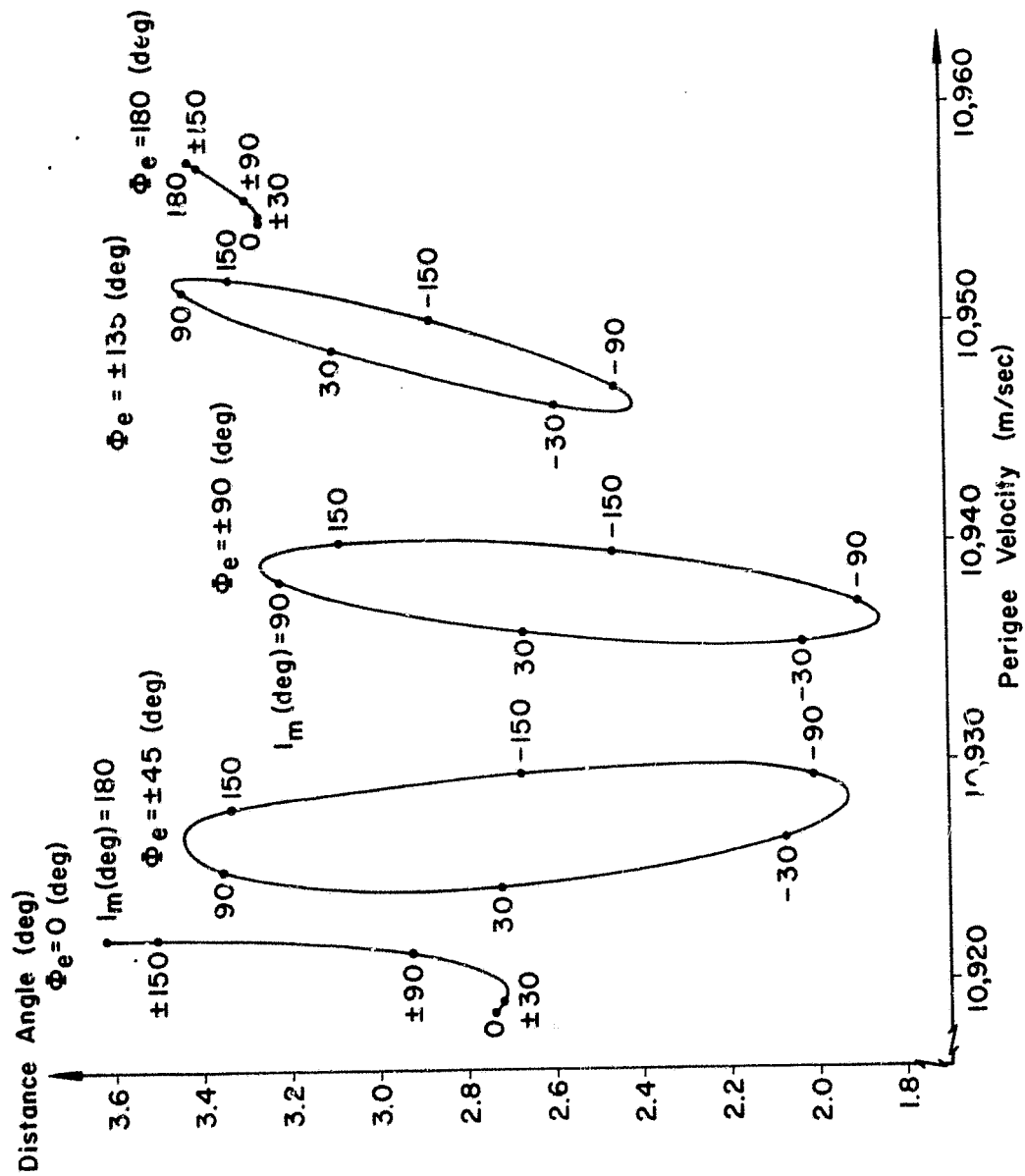


FIG. 35. VELOCITY REQUIREMENTS FOR THE INDICATED DEPARTURE PHASE ANGLES VS THE DISTANCE ANGLE FOR C (96 HR, 6555 KM, 1923 KM)

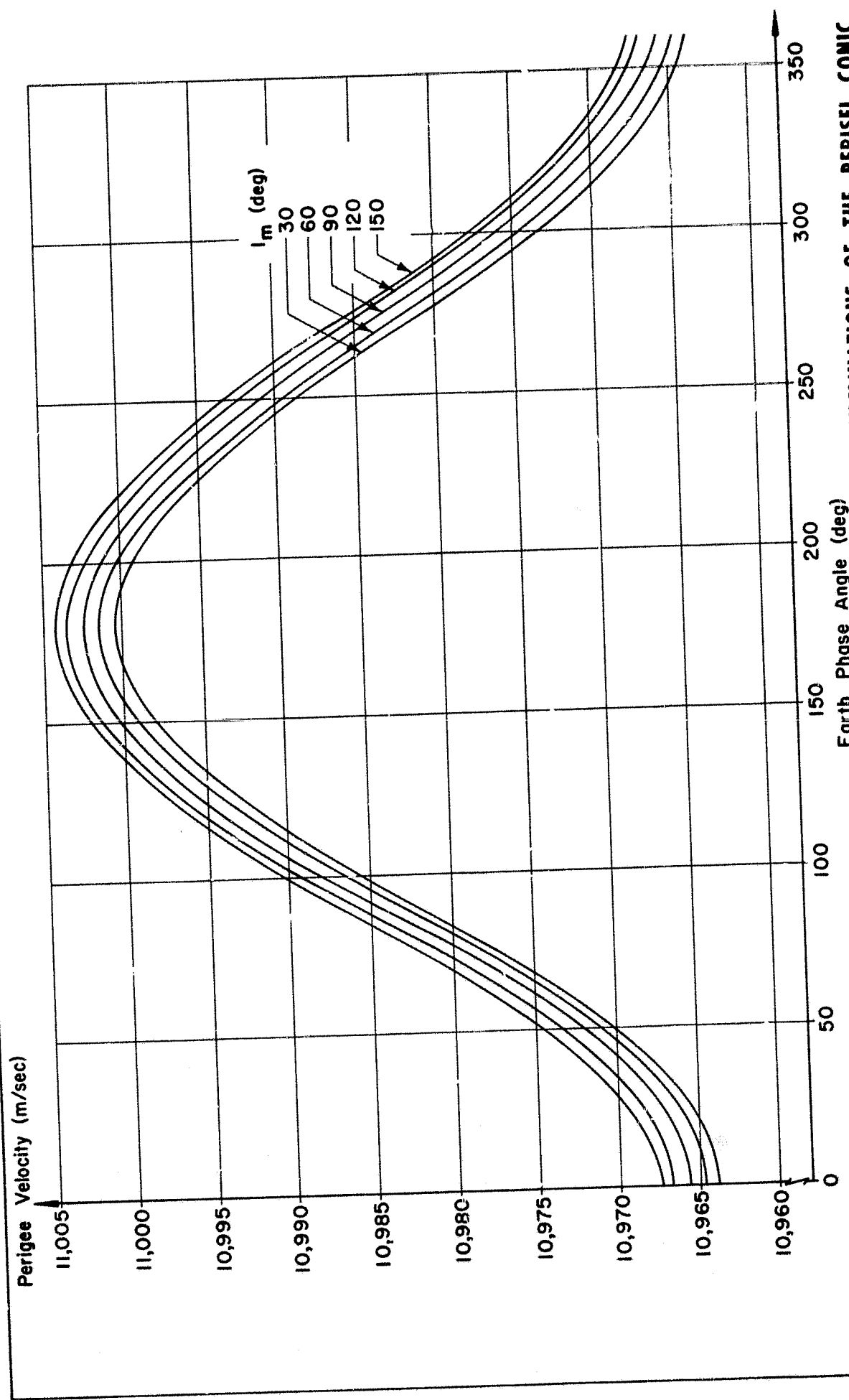


FIG. 36. PERIGEE VELOCITY VS EARTH PHASE ANGLE, Φ_p , FOR VARIOUS INCLINATIONS OF THE PERISEL CONIC FOR THE CLASS C (60 HR, 6555 KM, 1923 KM)

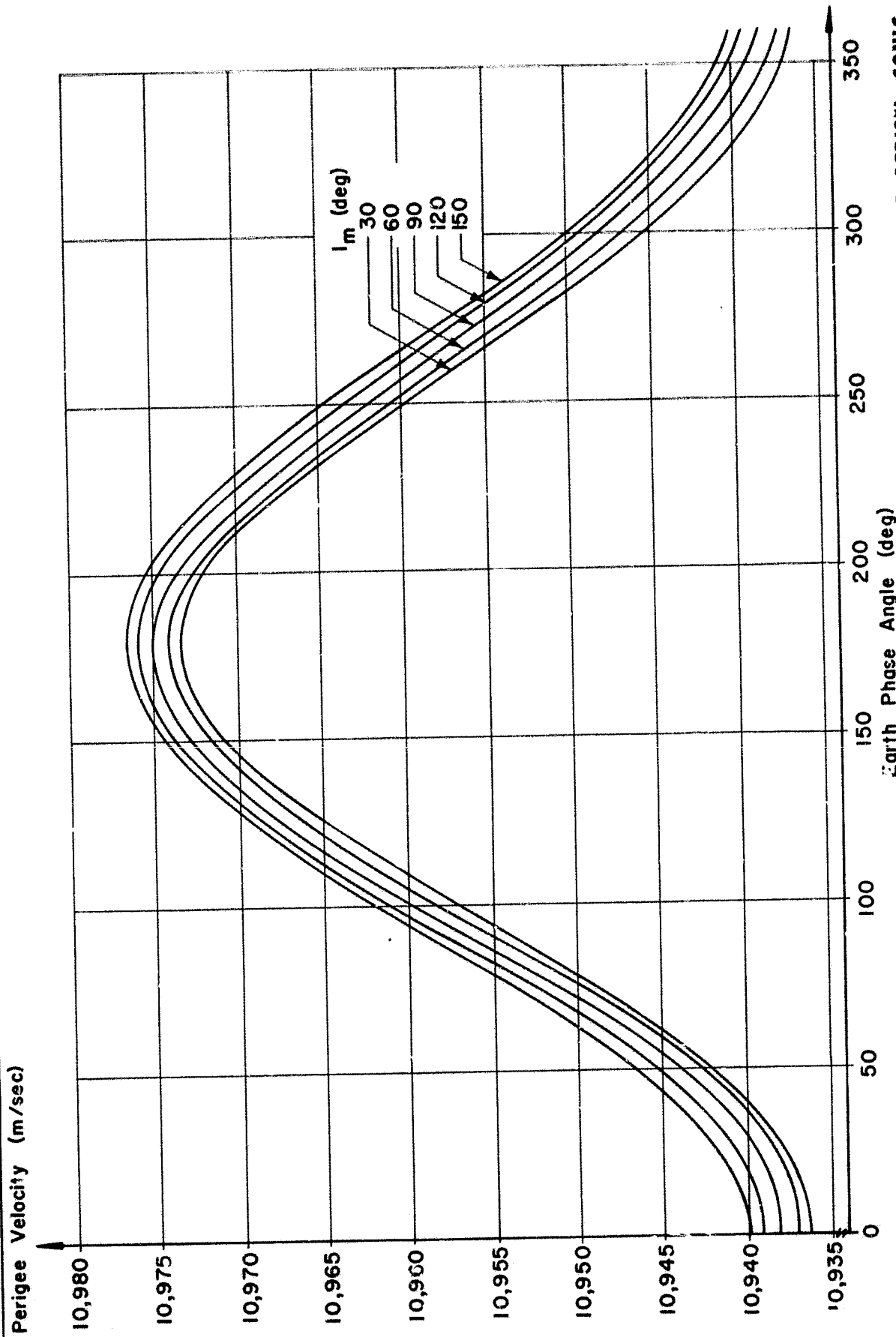


FIG. 37. PERIGEE VELOCITY VS EARTH PHASE ANGLE, Φ_e , FOR VARIOUS INCLINATIONS OF THE PERISEL CONIC FOR THE CLASS C (72 HR, 6555 KM, 1923 KM)

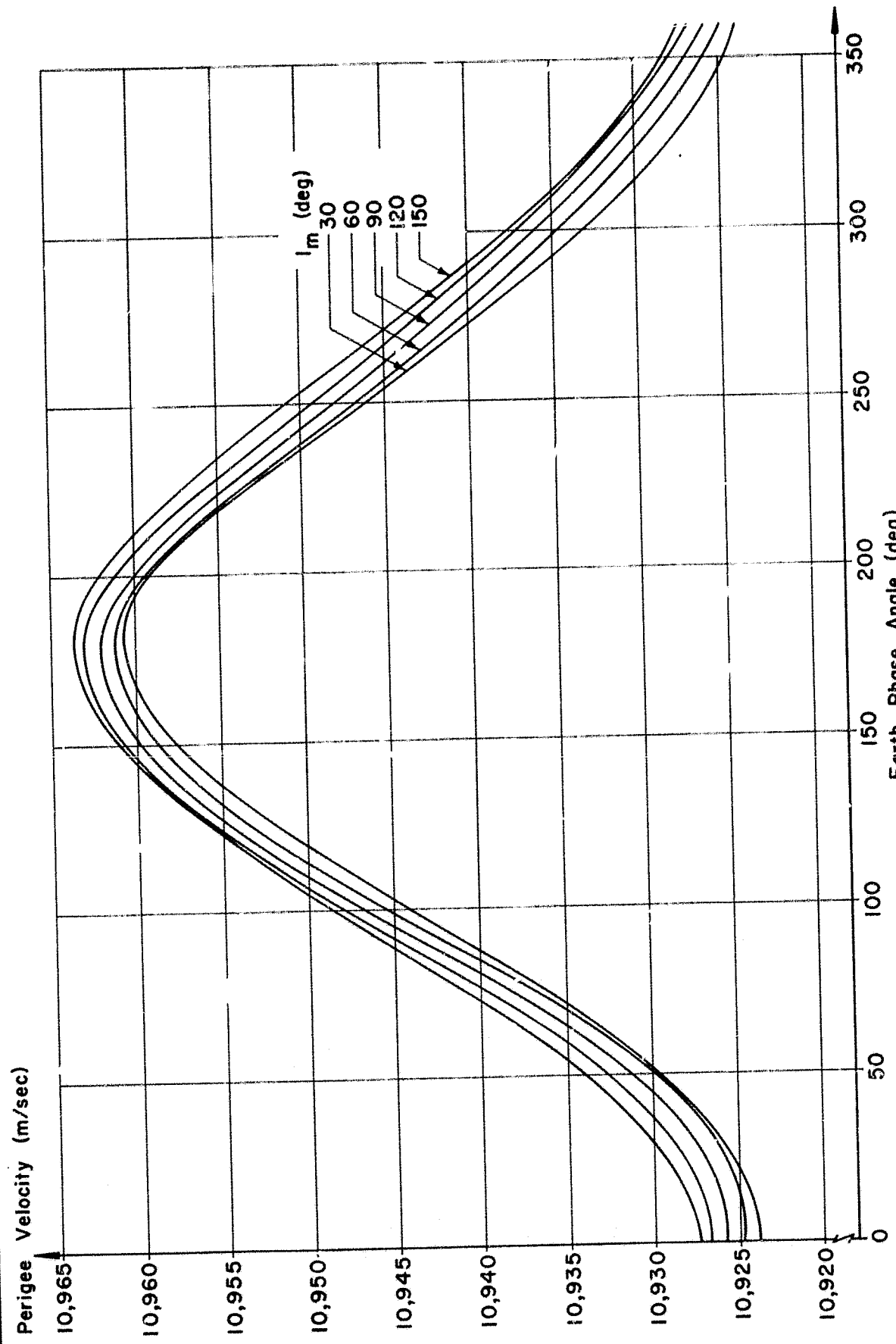


FIG. 38. PERIGEE VELOCITY VS EARTH PHASE ANGLE, Φ_e , FOR VARIOUS INCLINATIONS OF THE PERISEL CONIC FOR THE CLASS C (84 HR, 6555 KM, 1923 KM)

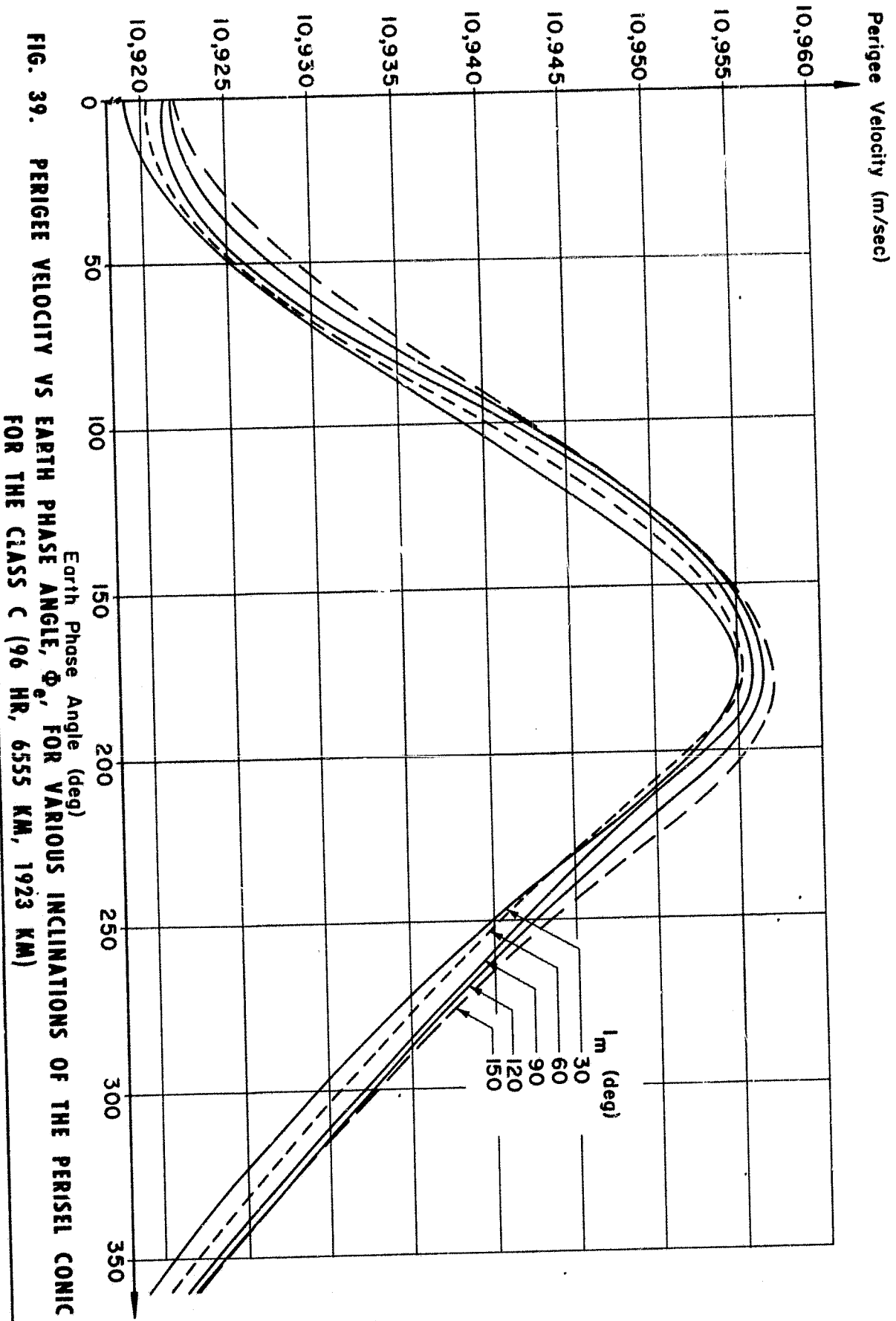


FIG. 39. PERIGEE VELOCITY VS EARTH PHASE ANGLE, Φ_e , FOR VARIOUS INCLINATIONS OF THE PERISEL CONIC FOR THE CLASS C (96 HR, 6555 KM, 1923 KM)

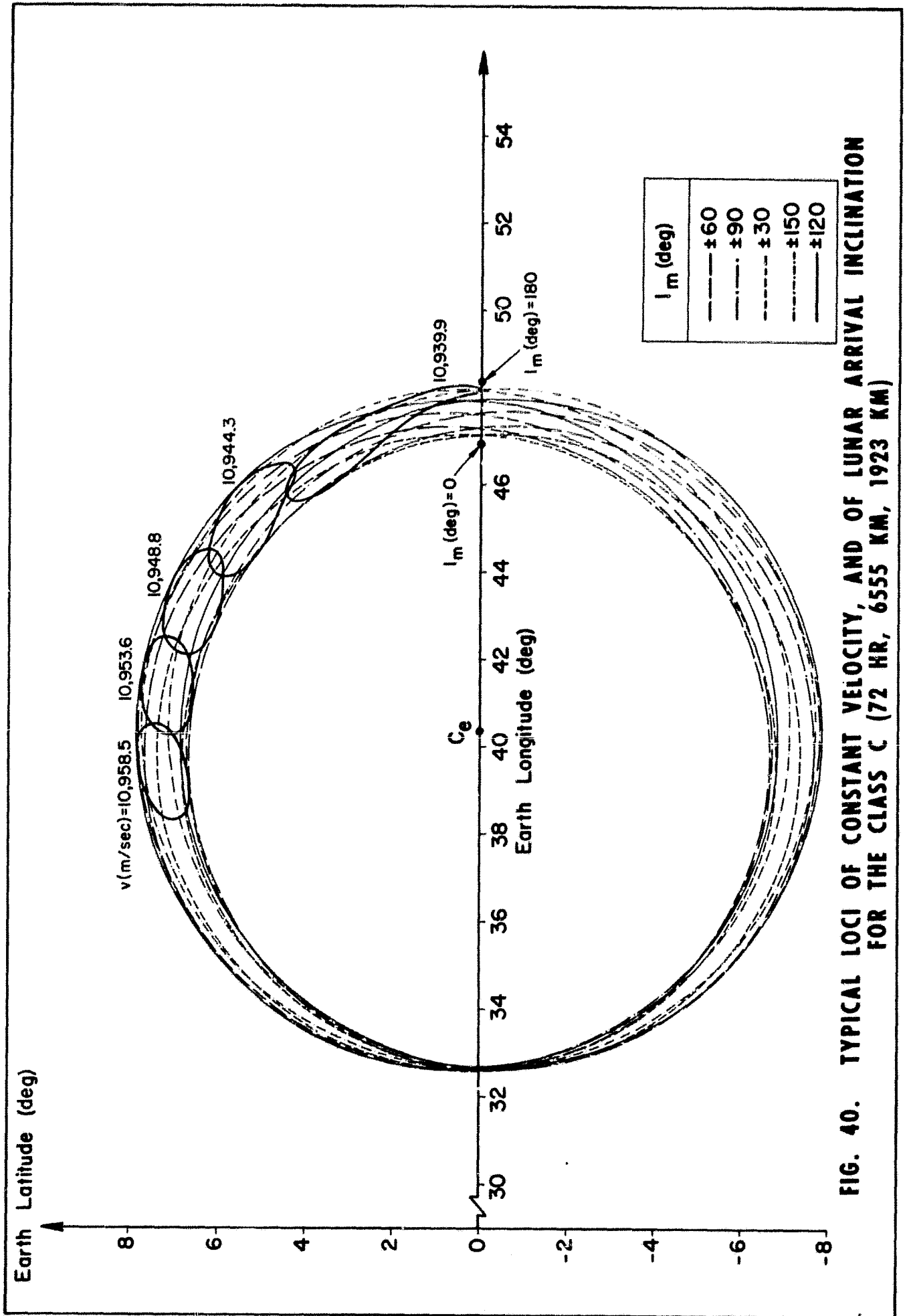


FIG. 40. TYPICAL LOCI OF CONSTANT VELOCITY, AND OF LUNAR ARRIVAL INCLINATION FOR THE CLASS C (72 HR, 6555 KM, 1923 KM)

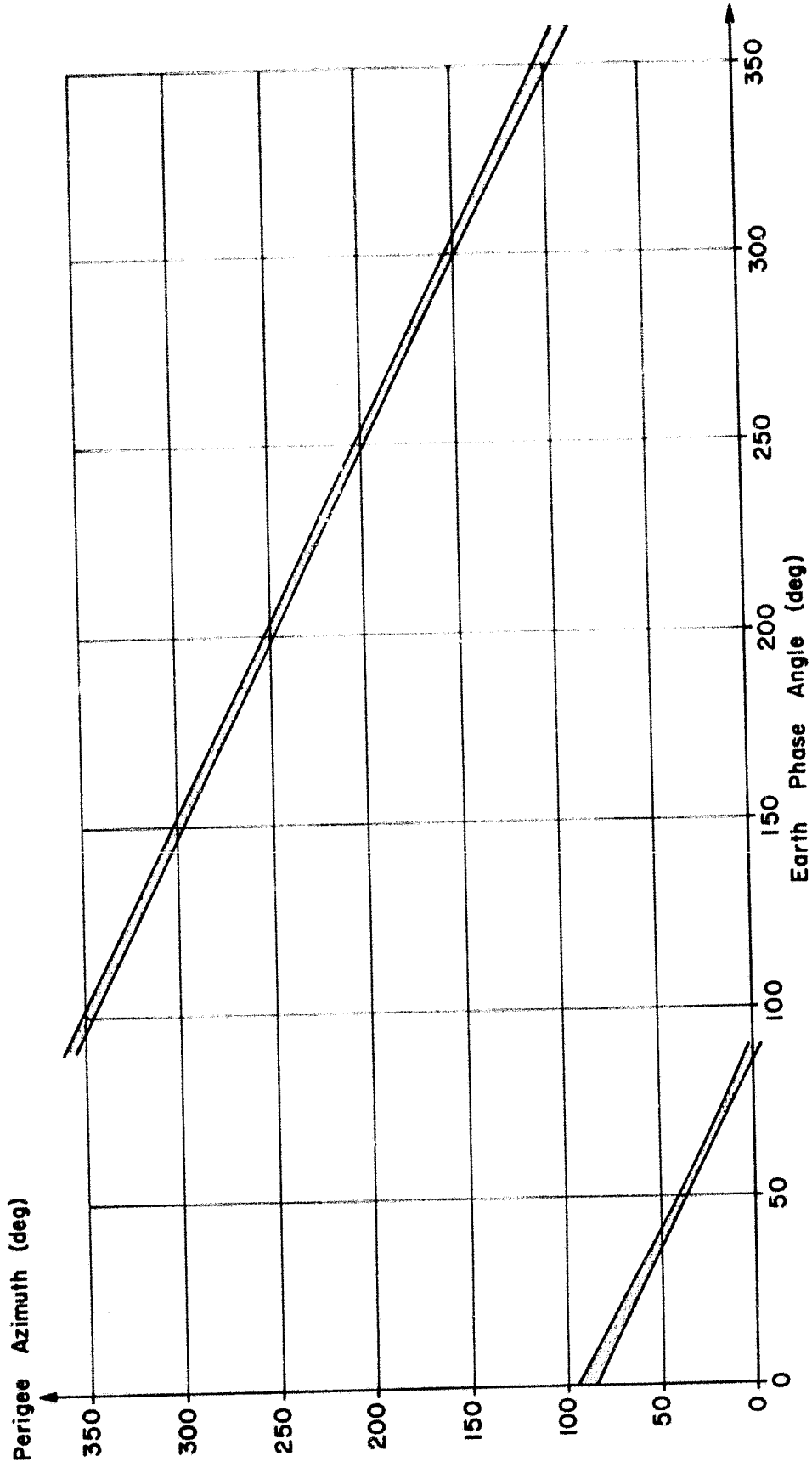


FIG. 41. AZIMUTH AT PERIGEE VS PHASE ANGLE FOR c (60 HR, 6555 KM, 1923 KM)

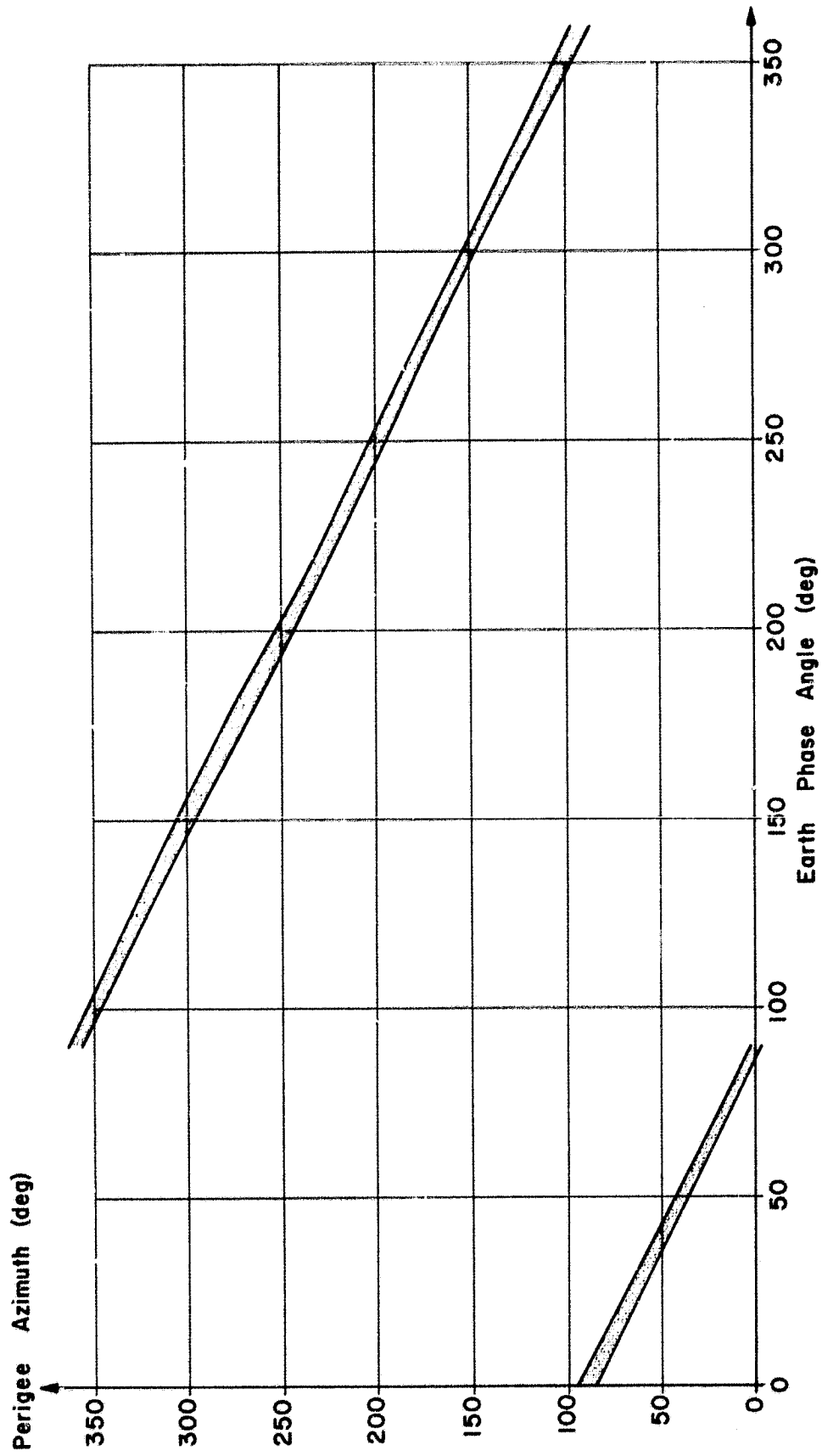


FIG. 42. AZIMUTH AT PERIGEE VS PHASE ANGLE FOR C (72 HR, 6555 KM, 1923 KM)

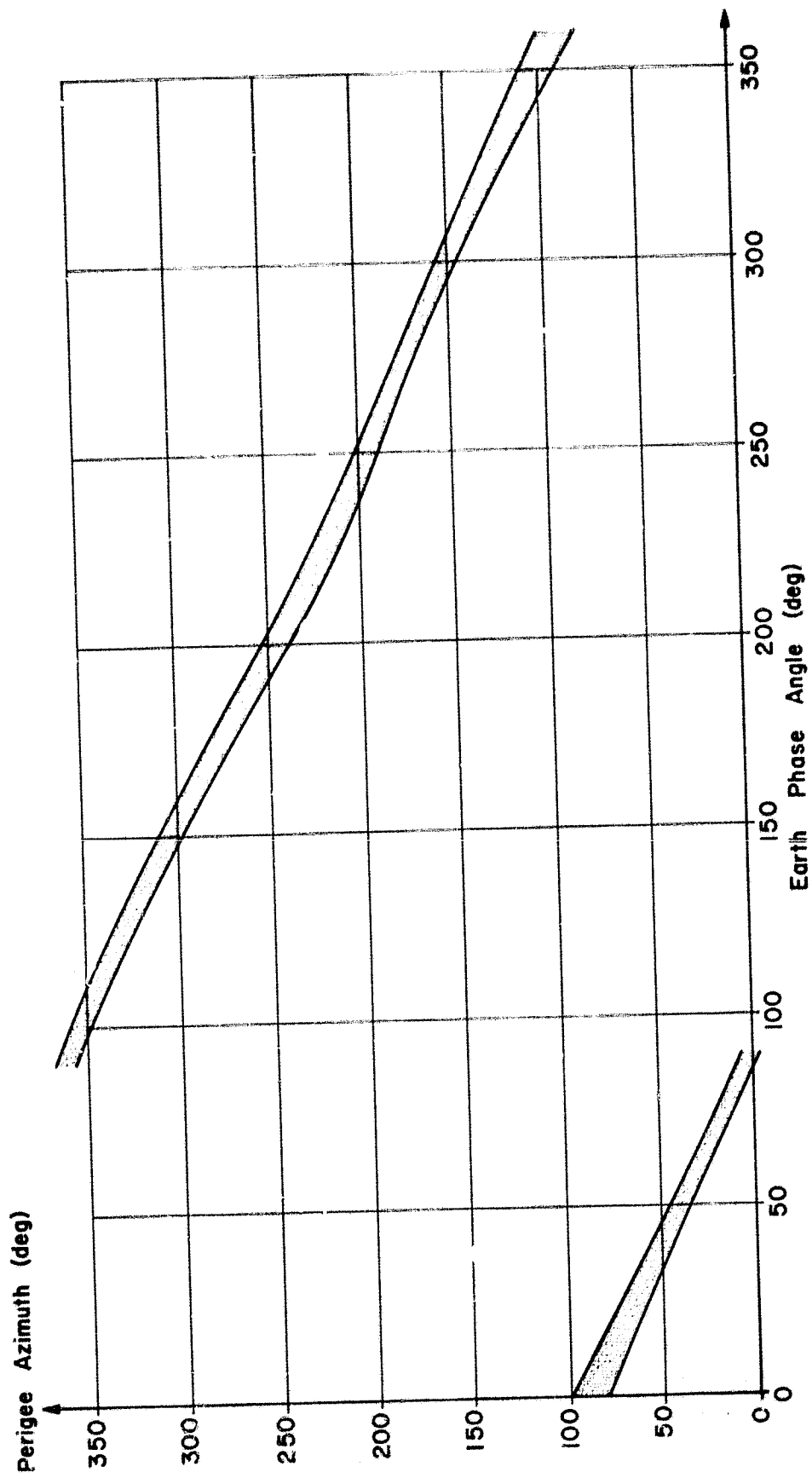


FIG. 43. AZIMUTH AT PERIGEE VS PHASE ANGLE FOR C (84 HR, 6555 KM, 1923 KM)

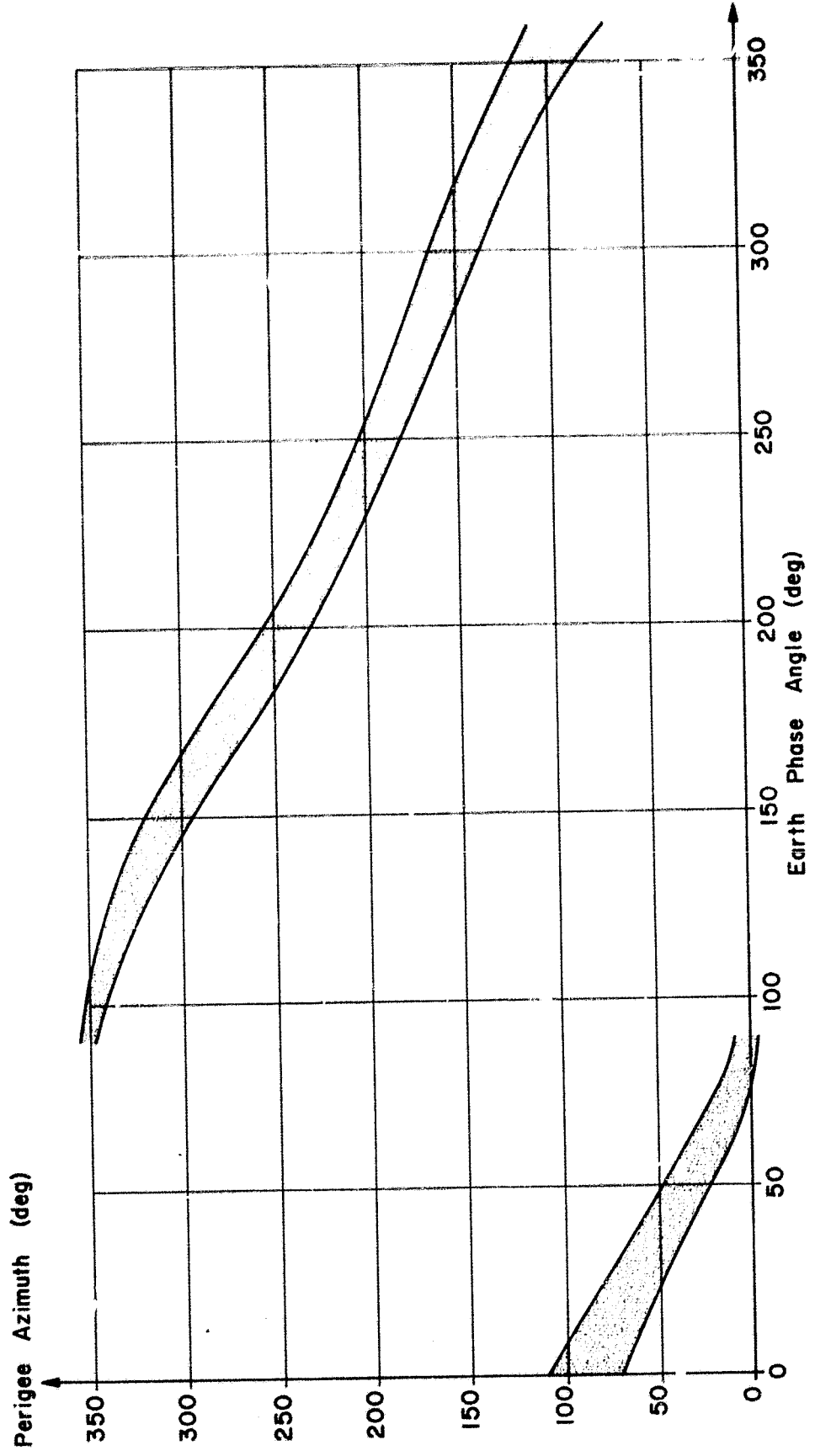


FIG. 44. AZIMUTH AT PERIGEE VS PHASE ANGLE FOR C (96 HR, 6555 KM, 1923 KM)

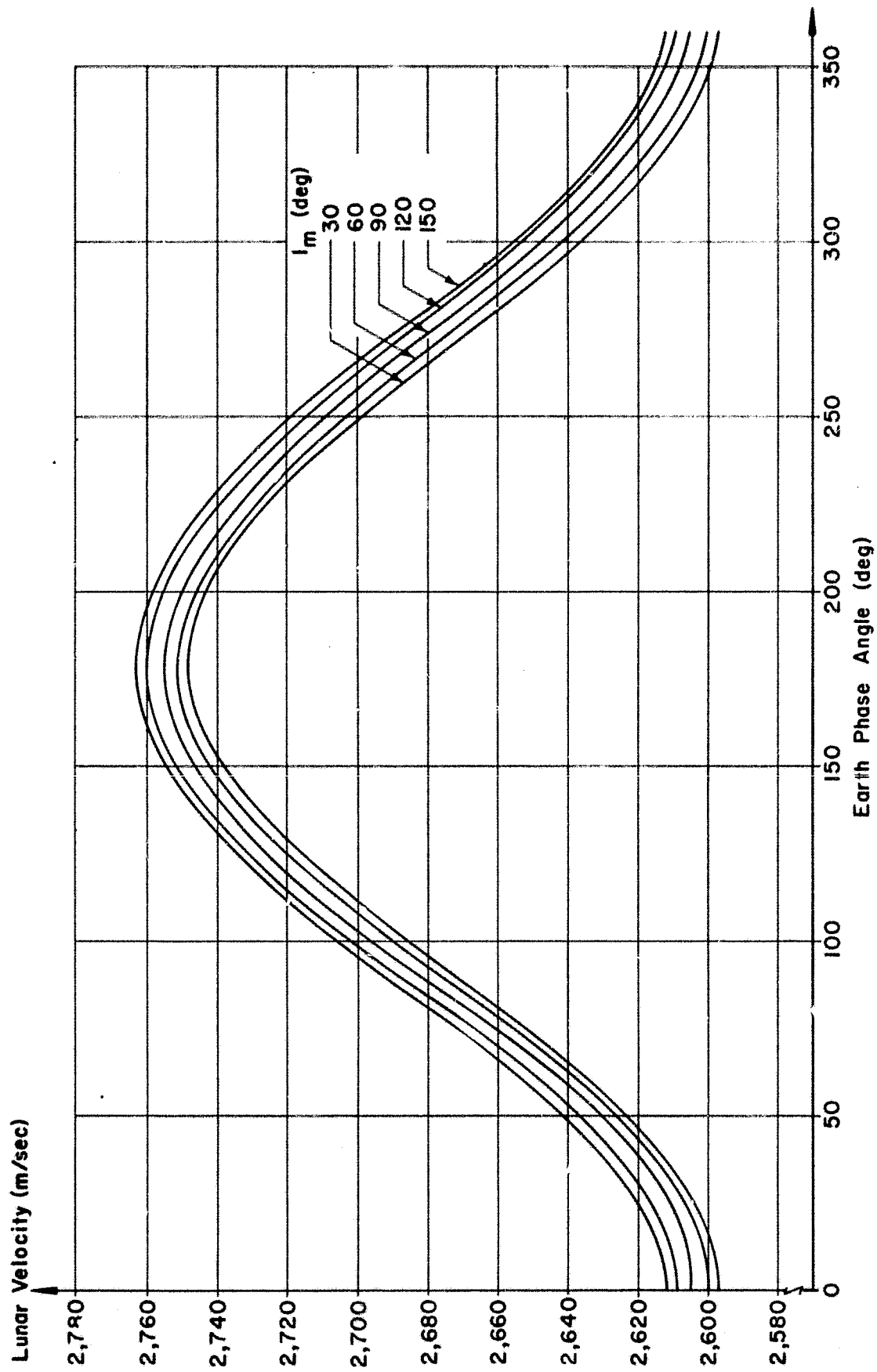


FIG. 45. LUNAR ARRIVAL VELOCITY CORRESPONDING TO THE INJECTION VELOCITIES SHOWN BY FIG. 36, C (60 HR, 6555 KM, 1923 KM)

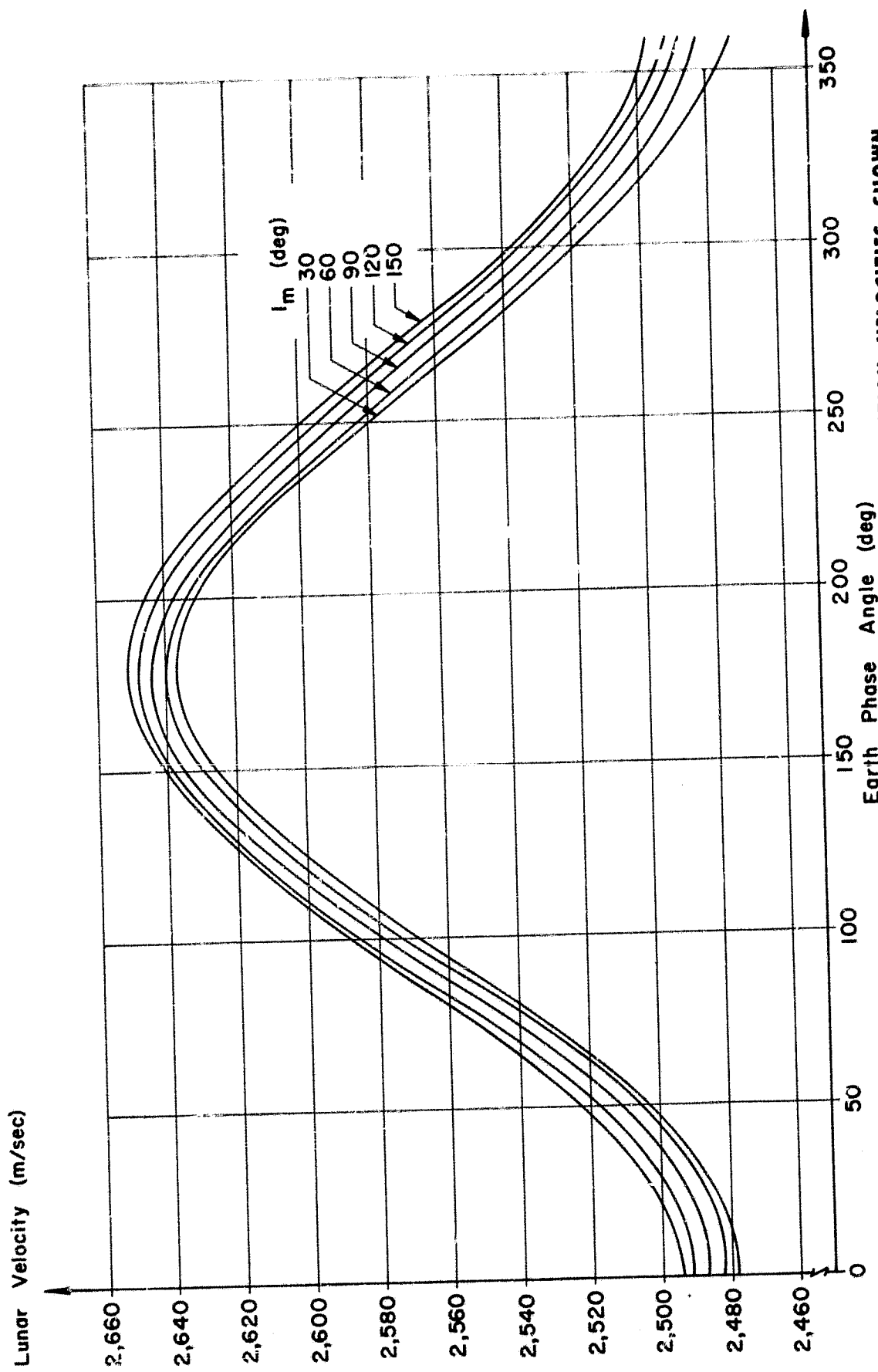


FIG. 46. LUNAR ARRIVAL VELOCITY CORRESPONDING TO THE INJECTION VELOCITIES SHOWN BY FIG. 37, C (72 HR, 6555 KM, 1923 KM)

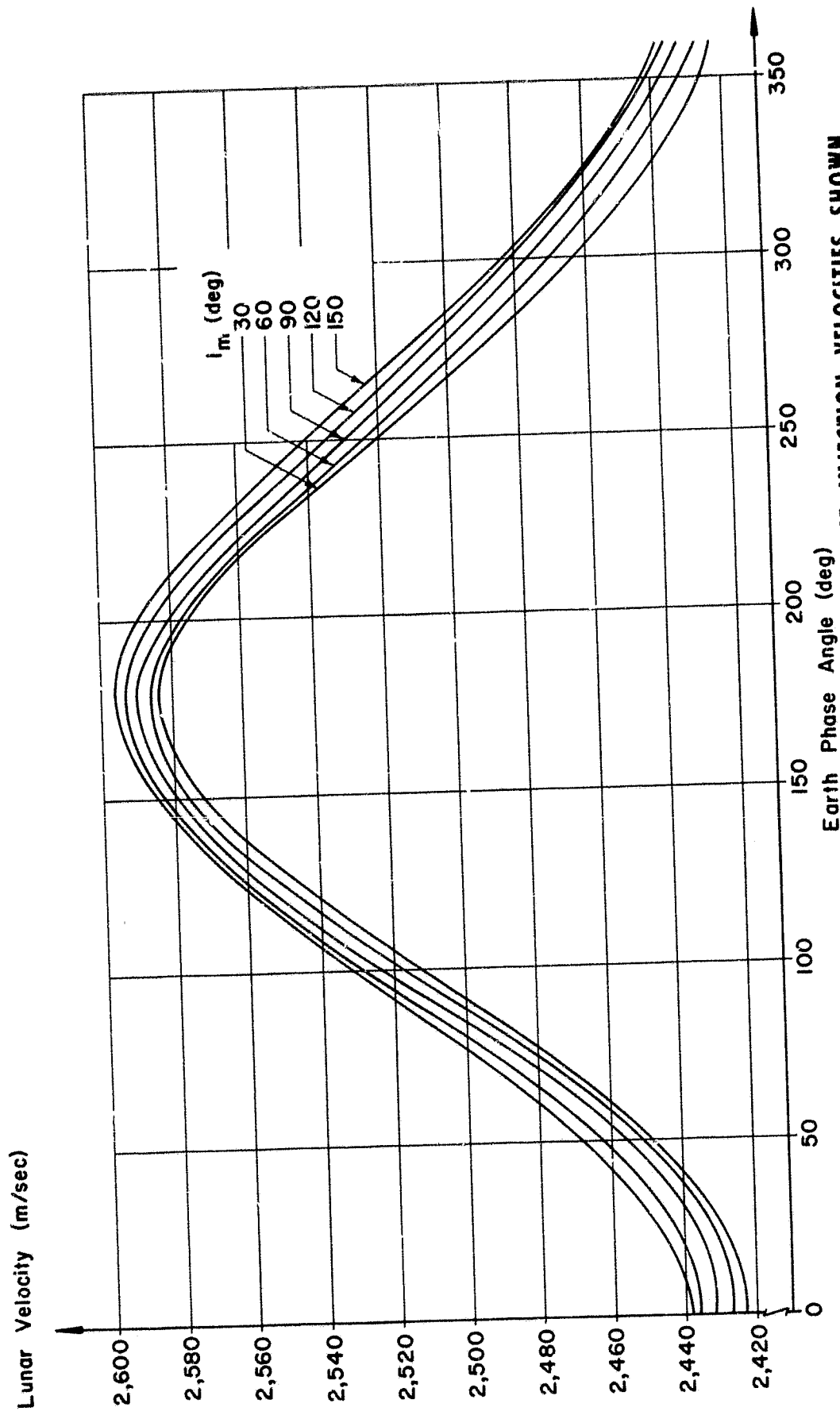


FIG. 47. LUNAR ARRIVAL VELOCITY CORRESPONDING TO THE INJECTION VELOCITIES SHOWN BY FIG. 38, C (84 HR, 6555 KM, 1923 KM)

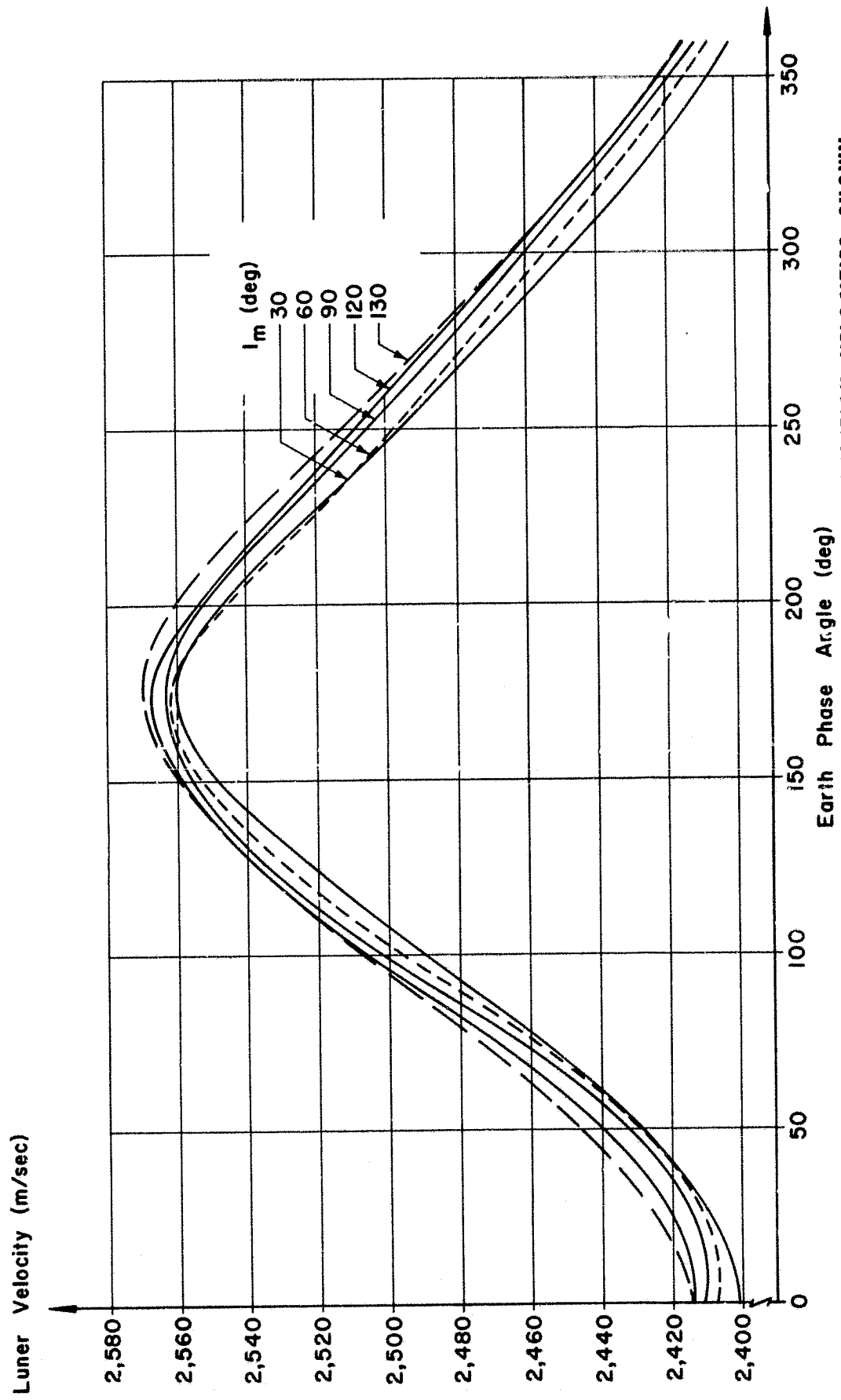


FIG. 48. LUNAR ARRIVAL VELOCITY CORRESPONDING TO THE INJECTION VELOCITIES SHOWN BY FIG. 39, C (96 HR, 6555 KM, 1923 KM)

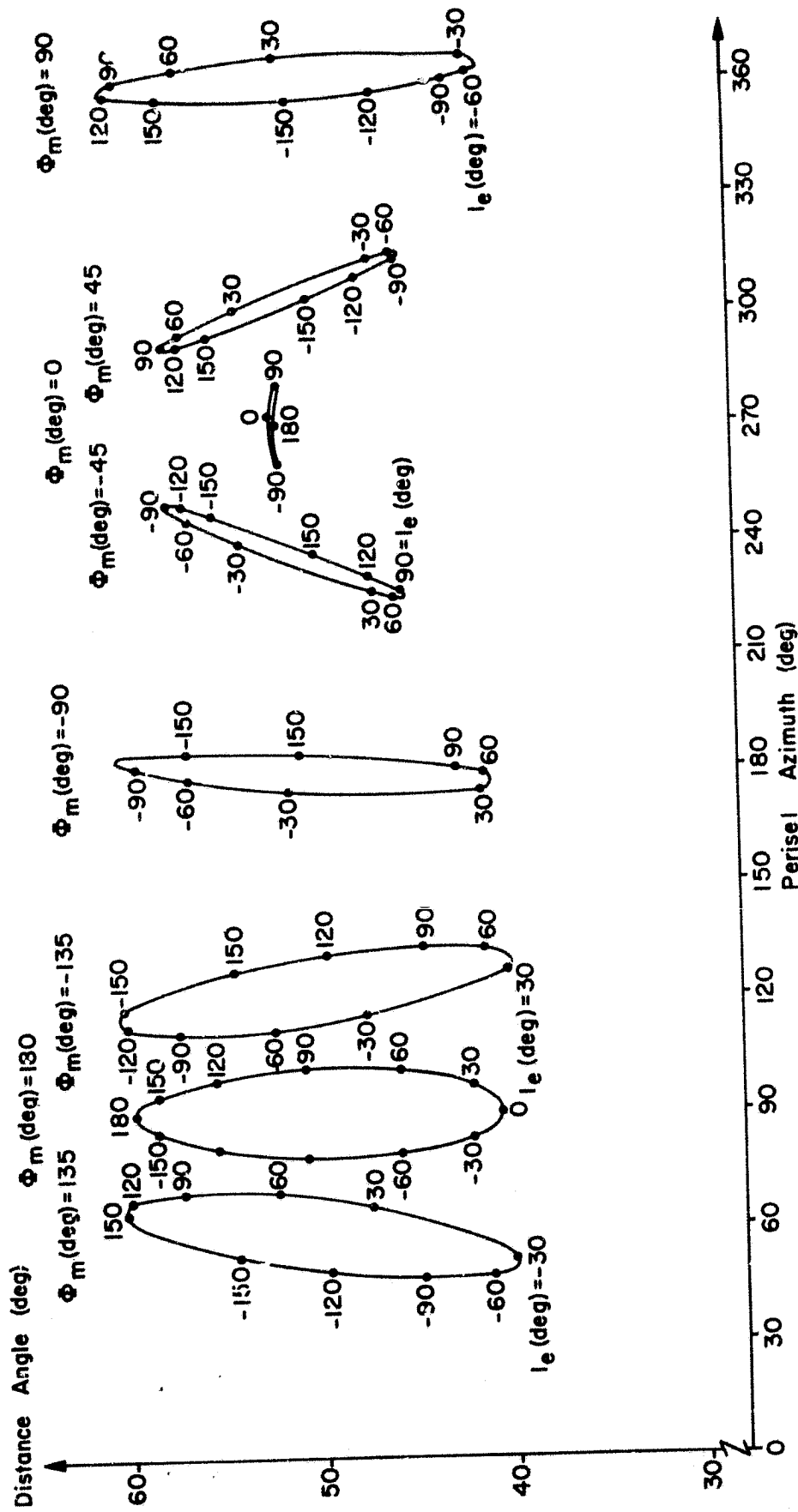


FIG. 49. PERISEL AZIMUTH VS DISTANCE ANGLE FOR VARIOUS Φ_m FOR C (72 HR, 6555 KM, 1923 KM)

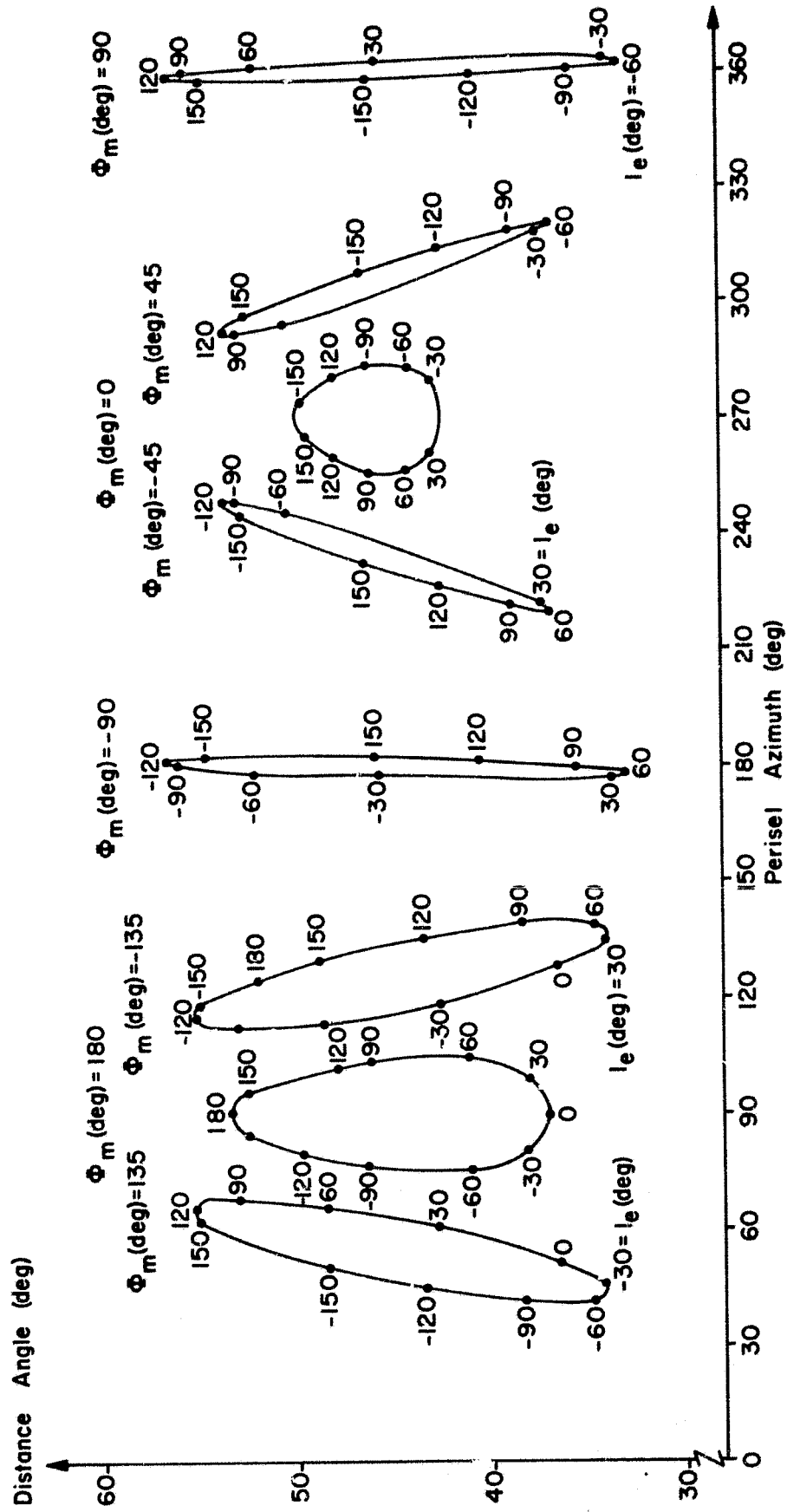


FIG. 50. PERISEL AZIMUTH VS Δ_m FOR VARIOUS Φ_m FOR C (96 HR, 6555 KM, 1923 KM)

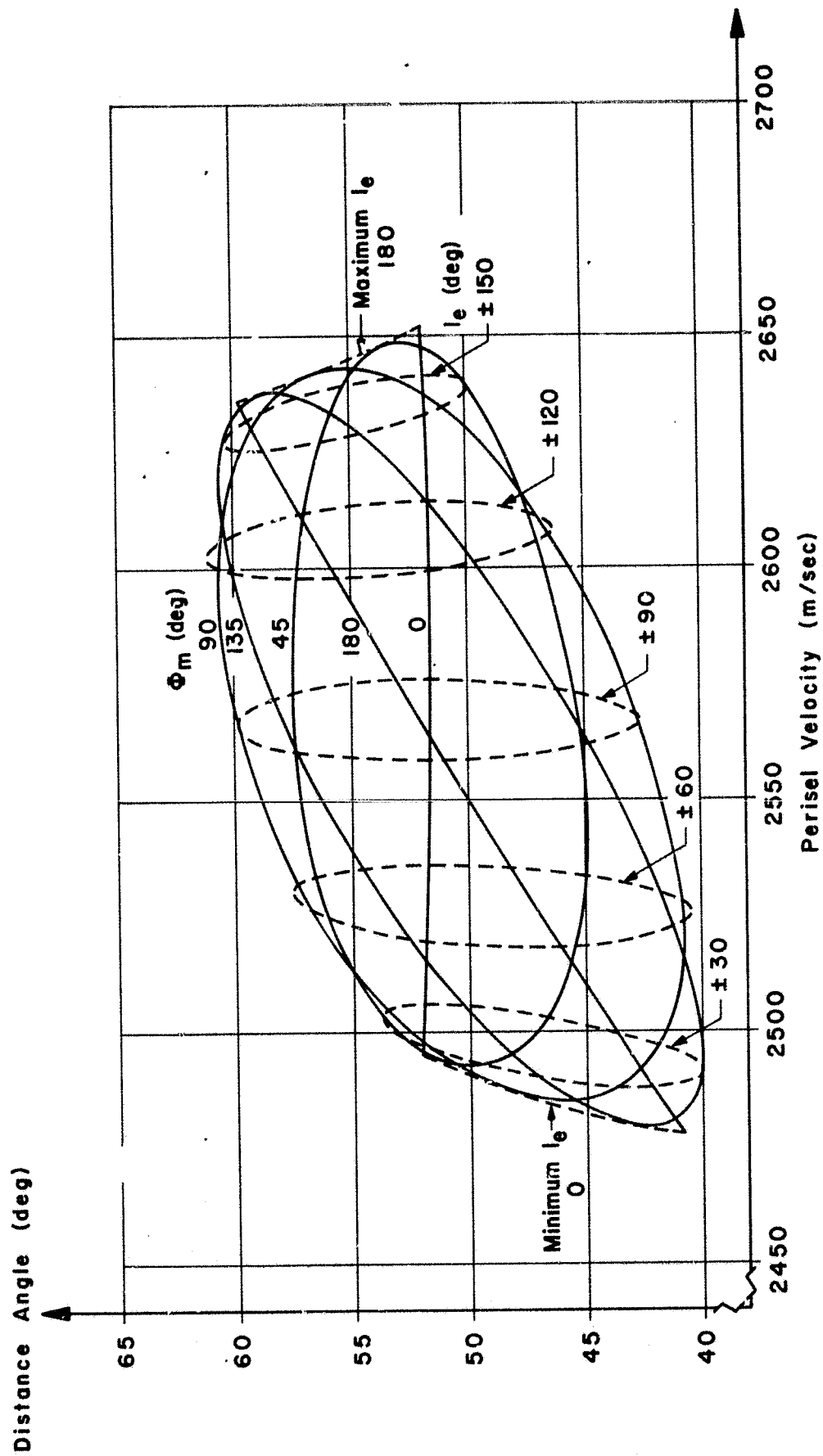


FIG. 51. PERISEL VELOCITY VS Δ_m WITH ϕ_m AND i_e AS PARAMETERS,
FOR THE CLASS C (72 HR, 6555 KM, 1923 KM)

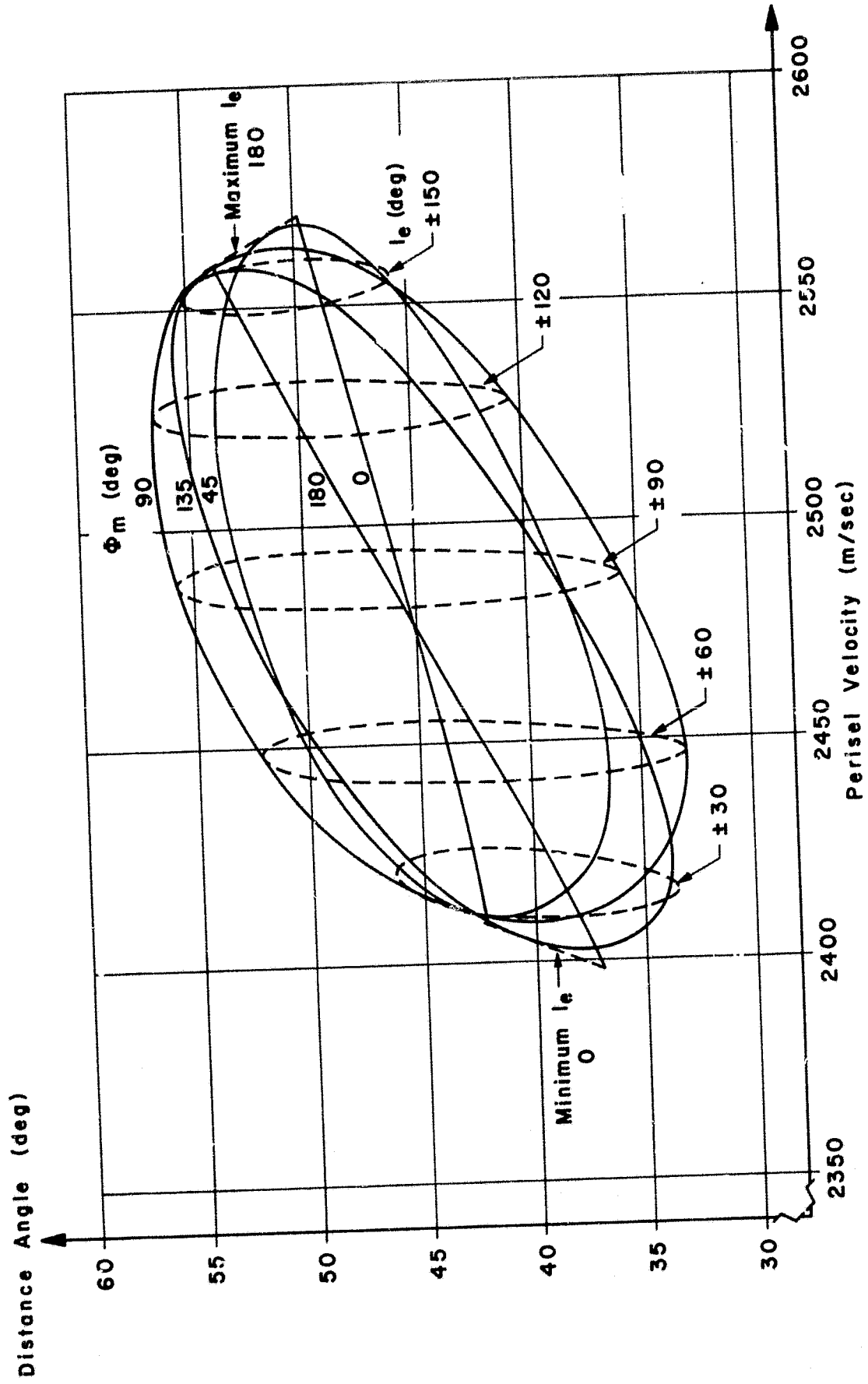


FIG. 52. PERISEL VELOCITY VS Δ_m WITH ϕ_m AND i_e AS PARAMETERS, FOR THE CLASS C (96 HR, 6555 KM, 1923 KM)

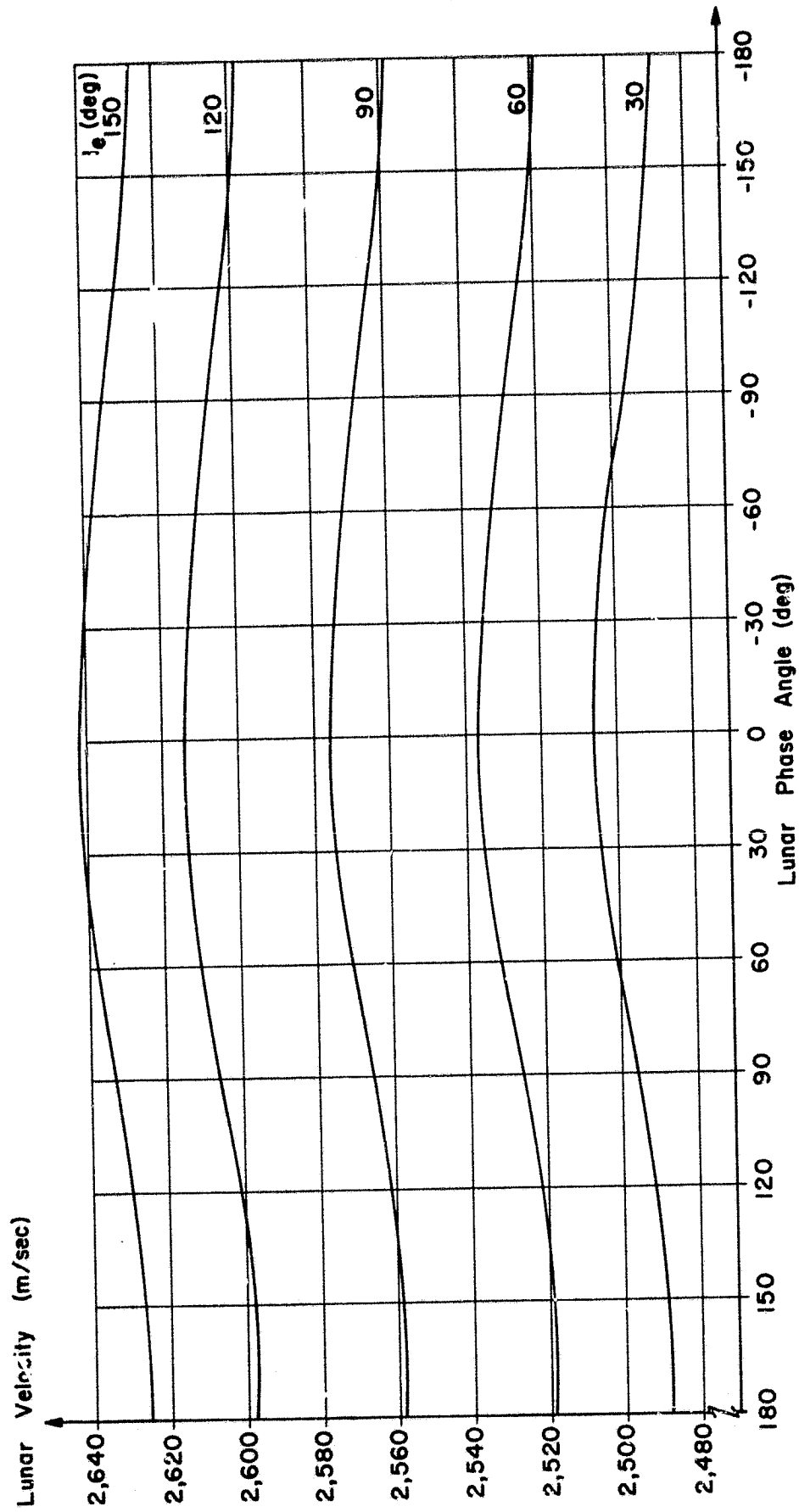


FIG. 53. PERIGEE CONIC INCLINATION RELATED TO PERISEL VELOCITY AND LUNAR PHASE ANGLE
FOR THE CLASS C (72 HR, 6555 KM, 1923 KM)

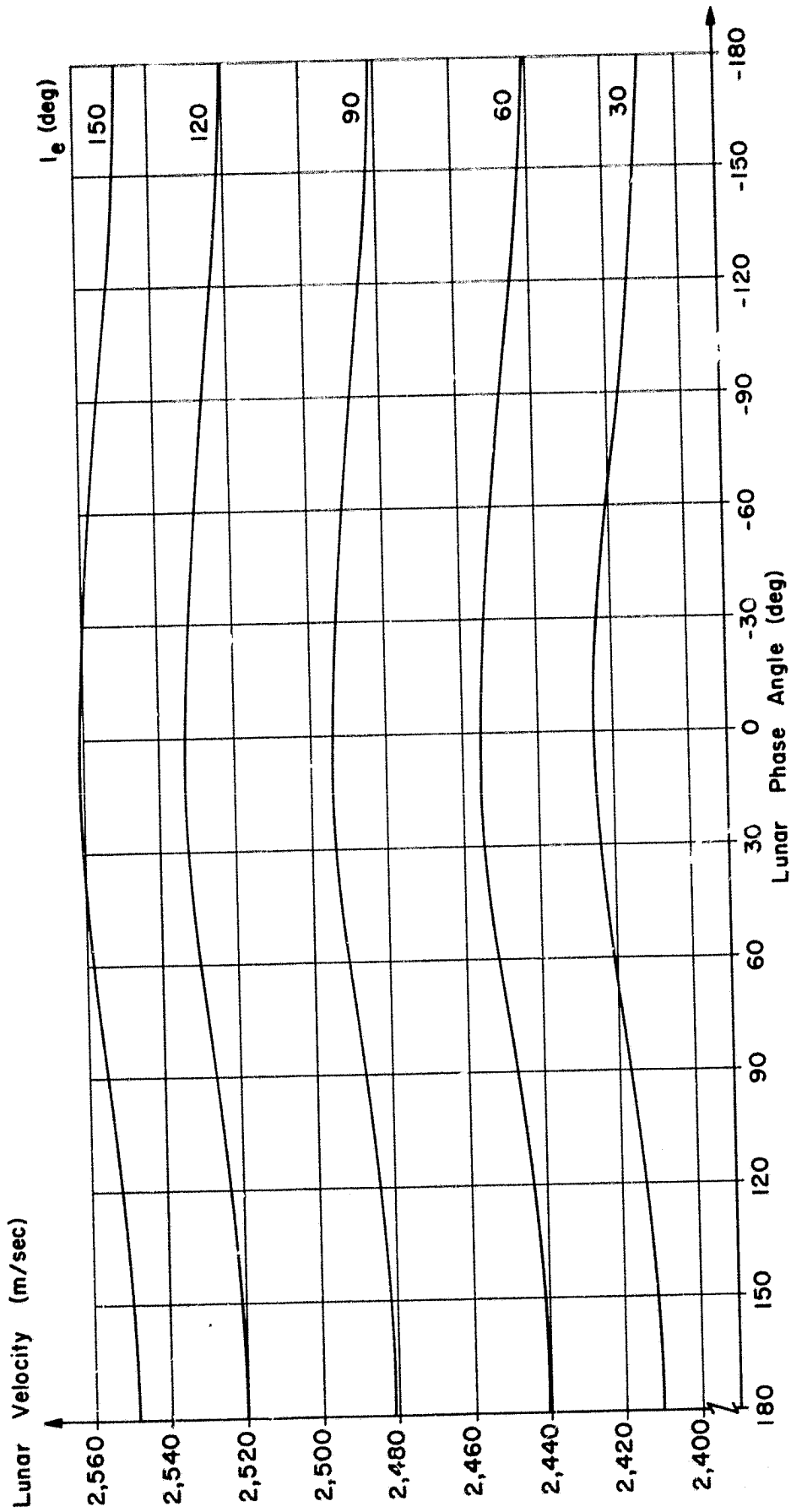


FIG. 54. PERIGEE CONIC INCLINATION RELATED TO PERISEL VELOCITY AND LUNAR PHASE ANGLE FOR THE CLASS C (96 HR, 6555 KM, 1923 KM)

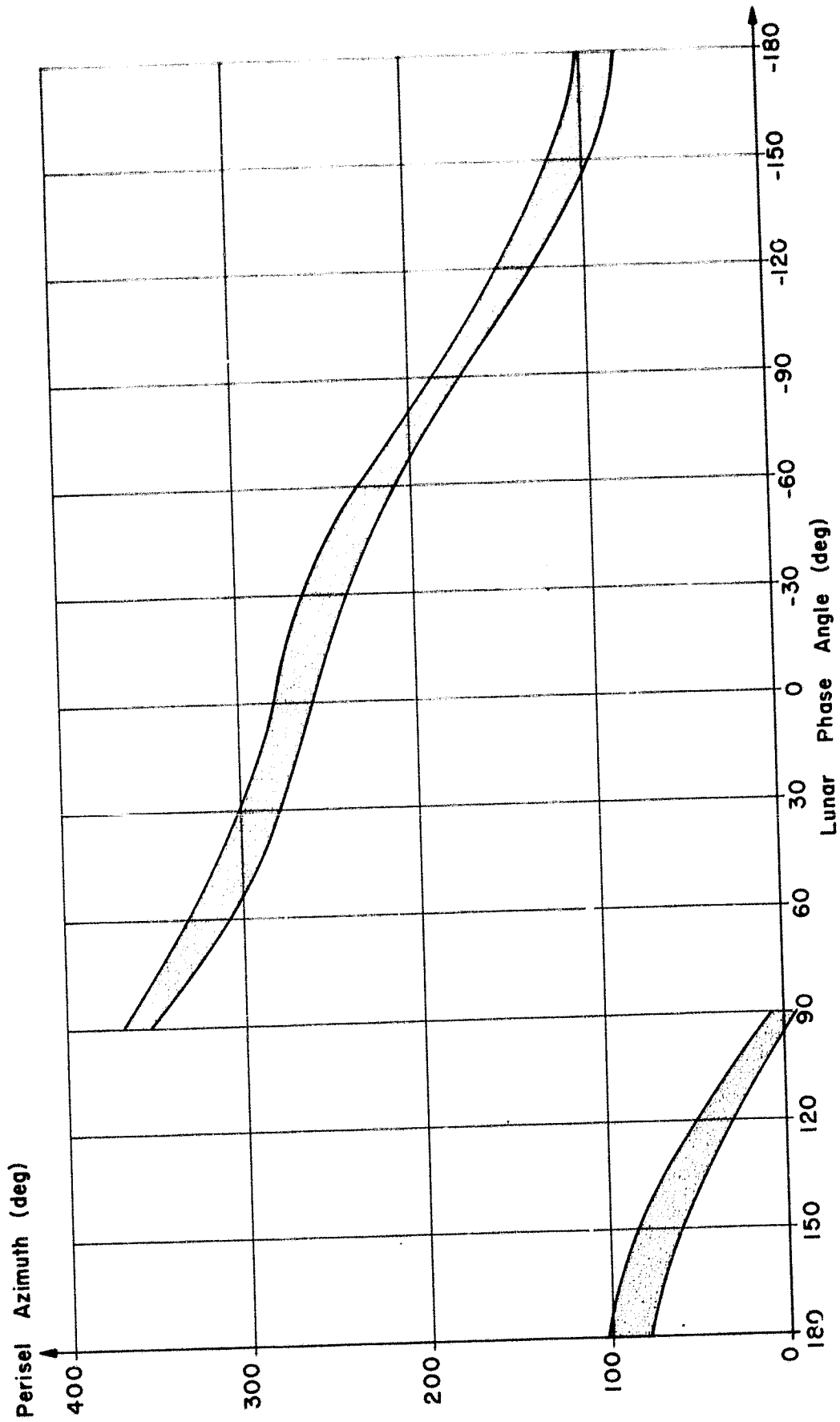


FIG. 55. PERISEL AZIMUTH VS LUNAR PHASE ANGLE FOR THE CLASS C (72 HR, 6555 KM, 1923 KM)

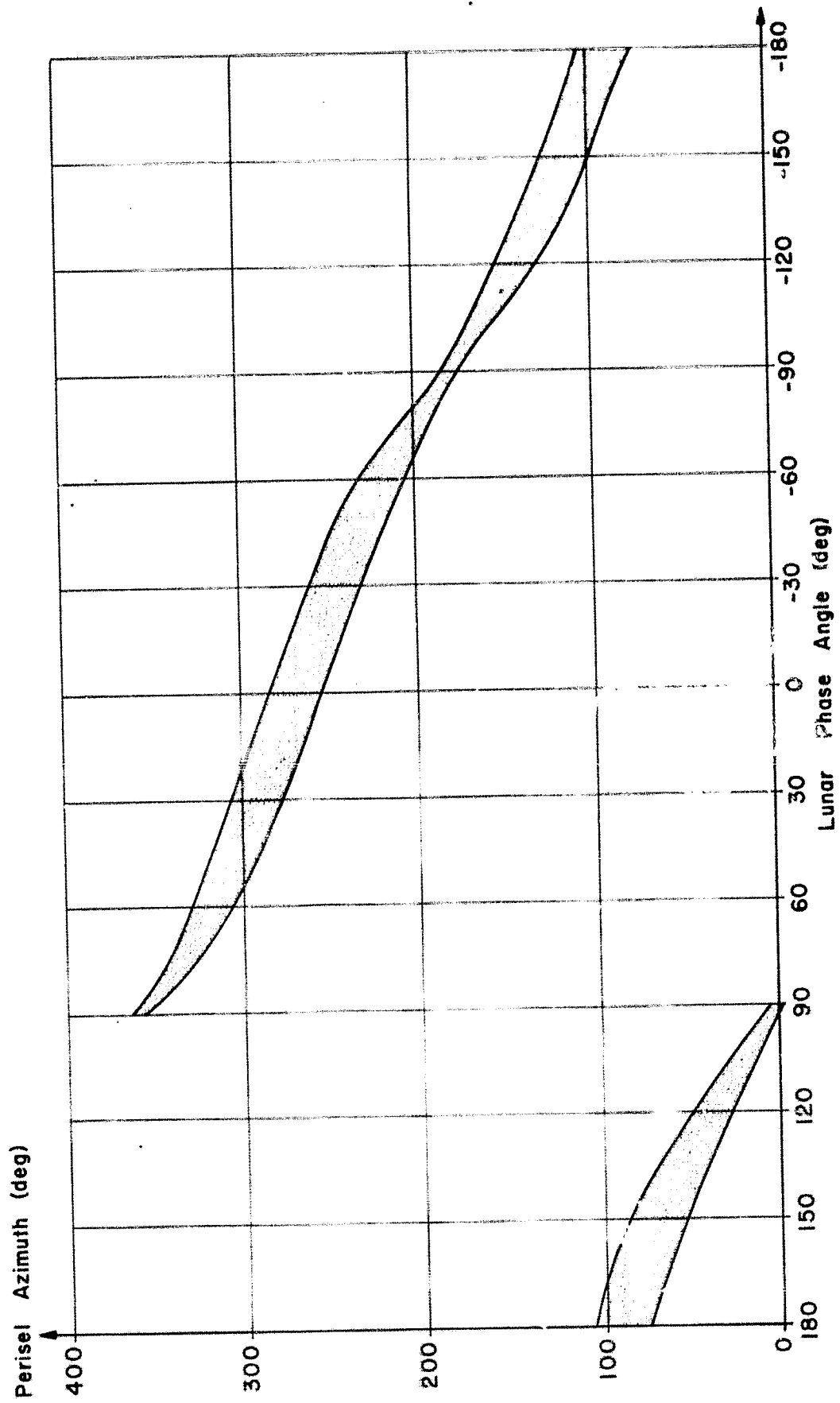


FIG. 56. PERISEL AZIMUTH VS LUNAR PHASE ANGLE FOR THE CLASS C (96 HR, 6555 KM, 1923 KM)

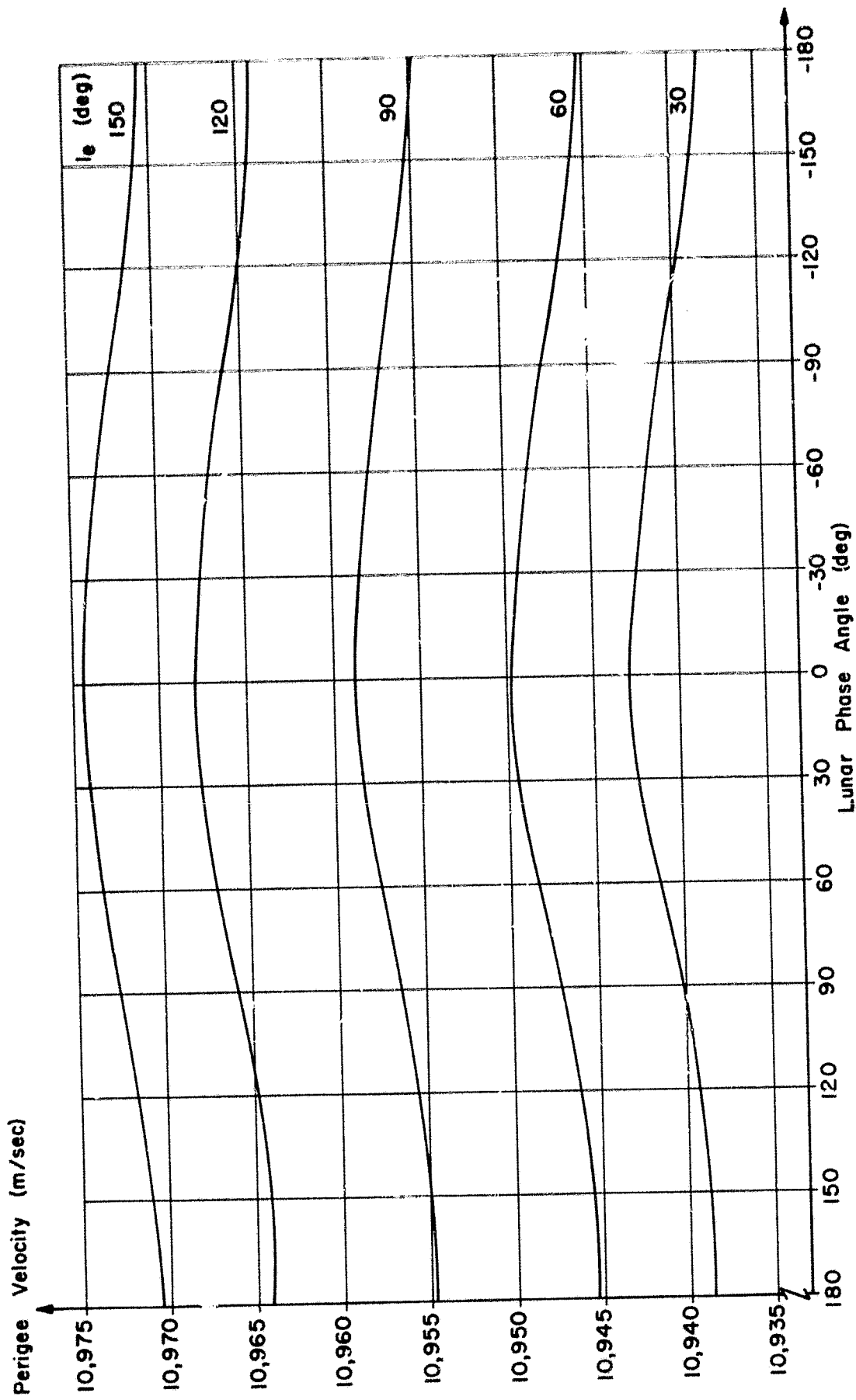


FIG. 57. PERIGEE VELOCITY VS LUNAR PHASE ANGLE FOR VARIOUS i_e FOR C (72 HR, 6555 KM, 1923 KM)

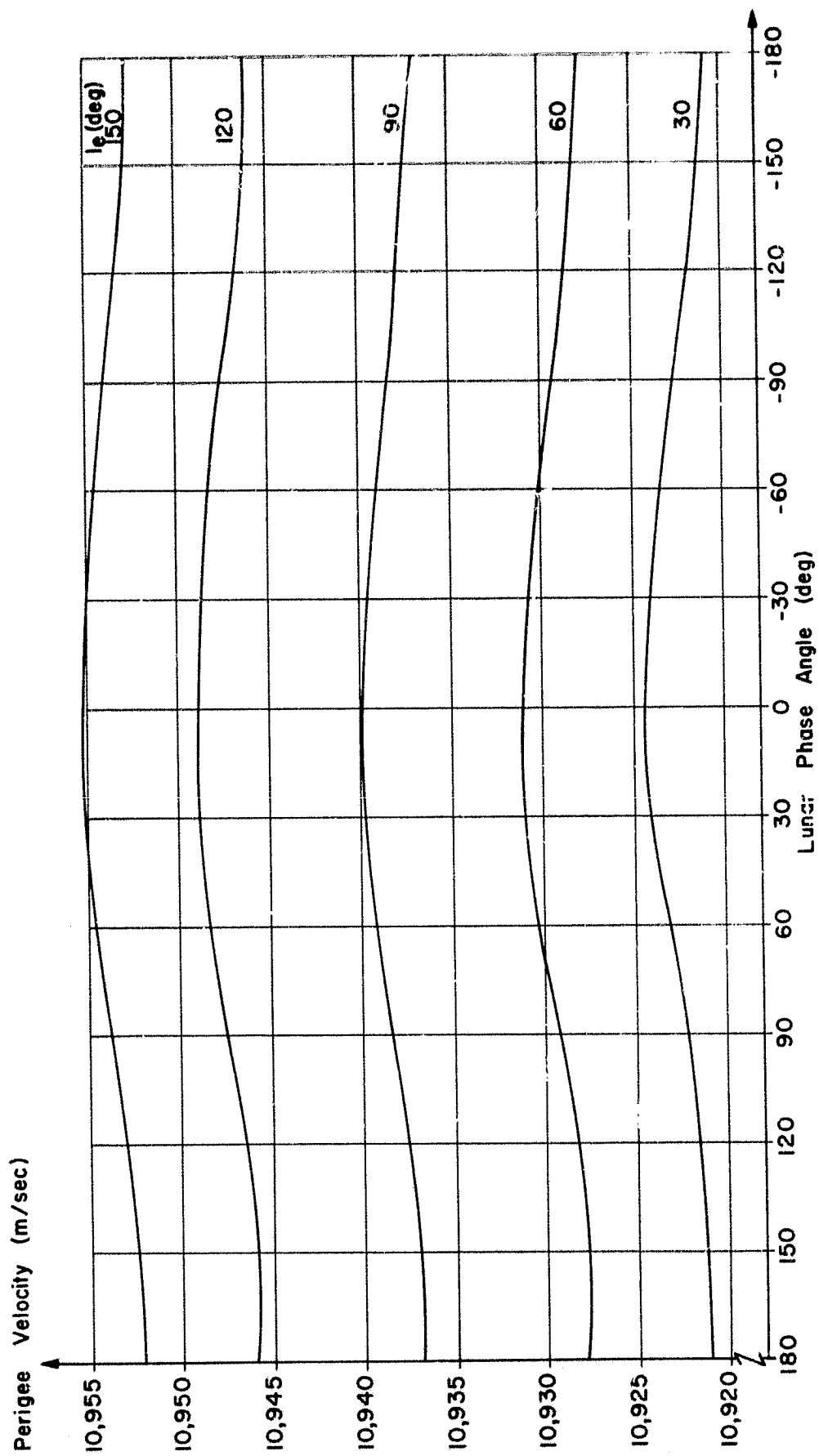
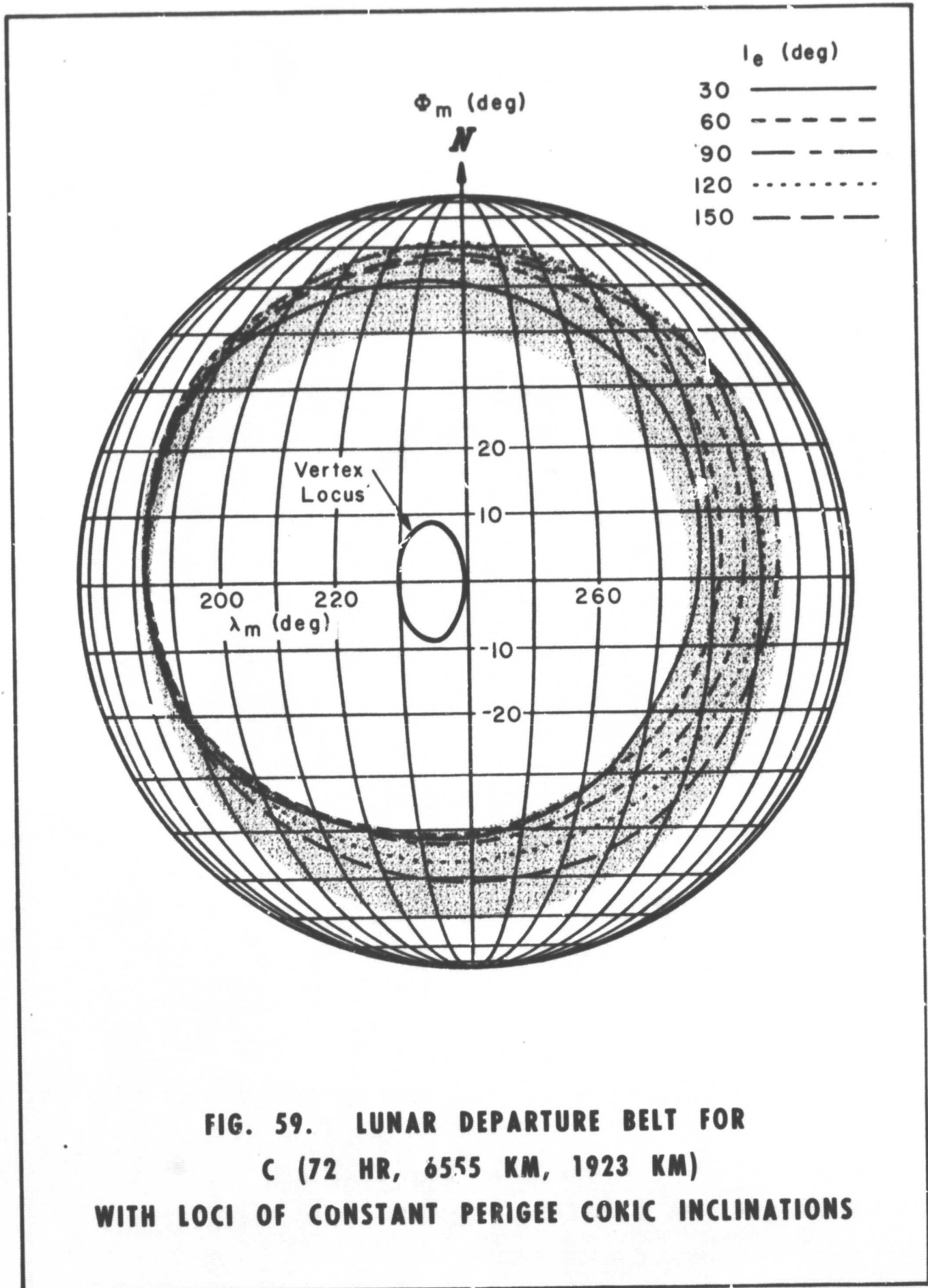
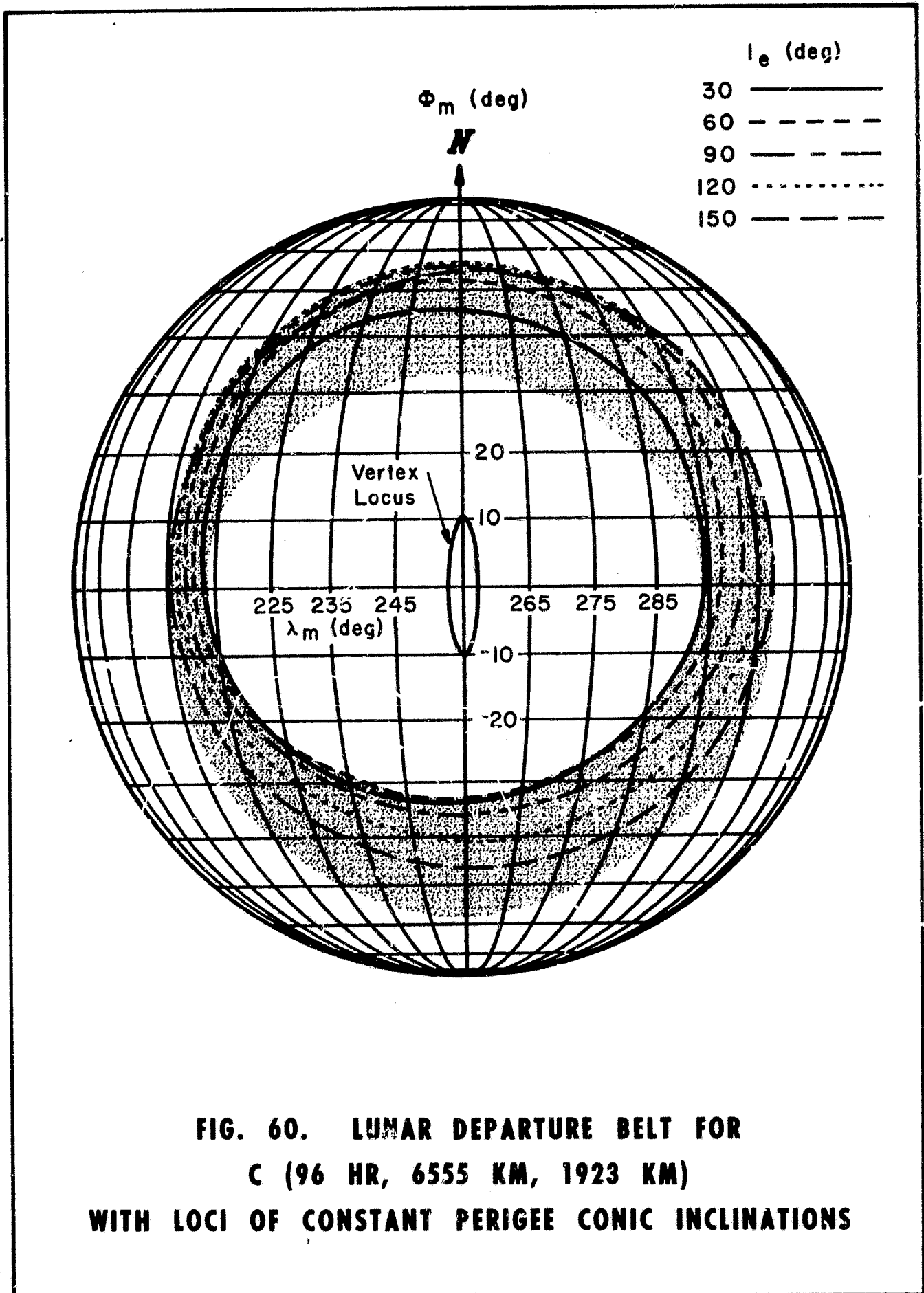


FIG. 58. PERIGEE VELOCITY VS LUNAR PHASE ANGLE FOR VARIOUS I_e FOR C (96 HR, 6555 KM, 1923 KM)



**FIG. 59. LUNAR DEPARTURE BELT FOR
C (72 HR, 6555 KM, 1923 KM)
WITH LOCI OF CONSTANT PERIGEE CONIC INCLINATIONS**



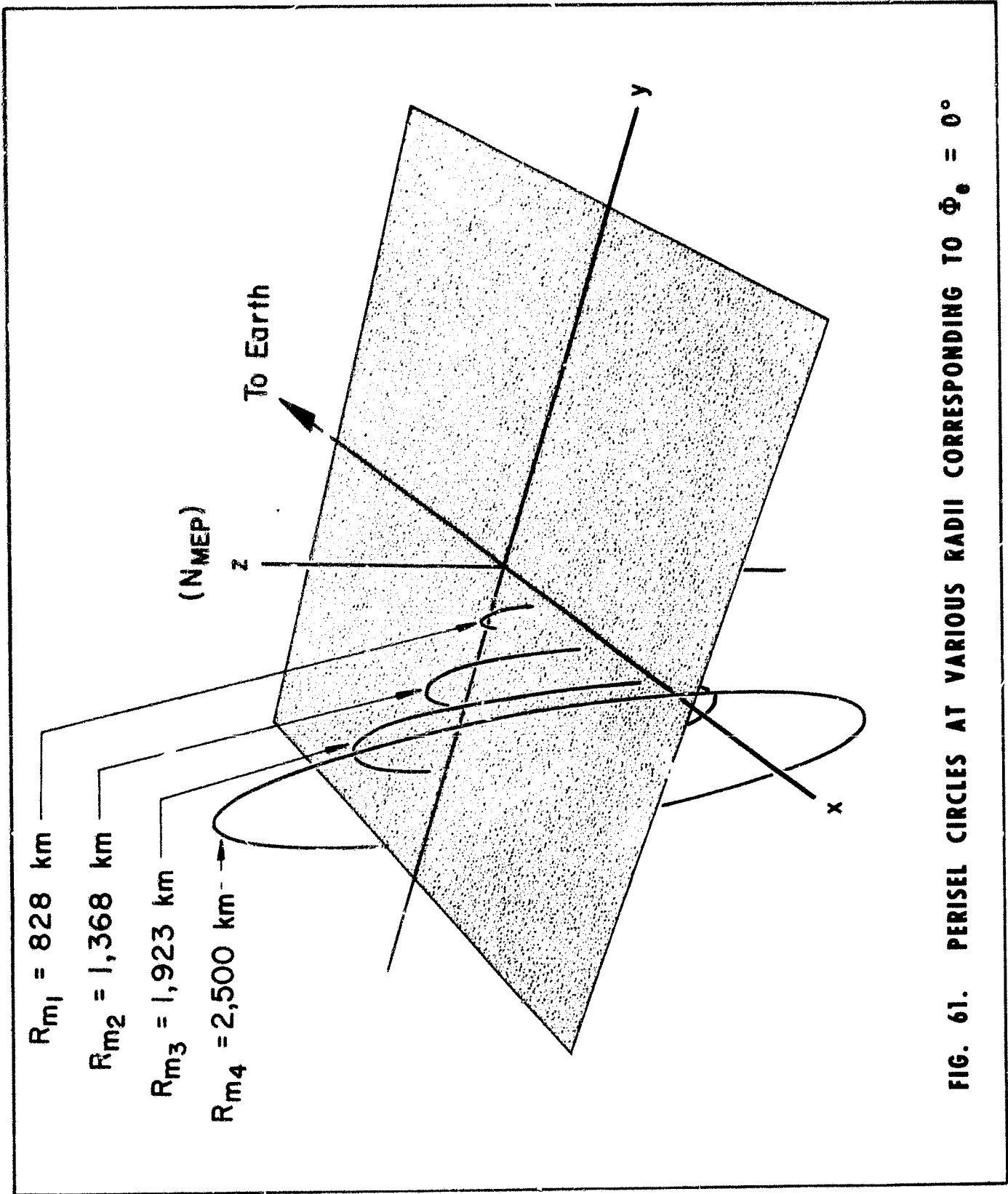
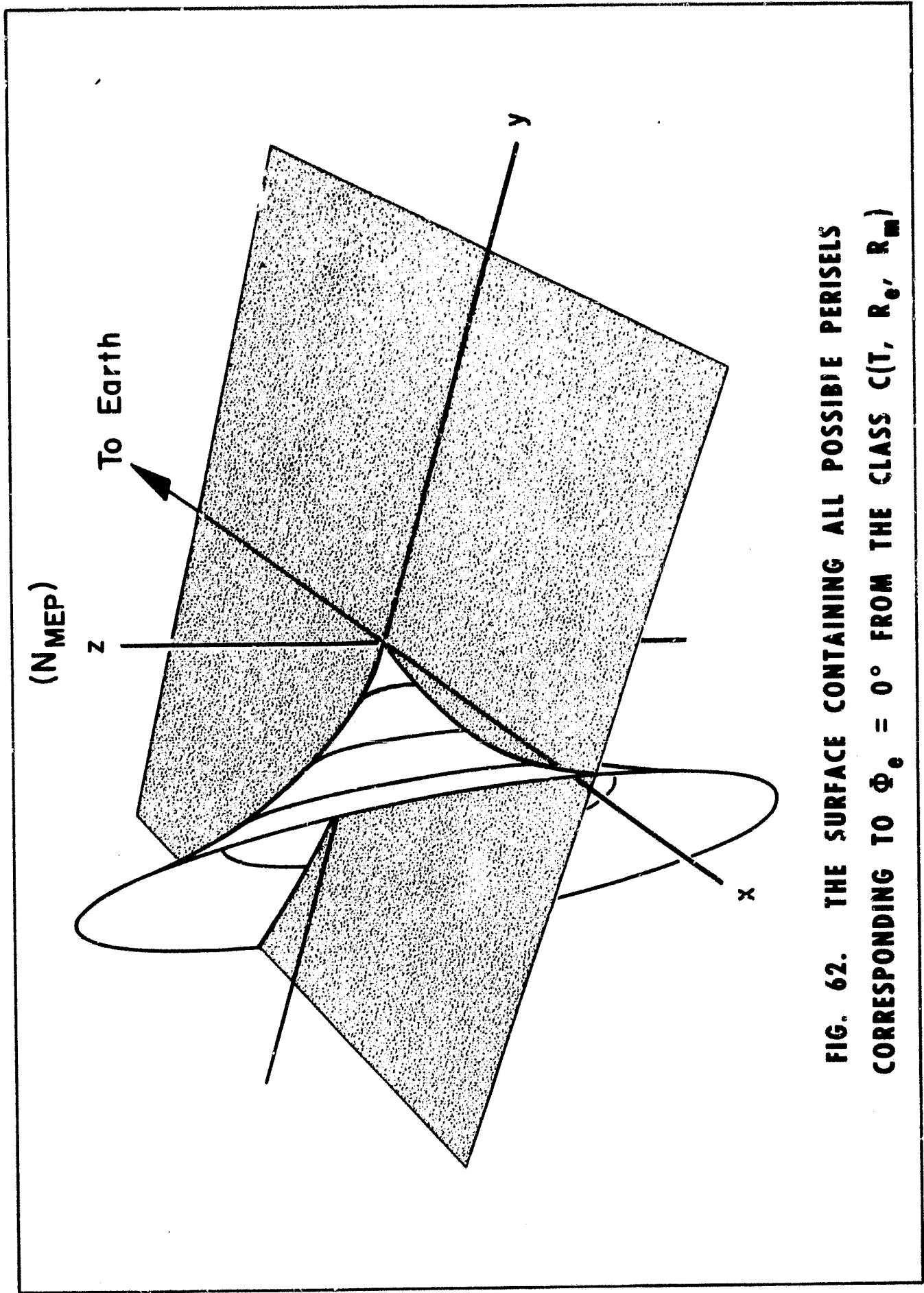


FIG. 61. PERISEL CIRCLES AT VARIOUS RADII CORRESPONDING TO $\Phi_0 = 0^\circ$



**FIG. 62. THE SURFACE CONTAINING ALL POSSIBLE PERISELS
CORRESPONDING TO $\Phi_e = 0^\circ$ FROM THE CLASS C(T, R_e, R_m)**

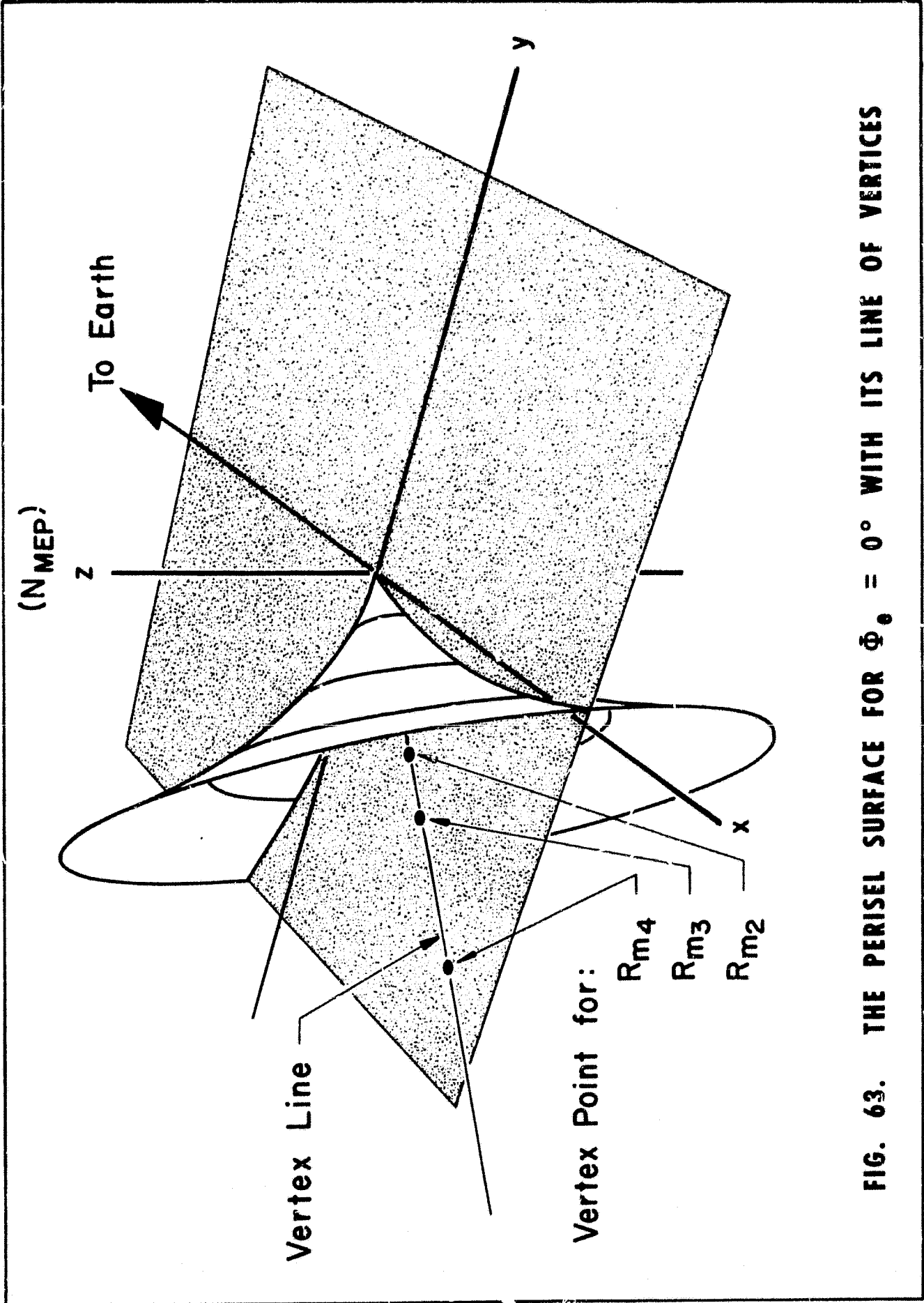


FIG. 63. THE PERISEL SURFACE FOR $\Phi_0 = 0^\circ$ WITH ITS LINE OF VERTICES

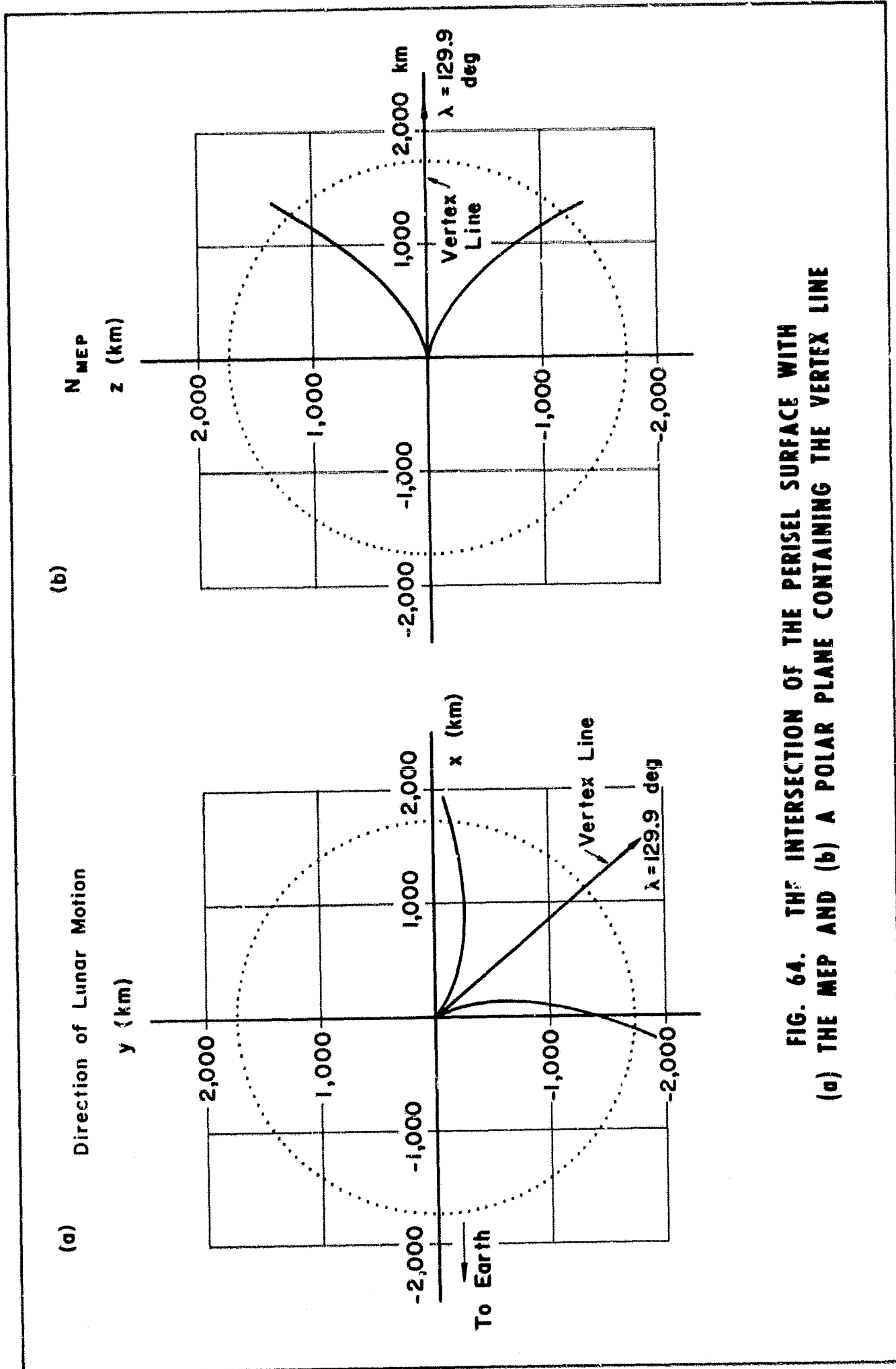


FIG. 64. THE INTERSECTION OF THE PERISEL SURFACE WITH
 (a) THE MEP AND (b) A POLAR PLANE CONTAINING THE VERTEX LINE

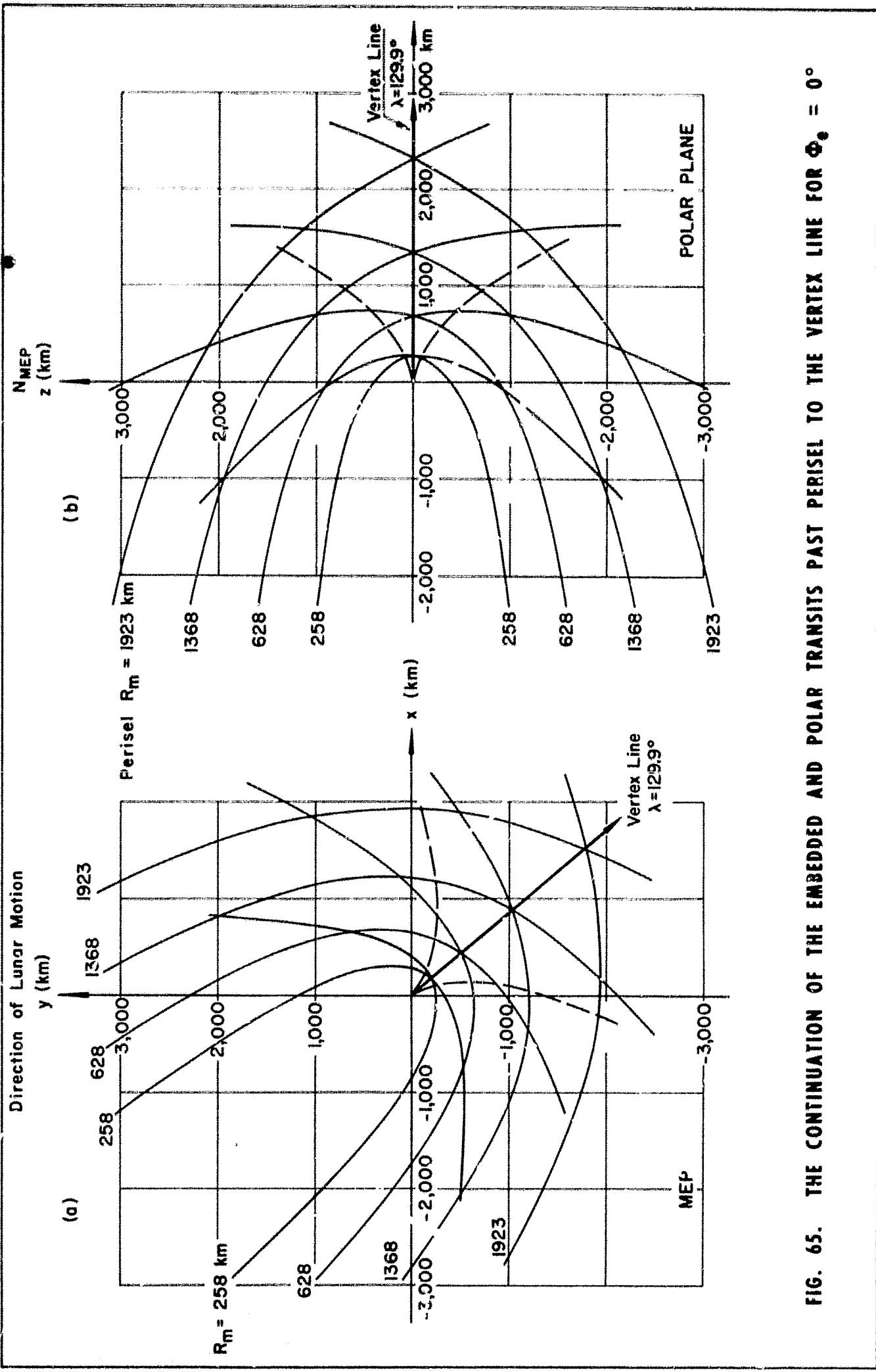


FIG. 65. THE CONTINUATION OF THE EMBEDDED AND POLAR TRANSITS PAST PERISEL TO THE VERTEX LINE FOR $\Phi_0 = 0^\circ$

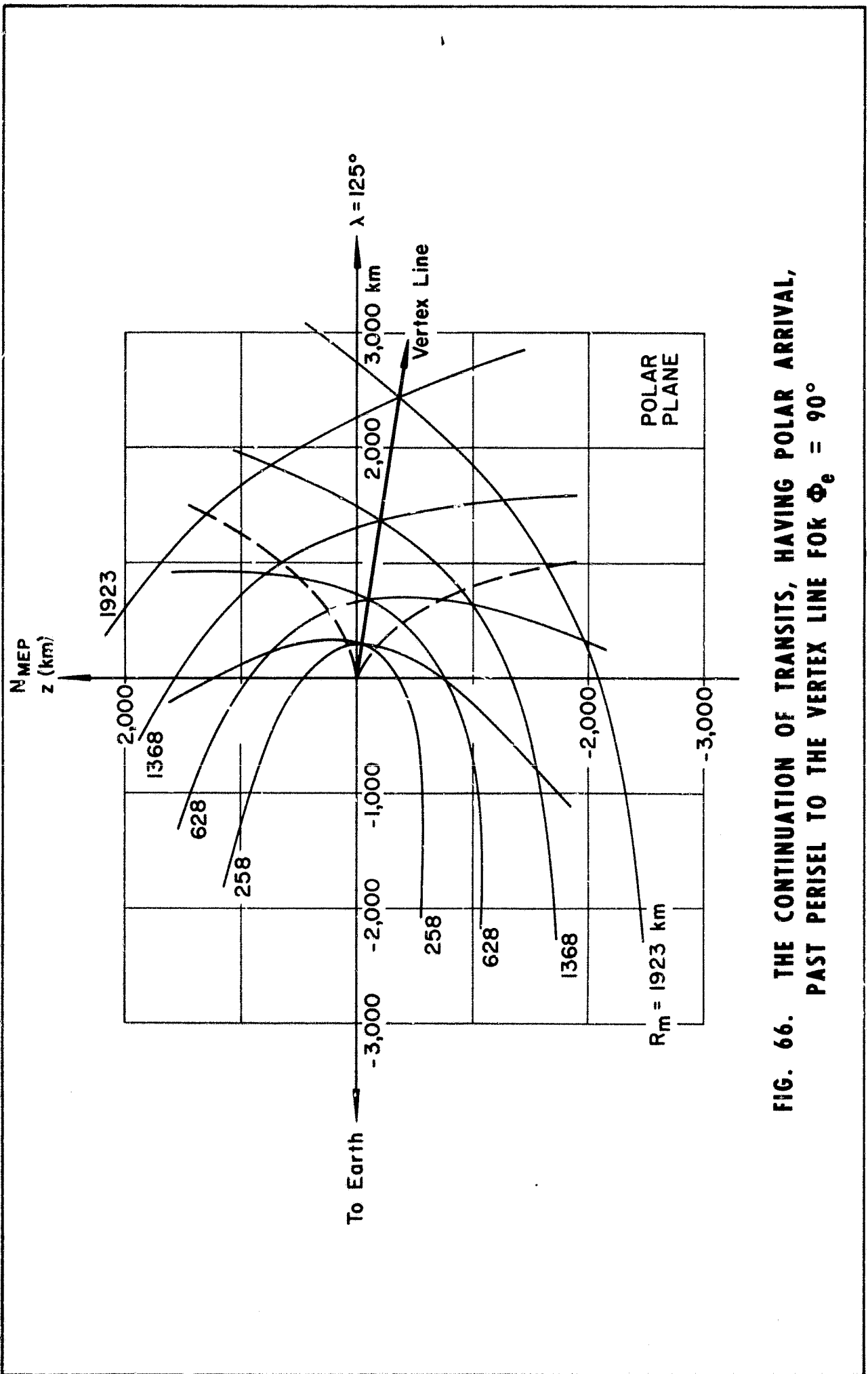


FIG. 66. THE CONTINUATION OF TRANSITS, HAVING POLAR ARRIVAL, PAST PERISEL TO THE VERTEX LINE FOR $\Phi_e = 90^\circ$

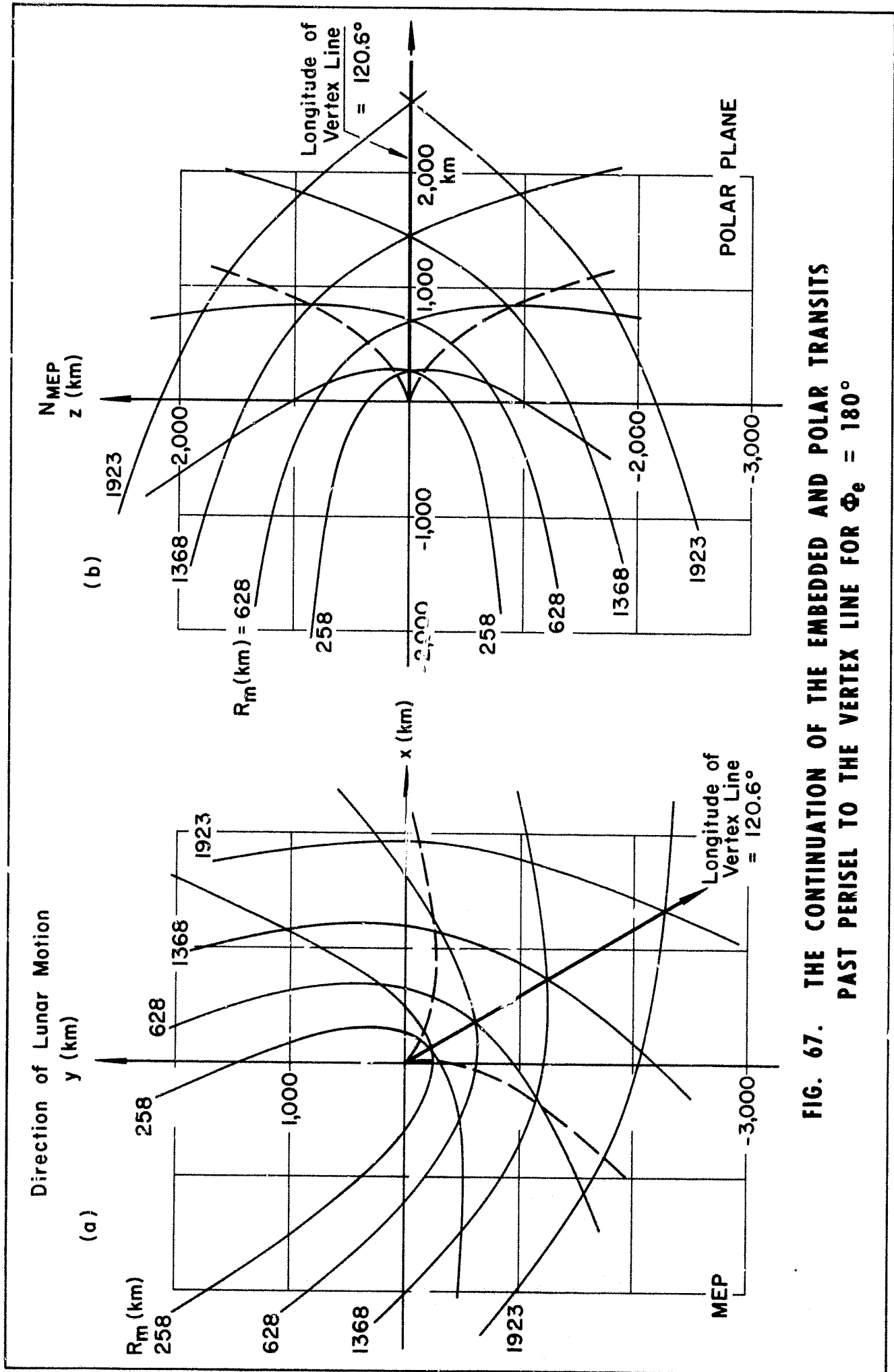
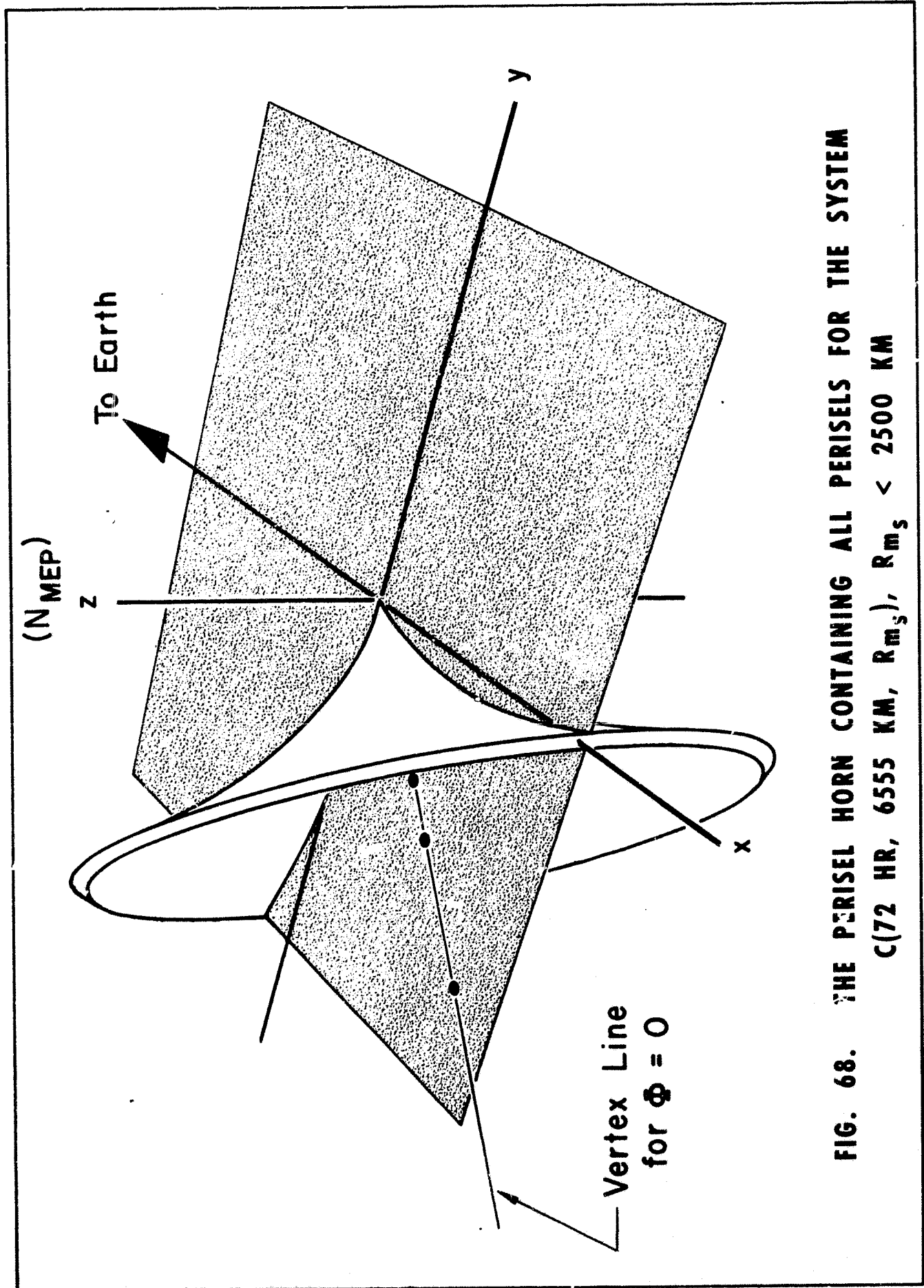


FIG. 67. THE CONTINUATION OF THE EMBEDDED AND POLAR TRANSITS PAST PERISEL TO THE VERTEX LINE FOR $\Phi_e = 180^\circ$



**FIG. 68. THE PERISEL HORN CONTAINING ALL PERISELS FOR THE SYSTEM
C(72 HR, 6555 KM, R_{ms}), $R_{ms} < 2500$ KM**

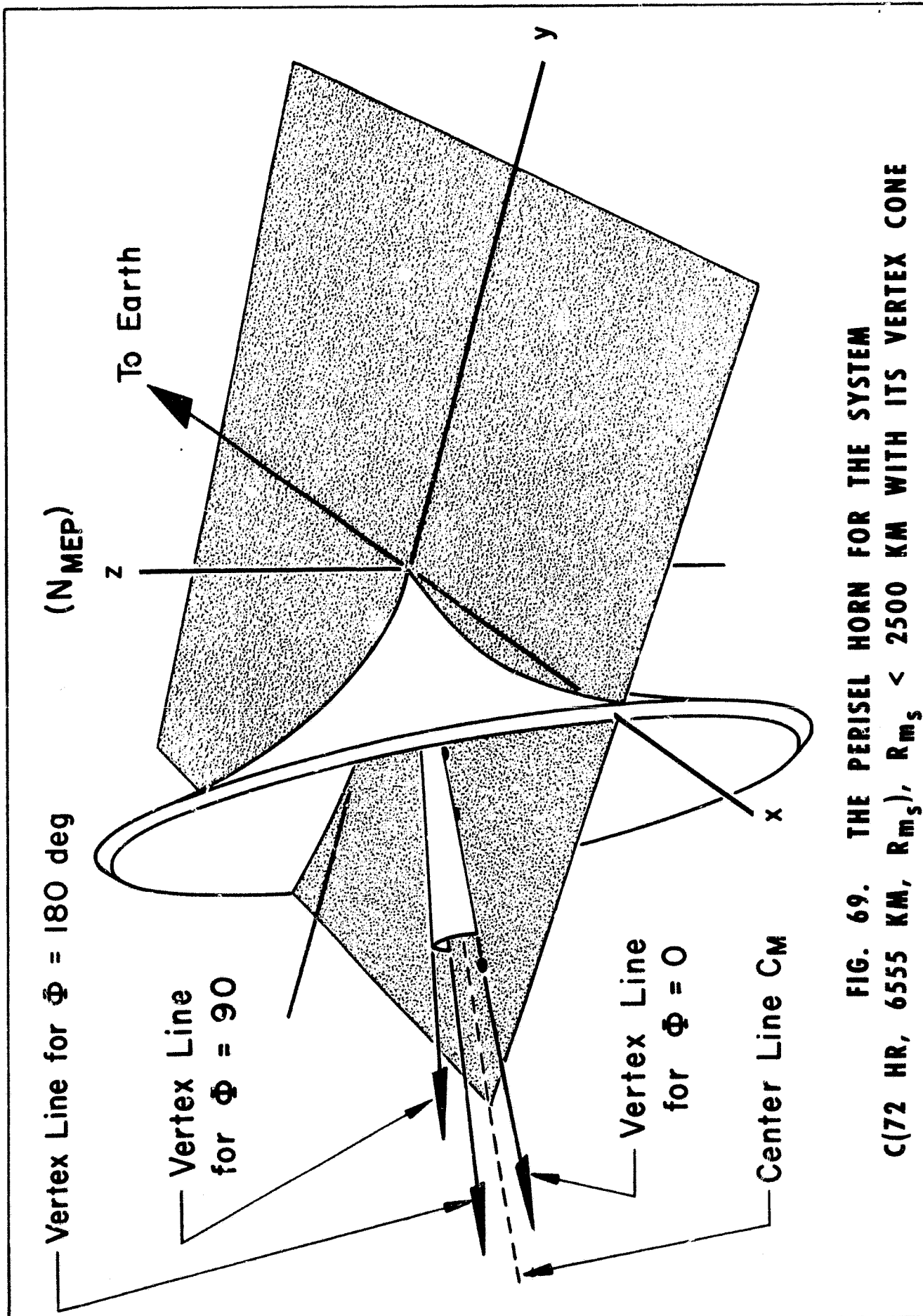


FIG. 69. THE PERISEL HORN FOR THE SYSTEM
 C(72 HR, 6555 KM, R_{m_s}), $R_{m_s} < 2500$ KM WITH ITS VERTEX CONE

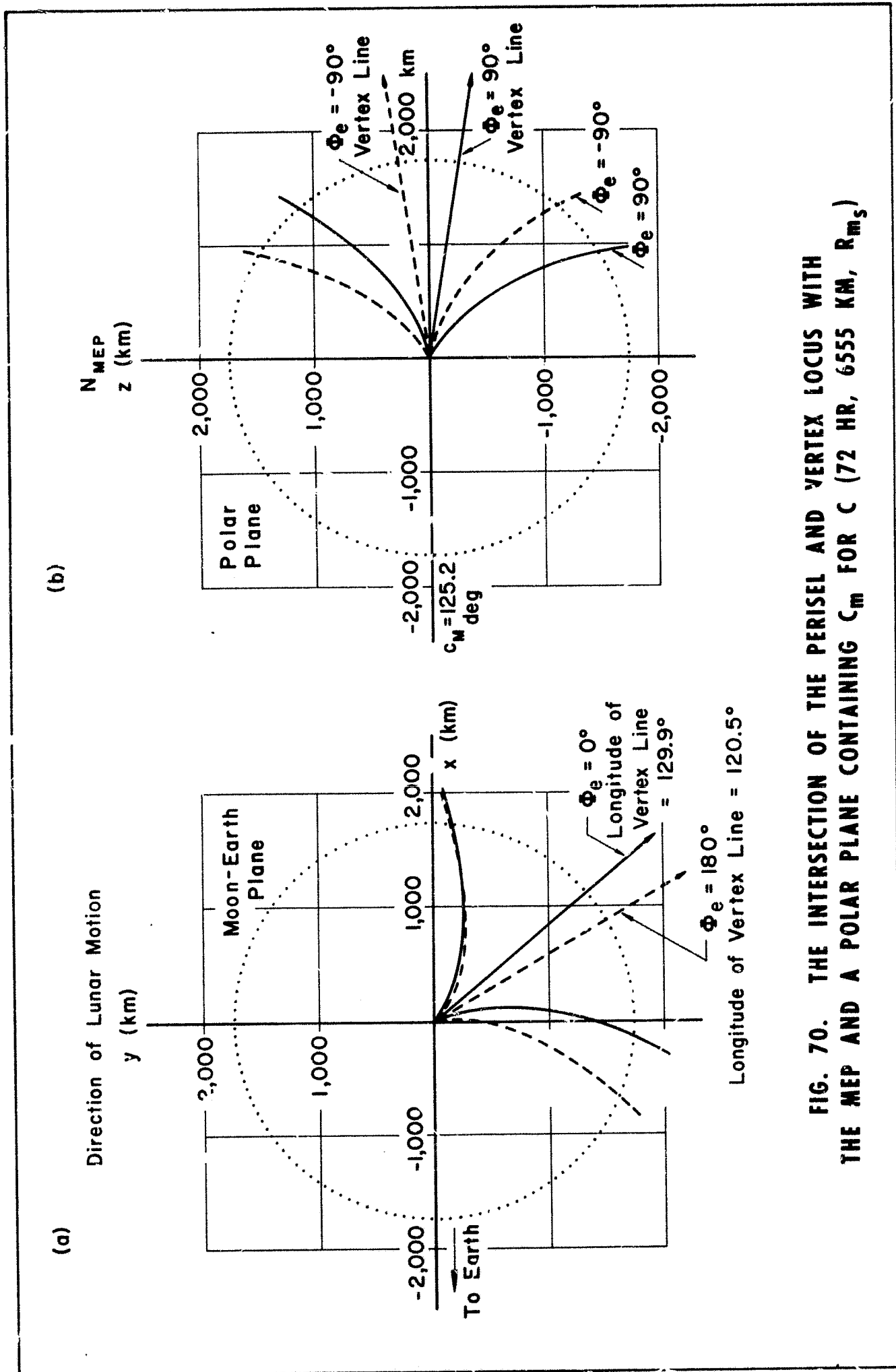


FIG. 70. THE INTERSECTION OF THE PERISEL AND VERTEX LOCUS WITH THE MEP AND A POLAR PLANE CONTAINING C_M FOR C (72 HR, 6555 KM, R_{m_s})

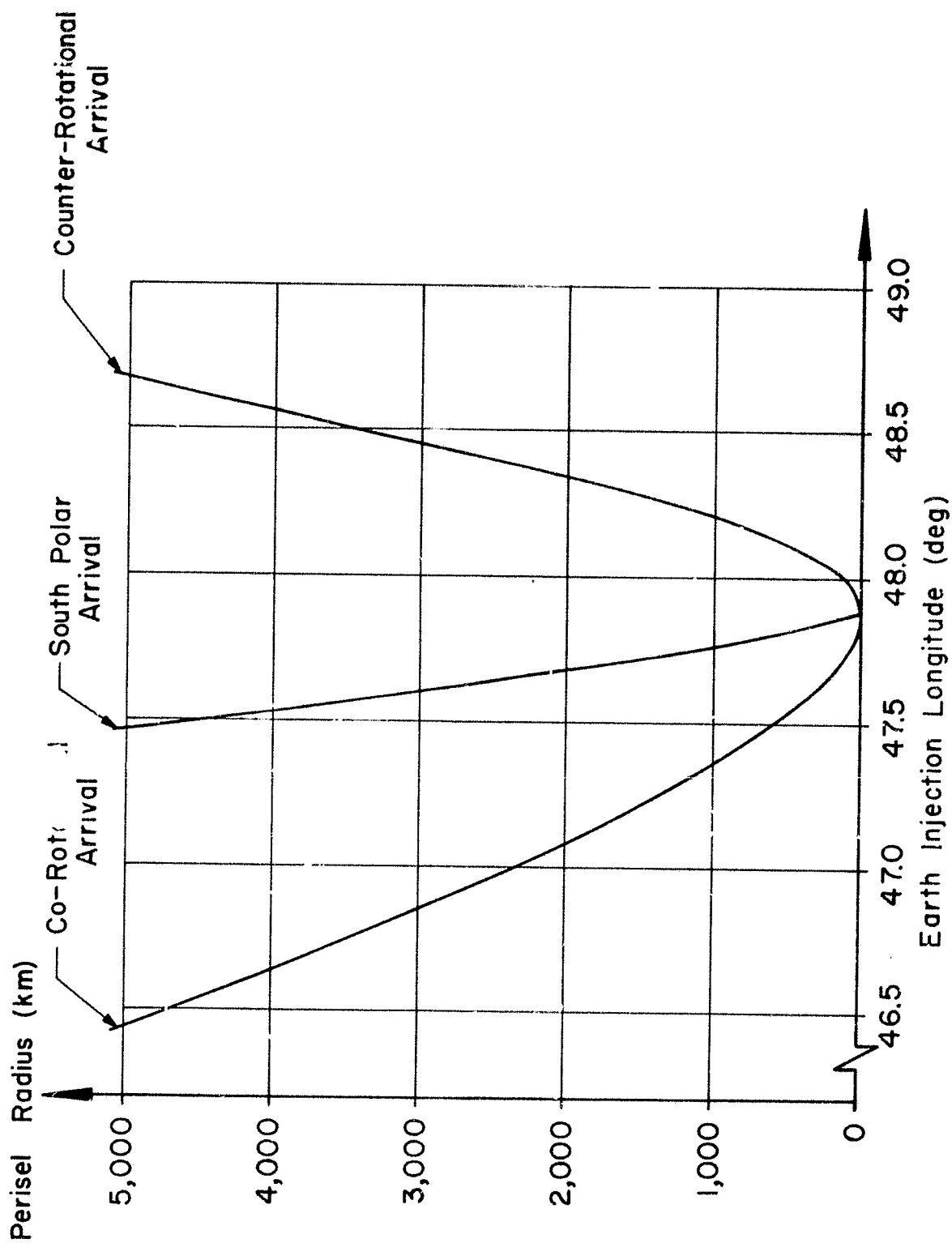


FIG. 71. LOCATION OF PERIGEE FOR TRANSITS FROM $\Phi_e = 0^\circ$ BELONGING TO THE SYSTEM C (72 HR, 6555 KM, R_{ms})

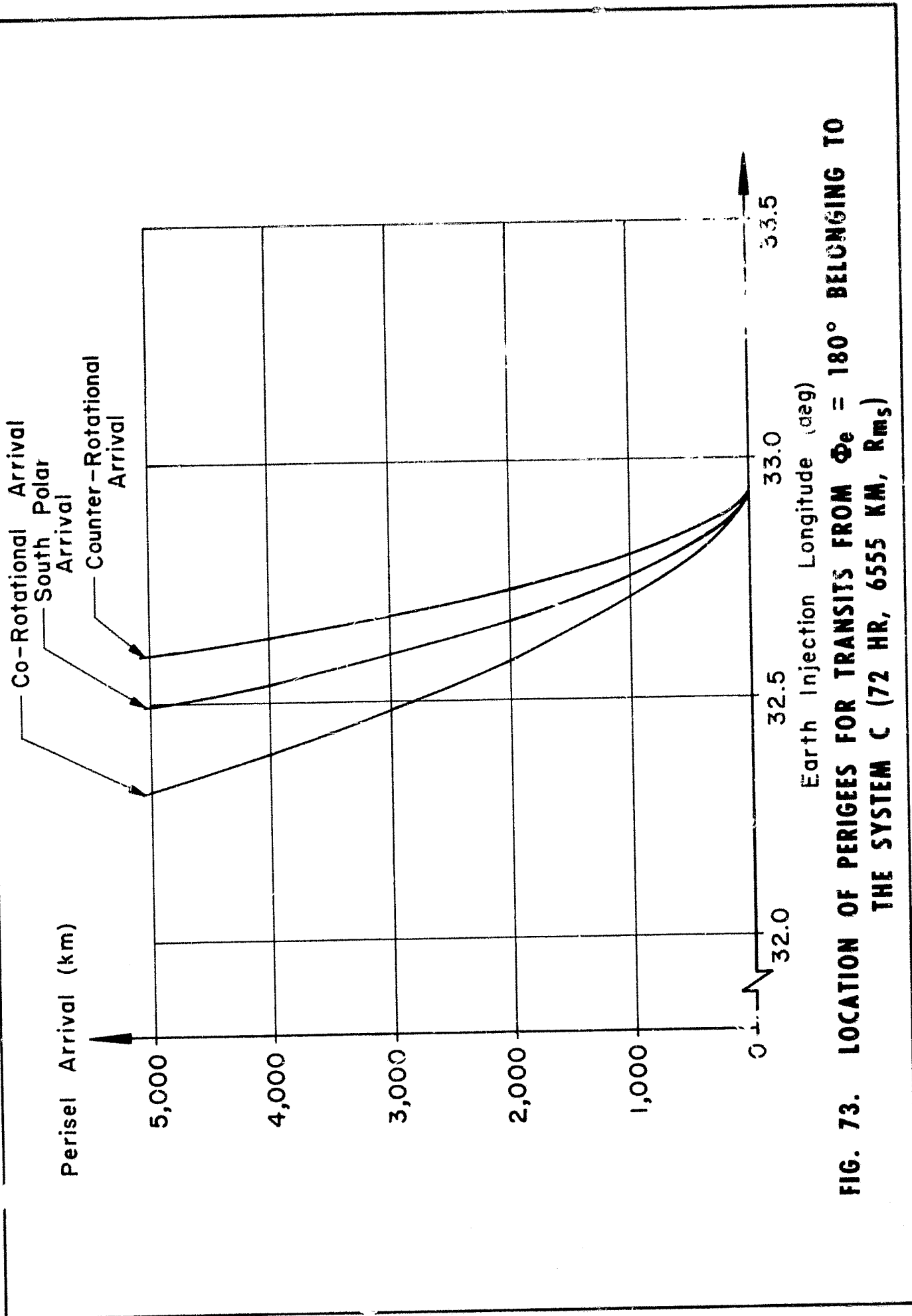


FIG. 73. LOCATION OF PERIGEEES FOR TRANSITS FROM $\Phi_e = 180^\circ$ BELONGING TO THE SYSTEM C (72 HR, 6555 KM, R_{ms})

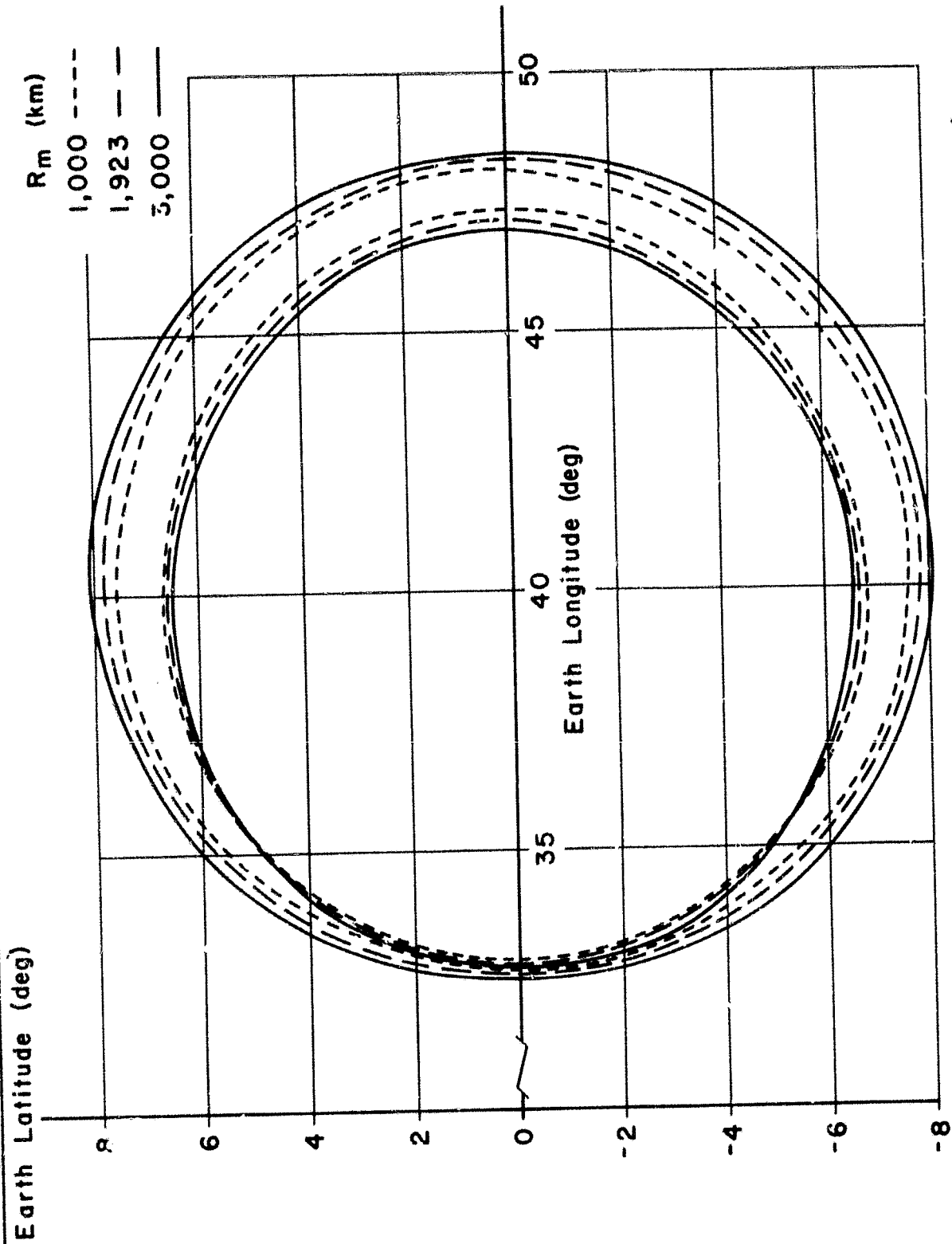
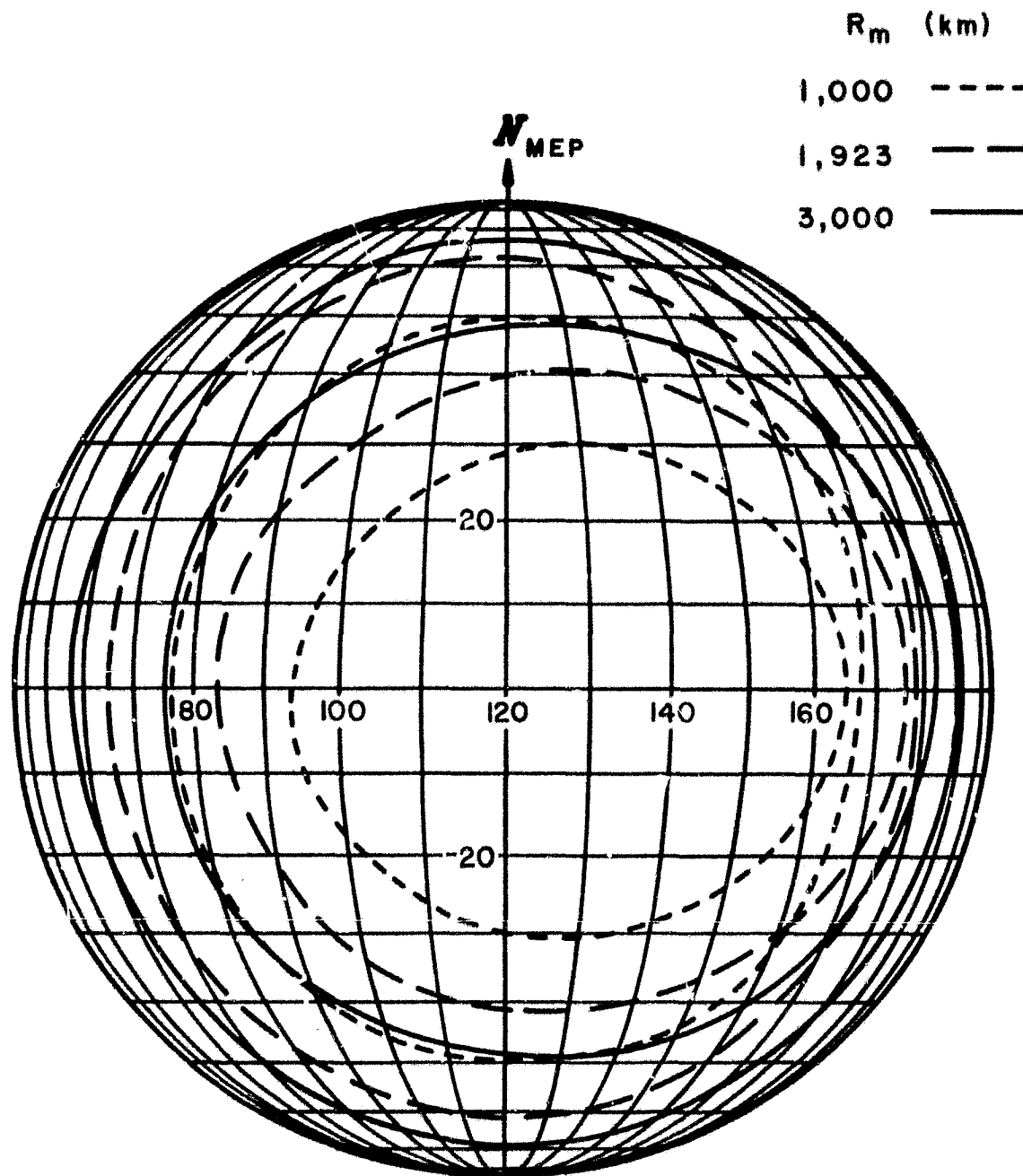


FIG. 75. PERIGEE BELTS FROM THE SYSTEM C (72 HR, 6555 KM, R_{ms}),
 $R_m = 1000$ KM, 1923 KM, AND 3000 KM



**FIG. 76. PROJECTIONS OF PERISEL BELTS AT
 $R_m = 1,000$ km, $1,923$ km AND $3,000$ km FROM THE SYSTEM
 $C(72$ hr, $6,555$ km, $R_{m_s})$ ONTO A COMMON SPHERE**

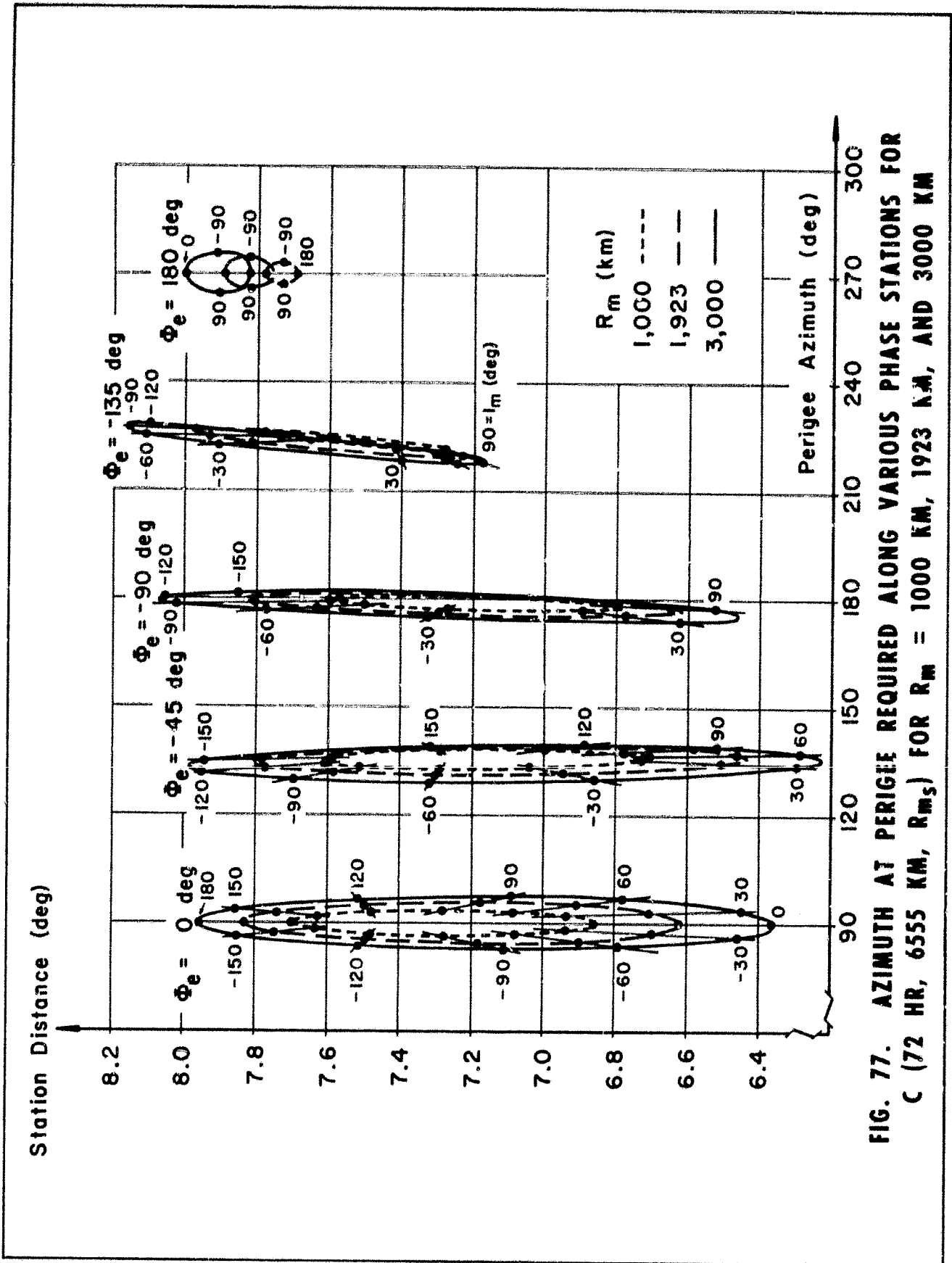
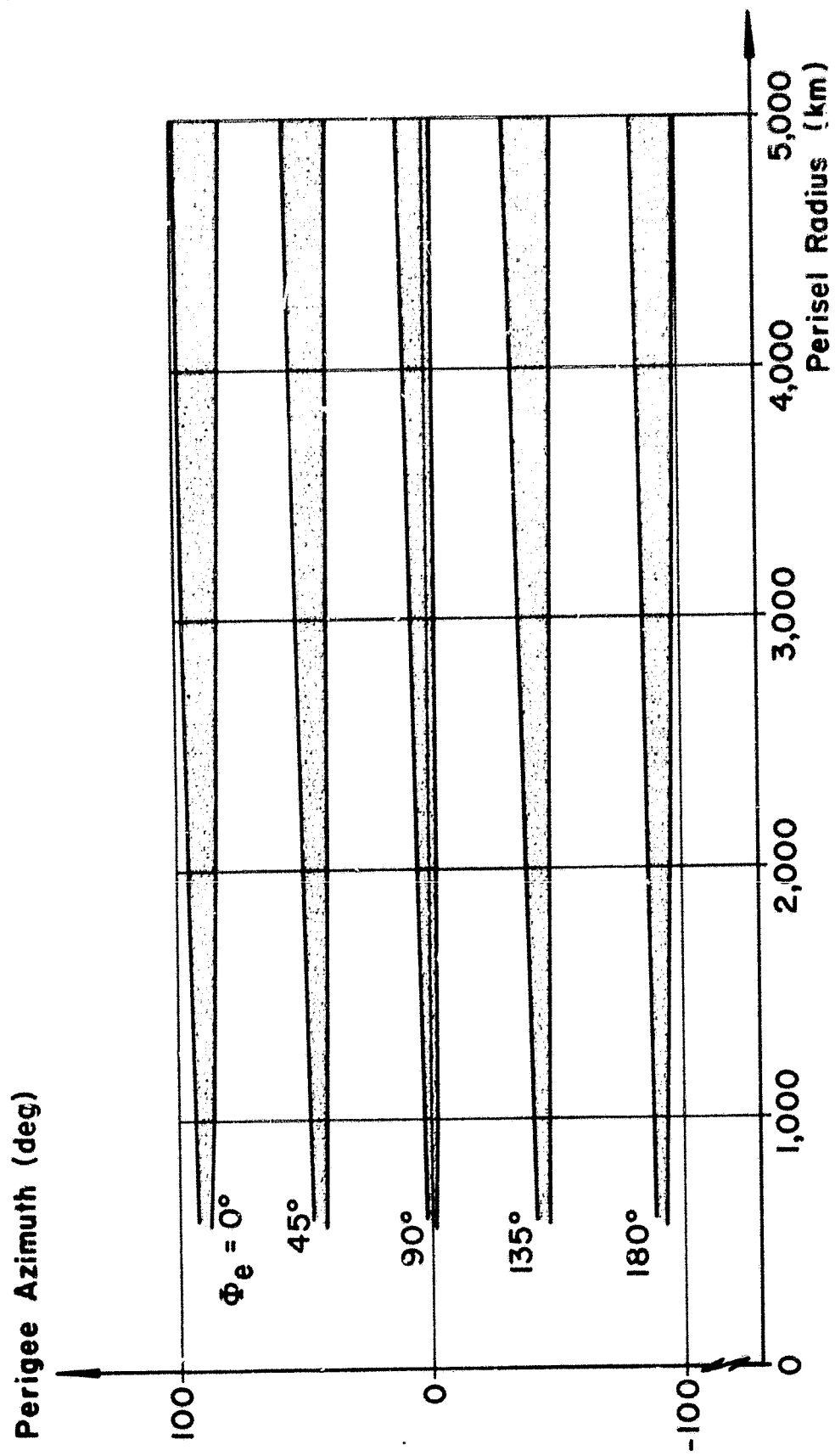


FIG. 77. AZIMUTH AT PERIGEE REQUIRED ALONG VARIOUS PHASE STATIONS FOR C (72 HR, 6555 KM, R_{m5}) FOR $R_m = 1000$ KM, 1923 KM, AND 3000 KM



**FIG. 78. AZIMUTHS REQUIRED TO ENVELOP THE MOON
FROM VARIOUS PHASE STATIONS
VS PERISEL RADIUS FOR THE SYSTEM C (72 HR, 6555 KM, R_{ms})**

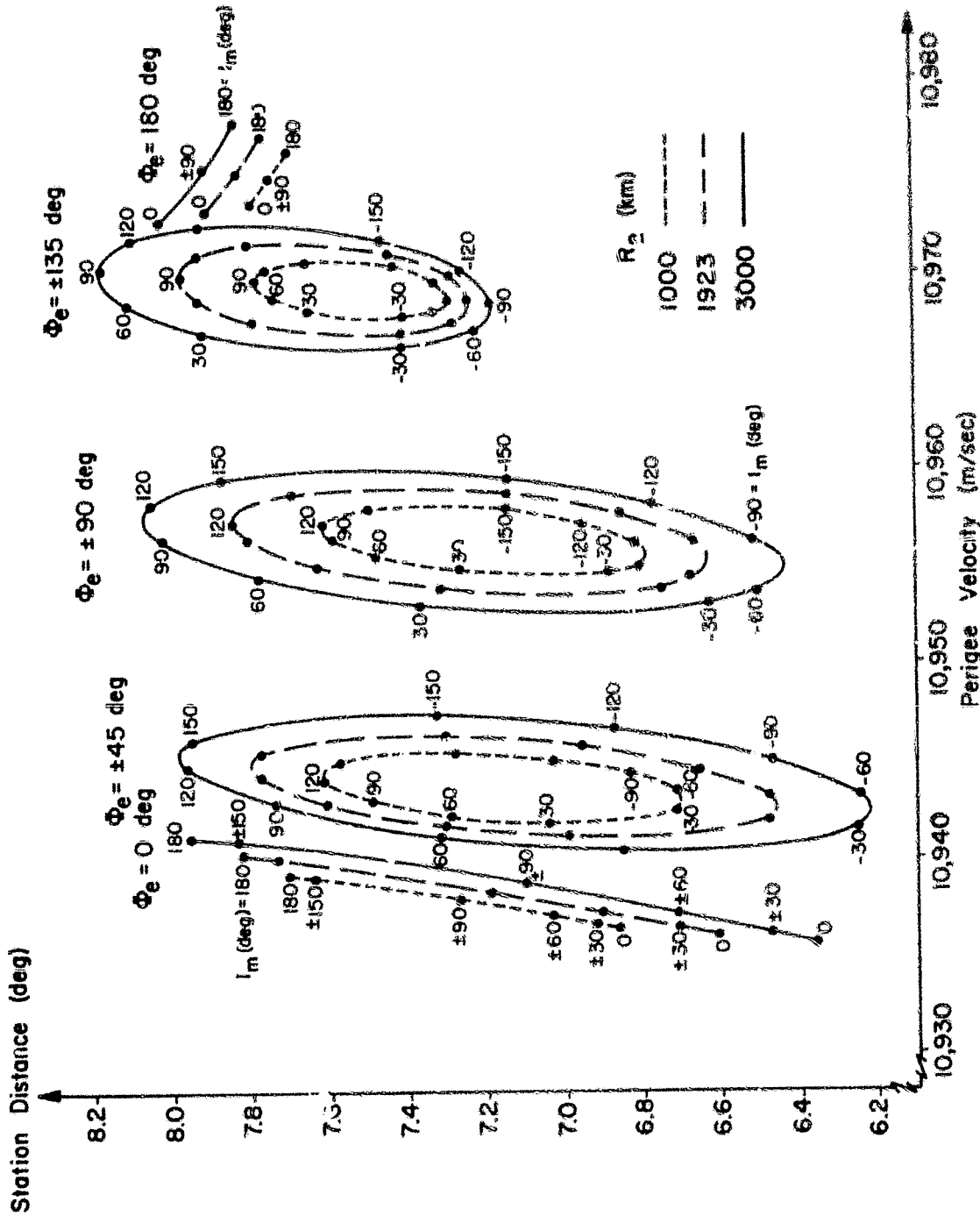


FIG. 79. PERIGEE VELOCITY REQUIREMENTS FOR POINTS ALONG THE GIVEN PHASE STATIONS FOR PERISEL RADIUS OF 1000 KM, 1923 KM, AND 3000 KM FROM THE CLASSES C (72 HR, 6555 KM, R_{m_2})

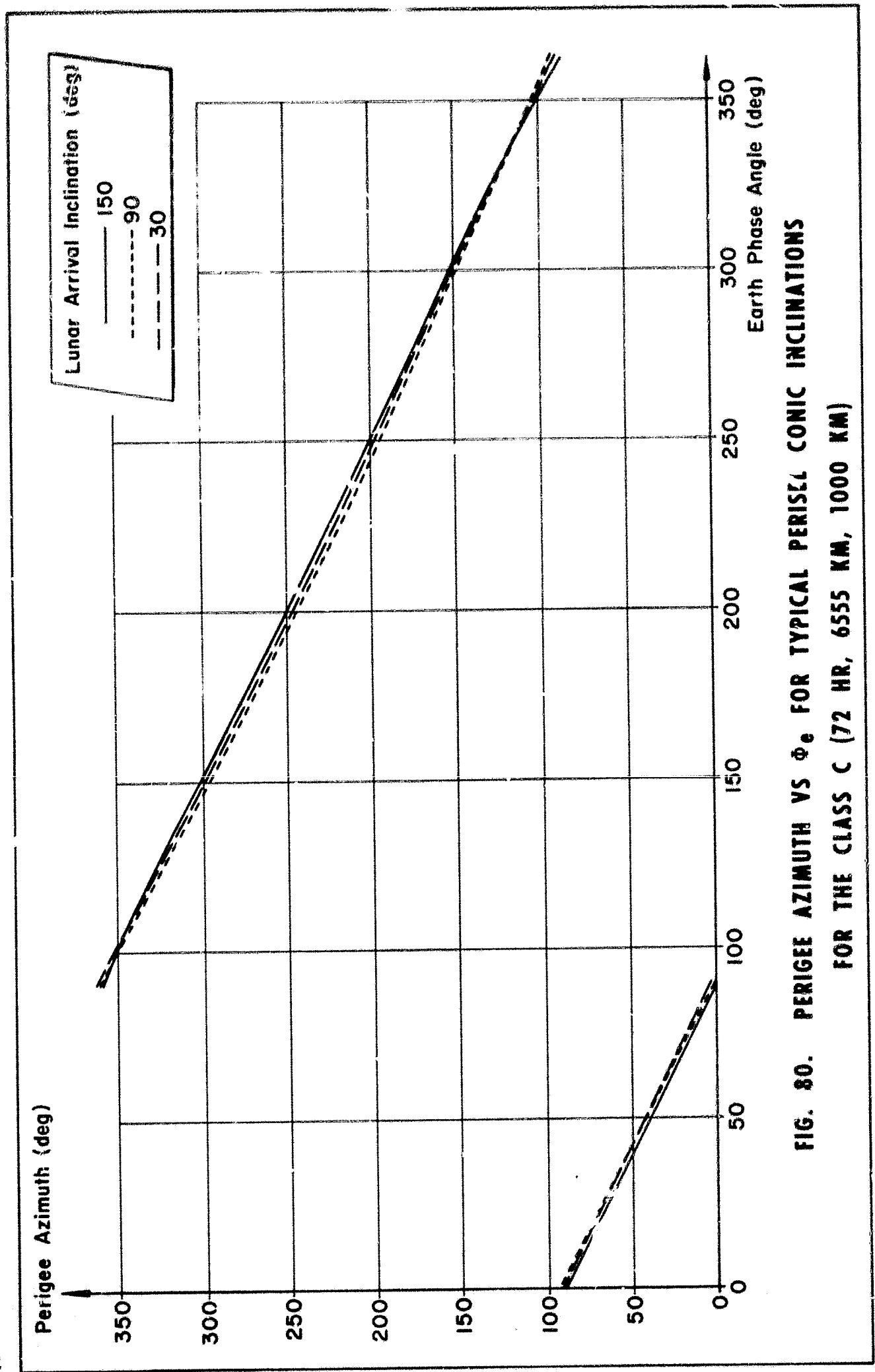


FIG. 80. PERIGEE AZIMUTH VS ϕ_e FOR TYPICAL PERISEL CONIC INCLINATIONS FOR THE CLASS C (72 HR, 6555 KM, 1000 KM)

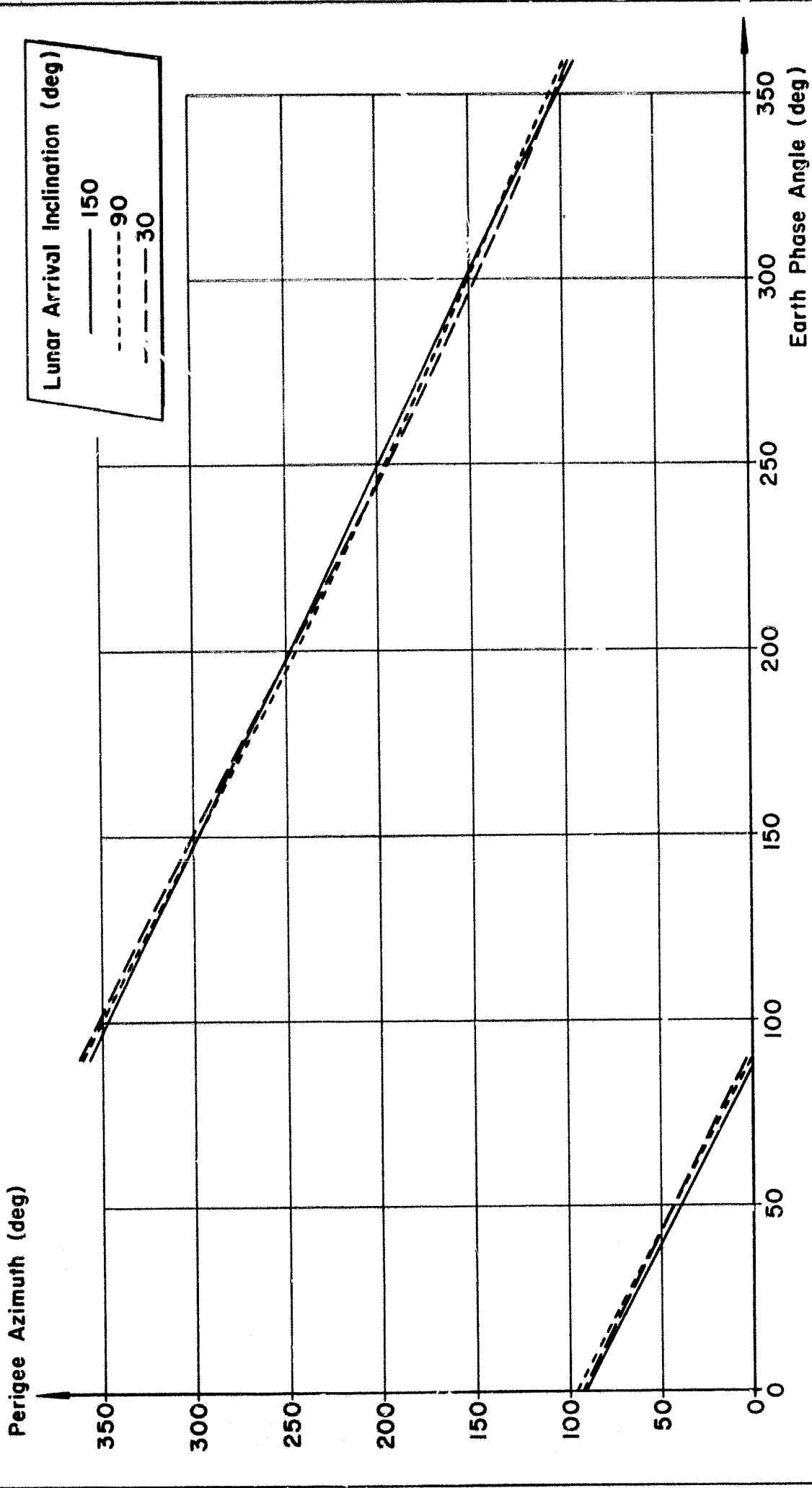
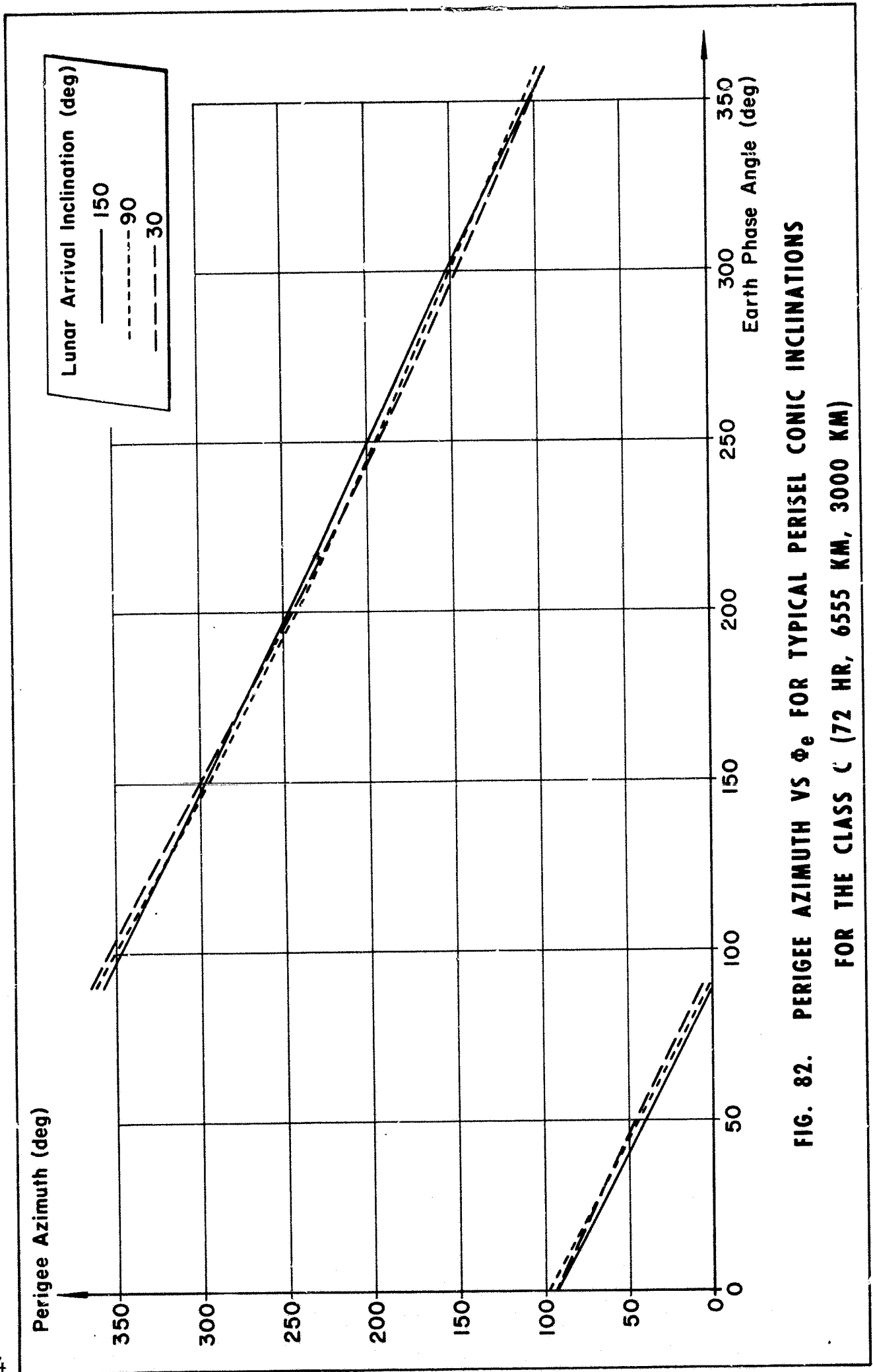


FIG. 81. PERIGEE AZIMUTH VS ϕ_e FOR TYPICAL PERISEL CONIC INCLINATIONS FOR THE CLASS C (72 HR, 6555 KM, 1923 KM)



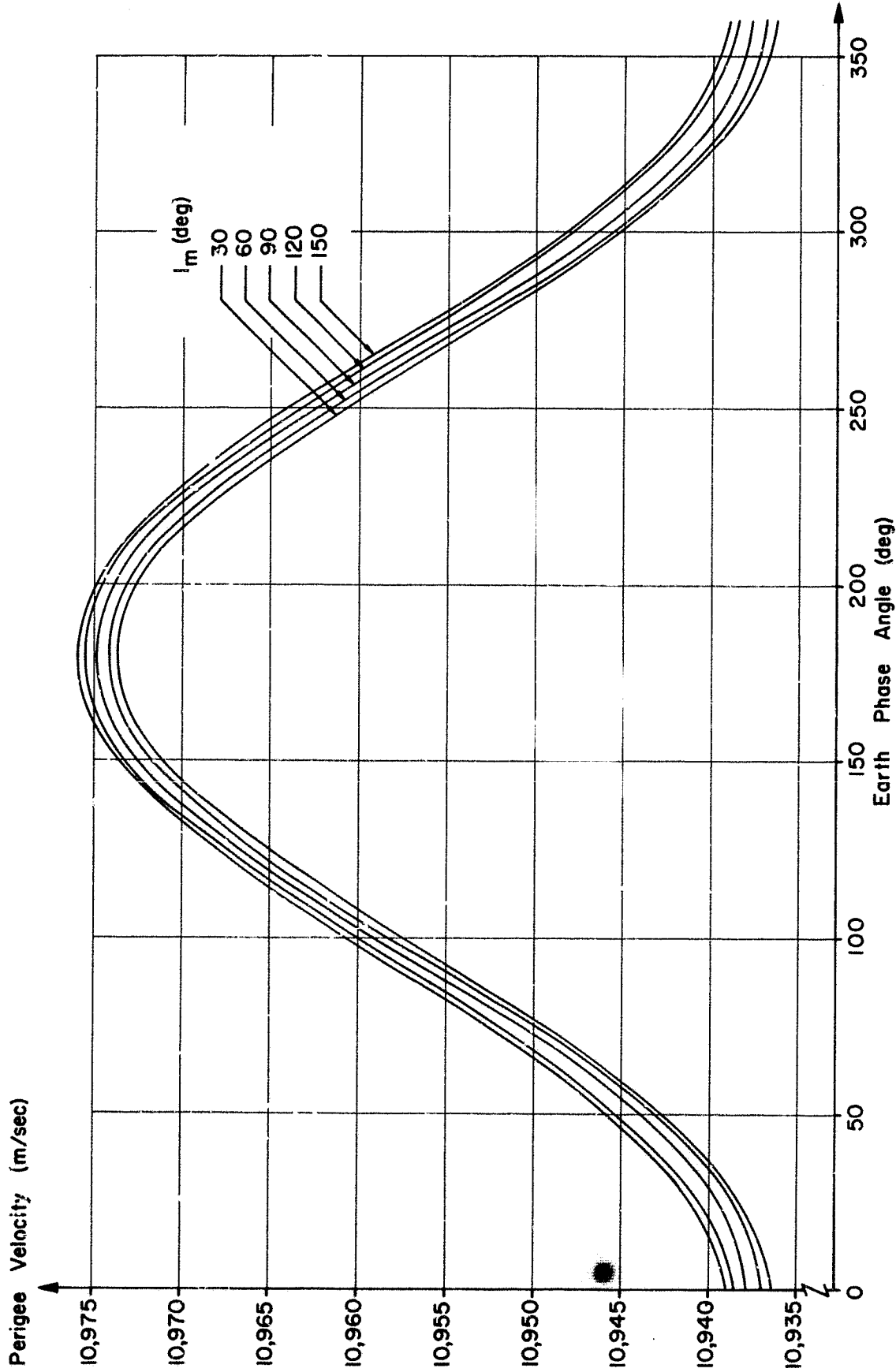


FIG. 83. PERIGEE VELOCITY REQUIRED FOR LUNAR ARRIVAL INCLINATIONS OF 30°, 60°, 90°, 120°, AND 150° FOR PERISEL RADIUS OF 1000 KM, C (72 HR, 6555 KM, 1000 KM)

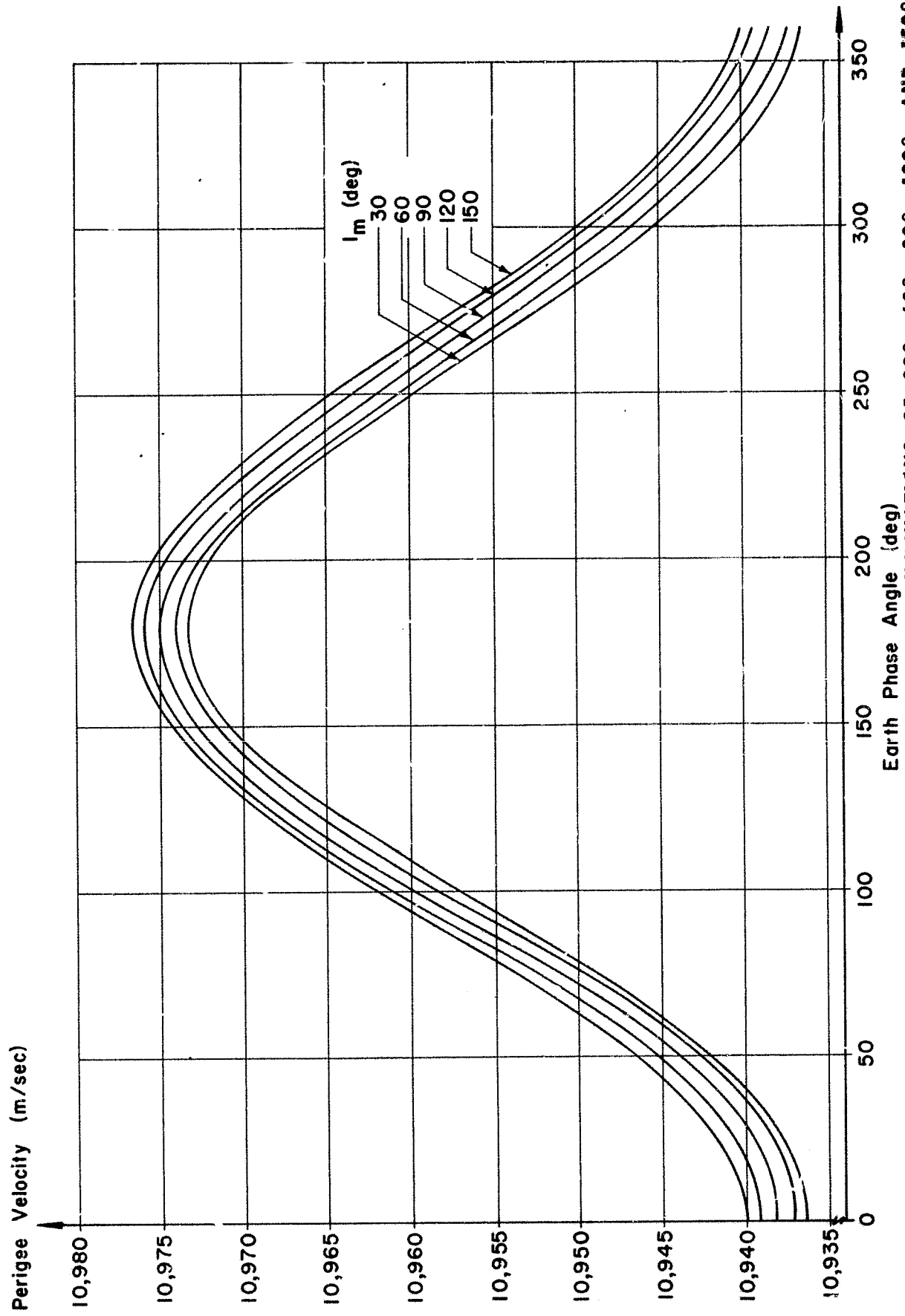


FIG. 84. PERIGEE VELOCITY REQUIRED FOR LUNAR ARRIVAL INCLINATIONS OF 30°, 60°, 90°, 120°, AND 150° FOR PERISEL RADIUS OF 1923 KM, C (72 HR, 6555 KM, 1923 KM)

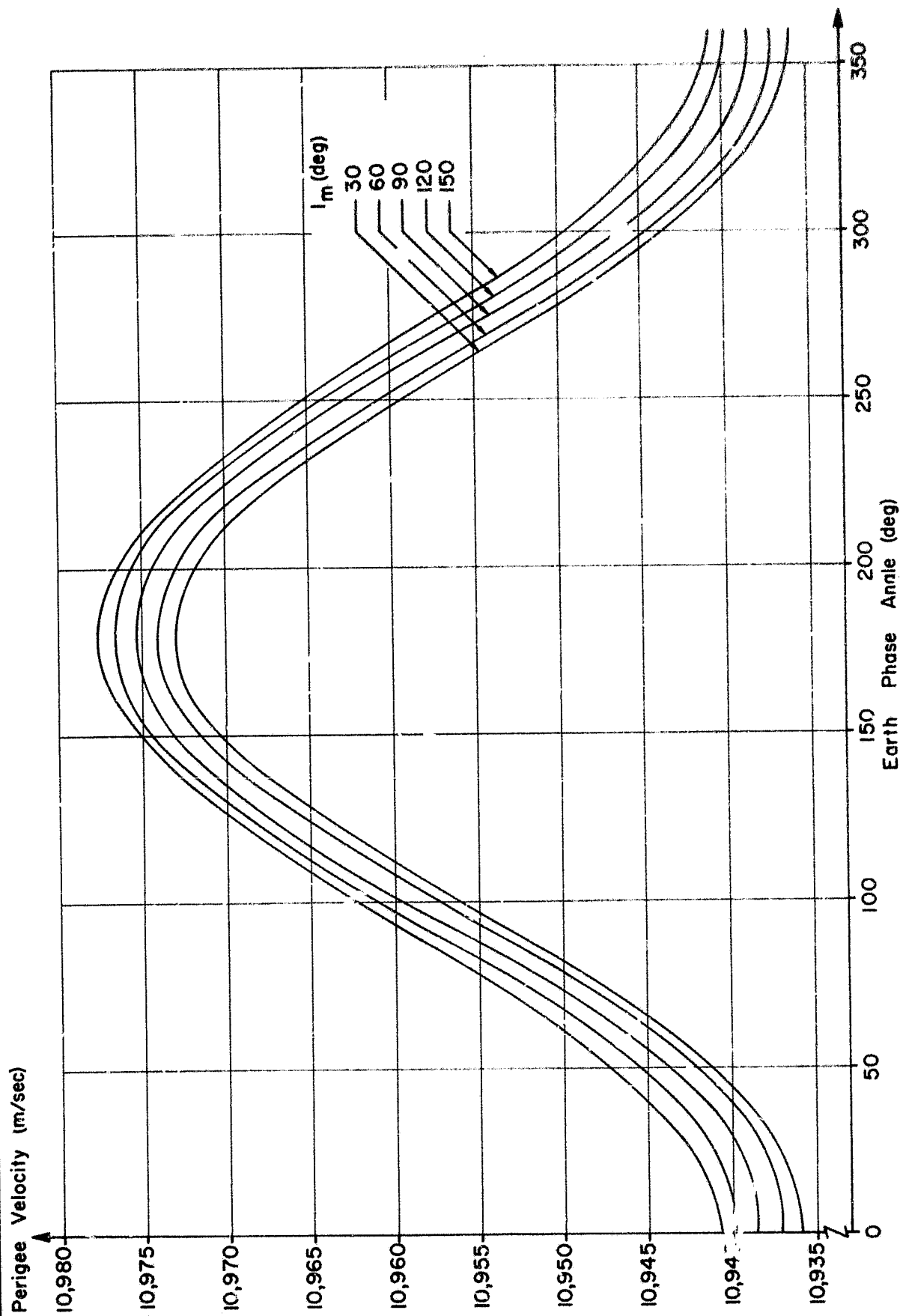


FIG. 85. PERIGEE VELOCITY REQUIRED FOR LUNAR ARRIVAL INCLINATIONS OF 30°, 60°, 90°, 120°, AND 150° FOR PERISEL RADIUS OF 3000 KM, C (72 HR, 6555 KM, 3000 KM)

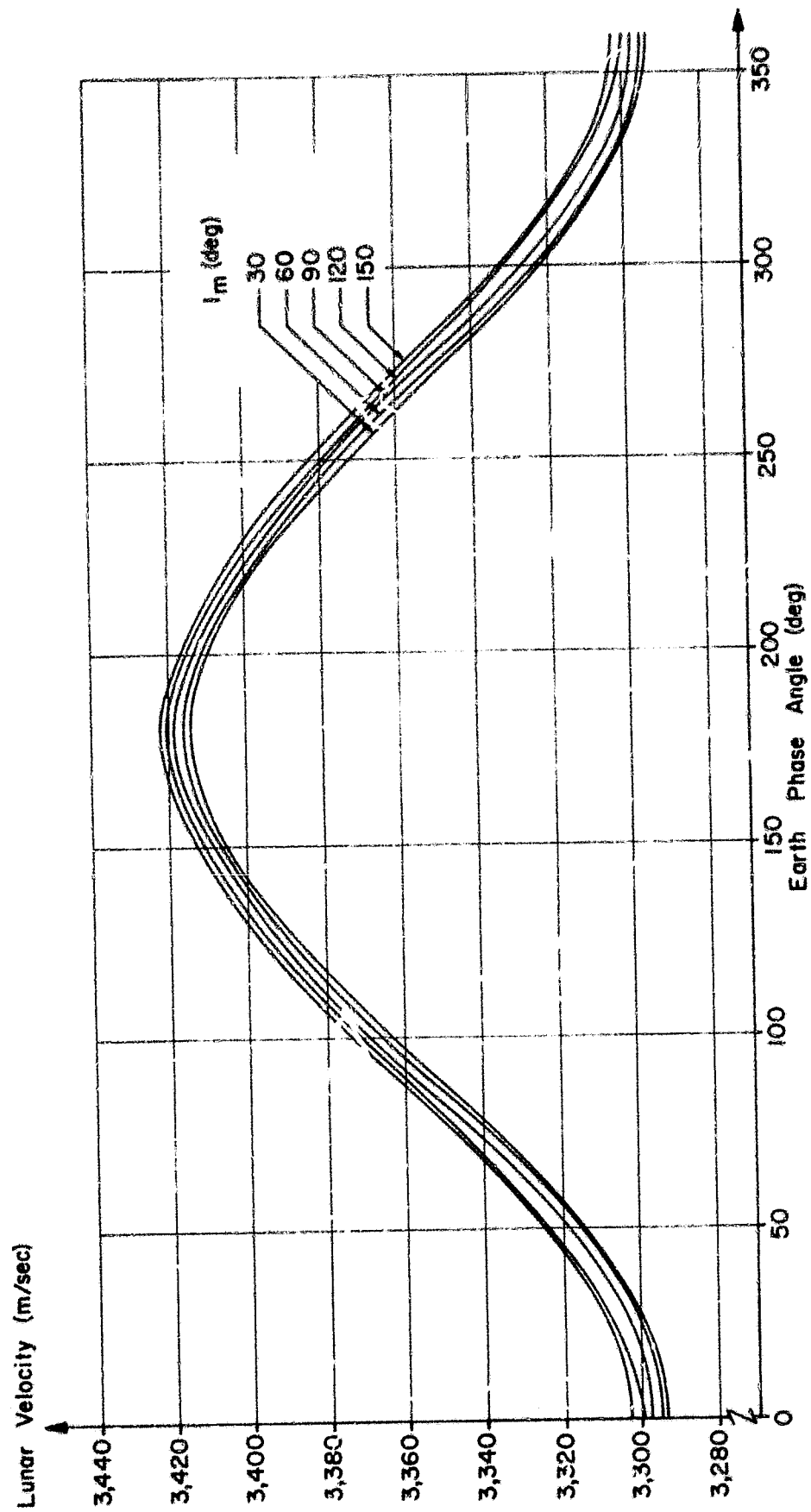


FIG. 86. LUNAR ARRIVAL VELOCITY FOR VARIOUS ARRIVAL INCLINATIONS AT PERISEL RADIUS OF 1000 KM, C (72 HR, 6555 KM, 1000 KM)

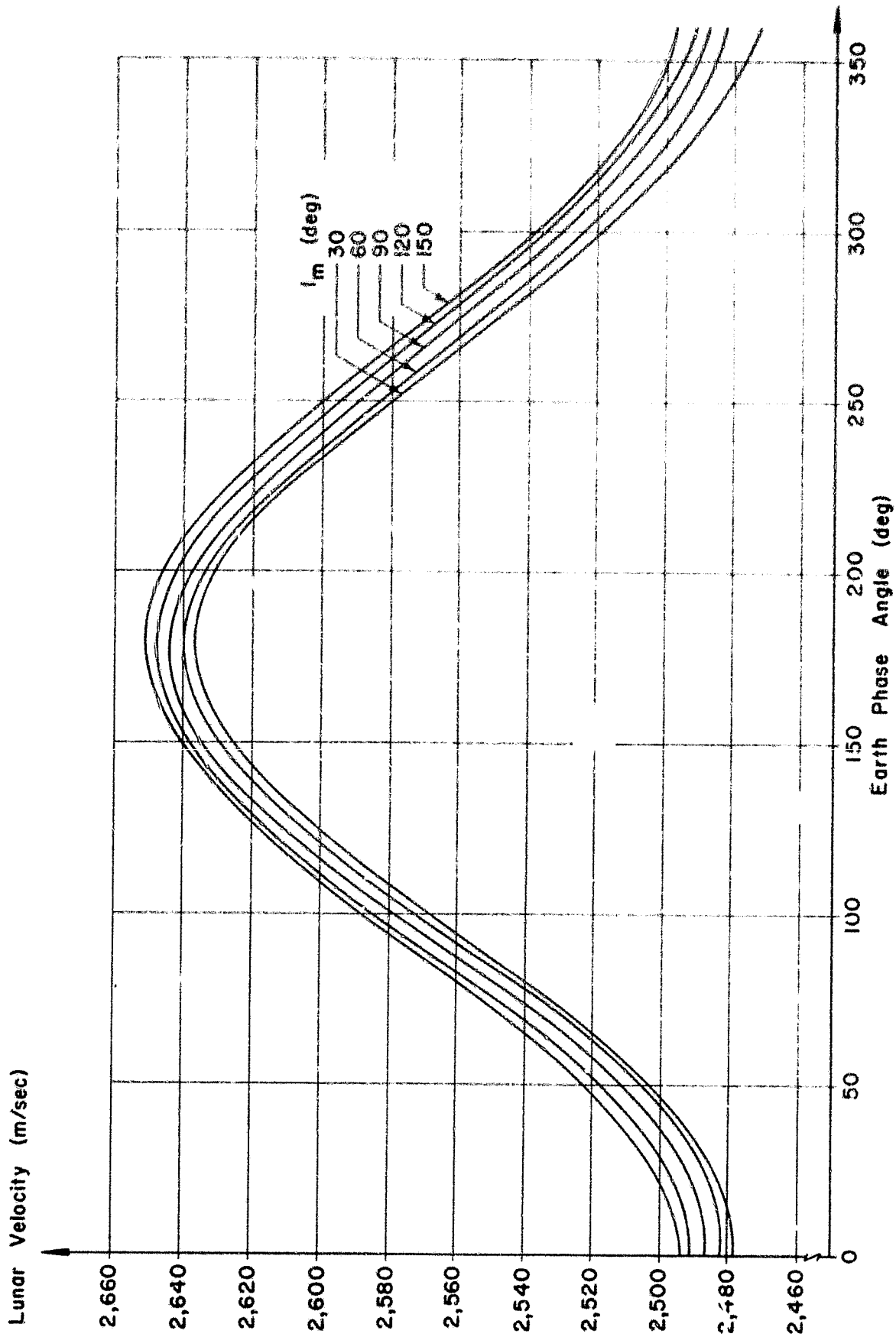


FIG. 87. LUNAR ARRIVAL VELOCITY FOR VARIOUS ARRIVAL INCLINATIONS AT PERISEL RADIUS OF 1923 KM, C (72 HR, 6555 KM, 1923 KM)

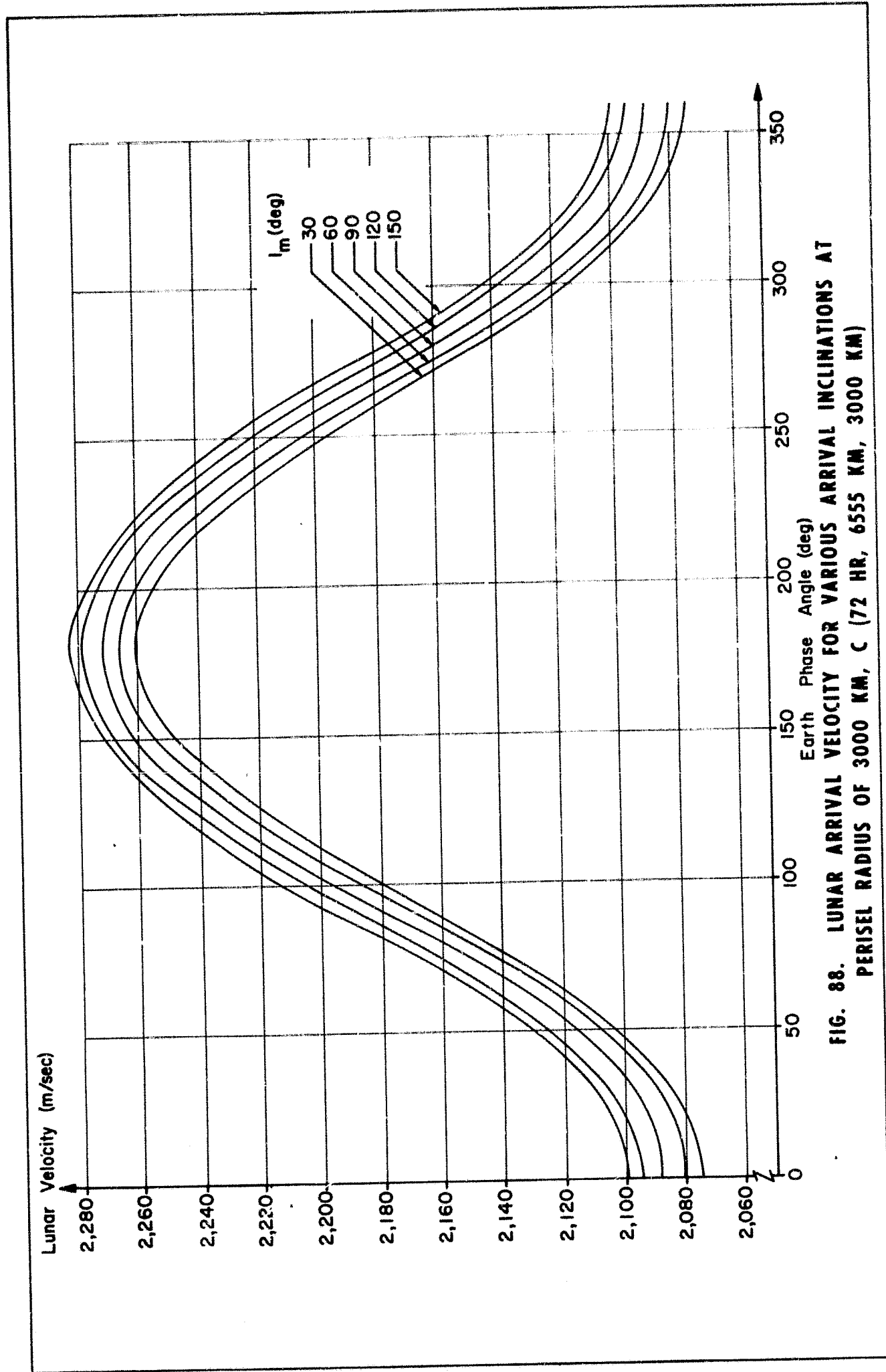


FIG. 88. LUNAR ARRIVAL VELOCITY FOR VARIOUS ARRIVAL INCLINATIONS AT PERISEL RADIUS OF 3000 KM, C (72 HR, 6555 KM, 3000 KM)

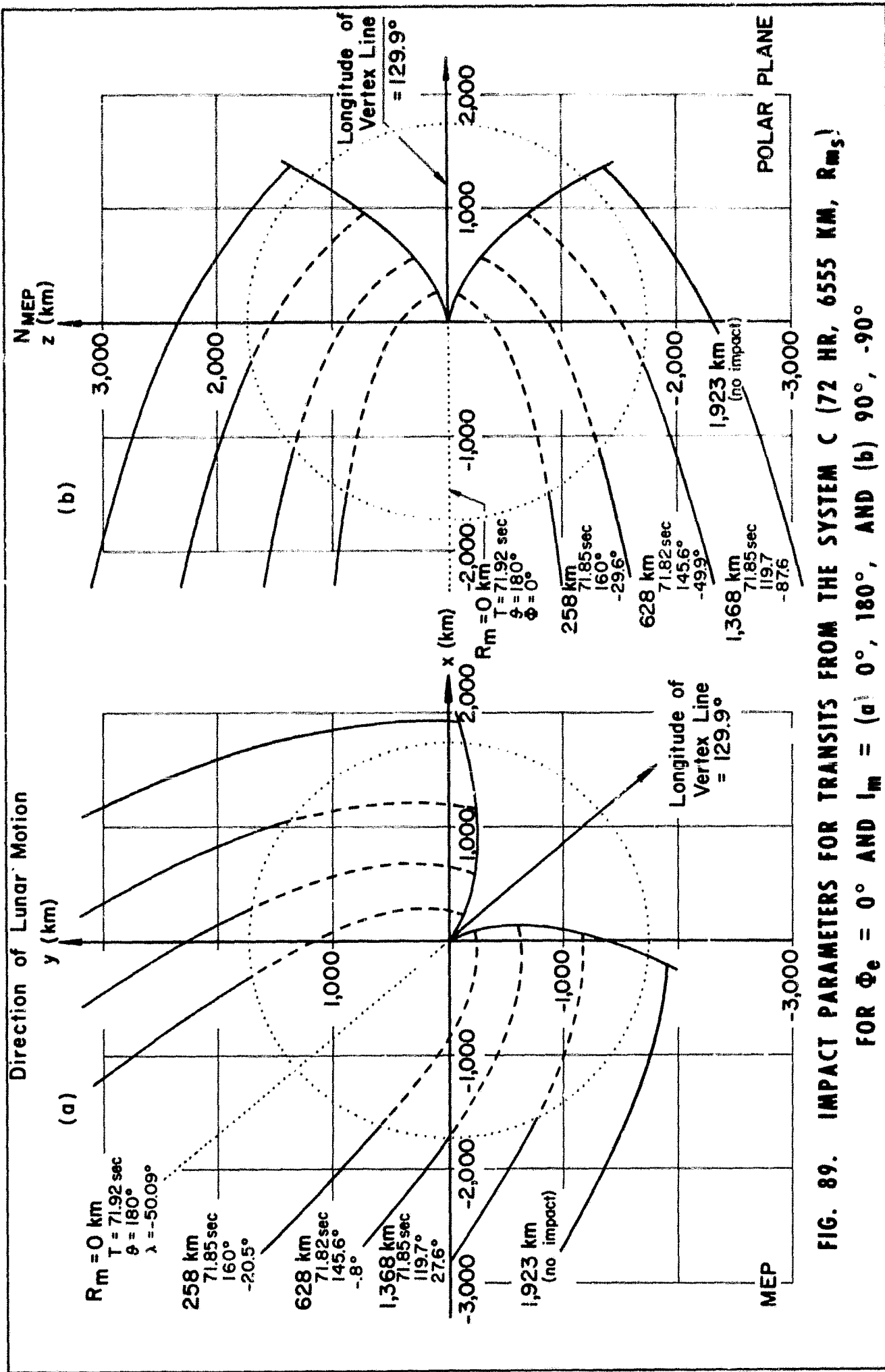


FIG. 89. IMPACT PARAMETERS FOR TRANSITS FROM THE SYSTEM C (72 HR, 6555 KM, R_{ms}) FOR $\phi_e = 0^\circ$ AND $I_m = (a) 0^\circ, 180^\circ$, AND (b) $90^\circ, -90^\circ$

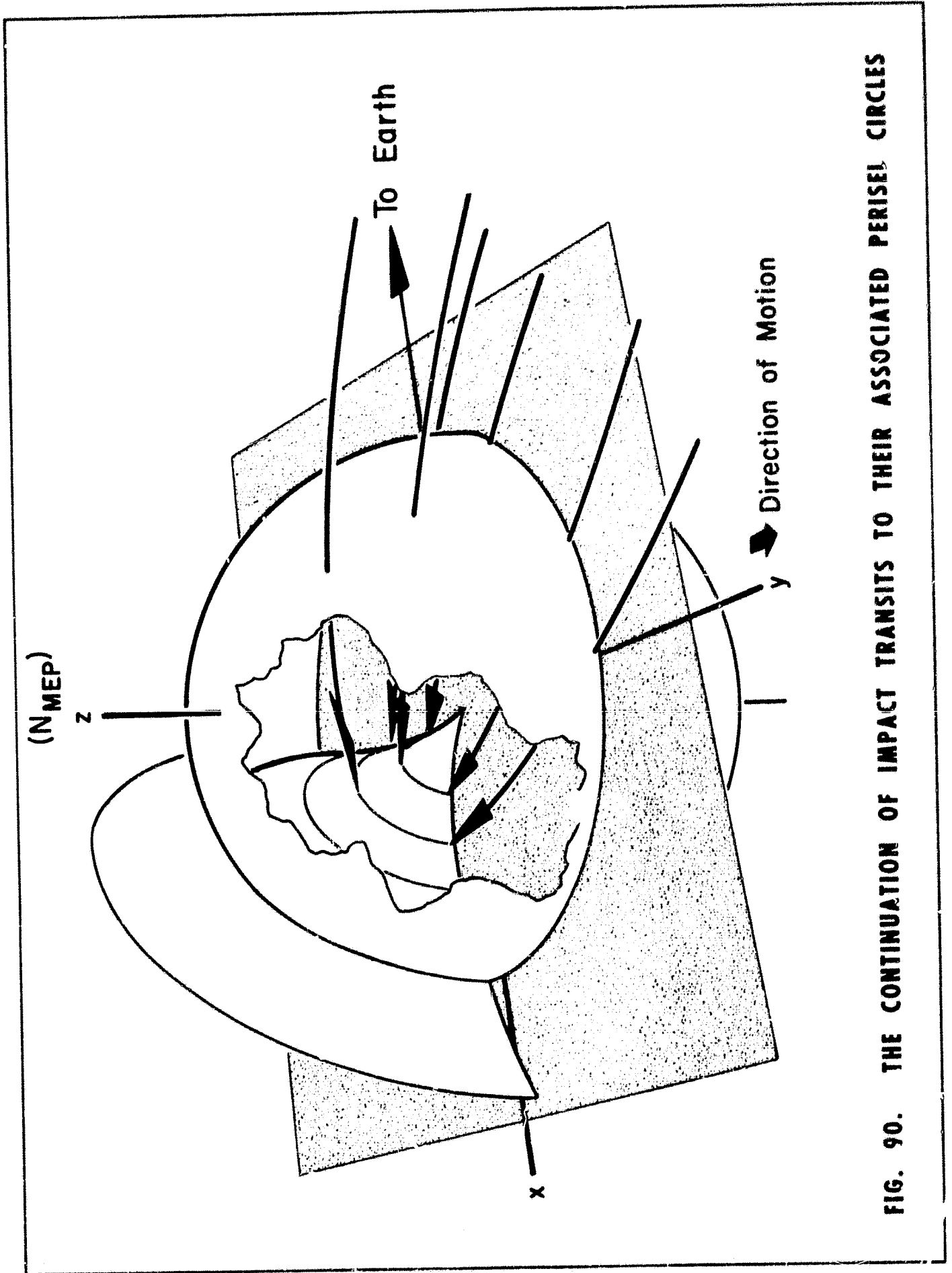


FIG. 90. THE CONTINUATION OF IMPACT TRANSITS TO THEIR ASSOCIATED PERISEL CIRCLES

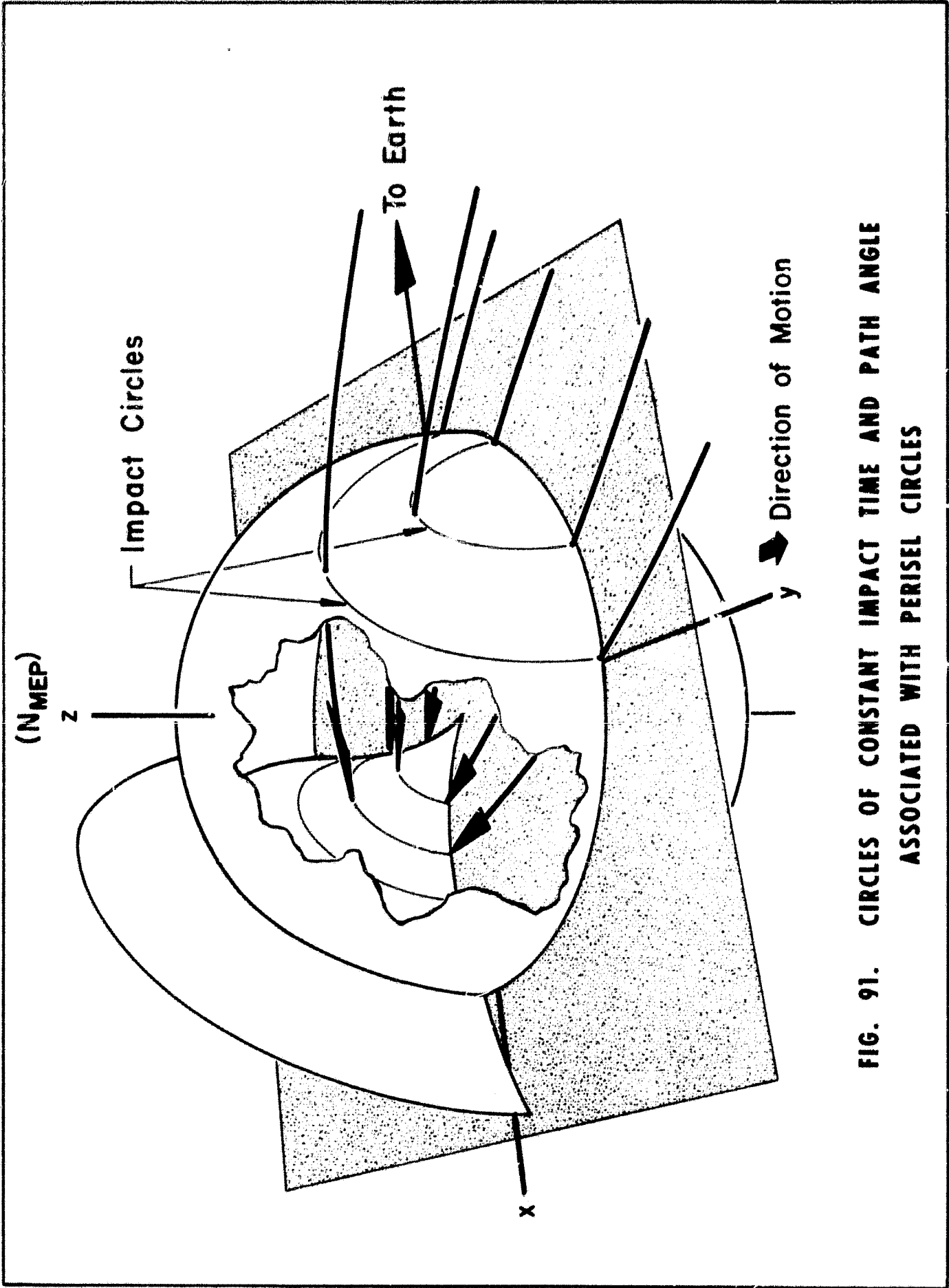


FIG. 91. CIRCLES OF CONSTANT IMPACT TIME AND PATH ANGLE ASSOCIATED WITH PERISEL CIRCLES

$R_m = 627 \text{ km}$

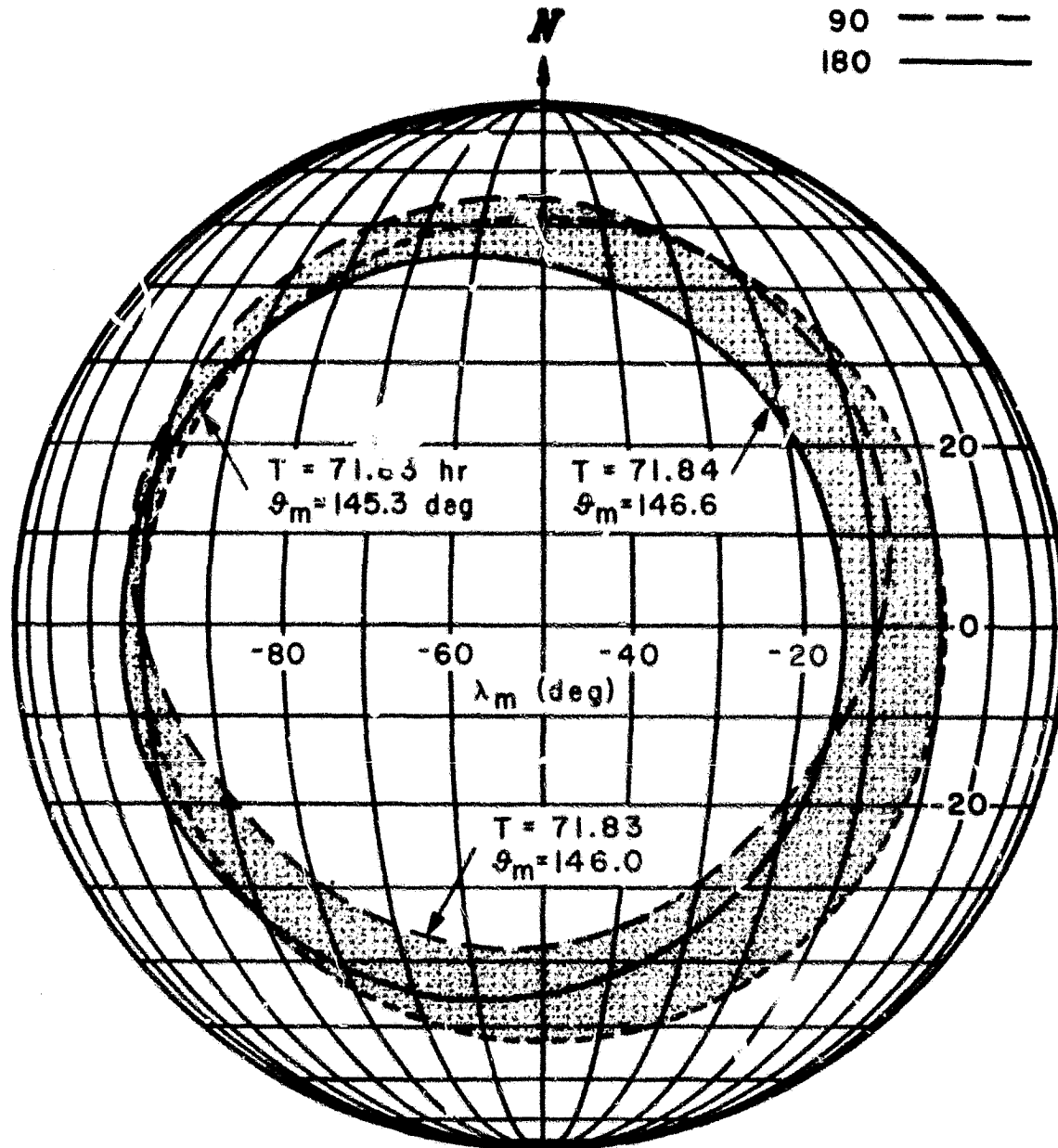
$\Phi_m \text{ (deg)}$

$\Phi_e \text{ (deg)}$

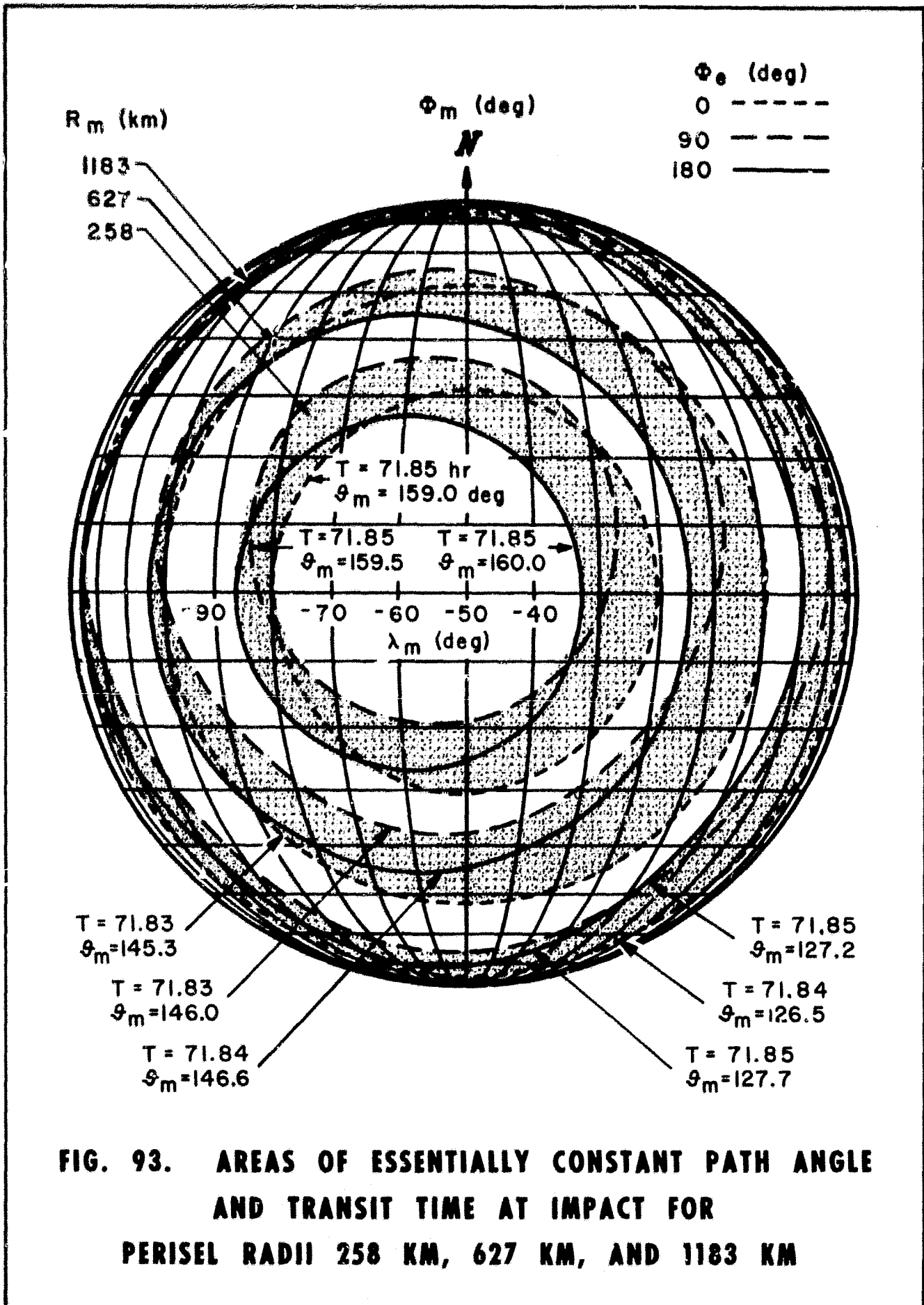
0 - - - - -

90 - - - - -

180 - - - - -



**FIG. 92. IMPACT AREA DEFINED BY
A PERISEL RADIUS OF 627 KM IN WHICH
ESSENTIALLY CONSTANT TIME AND PATH ANGLE
MAY BE OBTAINED**



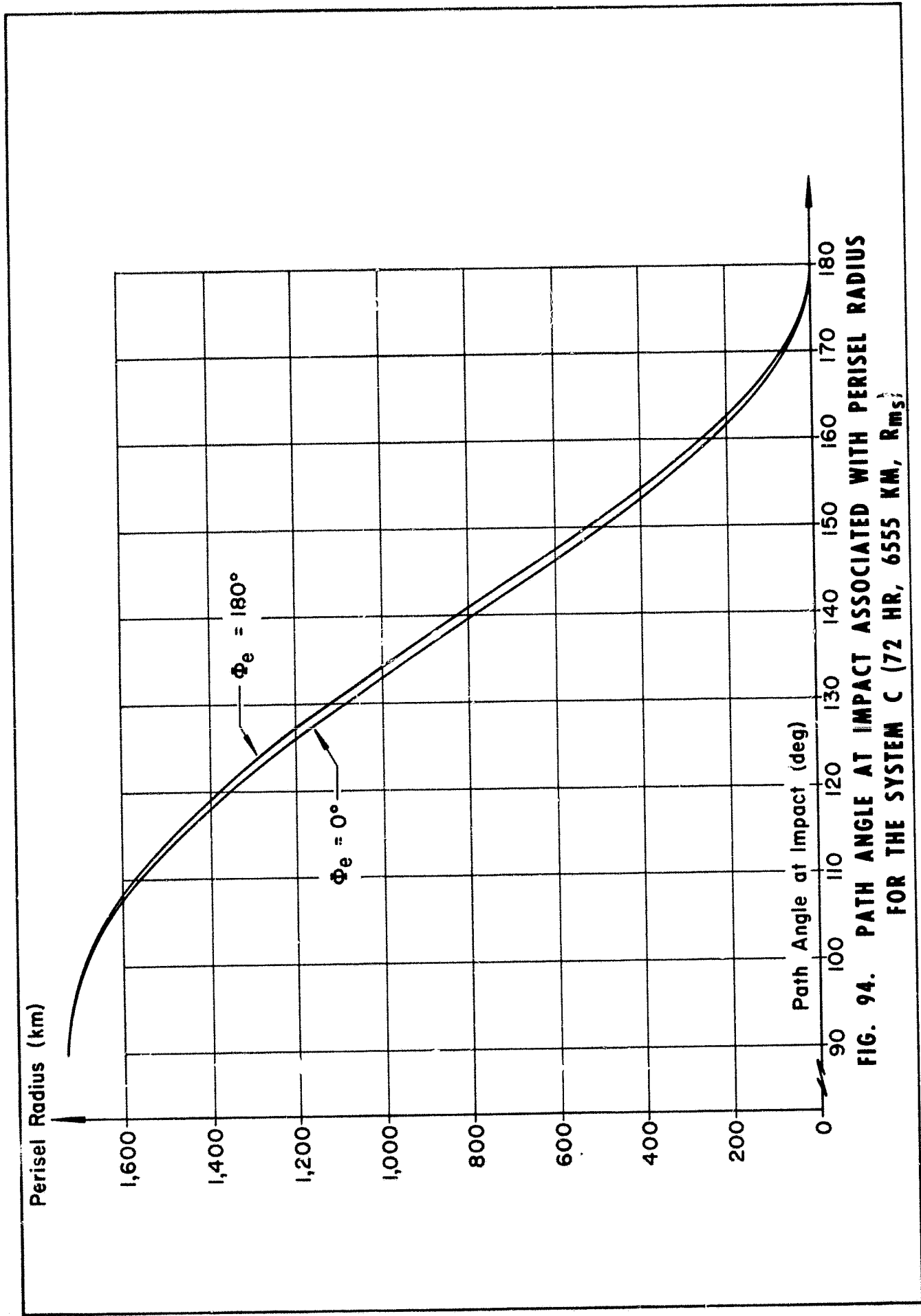


FIG. 94. PATH ANGLE AT IMPACT ASSOCIATED WITH PERISEL RADIUS FOR THE SYSTEM C (72 HR, 6555 KM, R_{ms})

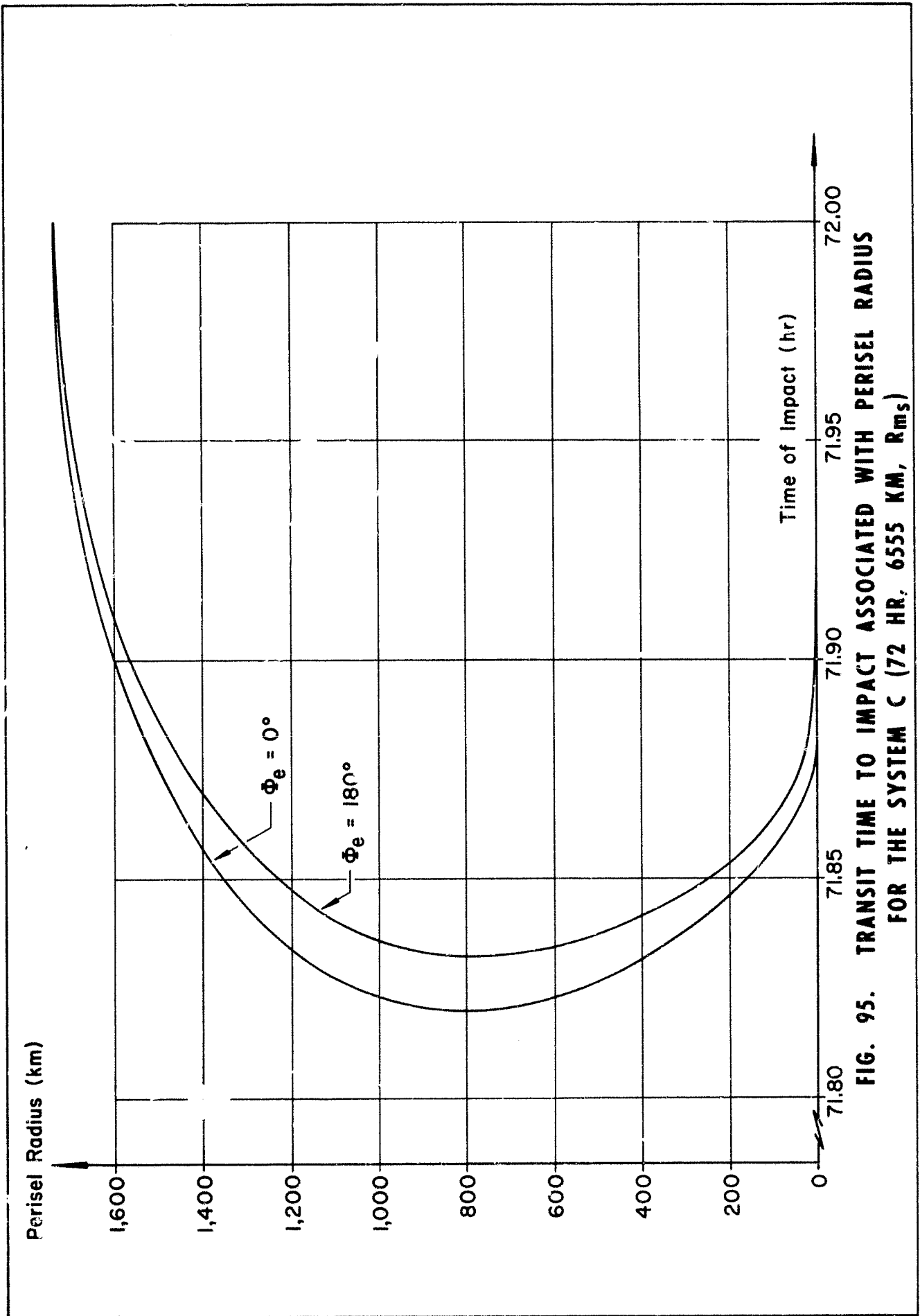


FIG. 95. TRANSIT TIME TO IMPACT ASSOCIATED WITH PERISEL RADIUS FOR THE SYSTEM C (72 HR, 6555 KM, R_{ms})

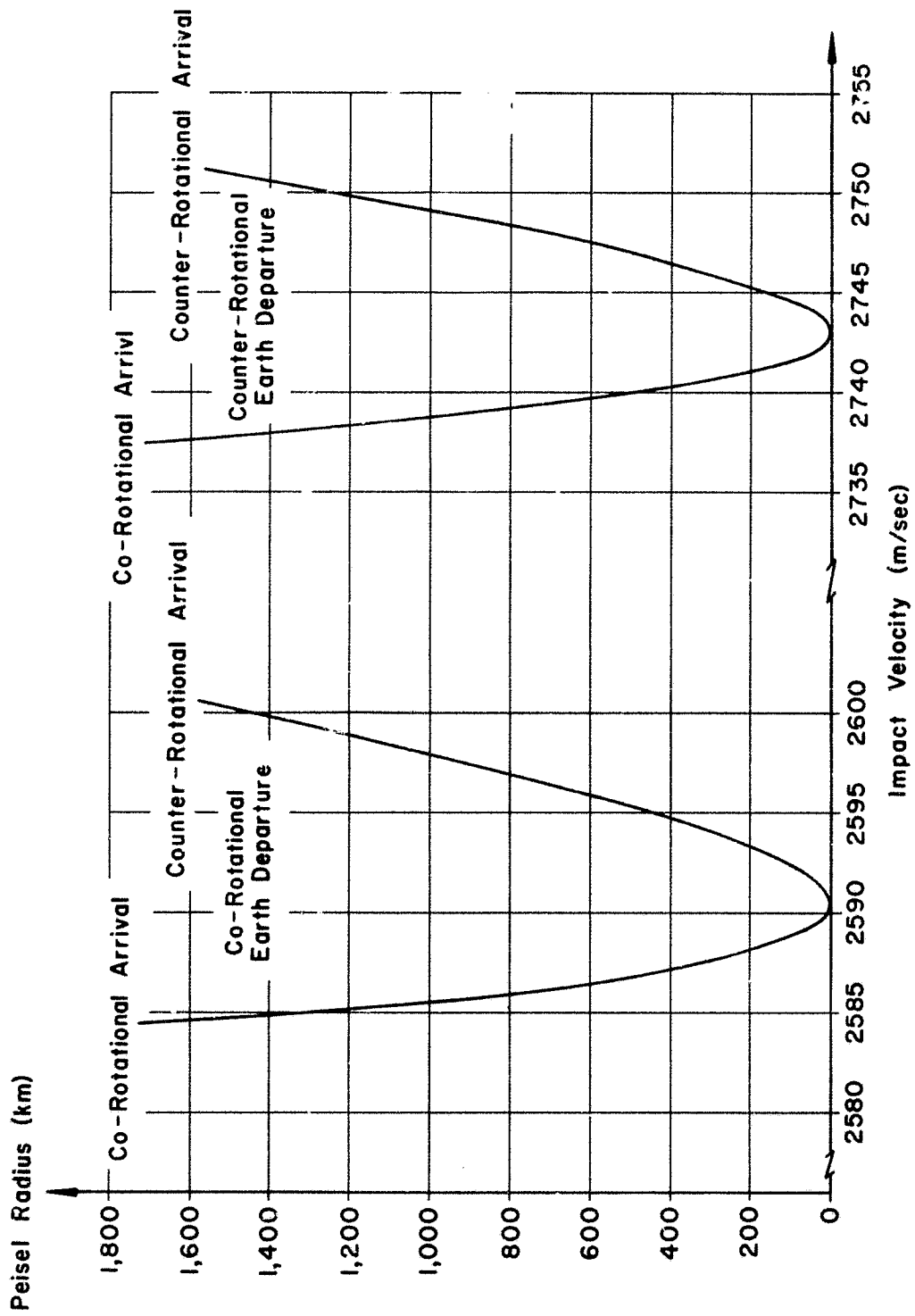


FIG. 96. VELOCITY AT IMPACT FOR COUNTER AND CO-ROTATIONAL EARTH DEPARTURE, C (72 HR, 6555 KM, R_{m_s})

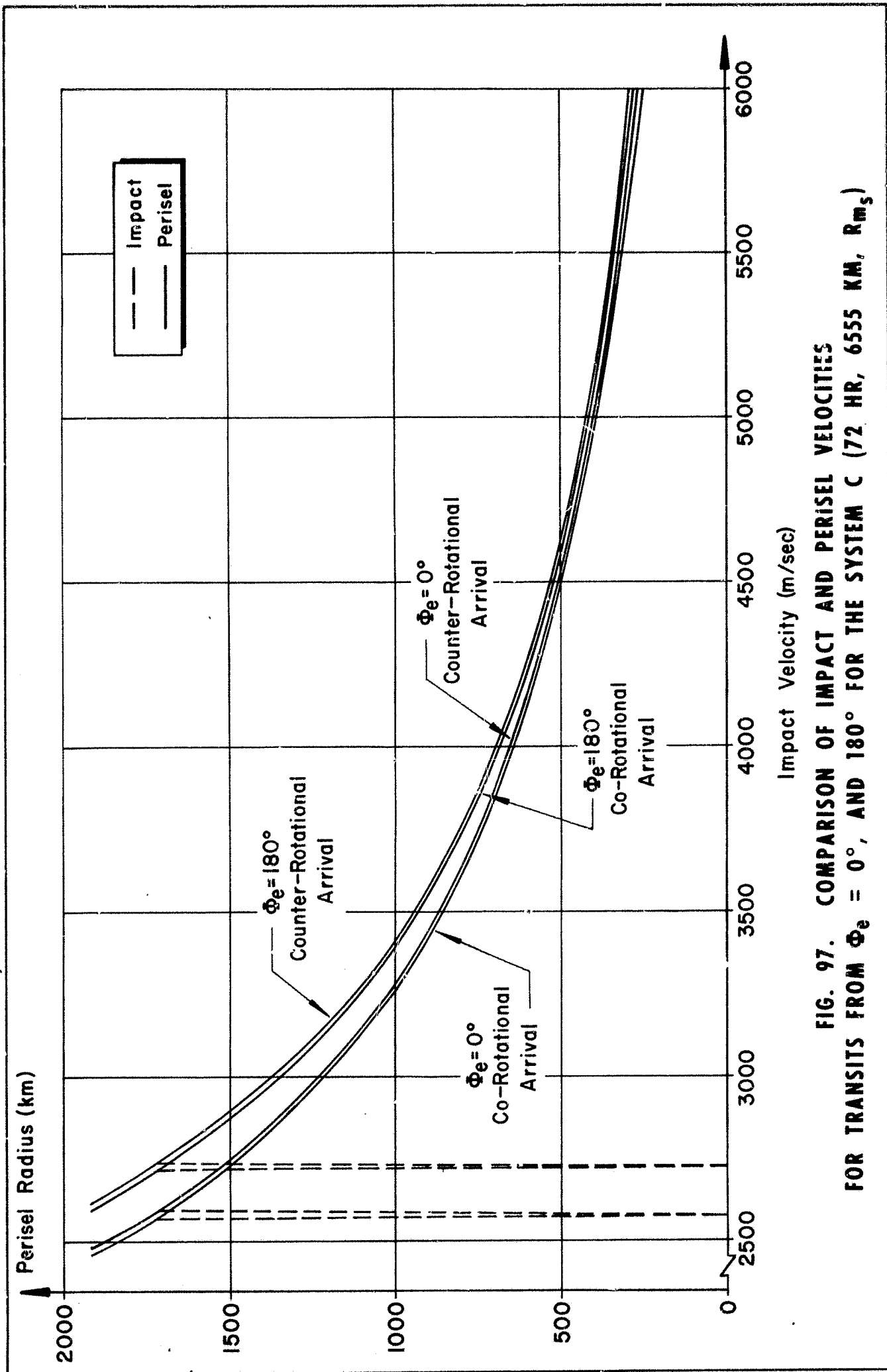


FIG. 97. COMPARISON OF IMPACT AND PERISEL VELOCITIES FOR TRANSITS FROM $\phi_e = 0^\circ$, AND 180° FOR THE SYSTEM C (72 HR, 6555 KM, R_{m_s})

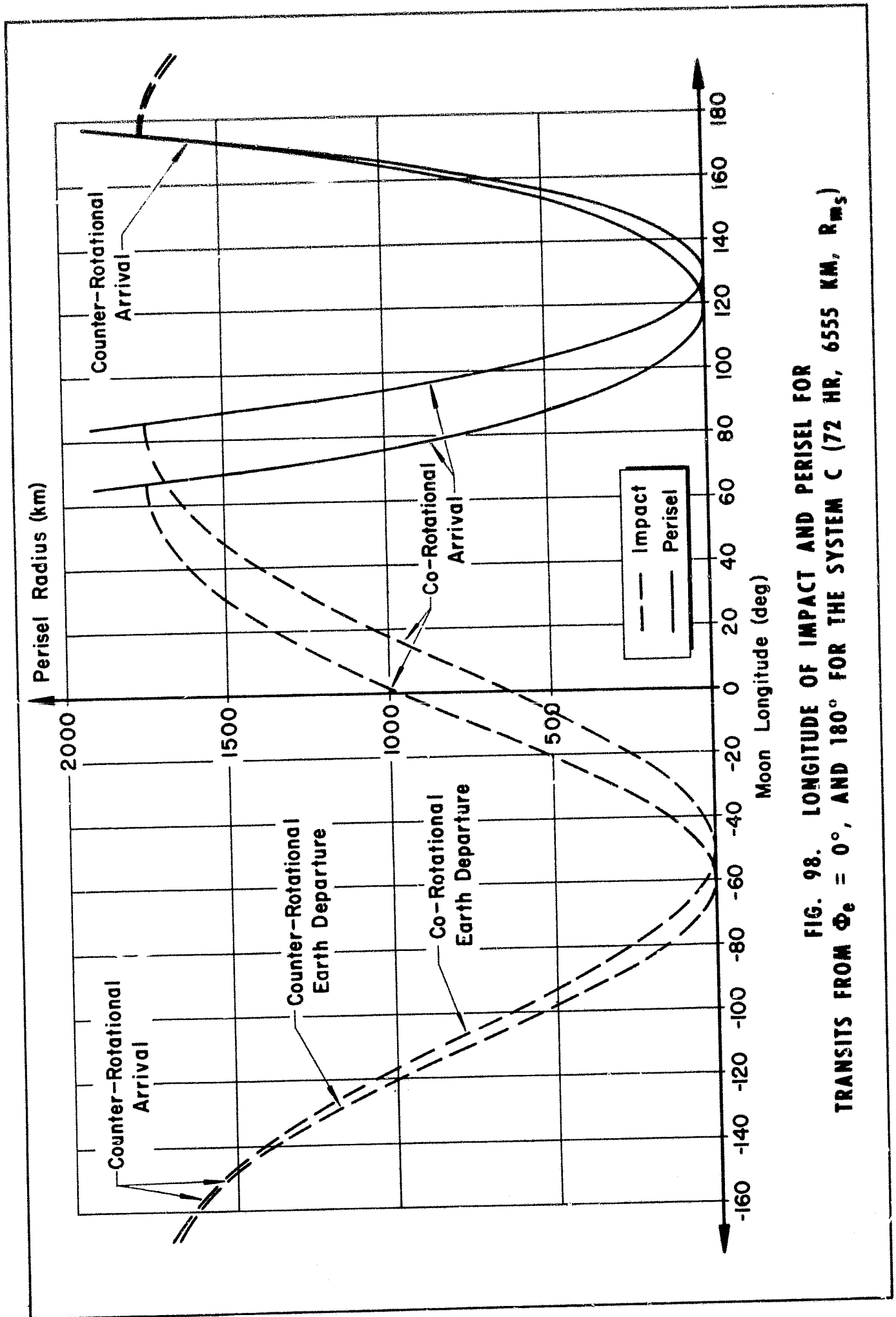


FIG. 98. LONGITUDE OF IMPACT AND PERISEL FOR TRANSITS FROM $\Phi_e = 0^\circ$, AND 180° FOR THE SYSTEM C (72 HR, 6555 KM, R_{ms})

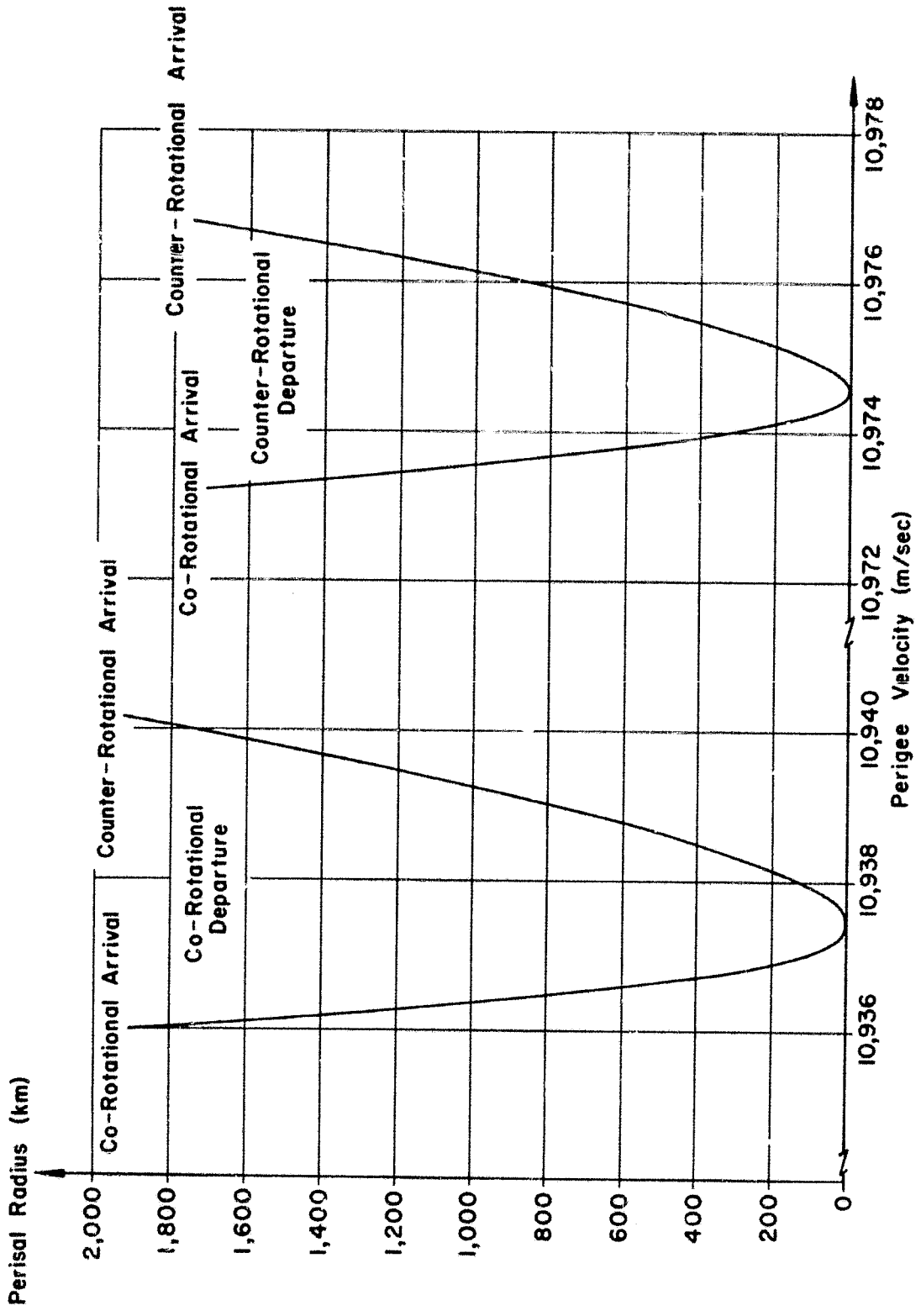


FIG. 99. PERIGEE VELOCITY REQUIRED FOR THE EMBEDDED TRANSITS VS PERISEL RADIUS, C (72 HR, 6555 KM, R_{m_s})

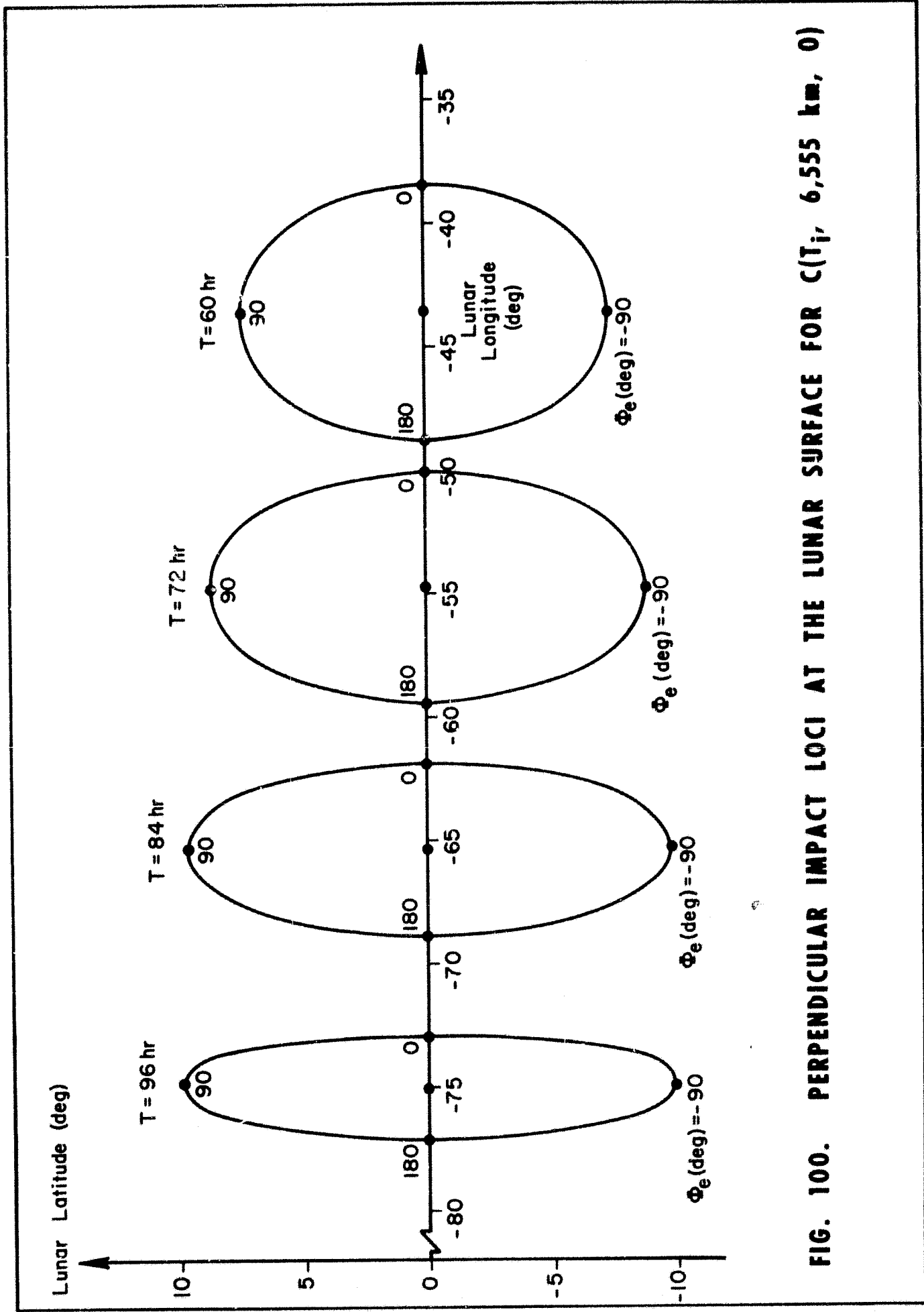


FIG. 100. PERPENDICULAR IMPACT LOCI AT THE LUNAR SURFACE FOR $C(T_i, 6,555 \text{ km}, 0)$

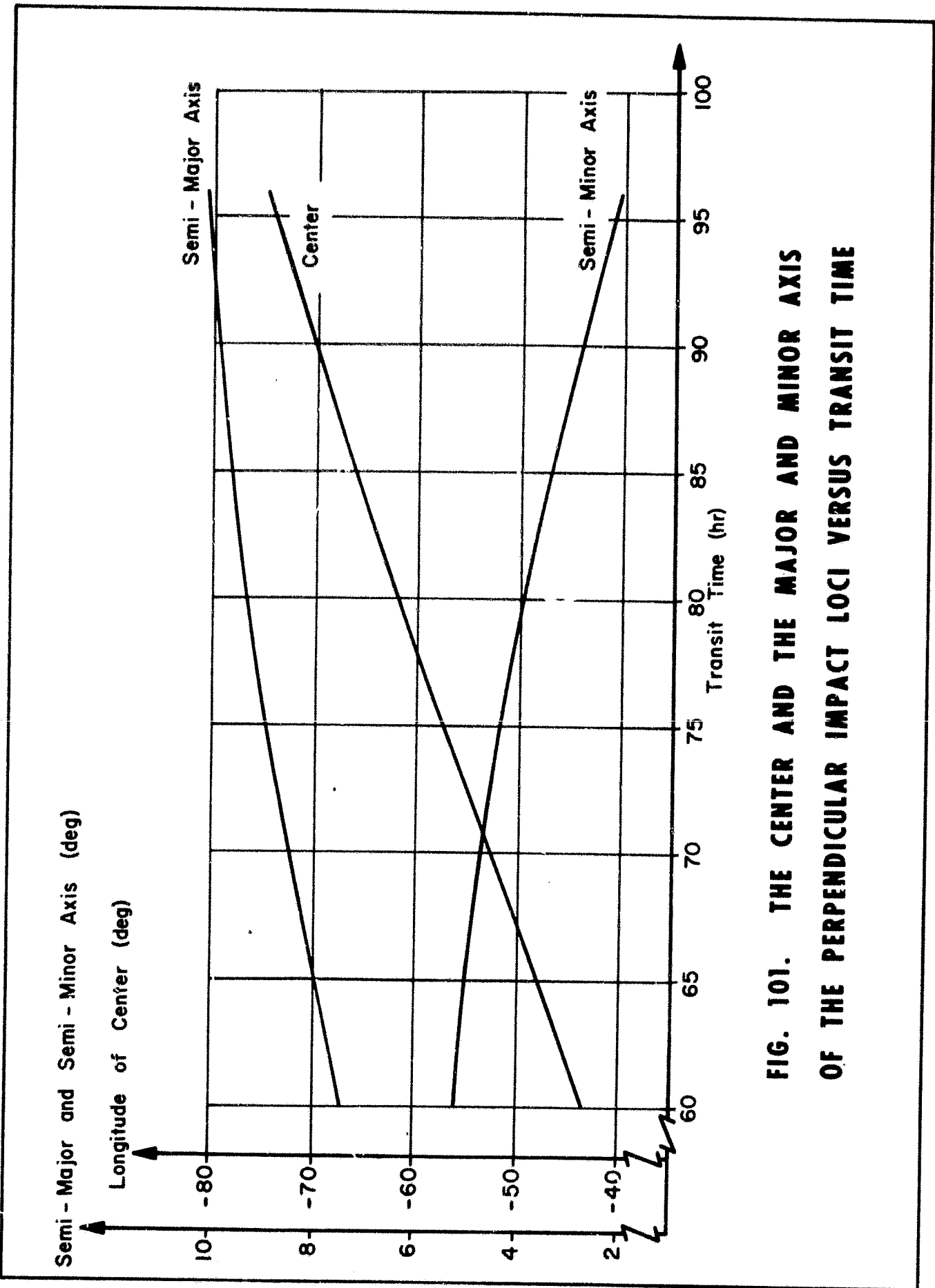


FIG. 101. THE CENTER AND THE MAJOR AND MINOR AXIS OF THE PERPENDICULAR IMPACT LOCI VERSUS TRANSIT TIME

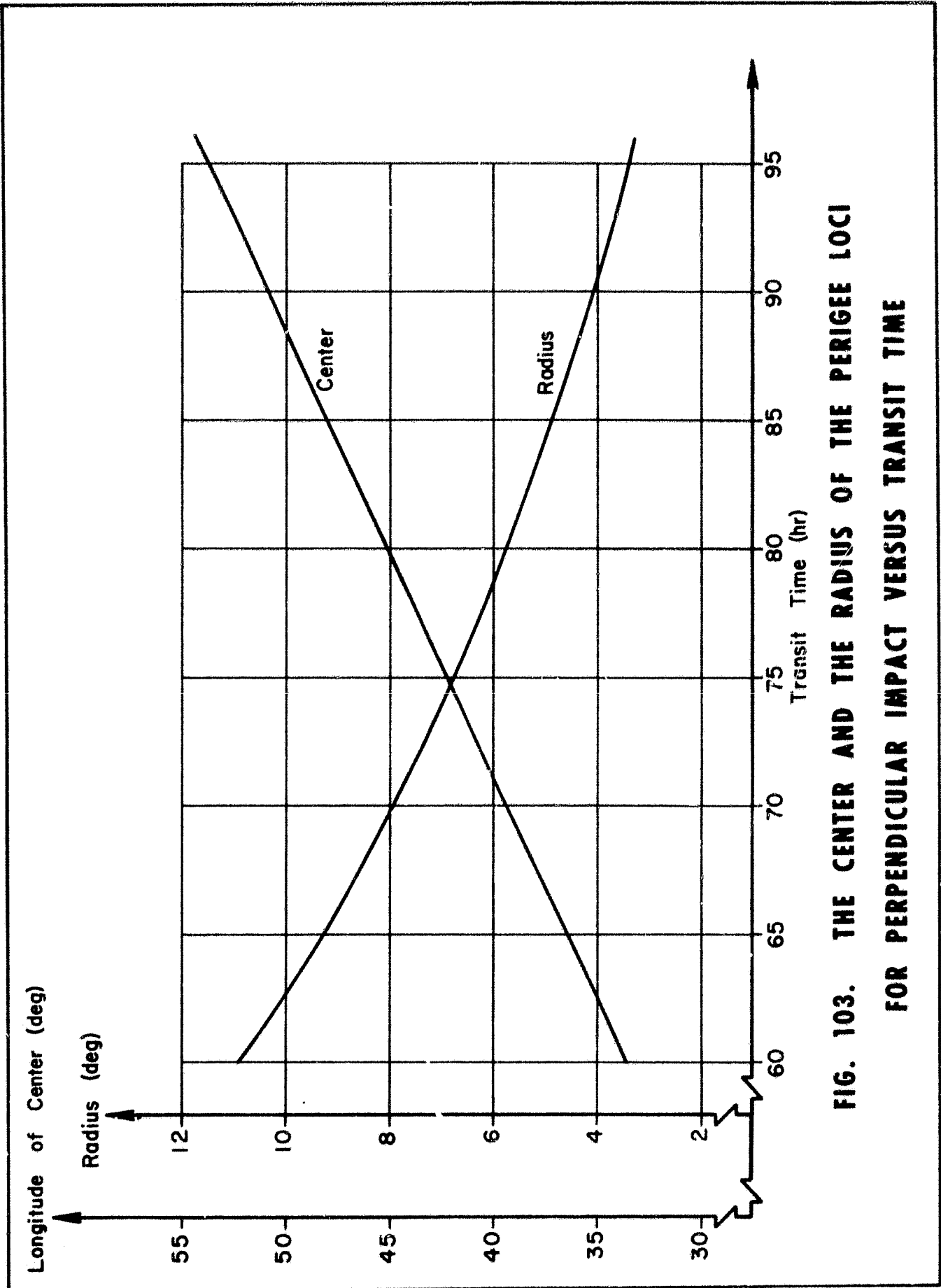


FIG. 103. THE CENTER AND THE RADIUS OF THE PERIGEE LOCI FOR PERPENDICULAR IMPACT VERSUS TRANSIT TIME

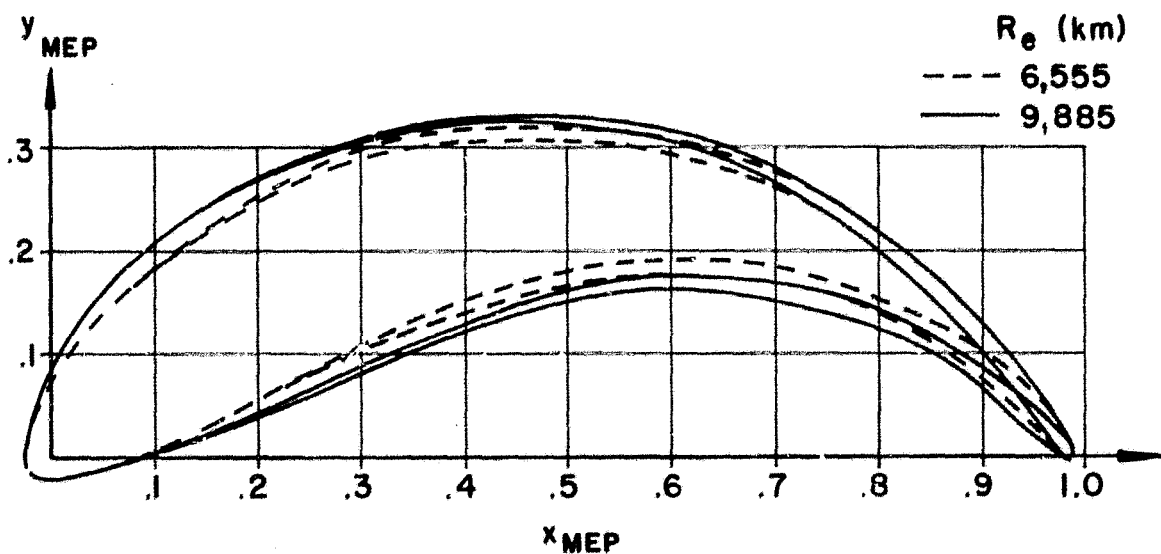
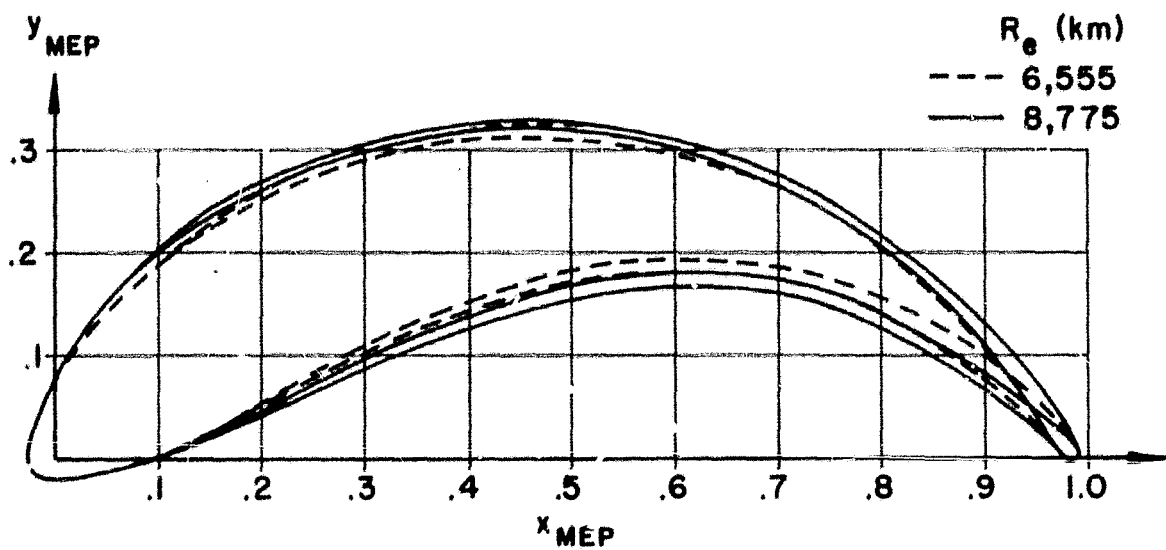
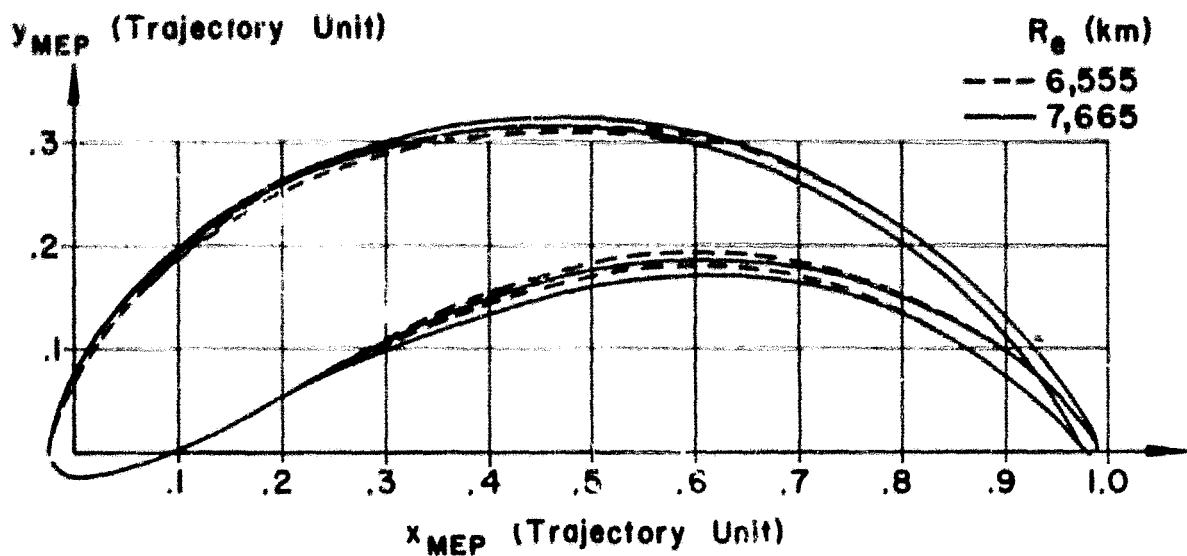


FIG. 104. COMPARISON OF THE PERTURBATIONS IN THE SHAPE OF THE EMBEDDED TRANSITS FOR VARIATIONS IN R_e FOR THE SYSTEM C (72 HR, R_{e_s} , 1923 KM)

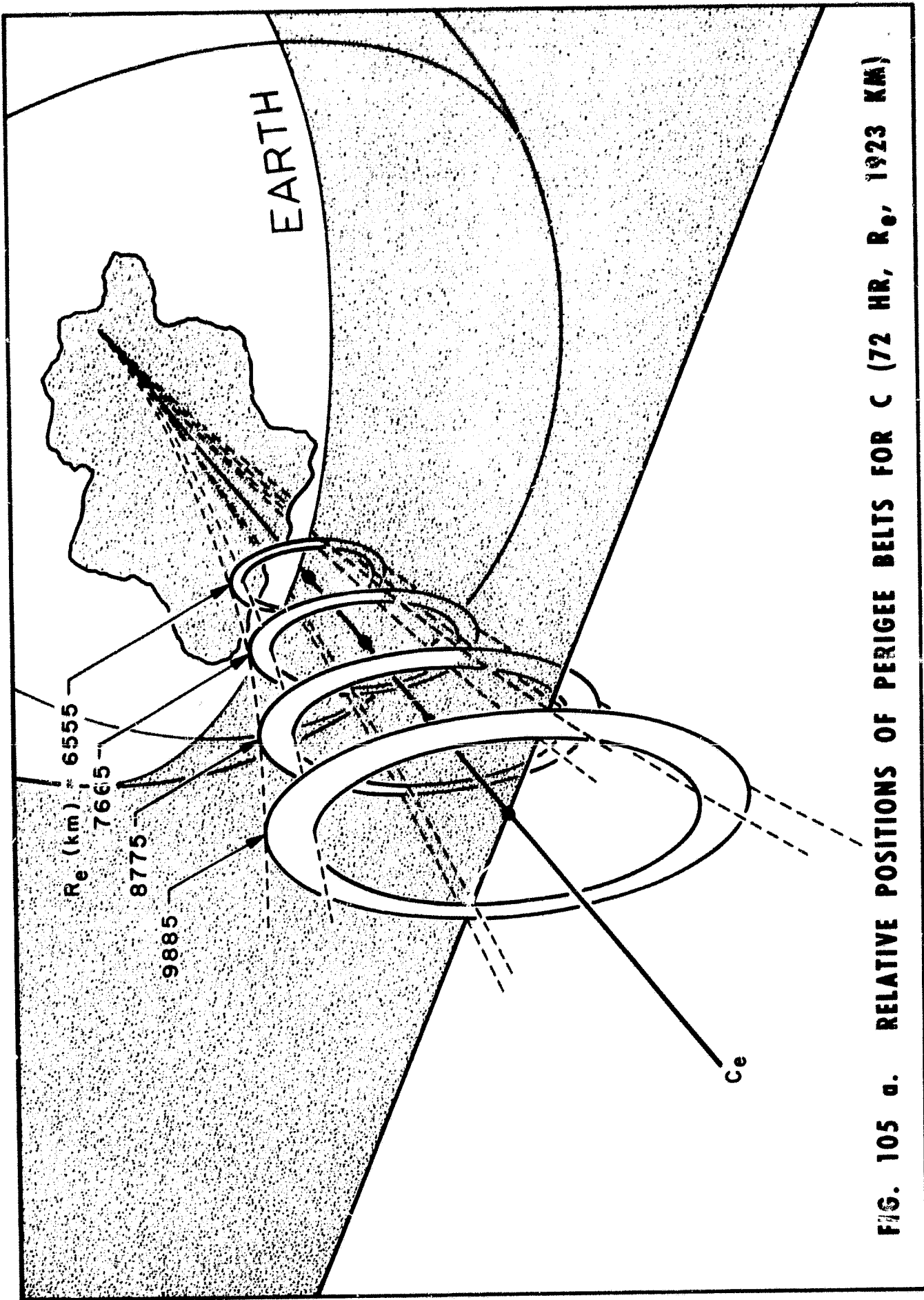


FIG. 105 a. RELATIVE POSITIONS OF PERIGEE BELTS FOR C (72 HR, R_e , 1923 KM)

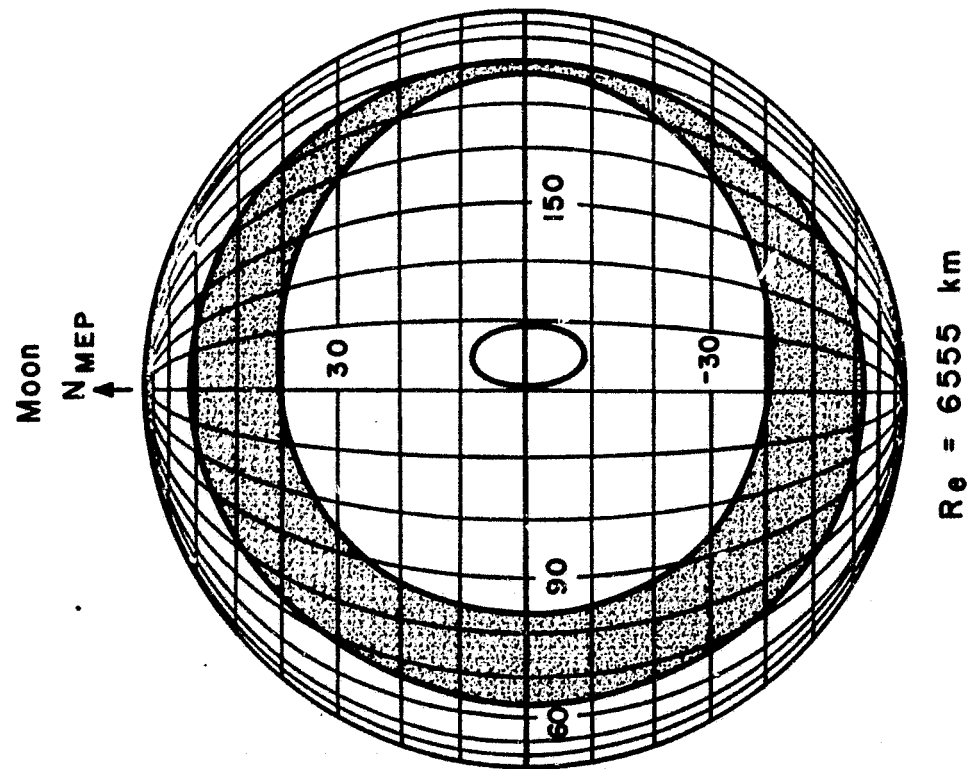
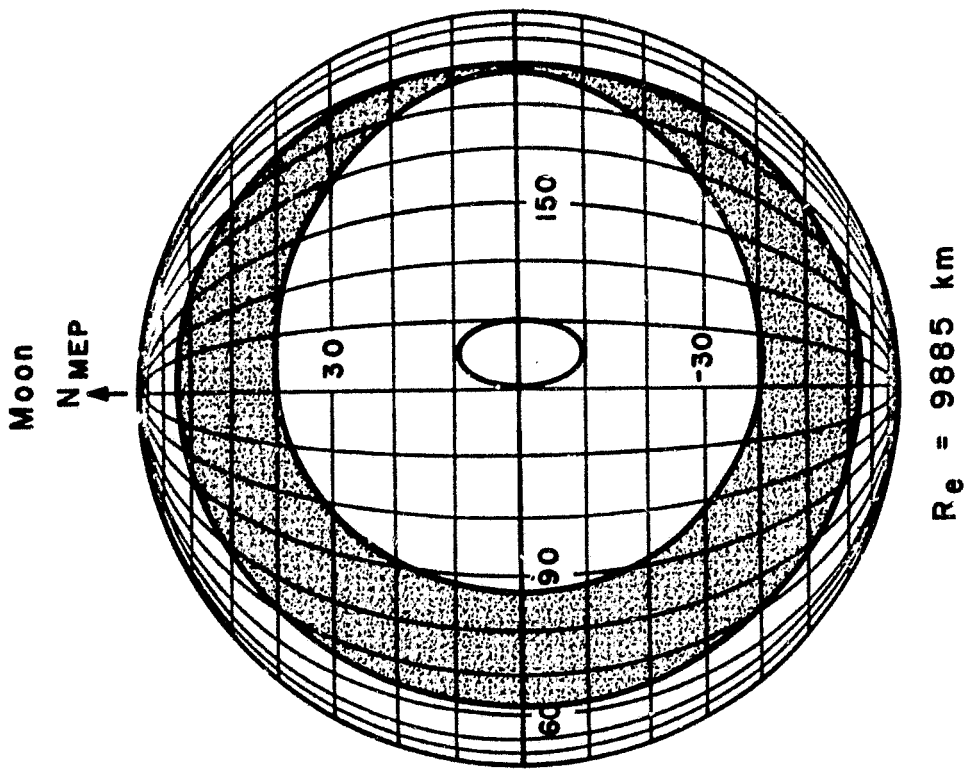


FIG. 105 b. PERISEL BELTS FOR C (72 HR, R_e , 1923 KM)

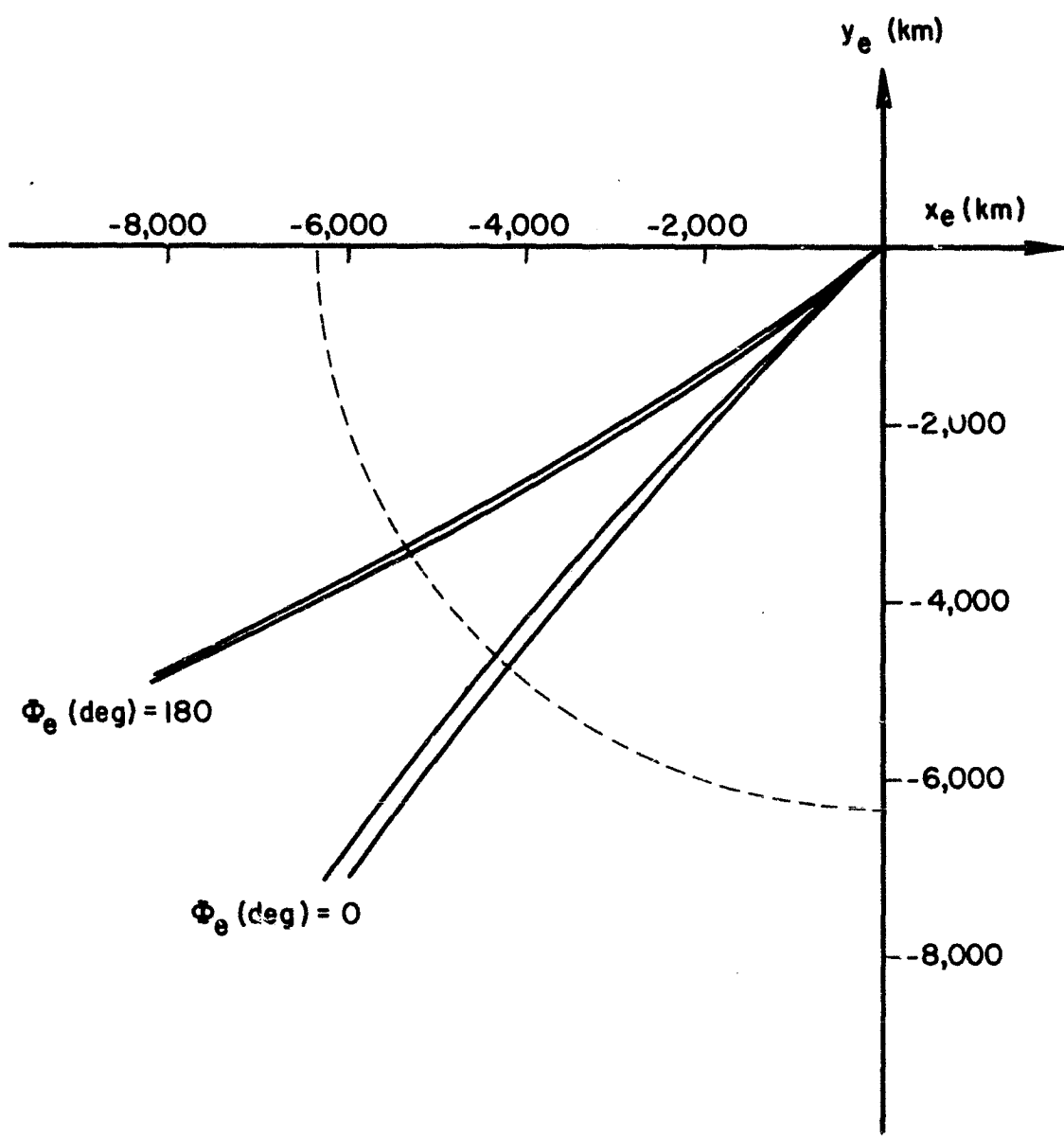
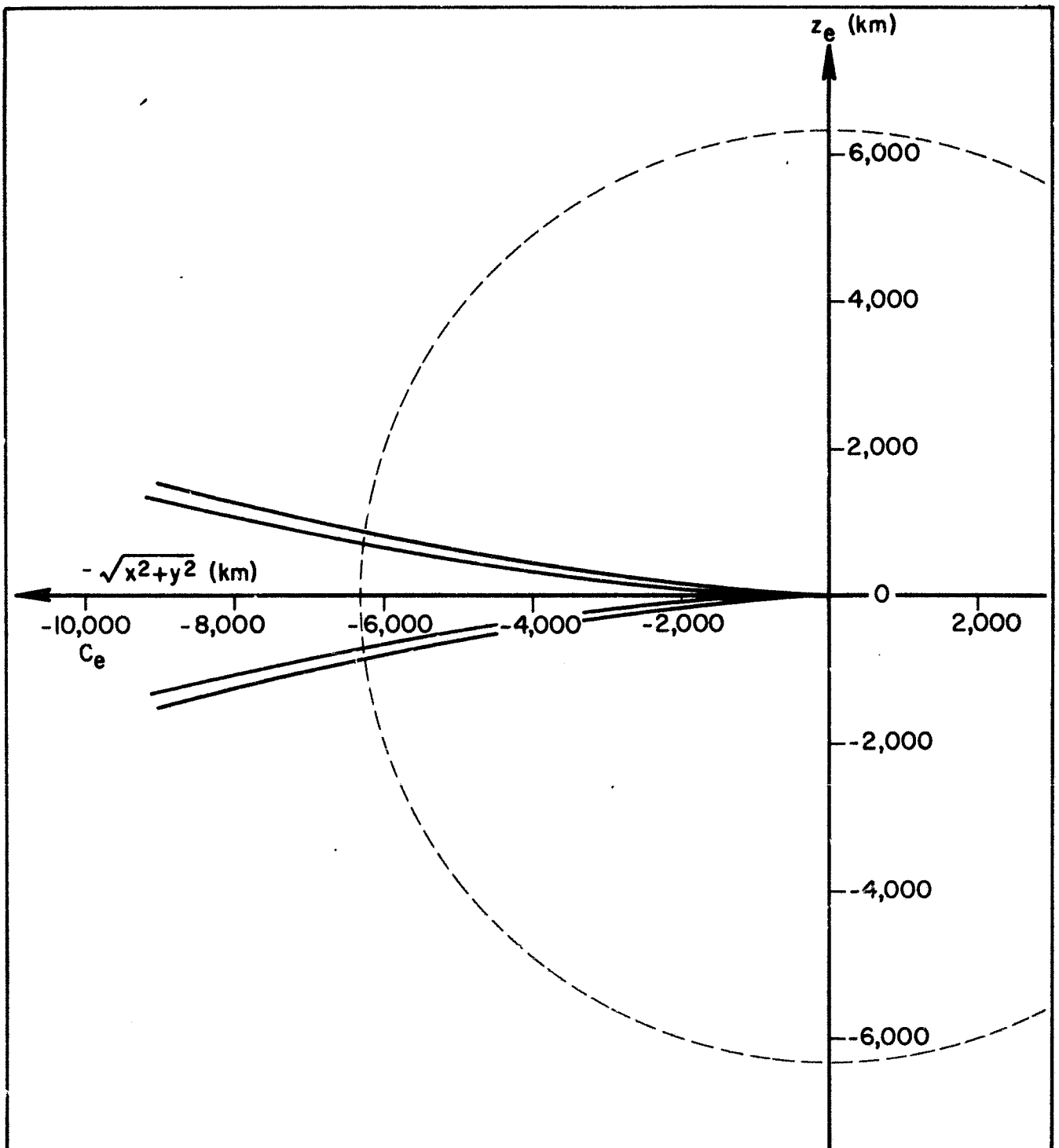


FIG. 106. THE INTERSECTION OF THE PERIGEE HORN WITH THE MEP FOR THE SYSTEM C(72 hr, R_{e_s} , 1,923 km)



**FIG. 107. THE INTERSECTION OF THE PERIGEE HORN
WITH A POLAR PLANE CONTAINING C_e ,
FOR THE SYSTEM C(72 hr, R_{e_s} , 1,923 km)**

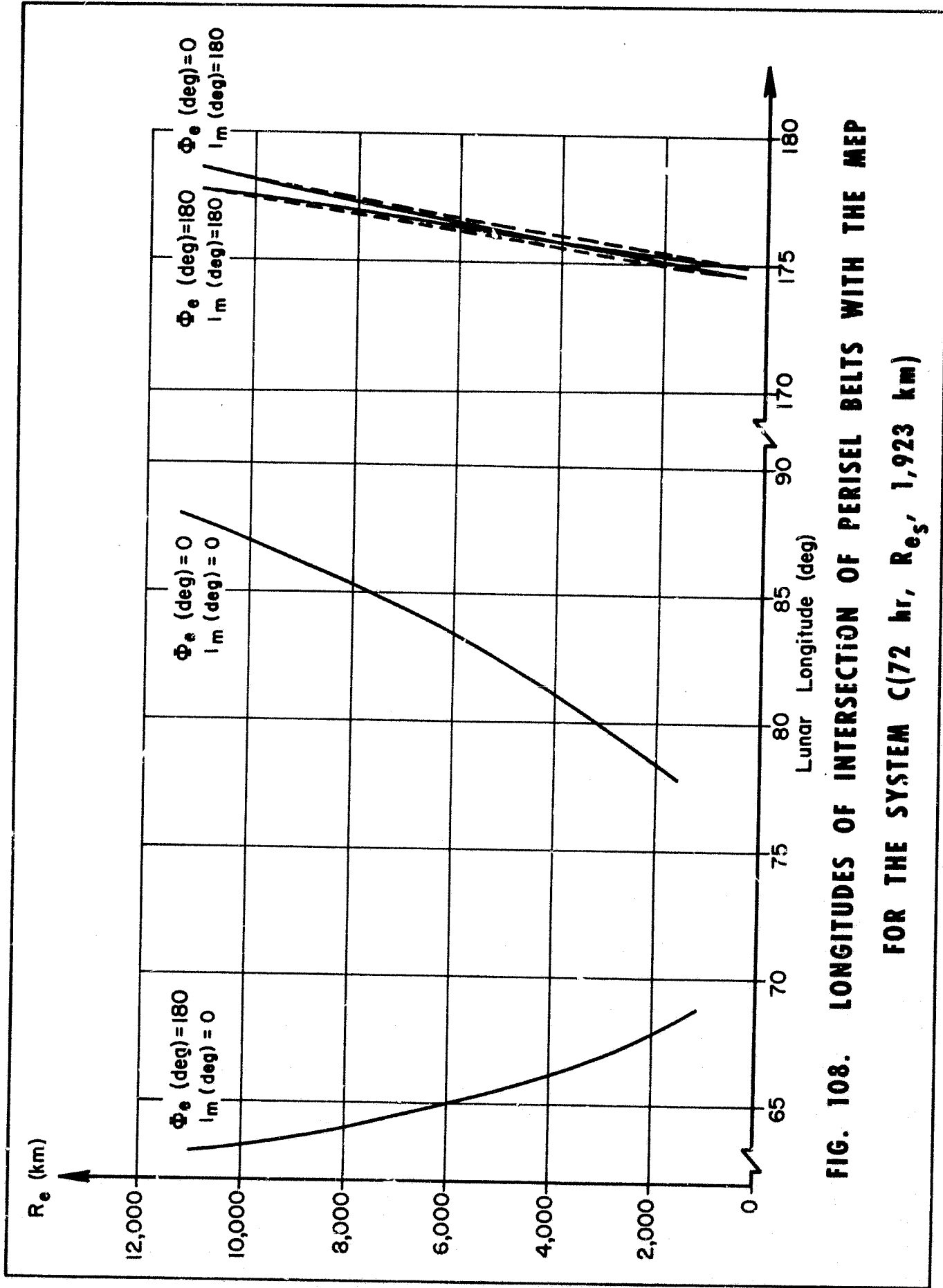


FIG. 108. LONGITUDES OF INTERSECTION OF PERISEL BELTS WITH THE MEP FOR THE SYSTEM C(72 hr, R_{e_s} , 1,923 km)

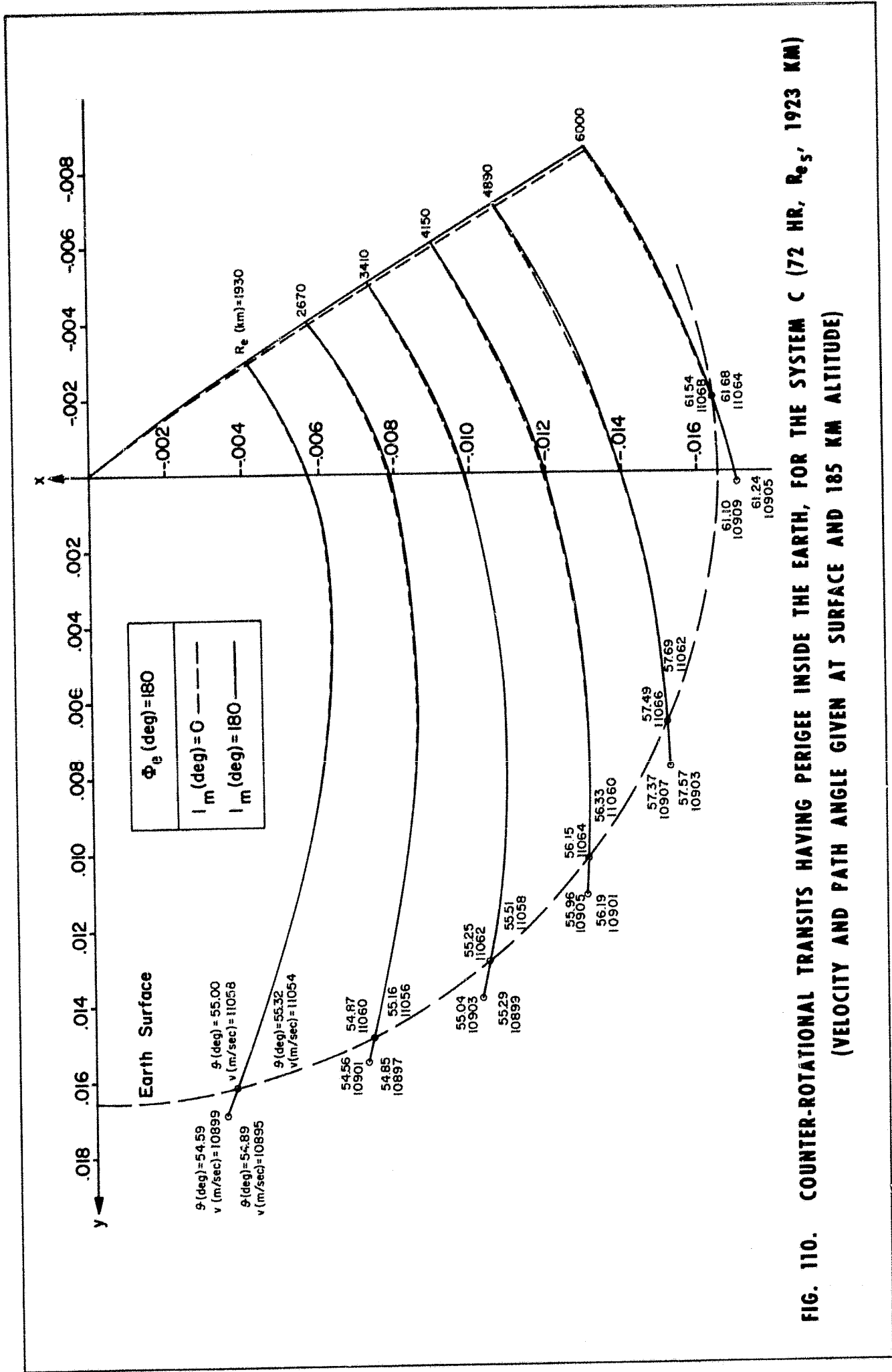


FIG. 110. COUNTER-ROTATIONAL TRANSITS HAVING PERIGEE INSIDE THE EARTH, FOR THE SYSTEM C (72 HR, R_{e_s} , 1923 KM)
(VELOCITY AND PATH ANGLE GIVEN AT SURFACE AND 185 KM ALTITUDE)

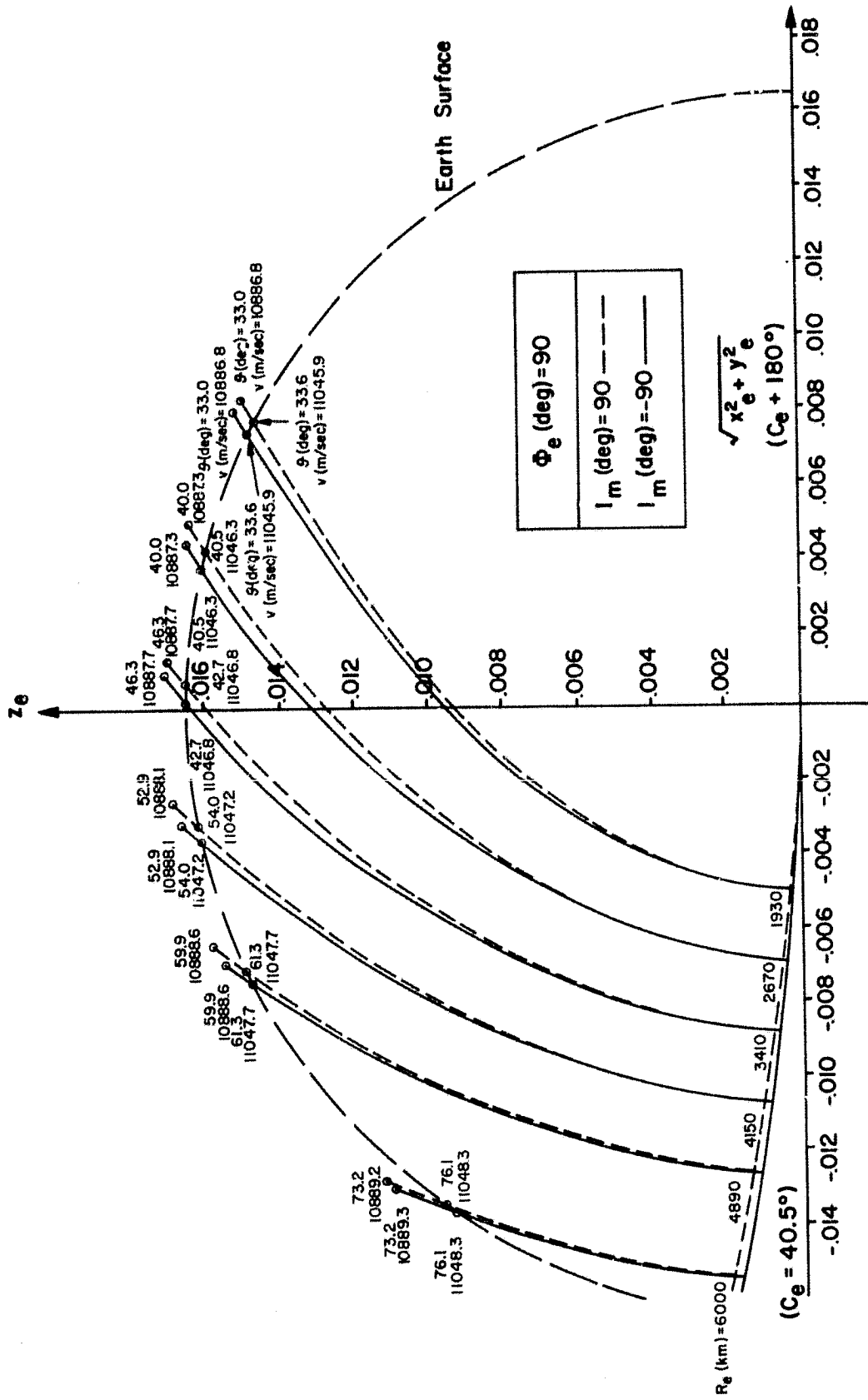


FIG. 111. POLAR TRANSITS HAVING PERIGEE INSIDE THE EARTH FOR THE SYSTEM C (72 HR, R_{e_s} , 1923 KM)

(VELOCITY AND PATH ANGLE GIVEN AT SURFACE AND 185 KM ALTITUDE)

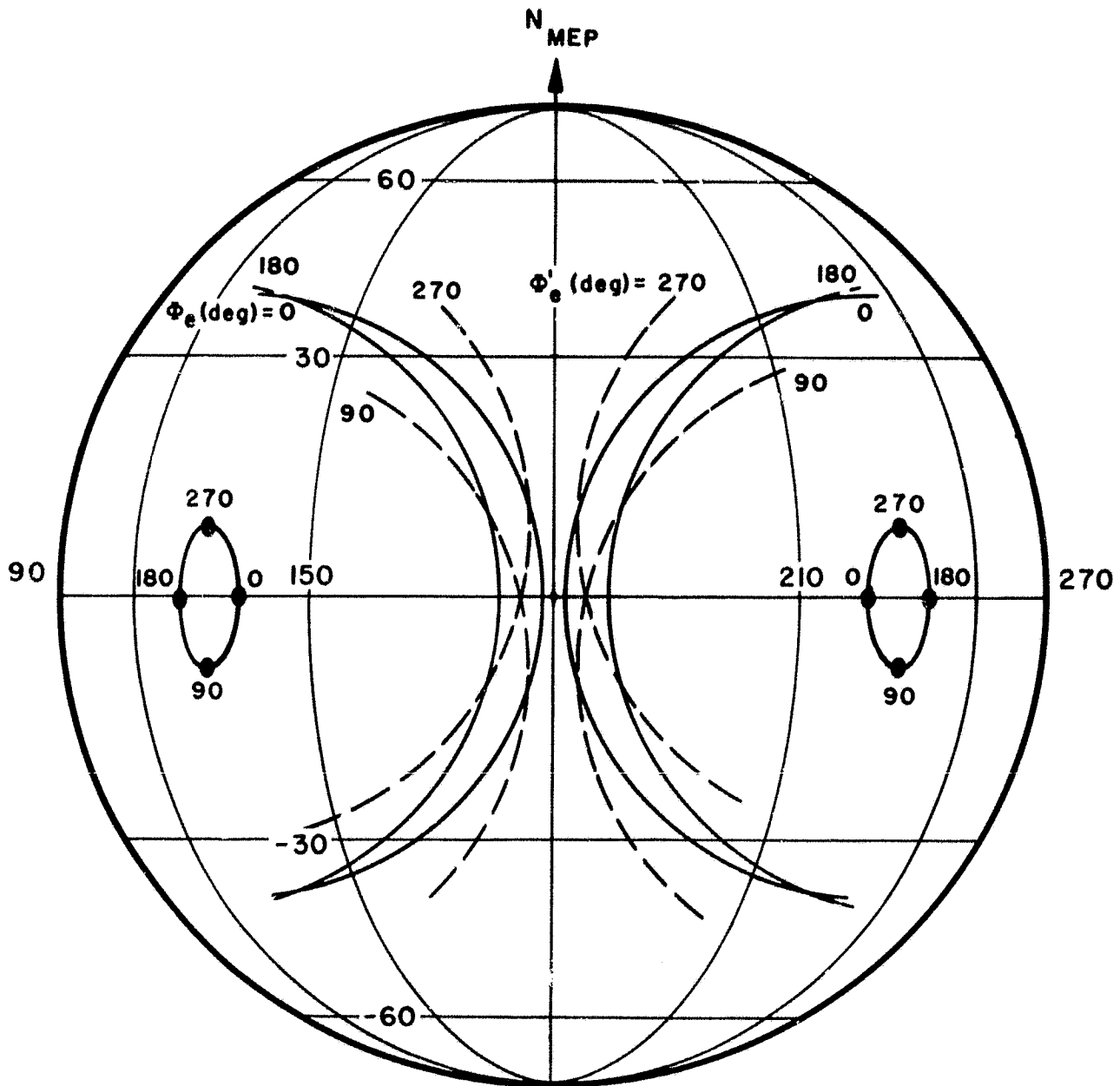


FIG. 112. SCHEMATIC OF SEGMENTS OF THE PERISEL BELTS FOR THE CLASSES $C(T^*, 6,555 \text{ km}, R_1^*)$ AND $C'(T^*, 6,555 \text{ km}, R_1^*)$

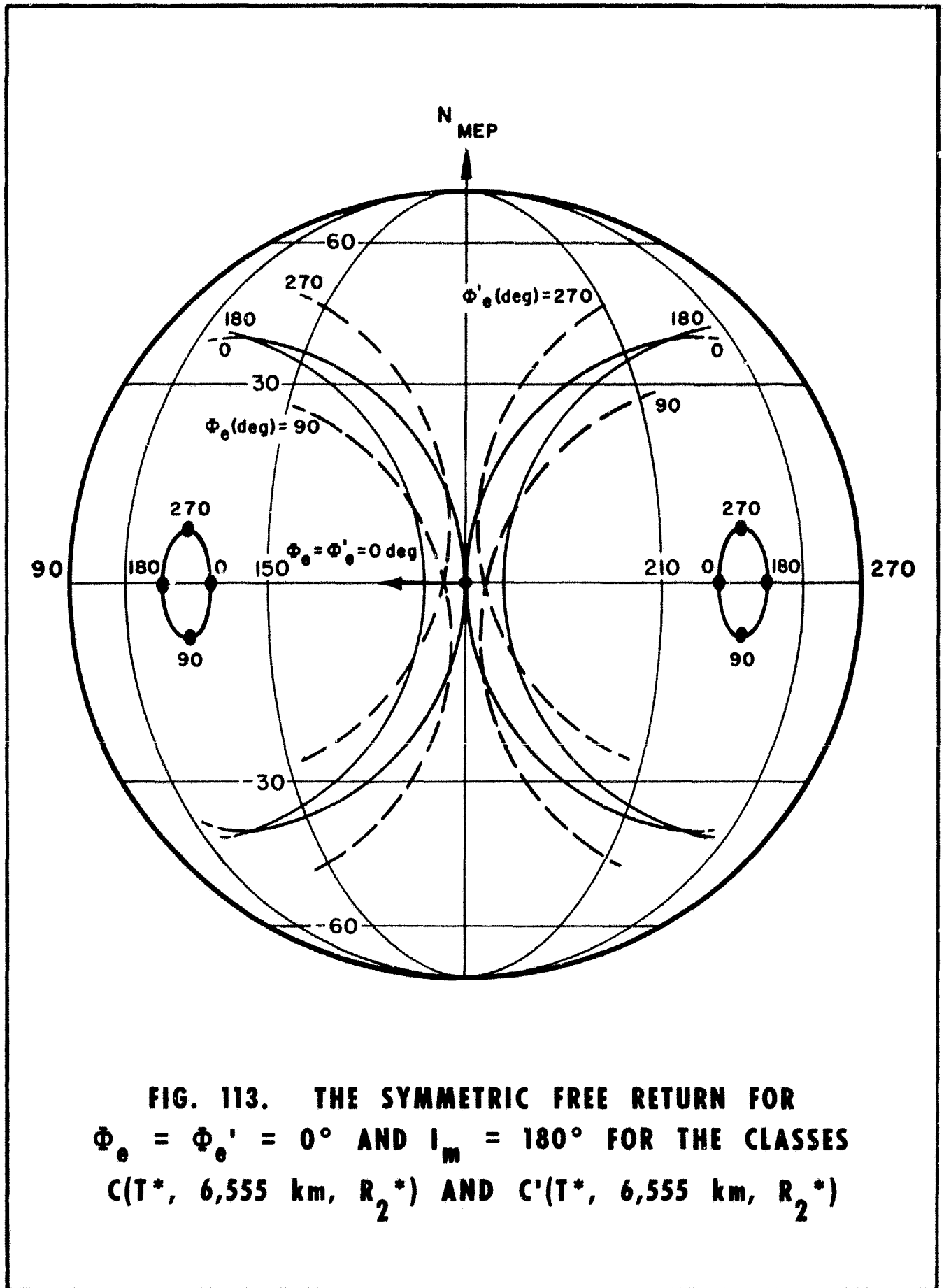


FIG. 113. THE SYMMETRIC FREE RETURN FOR $\Phi_e = \Phi'_e = 0^\circ$ AND $i_m = 180^\circ$ FOR THE CLASSES $C(T^*, 6,555 \text{ km}, R_2^*)$ AND $C'(T^*, 6,555 \text{ km}, R_2^*)$

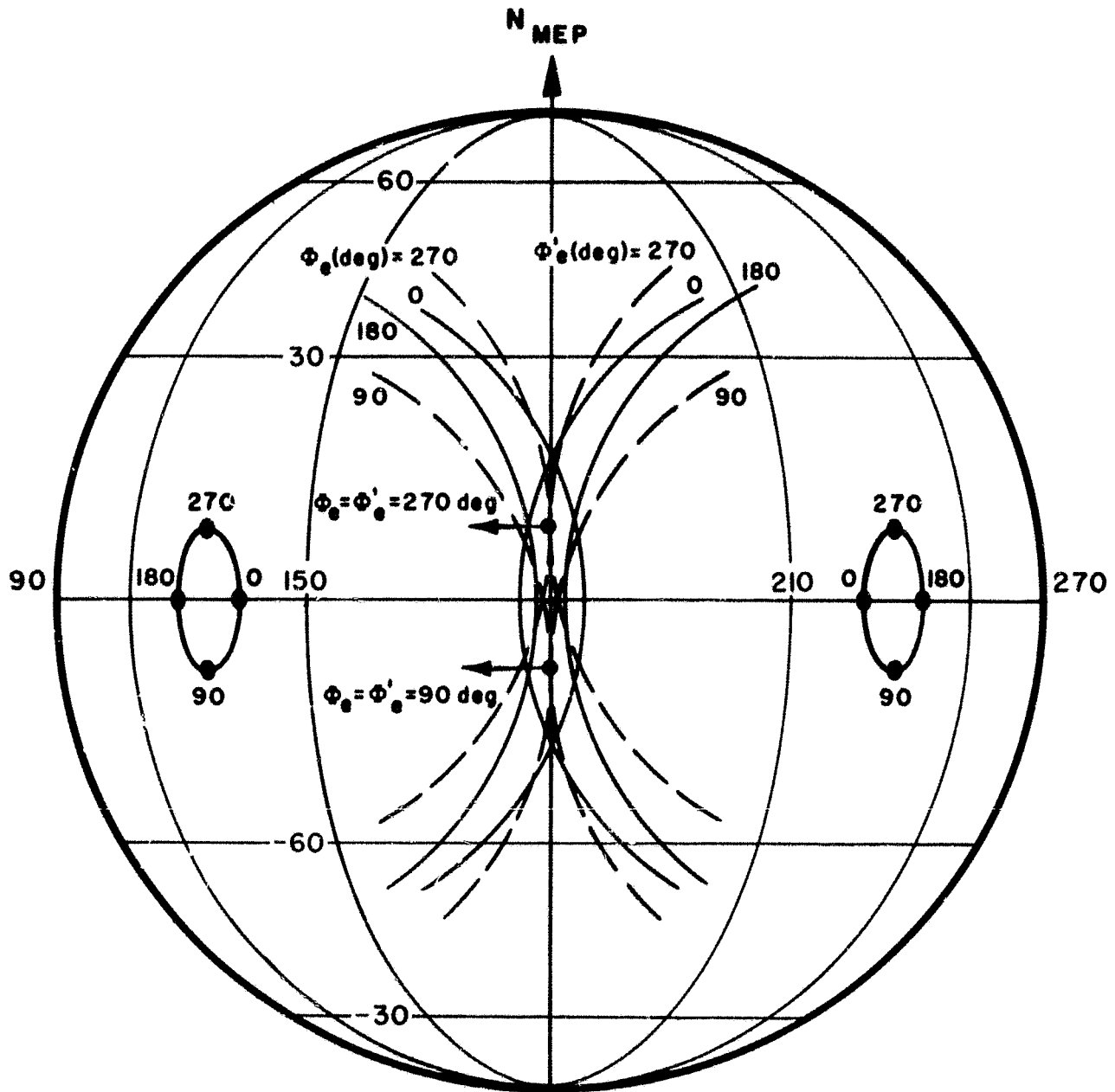


FIG. 114. THE PLANE SYMMETRIC FREE RETURN FOR
 $\Phi_e = \Phi'_e = 90^\circ, 270^\circ$ **AND MAXIMUM AND MINIMUM I_m**
FOR THE CLASSES $C(T^*, 6,555 \text{ km}, R_3^*)$
AND $C'(T^*, 6,555 \text{ km}, R_3^*)$

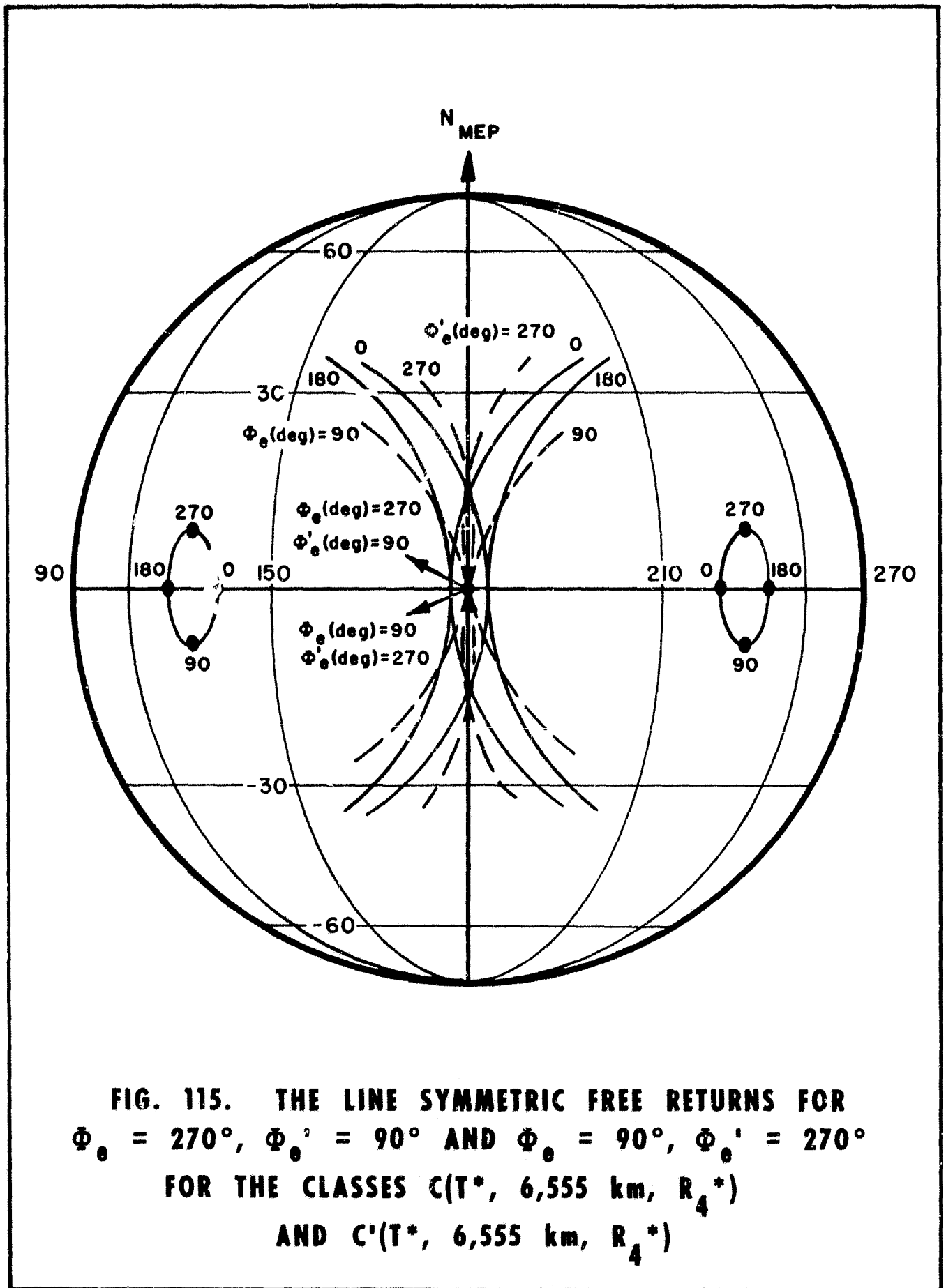


FIG. 115. THE LINE SYMMETRIC FREE RETURNS FOR
 $\Phi_e = 270^\circ, \Phi'_e = 90^\circ$ AND $\Phi_e = 90^\circ, \Phi'_e = 270^\circ$
FOR THE CLASSES $C(T^*, 6,555 \text{ km}, R_4^*)$
AND $C'(T^*, 6,555 \text{ km}, R_4^*)$

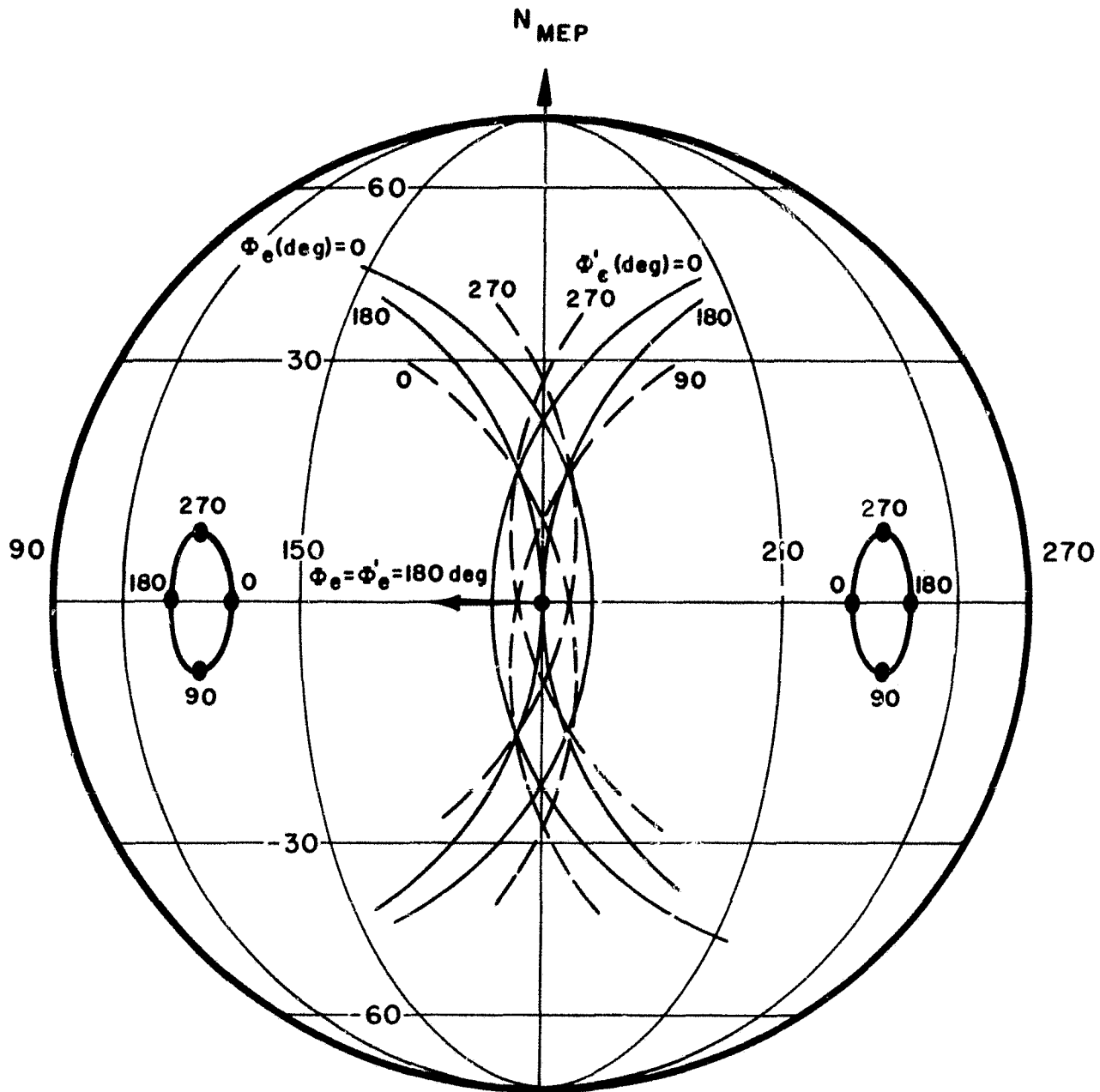
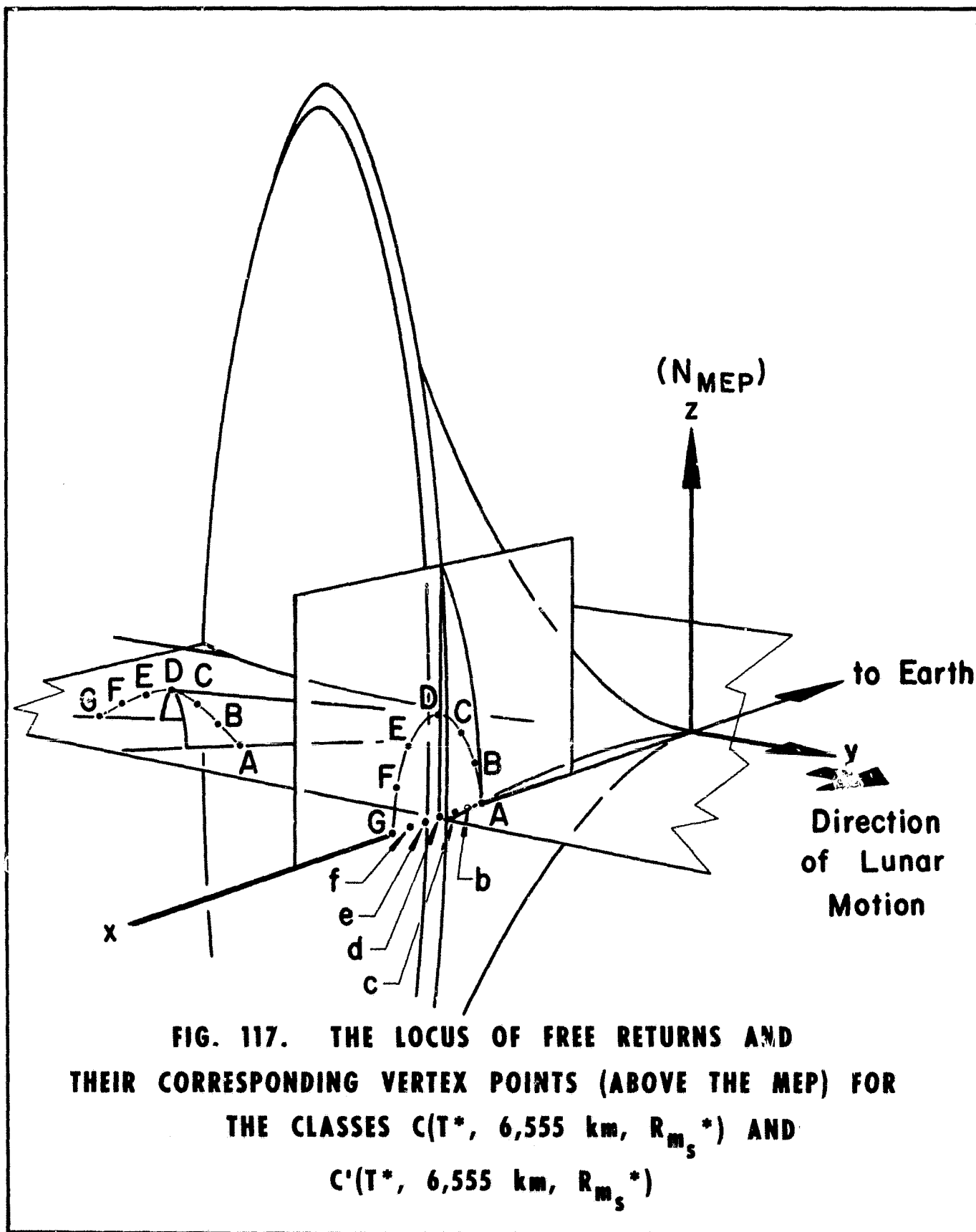


FIG. 116. THE SYMMETRIC FREE RETURN FOR $\Phi_e = \Phi'_e = 180^\circ$ AND $I_m = 180^\circ$ FOR THE CLASSES $C(T^*, 6,555 \text{ km}, R_5^*)$



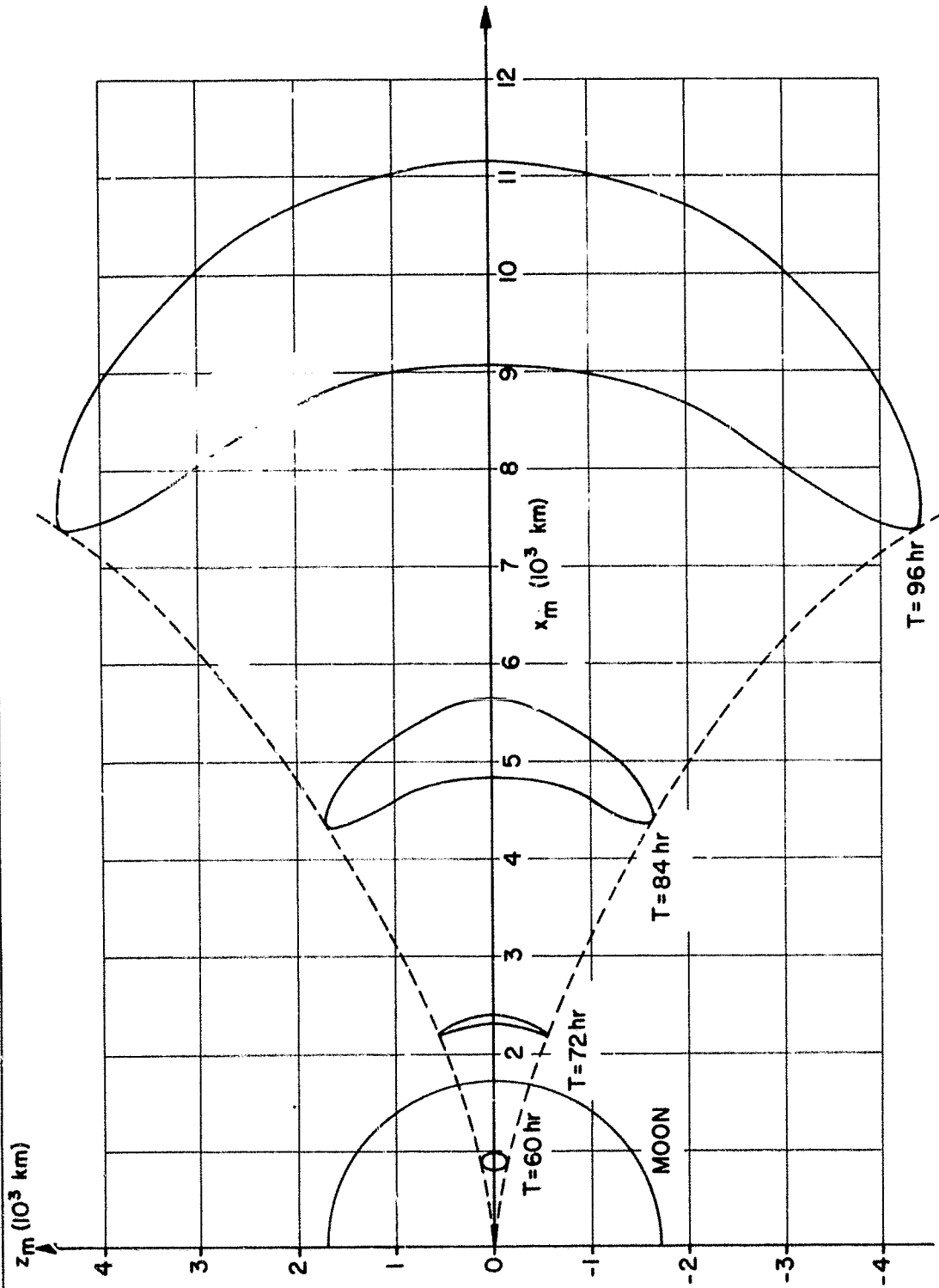


FIG. 118. PERISEL LOCI FOR SYMMETRIC FREE RETURNS
 FOR THE SYSTEM C (T_s , 6555 KM, R_{ms}), $T_s = 60, 72, 84, \text{ AND } 96$ HR

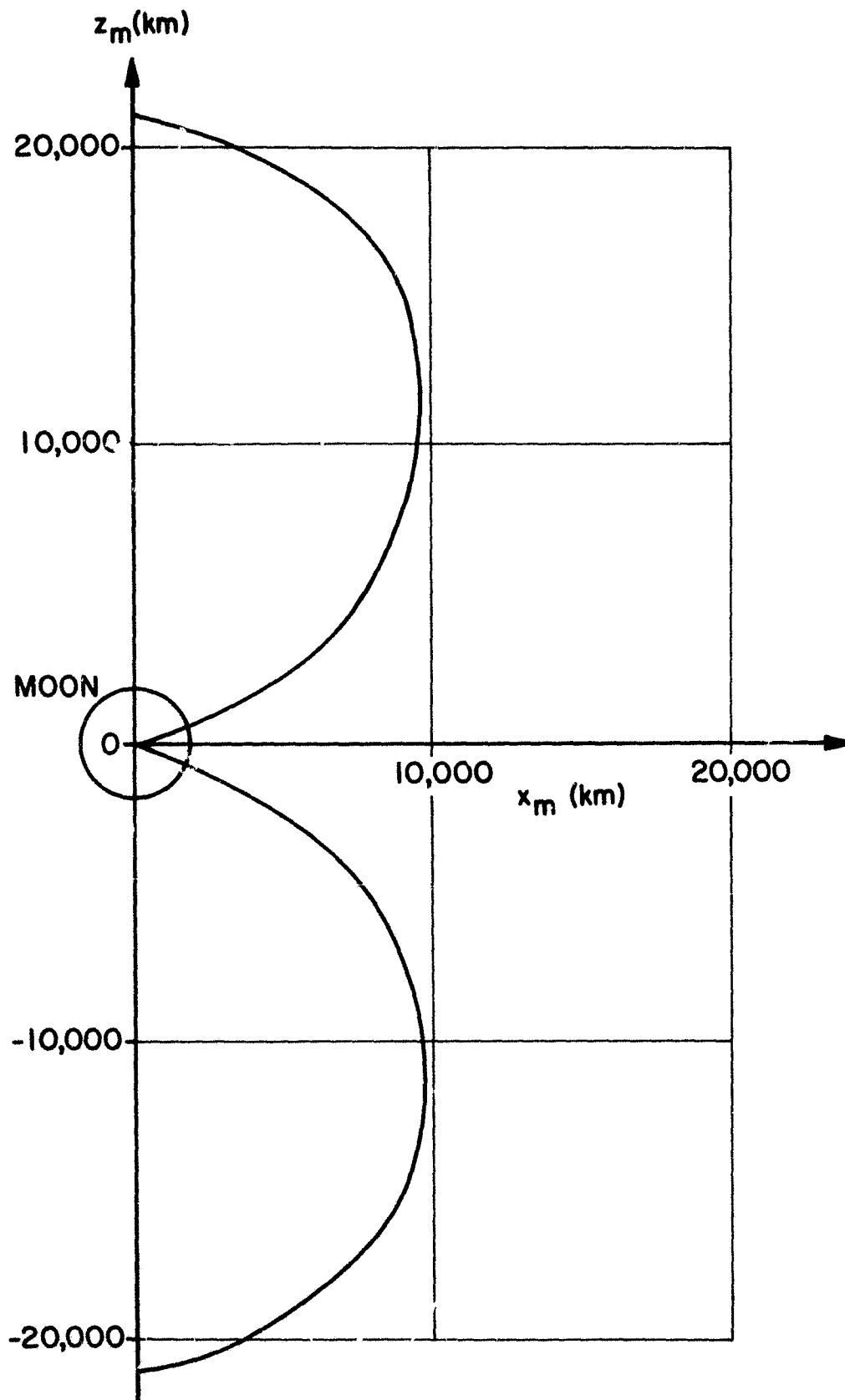


FIG. 119. NEAR MOON BOUNDARY FOR SYMMETRIC FREE RETURNS REPRESENTING MAXIMUM AND MINIMUM INCLINATION OF PERISEL CONIC AT ANY R_m

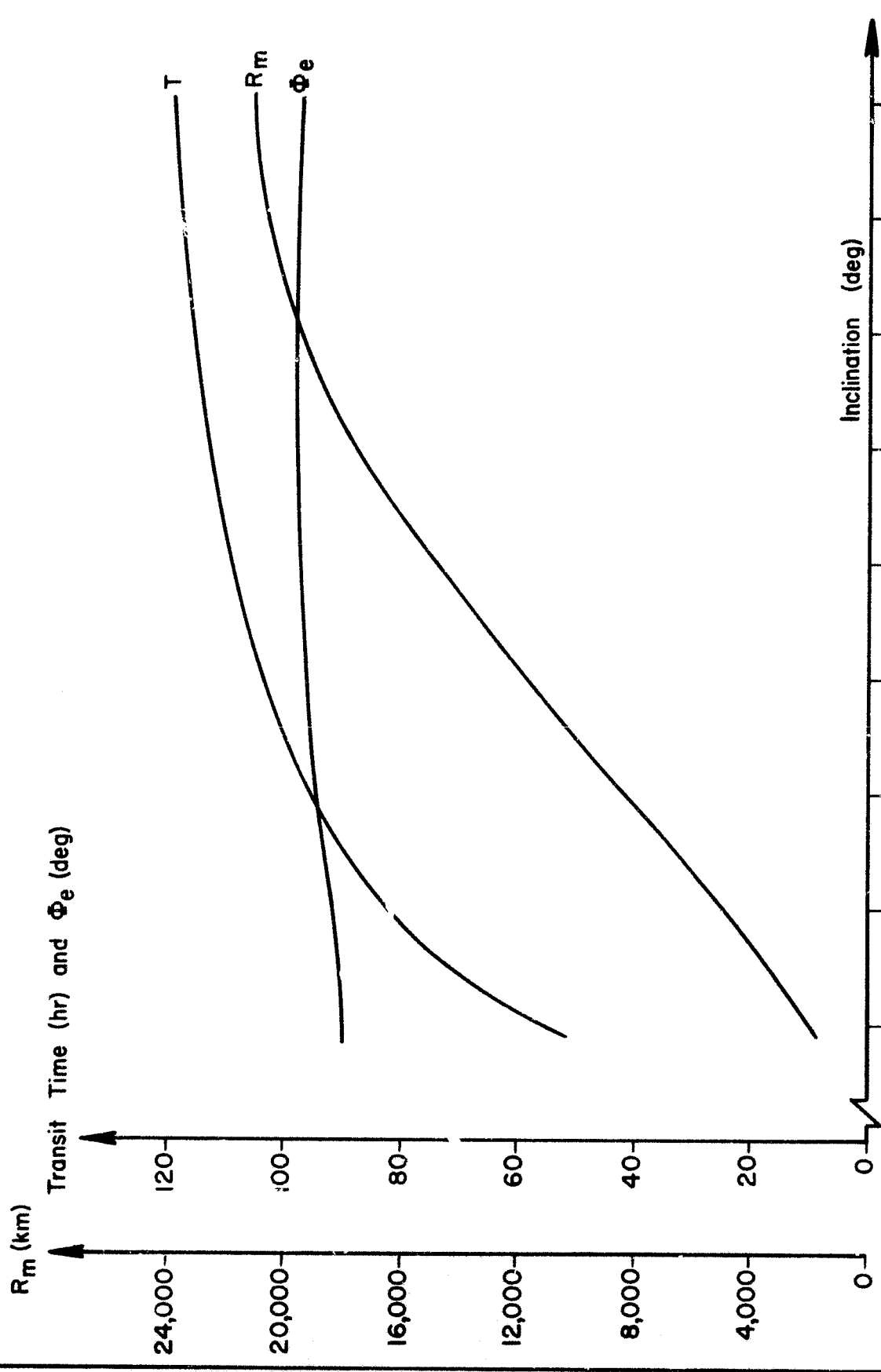


FIG. 120. TRANSIT TIME AND Φ_e FOR MAXIMUM INCLINATION OF PERISEL CONIC FOR FREE RETURNS IN NEIGHBORHOOD OF MOON

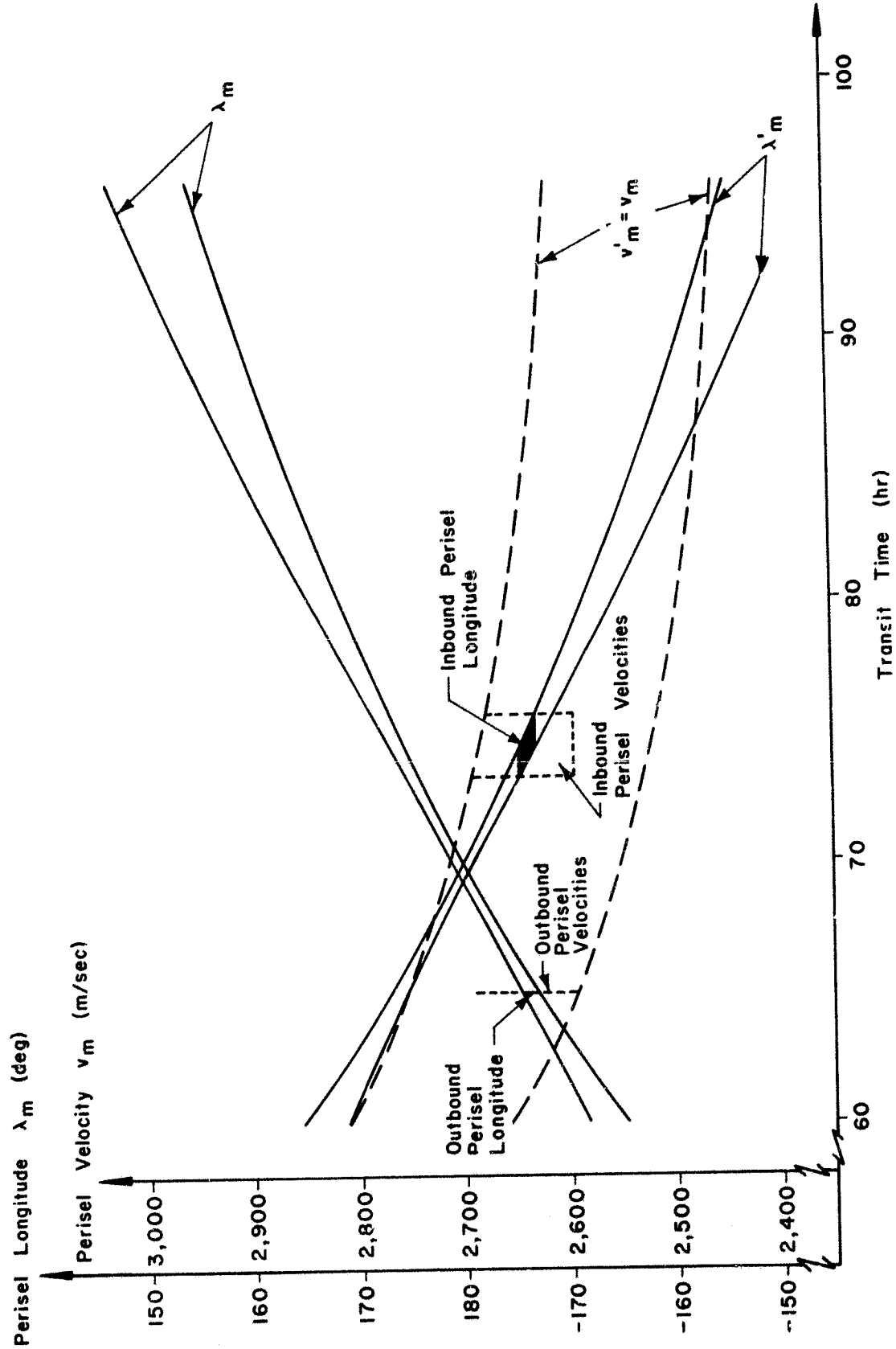


FIG. 121. VELOCITY AND LONGITUDE OF PERISELS IN THE MEP VS TRANSIT TIME FOR C (T_s , 6555 KM, 1923 KM) AND C' (T_s , 6555 KM, 1923 KM) FOR DETERMINATION OF FREE RETURN BOUNDARIES IN THE THREE PARAMETERS

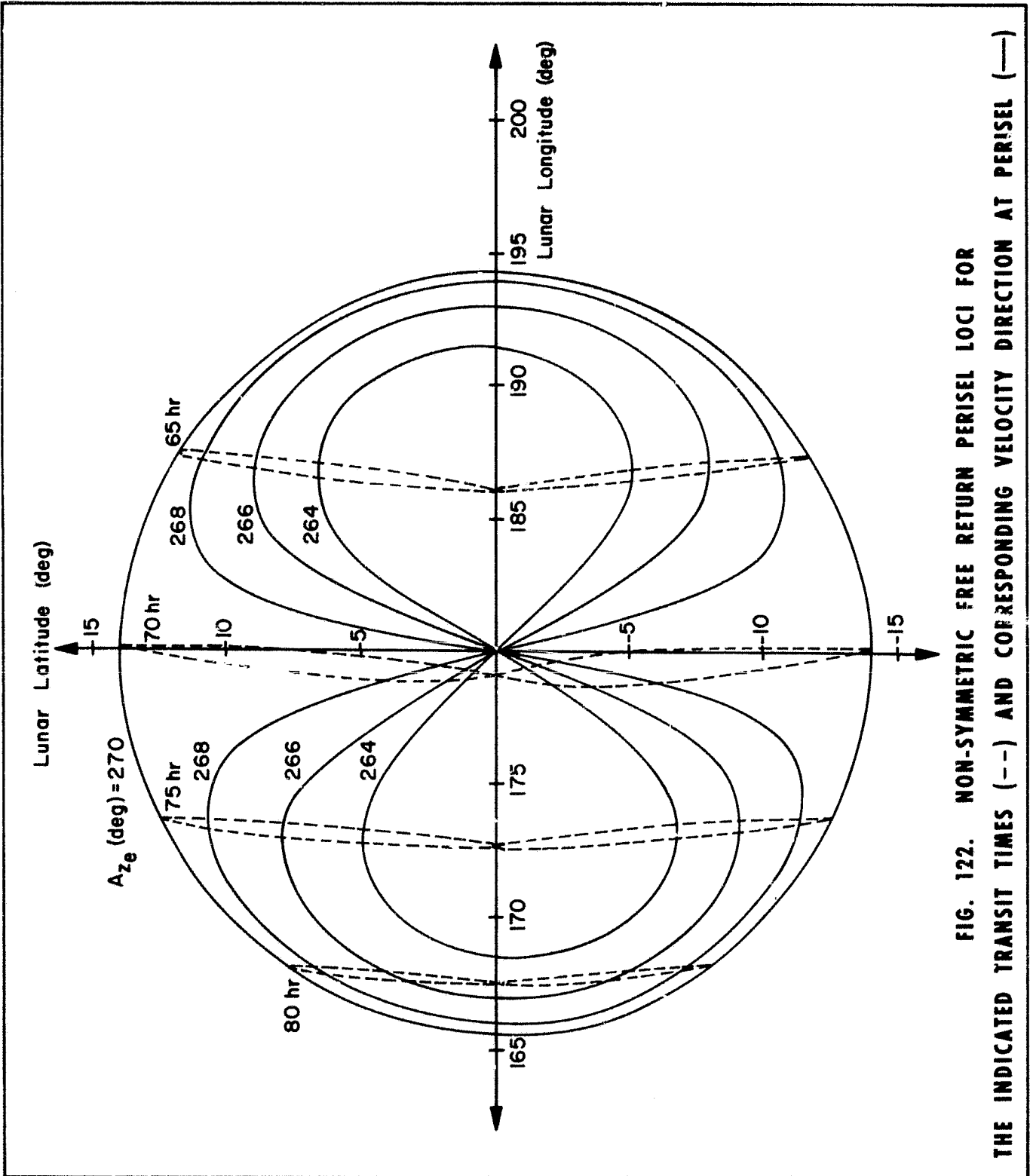


FIG. 122. NON-SYMMETRIC FREE RETURN PERISEL LOCI FOR THE INDICATED TRANSIT TIMES (---) AND CORRESPONDING VELOCITY DIRECTION AT PERISEL (—)

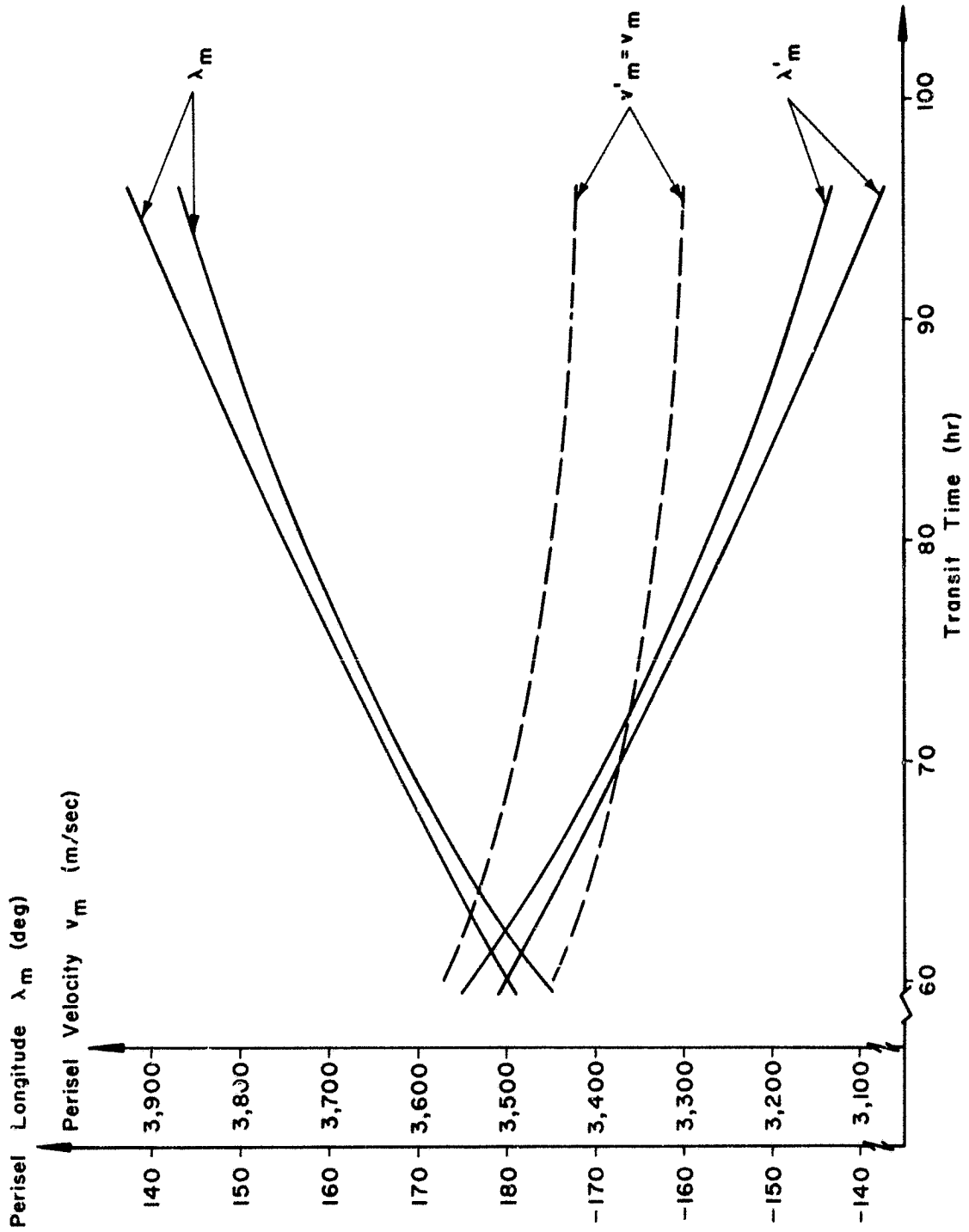


FIG. 123. VELOCITY AND LONGITUDE OF PERISELS IN THE MEP VS TRANSIT TIME FOR C (T_s , 6555 KM, 1000 KM) AND C' (T_s , 6555 KM, 1000 KM) FOR DETERMINATION OF FREE RETURN BOUNDARIES IN THE THREE PARAMETERS

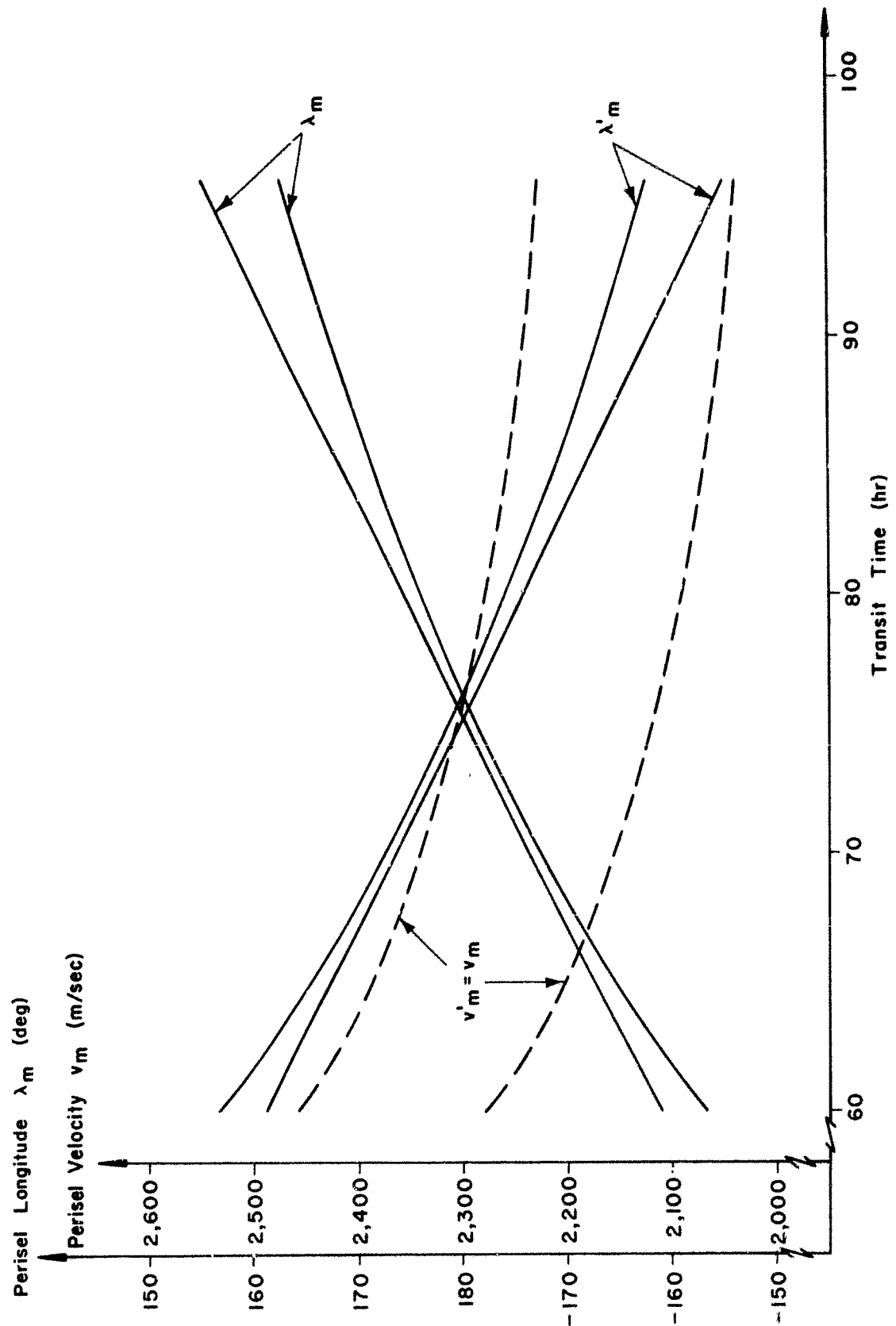


FIG. 124. VELOCITY AND LONGITUDE OF PERISELS IN THE MEP VS TRANSIT TIME FOR C (T_s , 6555 KM, 3000 KM) AND C' (T_s , 6555 KM, 3000 KM) FOR DETERMINATION OF FREE RETURN BOUNDARIES IN THE THREE PARAMETERS

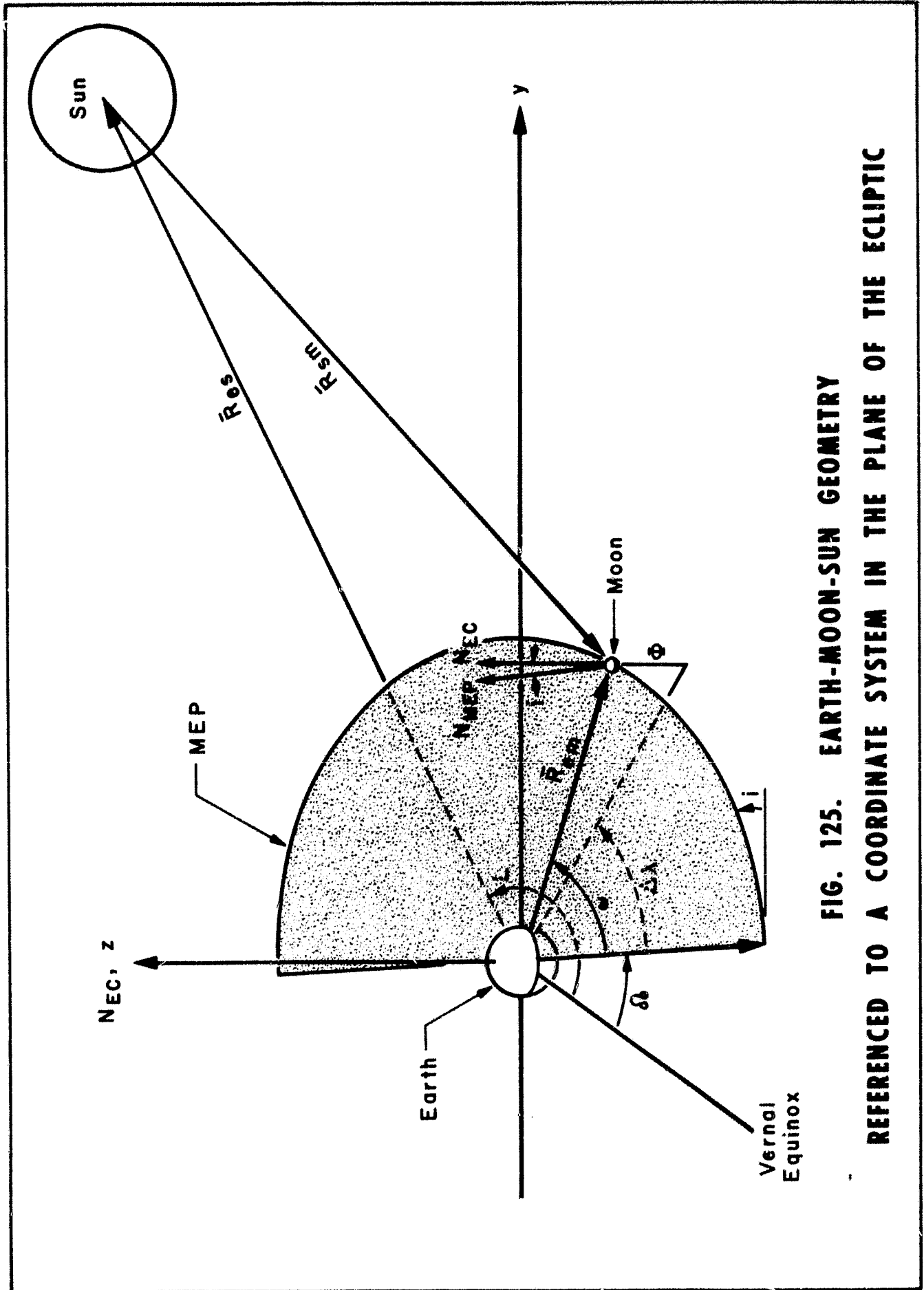


FIG. 125. EARTH-MOON-SUN GEOMETRY REFERENCED TO A COORDINATE SYSTEM IN THE PLANE OF THE ECLIPTIC

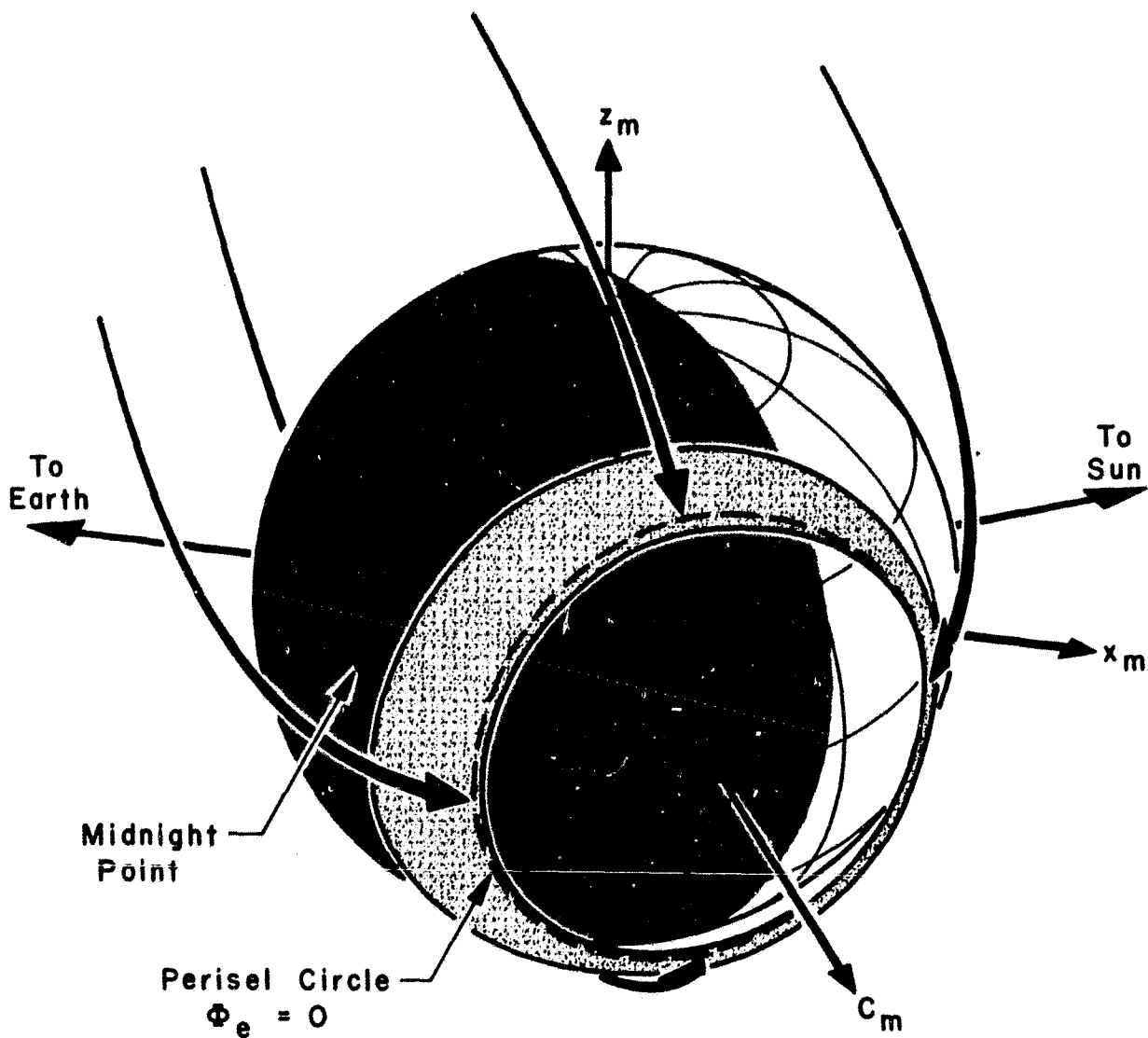
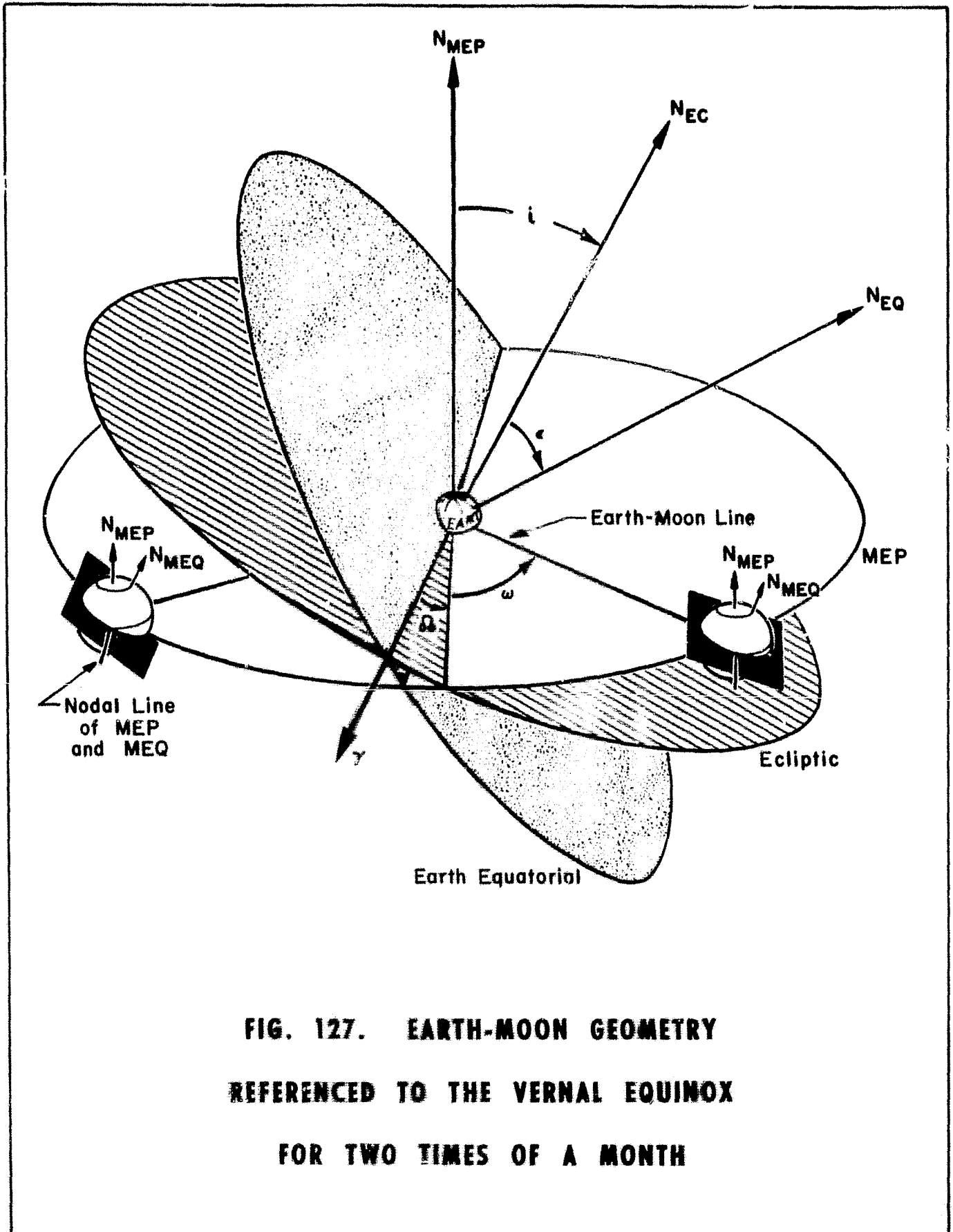


FIG. 126. LIGHTING CONDITIONS AT ARRIVAL FOR THE EMBEDDED AND POLAR TRANSITS FROM $\Phi_0 = 0$, AND PERISEL BELT FOR $T = 72$ HR FOR A PARTICULAR EARTH-MOON-SUN GEOMETRY



**FIG. 127. EARTH-MOON GEOMETRY
REFERENCED TO THE VERNAL EQUINOX
FOR TWO TIMES OF A MONTH**

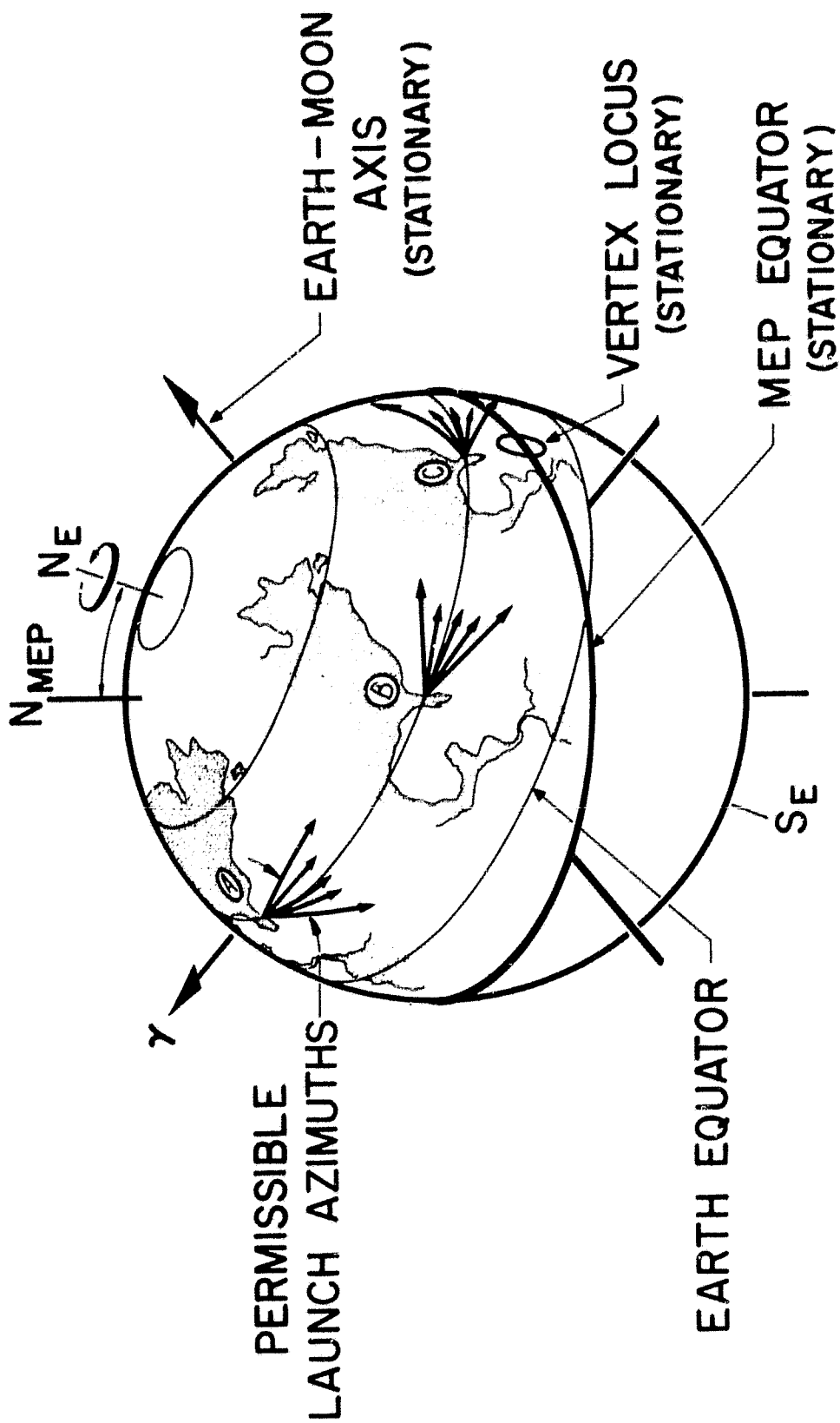


FIG. 128. AN ARBITRARY BUT TYPICAL POSITION OF THE TRUE EARTH AXIS AND EQUATOR TO THE MEP-REFERENCE SYSTEM

LAUNCH SITE LOCATIONS ARE INDICATED ACCORDING TO THREE DIFFERENT TIMES OF A DAY

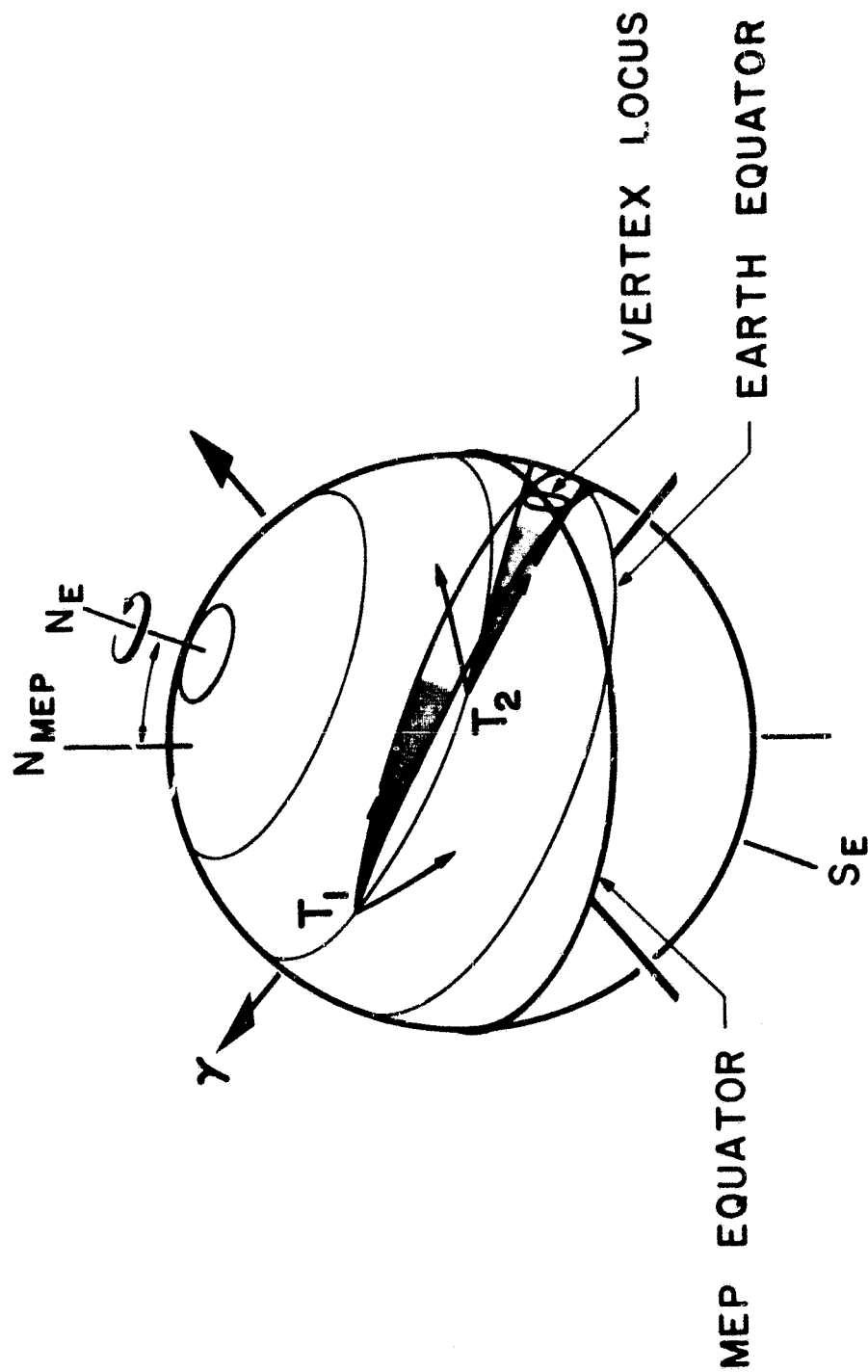


FIG. 129. ILLUSTRATIONS OF THE INITIAL AND LAST TIMEPOINTS OF THE PERIOD AT WHICH A FULL COVERAGE OF THE VERTEX LOCUS BY TWO-DIMENSIONAL TRAJECTORIES CAN BE ACCOMPLISHED

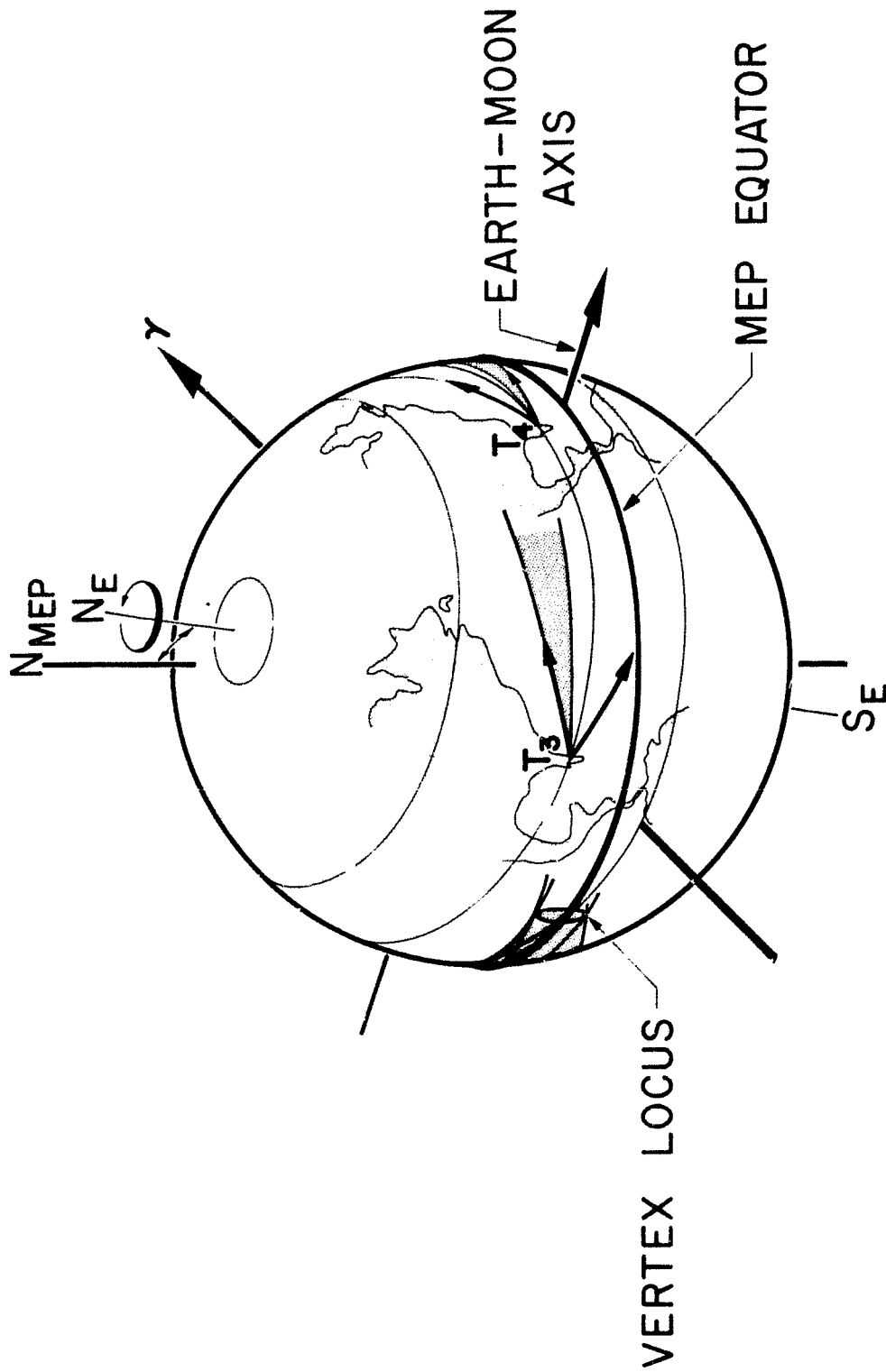


FIG. 130. ILLUSTRATION OF THE SECOND PERIOD FOR WHICH TWO-DIMENSIONAL FLIGHTS FROM THE LAUNCH SITE ALLOW FULL COVERAGE OF THE VERTEX LOCUS THESE FLIGHTS TAKE A LONGER CENTRAL ANGLE BEFORE REACHING THE VERTEX THAN THOSE OF FIG. 129

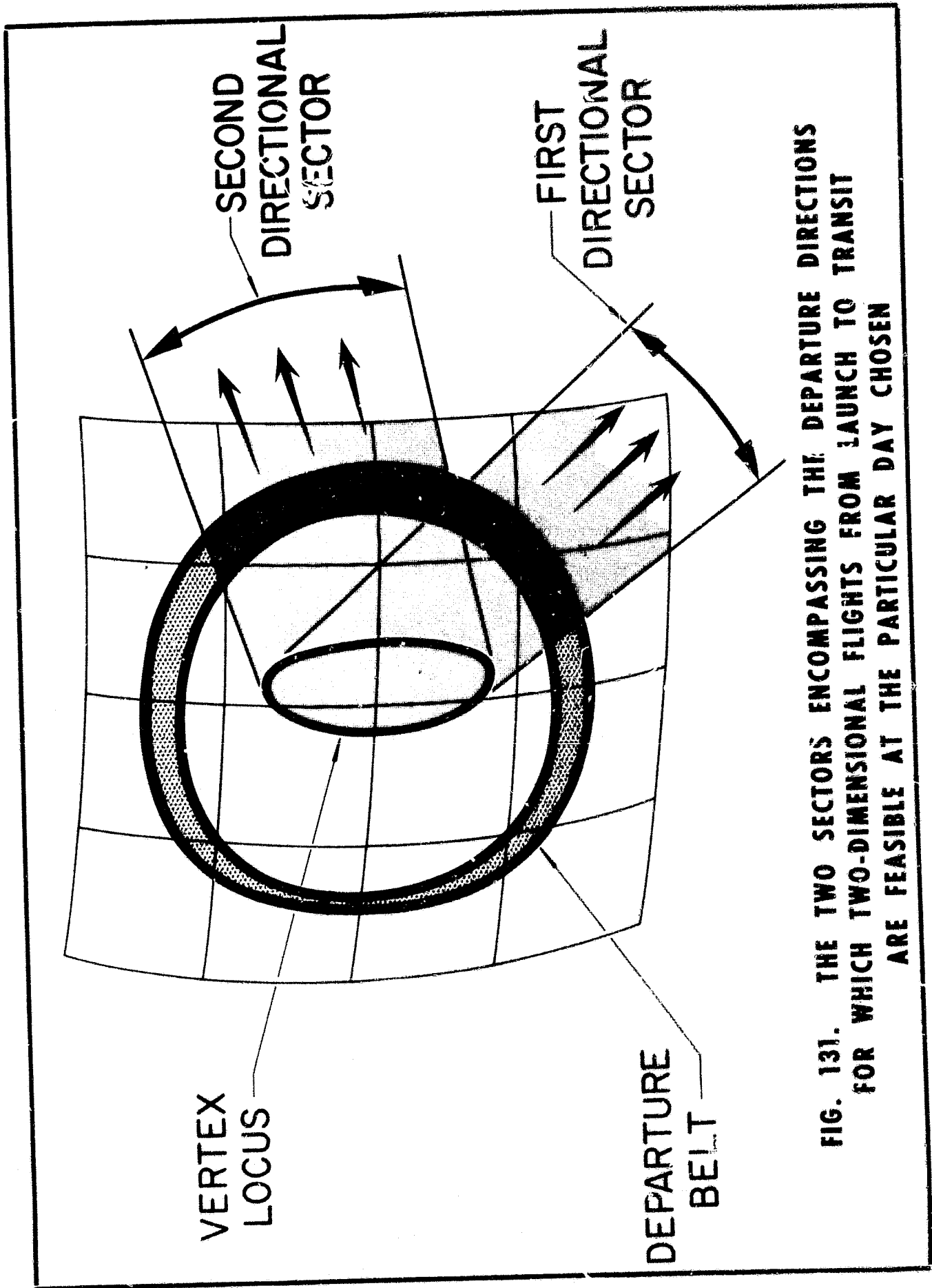


FIG. 131. THE TWO SECTORS ENCOMPASSING THE DEPARTURE DIRECTIONS FOR WHICH TWO-DIMENSIONAL FLIGHTS FROM LAUNCH TO TRANSIT ARE FEASIBLE AT THE PARTICULAR DAY CHOSEN

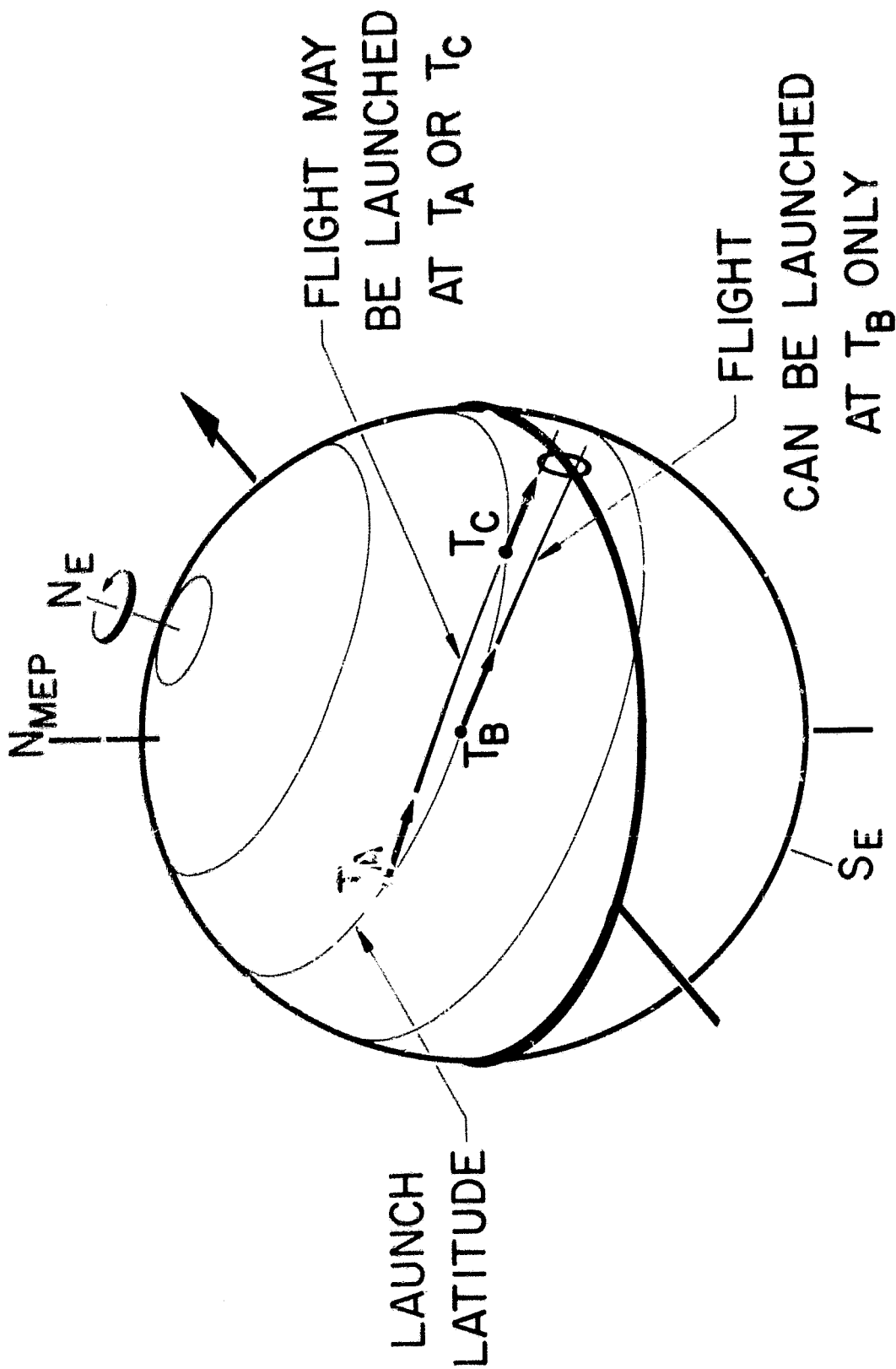
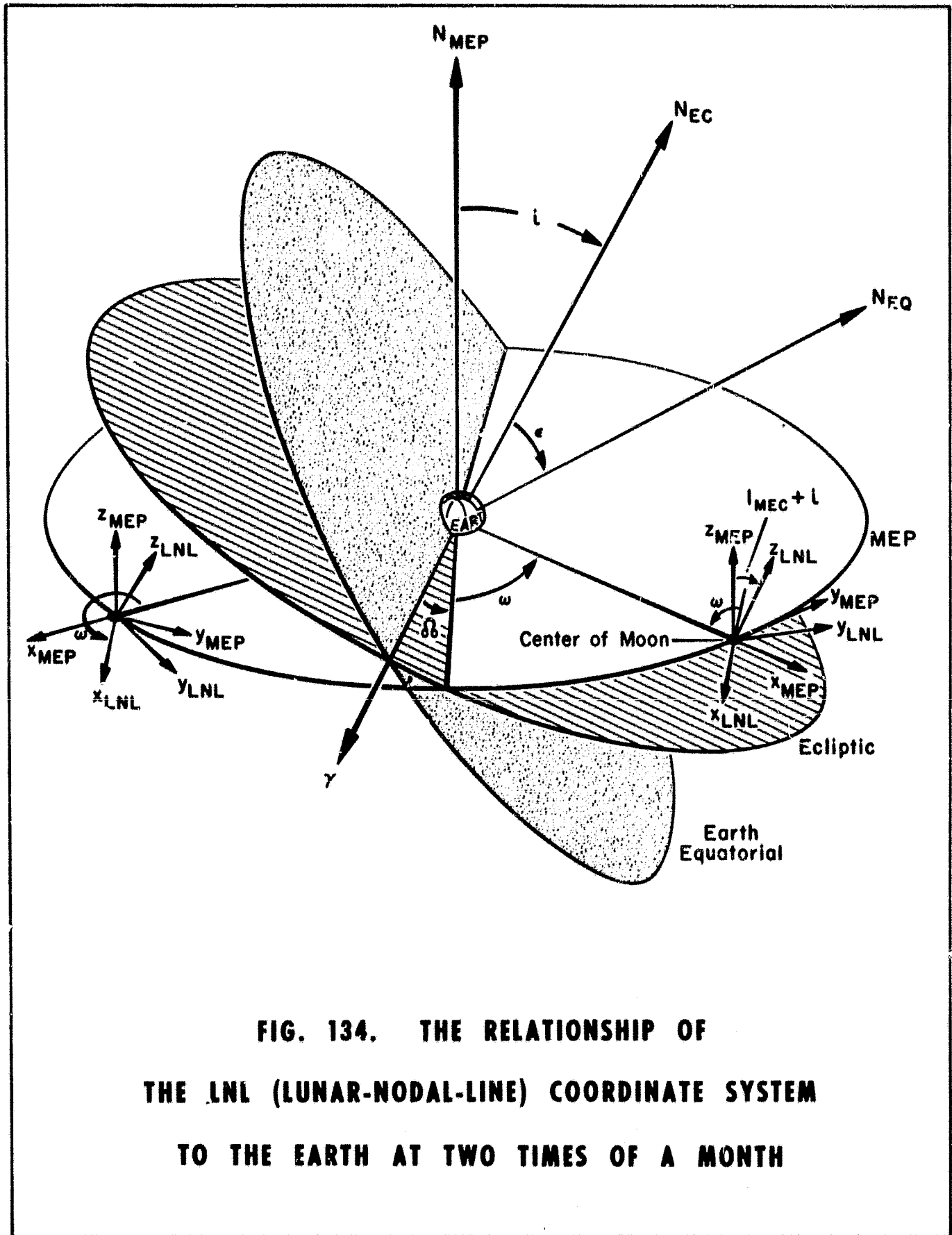
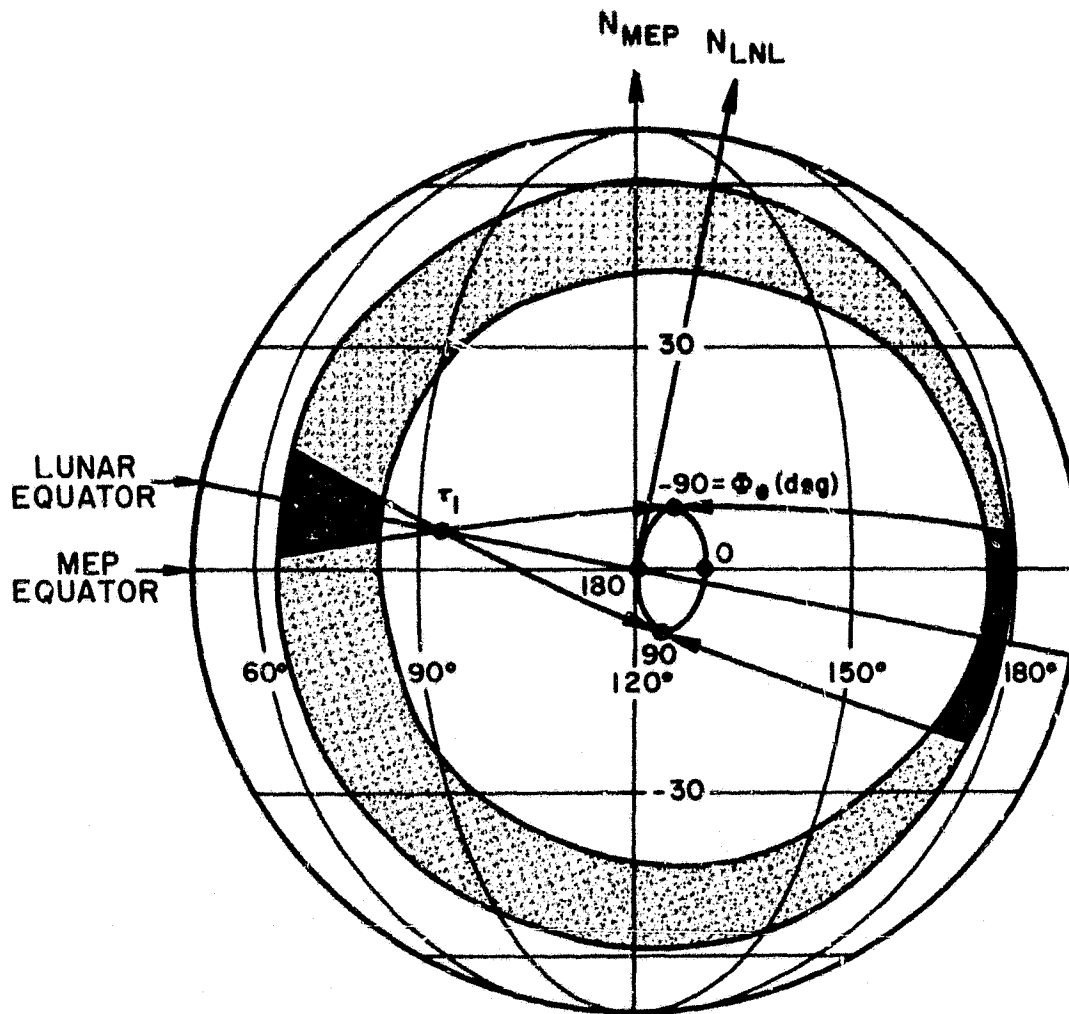


FIG. 132. EXAMPLES OF A TRAJECTORY WITH TWO LAUNCH OPPORTUNITIES (TA AND TC) AND OF ONE LAUNCHED DUE EAST ALLOWING ONLY ONE LAUNCH OPPORTUNITY (TB)



**FIG. 134. THE RELATIONSHIP OF
THE LNL (LUNAR-NODAL-LINE) COORDINATE SYSTEM
TO THE EARTH AT TWO TIMES OF A MONTH**



**FIG. 135. CO- AND COUNTER-ROTATIONAL ARRIVAL GEOMETRY
FOR TRANSITS FROM $C(T, R_e, R_m)$
WHICH PASS OVER A COMMON POINT ON THE LUNAR SURFACE**

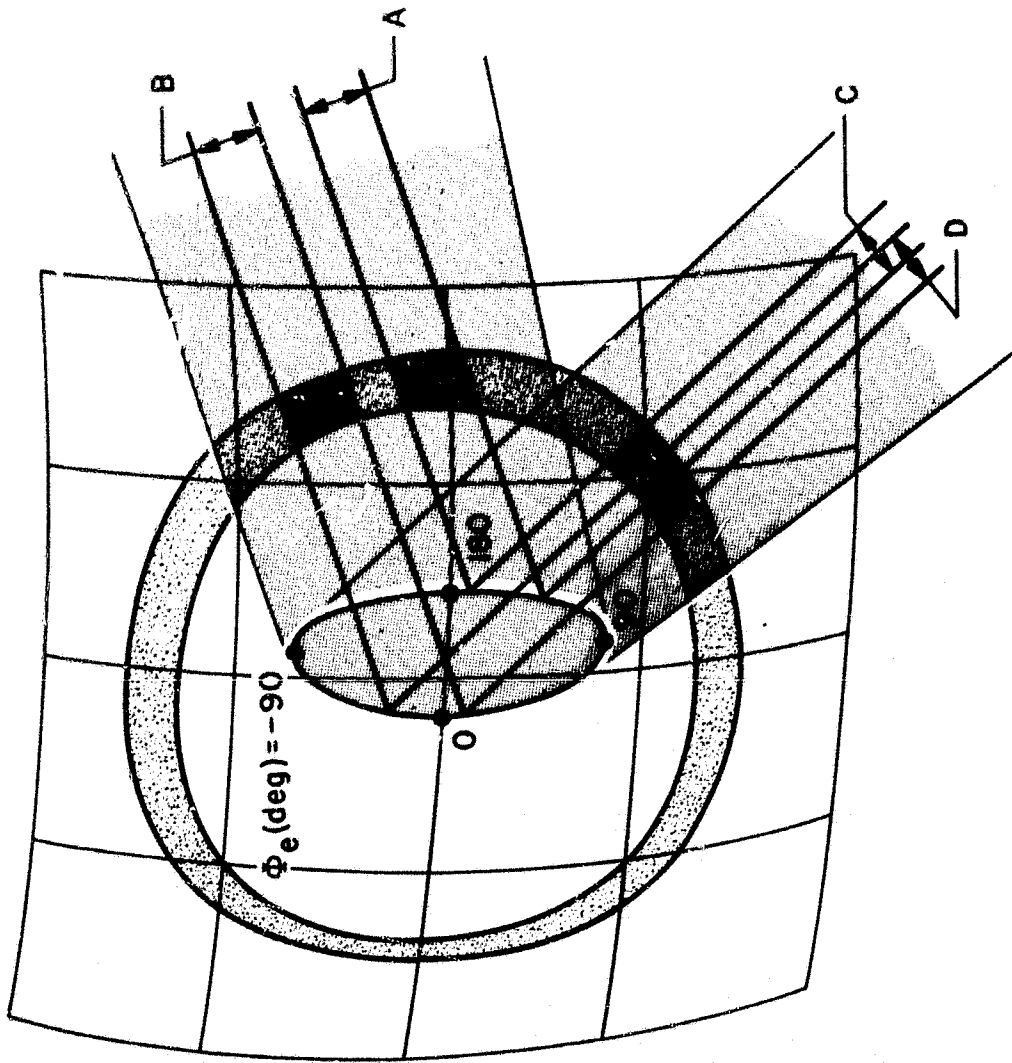
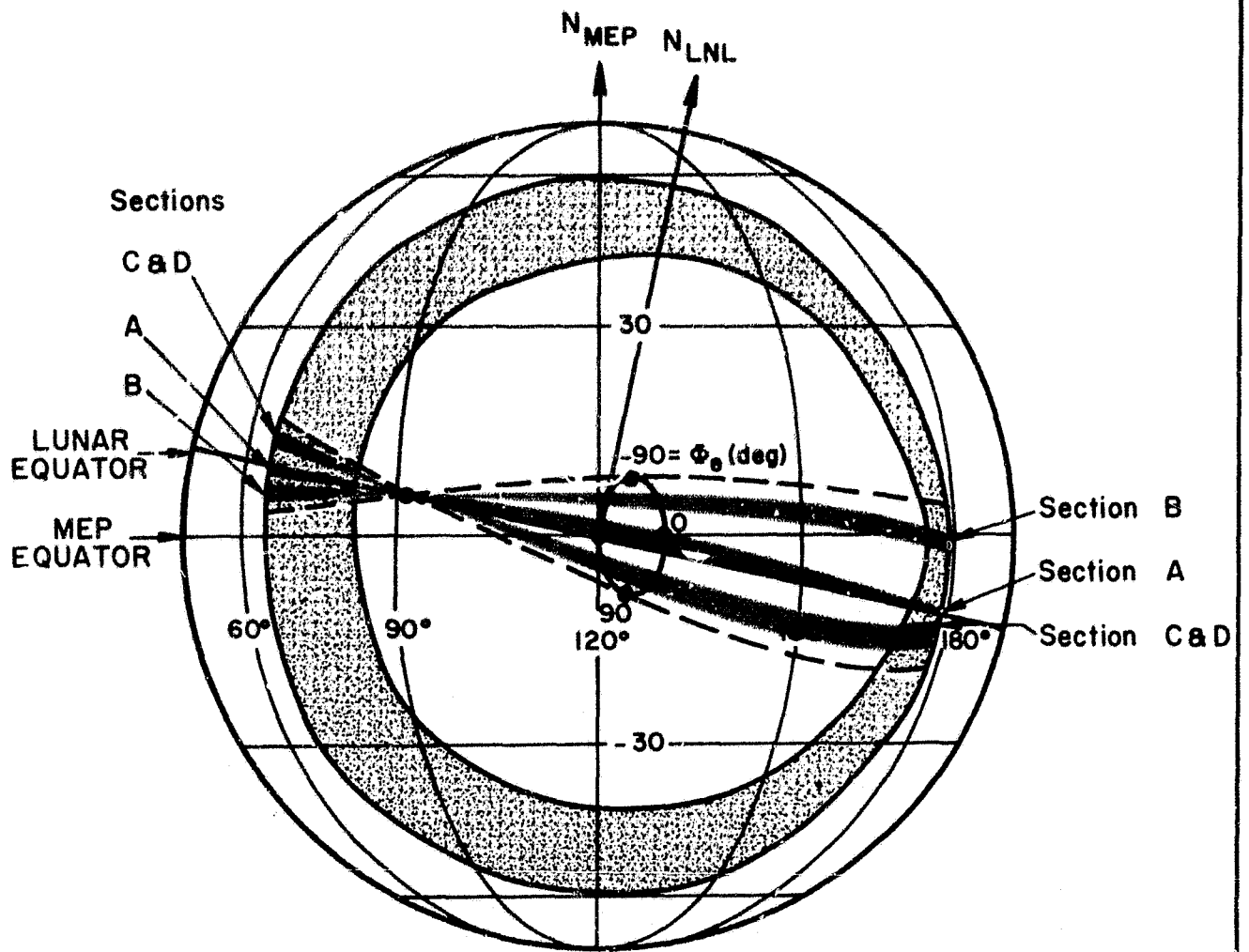


FIG. 136. THE EARTH LAUNCH SECTORS REDUCED BY REQUIREMENT THAT THE TRANSITS PASS OVER A GIVEN POINT ON THE LUNAR SURFACE



**FIG. 137. THE LUNAR ARRIVAL SECTORS
AS REDUCED BY LAUNCH RESTRICTIONS ON AZIMUTH,
THE TIME OF LAUNCH, AND THE LAUNCH SITE**

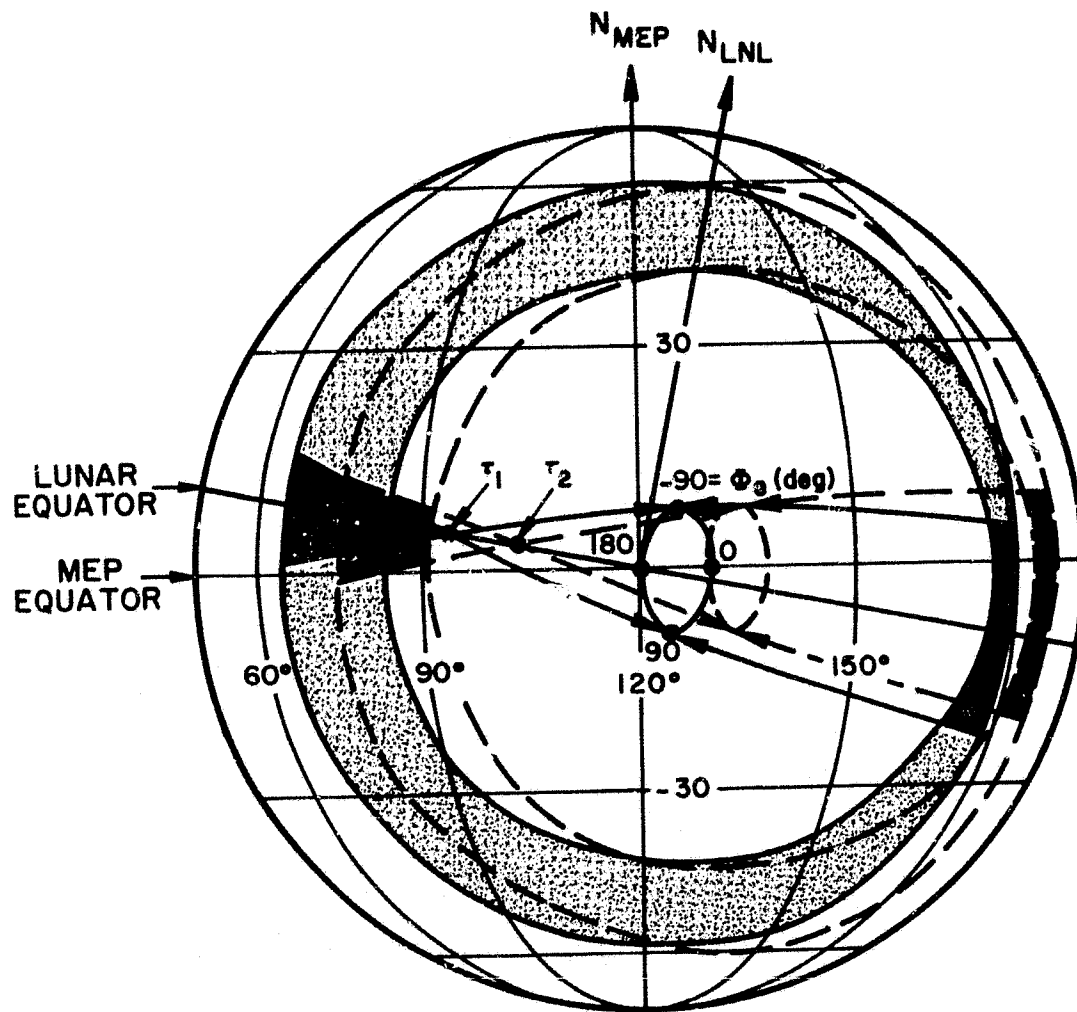


FIG. 138. AN INDICATION OF THE MOVEMENT OF THE SECTORS FOR LUNAR APPROACH AS TIME INCREASES ($\tau_1 < \tau_2$)

REFERENCES

1. Miele, Angelo, "Theorem of Image Trajectories in the Earth-Moon Space," Boeing Scientific Research Laboratories, D1-82-0039 (superseding a report of the same title and number in which several errors were found).
2. Miner, William E., "Methods for Trajectory Computation," MSFC, MTP-AERO-63-9, 1963.
3. "Explanatory Supplement to the Ephemeris," HMSO, 1961.
4. Hoelker, R. F., "Eine Uebersicht Ueber Freiflugbahnen zwischen Erde und Mond mit Herausstellung Charakteristischer Feldeigenschaften," presented at the German Rocket Society's 12th Rocket and Space Flight Symposium, Hamburg, West Germany, 20-22 Sept. 1963.
5. Hoelker, R. F. and N. J. Braud, "Mapping the Course for the Moon Trip," *Astronautics and Aerospace Engineering*, February 1964.
6. Schwaniger, A. J., "Lunar Flight Study Series: Volume 5, Trajectories in the Earth-Moon Space with Symmetrical Free Return Properties," NASA TN D-1833, June 1963.
7. Herring, G. P., "The Reduced Three-Body Problem: A Generalization of the Classical Restricted Three-Body Problem," NASA TM X-53083, July 1964, Unclassified.
8. "Fundamentals of Earth to Moon Trajectories," NASA Contract 410w, Work Order 110, Line Item 4.2.1.3, 1964.
9. Schwaniger, A. J., "A Survey of Free Return Transits in Earth-Moon Space," presented at XVth International Astronautical Congress, Sept. 7-13, 1964, Warsaw, Poland.
10. Kurtz, F., "Stability and Visibility of Lunar Orbits," MSFC AIN-14-62, April 1962, Unclassified.
11. Kalensher, B. E., "Selenographic Coordinates," Tech. Report No. 32-41, JPL, Pasadena, Calif., February 1961.

October 21, 1964

APPROVAL

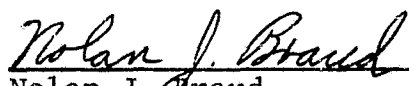
NASA TM X-53151

A COMPREHENSIVE ASTRODYNAMIC EXPOSITION AND
CLASSIFICATION OF EARTH-MOON TRANSITS

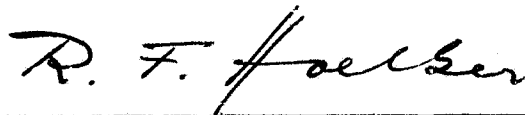
By Gary P. Herring

The information in this report has been reviewed for security classification. Review of any information concerning Department of Defense or Atomic Energy Commission programs has been made by the MSFC Security Classification Officer. This report, in its entirety, has been determined to be unclassified.

This document has also been reviewed and approved for technical accuracy.



Nolan J. Braud
Chief, Astrodynamics Branch



R. F. Hoelker
Chief, Astrodynamic and Guidance Theory Division



E. D. Geissler
Director, Aero-Astrodynamics Laboratory